CRANFIELD UNIVERSITY

ALESSANDRA SANSON

MODIFIED BISMUTH TITANATE PIEZOELECTRIC CERAMICS

SCHOOL OF INDUSTRIAL AND MANUFACTURING SCIENCE

PhD THESIS

CRANFIELD UNIVERSITY

SCHOOL OF INDUSTRIAL AND MANUFACTURING SCIENCE

PhD THESIS

ACADEMIC YEAR 2002-2003

ALESSANDRA SANSON

MODIFIED BISMUTH TITANATE PIEZOELECTRIC CERAMICS

Supervisor: Prof. R. W. Whatmore

December 2003

This thesis is submitted in partial fulfilment of the requirements for the degree of PhD

ABSTRACT

Bismuth compounds are considered the most suitable alternatives to lead-based systems for ferroelectric and piezoelectric applications. Nevertheless little has been done to systematically study the relationships that link the two main classes of ferroelectric bismuth compounds: perovskite and bismuth layer compounds (Aurivillius compounds). The knowledge of these relationships could be a key to improve the performances of the bismuth compounds and could help to better tailor their properties for specific applications.

The objective of this project was twofold:

1. To understand the structural and electrical relationships between perovskite and Aurivillius compounds within the $Na_{1/2}Bi_{1/2}TiO_3$-$Bi_4Ti_3O_{12}$-$BaTiO_3$ (NBT-BIT-BT) system;
2. To explore the possibility of obtaining a new perovskite of formula Bi_2MgTiO_6.

A study of 83 different compositions allowed us to sketch the possible phase diagram of the NBT-BIT-BT system. XRD structural characterisation highlighted the importance of low angle analysis in the study of layered compounds. The presence of monophasic regions in the phase diagram stressed the flexibility of this class of compounds that are able to withstand high percentage of vacancies before collapsing. It was shown that, after taking into account some electronic considerations, a simple geometrical model can be use as "rule of thumb" to predict the stability of Aurivillius compounds. New unreported compounds were found in the system and a mechanism for the formation of the Aurivillius compounds is proposed.

The dielectric and piezoelectric properties were linked to the fundamental layered structure of the Aurivillius phases showing that all these properties depend on the number of perovskite blocks present. The higher the number of perovskite blocks, higher the values of resistivity and relative permittivity.

It was proved that the formulation Bi_2MgTiO_6 does not lead to a perovskite compound but to a multiphasic system. Nonetheless, it was established that the doping of $Bi_4Ti_3O_{12}$ with magnesium improves its properties to a good extent modifying also the morphology of the grain of the ceramics. The addition of 1%mol MgO increases the permittivity by 50% and the resistivity by more than one order of magnitude. Magnesium strongly affects also the piezoelectric coefficient almost doubling the value relative to that previously reported for BIT.

ACKNOWLEDGEMENTS

First of all, I would like to thank my parents for their support during this period. Without them I would never be able to overcome the difficult moments that I had to face.

My warmest thanks to all my friends for reminding me what is really important in life.

I would like to thank Prof. Roger Whatmore for his advices and encouragement throughout this project and for being present whenever I needed.

Many thanks to Drs. Debbie Corker, Rob Dorey, Steve Dunn and Chris Shaw for their help and very useful suggestions.

Special thanks to the technical staff of Cranfield, in particular to Andrew Stallard and Mark Woodruff (especially for the cipping process) and to Colin Matthews for his patience and assistance in the XRD and SEM analyses.

Finally, I would like to thank all the persons in the Nanotechnology group for making me so hard to come back home!

The financial support of TDK Japan throughout this project is gratefully acknowledged.

TABLE OF CONTENTS

LIST OF FIGURES

LIST OF TABLES

LIST OF EQUATIONS

LIST OF SYMBOLS

□ = unoccupied site in the lattice
$\varnothing_g$ = diameter green pellet
$\varnothing_s$ = diameter sintered pellet
a = cell parameter
$\underline{a}$ = pseudo tetragonal lattice parameter of layered compounds
a_{orth} = cell parameter of orthorhombic cell
a_T = cell parameter of tetragonal cell
A = surface area
a'_P = lattice parameter of the unconstrained perovskite-like unit in Aurivillius compounds
a'_B = lattice parameter of the unconstrained bismuthyl unit in Aurivillius compounds
b = lattice parameter
b_{orth} = cell parameter of orthorhombic cell
b_T = cell parameter of tetragonal cell
c = cell parameter
C = capacitance
d_{ij} = piezoelectric coefficient
Dj = electric displacement
d_g = density green pellet
d_s = density sintered pellet
$d_s(G)$ = density of sintered pellet obtained by geometrical calculations
$d_s(A)$ = density sintered pellet obtained using the Archimedes technique
ΔV = Kikuchi parameter
ΔE_{AO} = electronegativity difference between ions A and oxygen
E_A = activation energy
E_C = coercive field
E = electric field
$\varepsilon'(\omega)$ = real permittivity as a function of frequency
$\varepsilon''(\omega)$= imaginary permittivity as a function of frequency
ε = permittivity
ε_0 = permittivity of free space
f_a = frequency of antiresonance
f_r = frequency of resonance
$f_r^{(2)}$ = frequency of resonance of the first overtone
(h,k,l) = Miller indexes
h_B = thickness of bismuthyl layer along c for Aurivillius compounds
h_P = thickness of perovskite-like unit along c for Aurivillius compounds
I = current
k = electromechanical coupling factor
k_{eff}, k_{ij} = effective electromechanical coupling factor
k_p = planar coupling factor
k_t = thickness coupling factor
K = ratio between the bulk moduli of the bismuthyl layer and perovskite block
K_B = bulk modulus of the bismuthyl layers of Aurivillius compounds
K_P = bulk modulus of the perovskite blocks of Aurivillius compounds

L = inductance
m = number of perovskite block in an Aurivillius compound
P_r = remanent polarisation
P_s = saturation polarisation
$\bar{r}_A$ = mean radius of the ions in the A-site of a perovskite
$\bar{r}_B$ = mean radius of the ions in the B-site of a perovskite
r_o = radius of oxygen
R = resistance
ρ = resistivity
s = compliance
S = Strain
σ = conductivity
σ_p = Poisson ratio
t = tolerance factor
tanδ = dielectric loss
t_g = thickness green pellet
t_s = thickness sintered pellet
T = stress
T_C = Curie temperature
τ = time constant
U = energy density
V = voltage
V'_B = volume unconstrained bismuthyl layer in Aurivillius compounds
V'_P = volume unconstrained perovskite blocks in Aurivillius compounds

INTRODUCTION

The toxicity of lead and lead compounds has been known since 200 B.C.. Pb can be absorbed into blood, bone and soft tissues causing nervous disorders, high blood pressure, anaemia, memory and concentration problems. While lead heavily affects adults, its neurotoxic effect is particular worrying in children for whom low levels of lead in the blood can cause severe damage[1]. There has been an intense debate around the impact of lead coming from electronic equipments other than batteries, especially since the convention of Rio de Janeiro in 1992 on "climate change"[2]. Pushed by a public opinion, more and more sensitive to public health and environmental issues, the scientific community and electronic industry have started to move towards the elimination of lead from ferroelectric and piezoelectric materials before local or global regulations come into force.

In looking for new lead-free ferroelectrics attention has been focused on bismuth based materials. These compounds present a promising option to replace lead materials in ferroelectric applications presenting good properties coupled with a decreased toxicity. The materials for this study were made using the conventional mixed oxide ceramic technique that is the easiest synthetic route for these materials.

The piezoelectric compounds of bismuth crystallise mainly in two forms: perovskite and layered perovskite-related materials (known as Aurivillius compounds).

The aim of this project was to understand the structural and electrical relationships between these two families in an attempt to improve the properties of the compounds already known, or to discover new ones. This was accomplished by studying the coupling of the best known piezoelectric bismuth compound ($Na_{0.5}Bi_{0.5}TiO_3$, NBT) with the prototype of the Aurivillius compound family ($Bi_4Ti_3O_{12}$, BIT).

In conjunction with this, a study was made to obtain a possible new perovskite of formula Bi_2MgTiO_6.

This thesis is divided in four sections: Literature Review, Experimental, Results and Discussion, and Final Remarks and Future work.

In the first section the phenomenon of piezoelectricity is introduced and examined with respect to ceramics. The project is put in the context of an increasing interest in

lead-free materials and the main compounds chosen (NBT and BIT) are examined in detail.

In the "Experimental" section, the primary production route is reviewed and the techniques used for the characterisation of the materials are presented.

The "Results and Discussion" presents the work performed and justifies it on the basis of the current knowledge. This part is divided into two subsections corresponding to the two main parts of the project: the coupling perovskite-Aurivillius and the possible new perovskite Bi_2MgTiO_6.

The thesis is concluded with "Final Remarks and Future Work", where the research is summarised, conclusions are drawn and future directions considered.

1. LITERATURE REVIEW

1.1. PIEZOELECTRICITY

In this introductory section the phenomenon of piezoelectricity is presented and located in the context of the project. After a brief historical excursion, the fundamentals of the effect are presented.

1.1.1. Historical outline

The first experimental proof of the piezoelectric effect was published in 1880 by Pierre and Jacques Curie as a result of their studies on monocrystals (quartz, tourmaline and Rochelle salt) undergoing mechanical stress[3]. They showed that some materials, due to their particular crystallographic structure, can develop electrical charges proportional to the applied mechanical stress (direct piezoelectric effect). Later, they proved that the same crystal can exhibit a converse effect, changing its dimensions when a voltage is applied through it. Unfortunately, the complexity of this phenomenon, that requires a tensorial analysis to define the relevant measurable quantities, prevented the deep comprehension of piezoelectricity for almost twenty five years. In 1910 Voigt published the "Lerbuch der Kristallphysik" in which he defined completely the twenty natural crystal classes in which the piezoelectric effect occurs and, with appropriate tensorial analysis, all the possible macroscopic non-zero piezoelectric coefficients[4]. Although the phenomenon had been reported, there were no commercial applications for piezoelectric materials until 1917, when Langevin began to perfect an ultrasonic submarine detector, using piezoelectric quartz crystal as transducer[5].

The success of the sonar stimulated the research on all kind of piezoelectric devices that culminate in the 1940's with the discovery of the advantages obtainable by the use of polycrystalline ceramics instead of single crystals. Although investigations into the applications of piezoelectricity were carried out all around the world, the American industries took the lead of the research animating also an intense patent activity. The American supremacy established during the Second World War was soon beaten by new Japanese companies, born from the active collaboration between industry and university[6], appeared in the market for the first time in 1951.

The discovery of lead zirconate titanate (PZT) gave additional impulse to an already vibrant research throughout the world. An analysis of the US patents in the years between 1990 and 1996[6], showed that with 41 and 42% of the total patents issued, US and Japanese companies represent the leaders of the piezoelectric market. The total US consumption of electronic ceramic components in 1999 was $5.5 billions and with an average annual growth rate (AAGR) of 8.7% is estimated to reach $8.6 billions by the year 2004[7]. Among them, piezoelectric ceramics, ceramic-polymer composites and polymer films equalled 222 million of US dollars in 2000. Likely to grow at an AAGR of 8%, the market of piezoelectric ceramic is expected to reach in the US only $284 by 2005[8]. These numbers stress the diffusion and importance of these materials that are not longer confined to a narrow sector of the electronics industry. In fact, since the appearance of the Langevin's sonar, the number of devices based on piezoelectricity have expanded dramatically and piezoelectric materials are now part of everyday life. Some of these devices are listed in Figure 1.1, divided in 4 groups by the functions they are designated to serve. A newer, and rapidly growing application of piezoelectrics, is the integral incorporation of mechanical actuation and sensing microstructure into electronic chips (micro electromechanical systems (MEMS)) and the development of a new generation of non volatile memories (NVFRAM)[9].

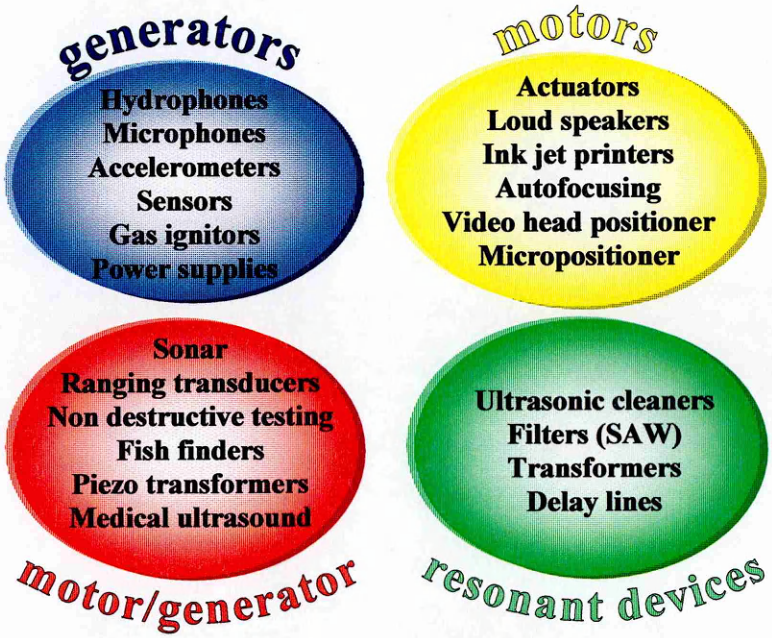

Figure 1.1: Applications of piezoelectric materials classified in base of their function

1.1.2. The environmental issue

- Lead zirconate titanate solid solutions (PZT) represent, from the time of their discovery in 1950, the most widely used ceramics for ferroelectric and piezoelectric applications. The high toxicity of lead oxide, however, is becoming a major concern all over the world as a consequence of a growing awareness on environmental issues. In addition, the volatilisation of PbO during sintering can change the stoichiometry of the ceramics affecting their performances obliging the manufacturer to carry out the high temperature processing in a Pb-rich atmosphere. For this reason the production of lead-based ceramics is not only a matter of public health but also a technological complication. Furthermore, the increasing interest in biocompatible materials to implant directly in living tissues, and in piezoelectrics operating at high temperature and pressure, has pushed the electronics industry to investigate lead-free materials to accomplish these new markets and possible new regulations. In a questionnaire about future R&D trends for piezoelectric and dielectric ceramics published in 1997, 61 Japanese technologists pointed out the necessity to find and develop non-lead containing piezoelectric ceramics for dielectric and piezoelectric applications[10].
  Although the environmental impact of lead released from electronic equipment may be extremely low, there has been (especially in the European Community) a progressive tightening of the legislation concerning lead-compounds. In two different directives (the Waste of Electric and Electronic Equipment (WEEE) and the limitation of hazardous substances in electrical and electronic equipment (ROHS)), ratified on the 7th of June 2001[11], the European Council stated that each state member must ensure that:

1. "Producers will pay for the collection, treatment, recovering and environmentally sound disposal of WEEE products from private house-hold" (WEEE);
2. By the 1st January 2007 at the latest, new electrical and electronic equipment put on market does not contain lead or other hazardous substances (ROHS).

The European approach was so aggressive both in terms of scopes and deadlines, to oblige the members of the World Semiconductor Council (representing the largest semiconductor makers in the European Union, Japan, U.S., Korea and Taiwan) to ask for the exemption of certain materials from the ban. PZT was exempted in consideration of the fact that no valid alternatives have yet been found to replace it[12].
It is clear that although there are no current regulations on eliminating PZT and related compounds, the electronic industry is very keen to discover and develop lead-free materials and processes, not only to be prepared for possible future legislations but also to find a breakthrough product for the market.

1.1.3. The effect

From a macroscopic point of view, piezoelectricity is the polarisation of a material due to the displacement of ions from their equilibrium positions by the action of an external stress. The piezoelectric effect is therefore strongly linked to the internal structure of the material: to show piezoelectric properties there must be a mismatch between the centre of the positive and negative charges, i.e. the crystal must be non-centrosymmetric. Of the 32 point groups in which all the crystals are classified, 21 classes are non-centrosymmetric and 20 of these are piezoelectric. For the class 432 the combination of symmetry elements excludes piezoelectric activity (Table 1.I). Out of the 20 piezoelectric classes, 10 are characterised by having a unique polar axis, i.e. an axis which shows different properties at the two ends[13]. Crystals belonging to these classes are called polar because they are spontaneously polarised. However, the spontaneous polarisation cannot be detected as charges on the surface, because these are compensated through external or internal conductivity.
Nevertheless, if the temperature of the crystal is altered, a change in the polarisation occurs and electric charges can be detected in the faces perpendicular to the polar axis. For this behaviour, these crystals are called pyroelectric. For some crystals belonging to these classes (called ferroelectrics), the direction of the spontaneous polarisation can be switched between two or more equivalent stable states by application of an electric field.

Centre simmetry	N° point groups	Crystal System											
		Cubic		Hexagonal		Tetragonal		Rhombohedral		Orthorhombic	Mono-clinic	Tri-clinic	
☑ (11)	11	m $\bar{3}$ m	m3	6/mmm	6/m	4/mmm	4/m	$\bar{3}$m	$\bar{3}$	mmm	2/m		$\bar{1}$
☐ (21)	11	432	23	622	$\bar{6}$	422	$\bar{4}$	32		222			
		$\bar{4}$3m		$\bar{6}$m2		$\bar{4}$2m							
	10			6mm	6	4mm	4	3m	3	2mm	2 m		1

Table 1-I: Crystalline classes classified considering the presence (☑) of absence (☐) of the centre of symmetry

The reversibility of the polarization can be strongly affected by temperature, pressure, electrical conductivity and crystal perfection so that the ferroelectric behaviour of a crystal (although theoretically predictable) can not be detected because of experimental limitations[14]. A summary of the relations between piezoelectricity, ferroelectricity and pyroelectricity is presented in Figure 1.2.

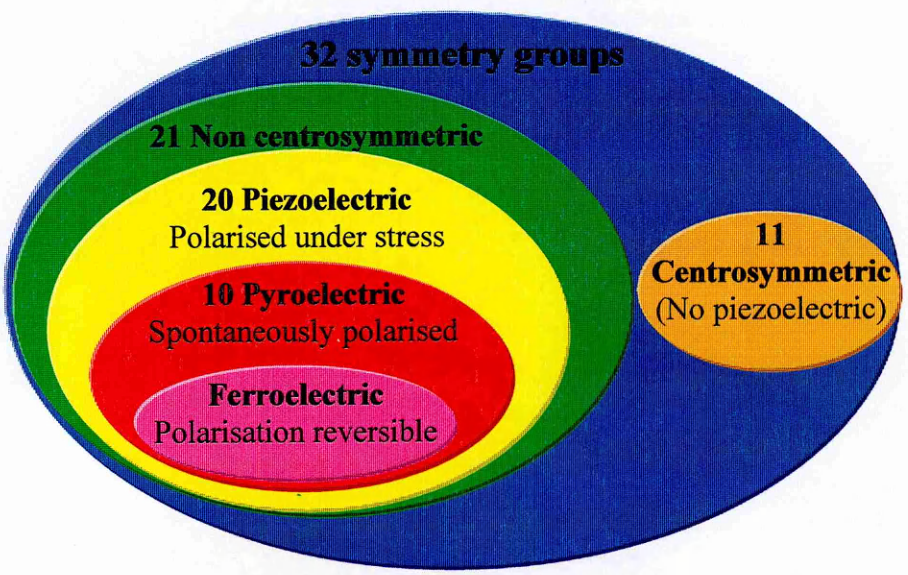

Figure 1.2: Relations between pyroelectric, ferroelectric and piezoelectric crystals

1.1.4. Ferroelectric crystals and ferroelectric domains

Ferroelectric crystals show spontaneous polarisation that decreases with increasing temperature to disappear at a specific temperature called the Curie temperature (T_C). The Curie point is characterised by a peak in the permittivity and disappearing of ferroelectric activity. This temperature therefore indicates the transition from a low temperature polar structure to a high symmetry, high temperature one (called paraelectric) in which no spontaneous dipole is present.

When the temperature is lowered below T_C without applying an electric field, the polarisation can develop in at least two directions. As a consequence, a depolarizing field E_o arises inside the crystal (Figure 1.3). To minimize the energy associated with E_o the crystal splits into regions called domains which are separated by interfaces called domains walls. The domains are therefore regions inside the crystals in which the polarisation is uniformly oriented along one of the directions allowed by symmetry. As an example of domain developing, we can consider the tetragonal phase of a perovskite crystal ABO_3. In this case, domains can have a polarization vector in one of the six {001} directions of the unit cell (Figure 1.4).

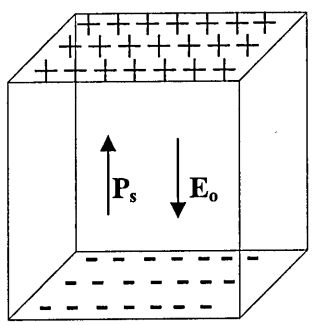

Figure 1.3: Surface charge associated with spontaneous polarisation. P_s= spontaneous polarisation, E_o= depolarizing field[15].

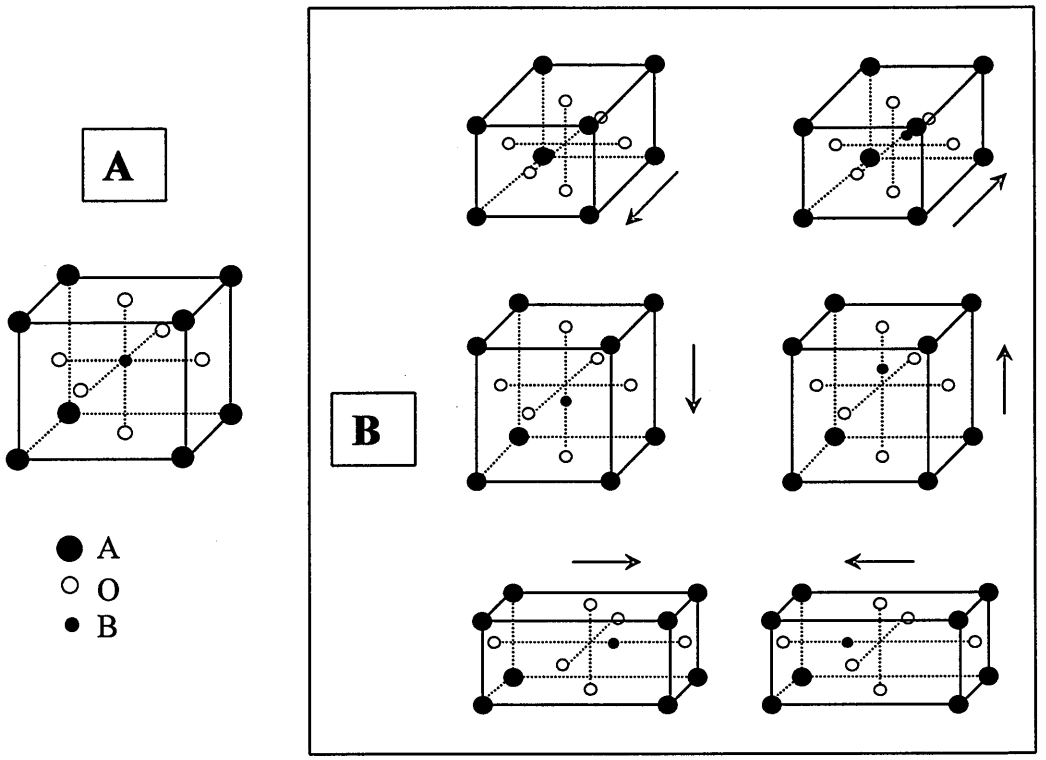

Figure 1.4: Representation of the possible distortion of the cell on cooling from the Curie temperature. A) Cubic cell in the paraelectric state; B) the six possible deformations that can lead to a tetragonal cell below the Curie temperature. The arrows indicate the direction of the cation displacement.

As a consequence, in tetragonal crystals, the domains wall can lie in the {100} or {110} planes forming what are called the 90° and 180° walls from the angles formed by the vectors of the two adjacent domains they divide (Figure 1.5).

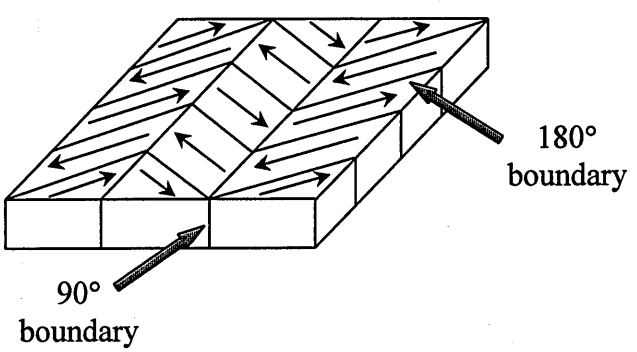

Figure 1.5: Example of domains pattern in a tetragonal material.

At room temperature, the domains compensate almost completely the polarisation in the crystal and as a consequence the latter shows almost no ferroelectric response at all. The polarity of the crystal can be easily restored exploiting the possibility of switching the polarisation, applying an external field. In these conditions the domains reorient themselves in the direction of the field leading to a "polarised" crystal. This process is called "poling". The presence of domains inside the materials is also responsible for the hysteretic behaviour of the polarisation when a variable field is applied (Figure 1.6).

By applying an electric field of increasing strength, an increasing number of domains will switch towards the direction of the field and the polarisation will increase rapidly. In these conditions the material has maximum domain allignment and the polarisation reaches the value of saturation (P_s). Decreasing the field to zero, some of the domains will remain aligned, producing a remanent polarisation (P_r). In order to eliminate this polarisation it is necessary to apply an electric field in the opposite direction: the value needed is called the coercive field (E_c). Further increase in the field causes the alignment of the dipoles in the opposite direction. The area within the loop is a measure of the energy required to reverse the polarisation twice.

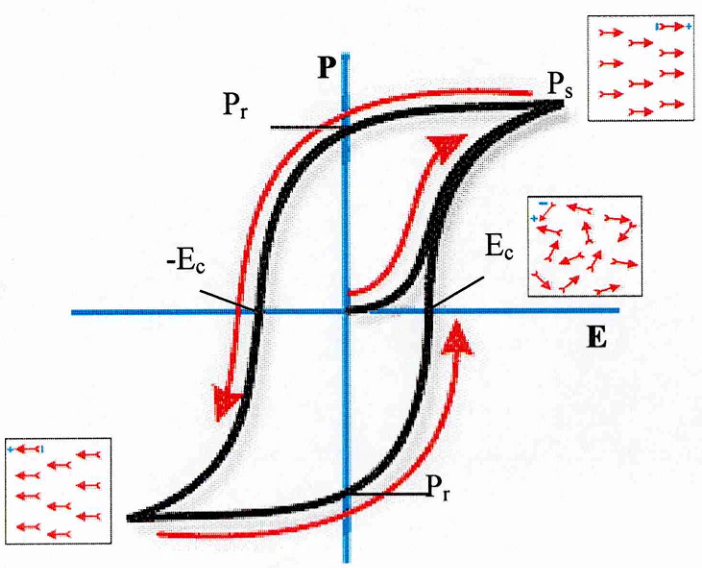

Figure 1.6: Hysteresis loop for a ferroelectric material. E_c=coercive field, P_s= saturation polarisation, P_r= remanent polarisation.

1.1.5. Equations of state

As stated above, the piezoelectric effect links mechanical and electrical properties. The equations of state can be expressed in terms of stress and strain (elastic variables) and field and displacement (electric variables) in the following way[3]:

$$D = dT + \varepsilon^T E \qquad \text{(Direct Effect)} \qquad \textbf{Equation 1.1}$$

$$S = s^E T + dE \qquad \text{(Converse effect)} \qquad \textbf{Equation 1.2}$$

In which D is the electric displacement, T the stress, E the electric field, S the strain, d the piezoelectric tensor, s the material compliance and ε the permittivity. The superscripts indicate a quantity held constant: constant stress means that the material is unconstrained, and electric field constant that the electrodes in the sample are short-circuited. From thermodynamic considerations, it can be proved that the piezoelectric coefficients of the direct and converse effects are equal. The previous equations are tensorial. The strain and the stress are second-rank tensors, the elastic compliance that expresses the relationship between them, is then a fourth-rank tensor. In the same way the permittivity, which links E and D, is a second rank tensor and the piezoelectric coefficient d, linking polarization and stress, is a third rank tensor. The tensorial nature of the equations becomes easy to see using the appropriate subscripts as in Equations 1.3 and 1.4.

$$D_j = d_{ijk}T_{jk} + \varepsilon^T{}_{ij}E_j \qquad \text{(Direct Effect)} \qquad \textbf{Equation 1.3}$$

$$S_{ij} = s^E{}_{ijkl}T_{kl} + d_{kij}E_k \qquad \text{(Converse effect)} \qquad \textbf{Equation 1.4}$$

If all the components of these tensors were independent, 117 coefficients would be necessary to completely describe the piezoelectric effect. The symmetry of s^E, ε^T and d, however, reduces the number to 45 independent tensor components: 21 for the elastic compliance, 6 for the relative permittivity and 18 for the piezoelectric coefficient. The crystal symmetry and the right choice of reference axes can reduce these numbers even further simplifying the problem as will be shown for ceramics in the following chapter.

1.2. PIEZOELECTRIC CERAMICS

The meaning of the word "ceramic" has changed in time according to the evolution of new technologies and materials. It was born to define products essentially based on silicates like pottery, and was extended to indicate oxides (MgO, Al_2O_3, ZrO_2 etc.) nitrides, borides and other inorganic materials. However, a definition based only on compositional considerations has become inadequate to describe a ceramic material especially after the discovery of borderline materials like cermets, glass-ceramics and ceramic-polymer composites. Bearing in mind that in a ceramic there are only ionic and covalent bonds, a possible definition could be: a polycrystalline inorganic material with a long-range order and essentially non metallic, that can exhibit electrical, magnetical or mechanical properties due to its structure and chemical composition.

1.2.1. Piezoelectricity and Ceramics

A ceramic can be roughly considered an agglomeration of small crystals, fitted together in a random way. As it is cooled from the high temperature paraelectric state to the ferroelectric state, the unit cell deforms usually with lengthening in the direction of the polar axis. Intergranular stresses are minimised by the formation of domains regions within each grain, which have common orientation of the spontaneous dipole, as already seen for single crystals. A ceramic of an ordinary piezoelectric or pyroelectric material is non piezoelectric, even though the individual crystals may be strongly piezoelectric, because the effects from the individual crystals cancel each other. This is initially true also for a ceramic specimen of a ferroelectric material. To make the ceramic piezoelectric, an electric field must be applied to switch the polar axes of the ferroelectric crystallites to those directions allowed by symmetry which are nearest to that of the electric field. After the poling, the ceramic has a net dipole moment, and will respond to an applied electric field or mechanical pressure similar to a single crystal as long as the field or pressure is well below that needed to switch the polar axis. As a result of the poling process much of the domain structure of the ceramic is eliminated. To pole a ceramic is more complicated than to

pole a single crystal. The process involves the alignment of the polarisation of each single grain. Since the original crystallographic directions of the grains in the ceramic were randomly oriented, the line-up of polar axes after the poling process cannot be as perfect as in a single crystal of the same material, but it will be the best possible in those conditions. In polycrystalline materials, in fact, the switching of the dipole moments is hindered by the elastic strain inside its body. On cooling from the paraelectric phase, large mechanical stress can be generated inside the ceramic body by the anisotropic strain caused by the deformation of the cells. This stress can affect the domain dynamics, clamping them and preventing in this way their switching in an electric field. The switching of domains by 180° do not change the strain of the grain but in the case of 90° switching, the difference in the **a** and **c** parameter of the cell obliges the latter to change its dimensions in respect to the crystallographic environment. This kind of "rotation of 90°" of the unit cell is not always possible due to the presence of the other grains and of the strain inside the material. The 90° domains are therefore more difficult to reorient than the 180° ones. Even if the field applied is high enough to reorient these domains, when it is removed they reverse back to their initial states immediately or after a certain time, in the phenomenon known as aging. The process of poling of a single crystal is represented in Figure 1.7.

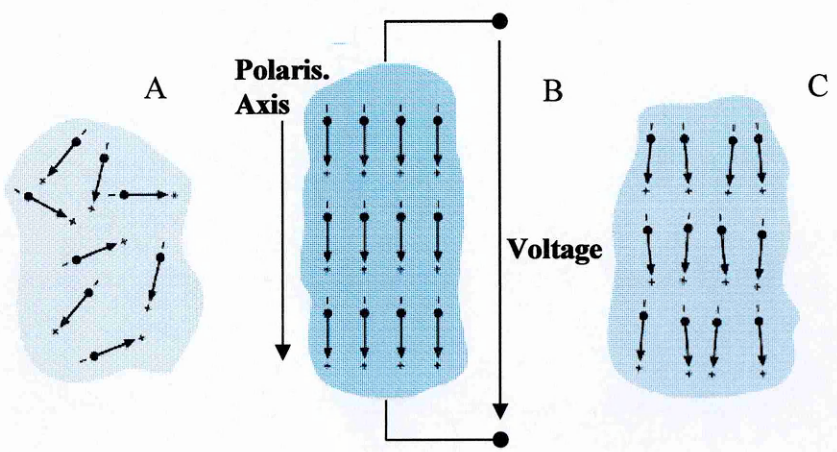

Figure 1.7: Schematic of the poling process. A) material before poling; B) During the application of the voltage the dipoles in the materials align with the direction of the field developing a polarisation; C) After poling, the dipoles rearrange themselves in the best condition considering the geometry of the system.

The fraction of the single crystal polarization value that can be obtained in ceramics has been calculated for the perovskites, the best known piezoelectric ceramics. The crystallites of these materials can have mainly three kind of structure: tetragonal, rhombohedric or orthorhombic. Depending on the nature of the constituent crystallites the fraction of alignment will then be 83% (tetragonal), 87% (rhombohedric) and 91% (orthorhombic)[15]. It is important to point out that these values refer to simple not-tilted perovskite like $BaTiO_3$.

Despite several types of symmetry of the constituent crystals, a piezoelectric ceramic shows only one kind of symmetry. Initially, the random disposition of its crystallites leads to an isotropic body. The poling process destroys this isotropy introducing a preferential orientation in the direction of the field: the symmetry of a poled ceramic can be described as cylindrical polar (∞m). The equations expressing the piezoelectric effect can then be simplified taking into account this symmetry and then be expanded as shown in Equations 1.5-1.7 for the direct effect and Equation 1.8-1.12 for the converse one[15].

$$D_1 = d_{15}T_5 + \varepsilon^T{}_1E_1 \qquad \textbf{Equation 1.5}$$

$$D_2 = d_{15}T_4 + \varepsilon^T{}_1E_2 \qquad \textbf{Equation 1.6}$$

$$D_3 = d_{31}(T_1+T_2) + d_{33}T_3 + \varepsilon^T{}_3E_3 \qquad \textbf{Equation 1.7}$$

$$S_1 = s^E{}_{11}T_1 + s^E{}_{12}T_2 + s^E{}_{13}T_3 + d_{31}E_3 \qquad \textbf{Equation 1.8}$$

$$S_2 = s^E{}_{11}T_2 + s^E{}_{12}T_1 + s^E{}_{13}T_3 + d_{31}E_3 \qquad \textbf{Equation 1.9}$$

$$S_3 = s^E{}_{13}(T_1+T_2) + s^E{}_{33}T_3 + d_{33}E_3 \qquad \textbf{Equation 1.10}$$

$$S_4 = s^E{}_{44}T_4 + d_{15}E_2 \qquad \textbf{Equation 1.11}$$

$$S_6 = 2(s^E{}_{11}-s^E{}_{12})T_6 \qquad \textbf{Equation 1.12}$$

It is worth remembering that in these equations it is considered that d and s are symmetrical tensors to use a more concise notation (suffix notation) that allowed to use only two suffix instead of the three generally used for a third rank tensor[16]. These coefficients are summarised in a more compact form in Table 1.II. Observing this table it is clear the massive simplification obtained using symmetry considerations.

s_{11}	s_{12}	s_{12}	0	0	0			
s_{12}	s_{11}	s_{13}	0	0	0	**∞ m**		
s_{13}	s_{13}	s_{33}	0	0	0	**(Cylindrical Symmetry = 6mm)**		
0	0	0	s_{44}	0	0			
0	0	0	0	s_{44}	0			
0	0	0	0	0	$2(s_{11}-s_{12})$			
0	0	0	0	d_{15}	0	$\varepsilon_1/\varepsilon_0$	0	0
0	0	0	d_{15}	0	0	0	$\varepsilon_1/\varepsilon_0$	0
d_{31}	d_{31}	d_{33}	0	0	0	0	0	$\varepsilon_3/\varepsilon_0$

Table 1-II: Matrix representation of the piezoelectric, dielectric and compliance for a piezoelectric ceramic.

The conventional labelling for reference axes and planes for piezoceramics, necessary for defining the previous coefficients, is shown in Figure 1.8. The poling direction is generally indicated as direction 3.

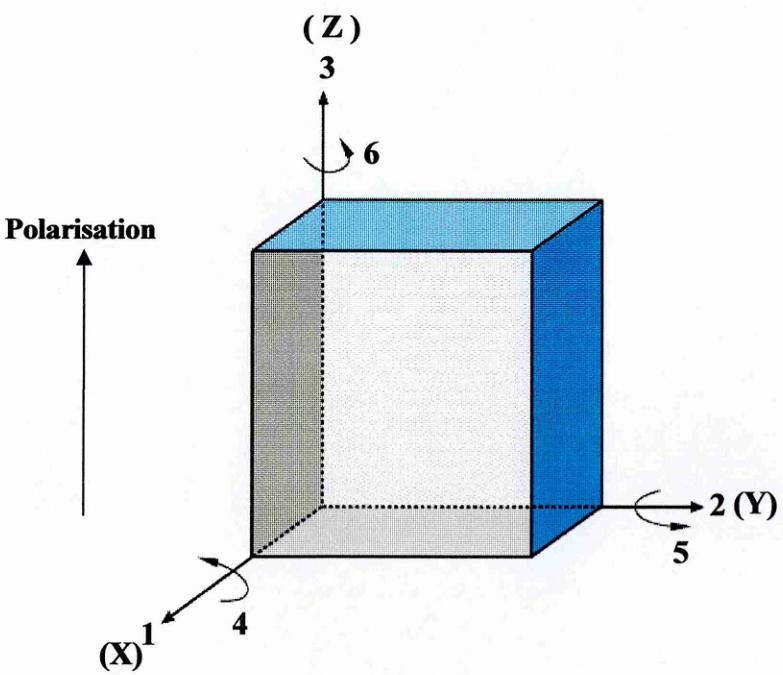

Figure 1.8: Definition of the directions for the piezoelectric coefficients. The direction of poling is generally indicated with 3.

In defining the piezoelectric coefficient d_{ij}, the first subscript describes the direction of the field (or the dielectric displacement) while the second indicates the component of strain or stress. In this way d_{31} relates the field along the polar axis to the strain perpendicular to it, while d_{33} is the coefficient of piezoelectricity when the field and the strain are parallel to the polar axis.

An important parameter to characterise a piezoelectric material is its electromechanical coupling factor (k). It is a measure of the efficiency of the electromechanical effect, i.e. of the conversion between the two forms of energy involved and it is espressed by the Equation 1.5.

$$k = \frac{U_{12}}{\sqrt{U_1 U_2}} \qquad \textbf{Equation 1.13}$$

where U_{12}, U_1 and U_2 are the piezoelectric, mechanical and electrical energy densities. It is important to have a high k for an efficient energy conversion, but the previous definition of k does not take into account the dielectric or mechanical losses nor the recovery of unconstrained energy. Hence it is not an exact indication of the effective energy conversion. The efficiency of the process is then better expressed by the ratio of converted, useable energy delivered by the piezoelectric sample to the total energy taken up by it. This ratio is commonly named "effective coupling coefficient, k_{eff}" and it is expressed by the following equations.

$$k^2_{eff} = \frac{\text{input electrical energy converted into mechanical}}{\text{Input electrical energy}}$$

$$k^2_{eff} = \frac{\text{input mechanical energy converted into electrical}}{\text{Input mechanical energy}}$$

The strain caused by the application of an electrical field or a mechanical stress has components in the three orthogonal directions, so the energy transfer from one form to the other occurs in a very complex 3-dimensional way. As a consequence, shape and dimensions of a ceramic element lead to unique expressions of k_{eff}. The

electromechanical coupling coefficient is written with two subscripts that indicate respectively, the direction along which the electrodes are applied and along which the mechanical energy is applied or developed. For example k_{31} links the electric field in the direction parallel to the one of poling (3) with the direction perpendicular to it (1). Special mention should be given to the planar coupling factor (k_p) and the thickness coupling factor (k_t). These two parameters are characteristic of ceramic samples shaped in the form of disc with electrodes on the major surfaces and thickness small compared to them. k_p expresses the coupling between an electric field applied along 3 (the poling direction) and the radial vibrations (directions 1 and 2) (Figure 1.9A). The thickness coupling coefficient k_t on the other hand links an electric field along 3 with mechanical vibrations in the same direction (Figure 1.9B).

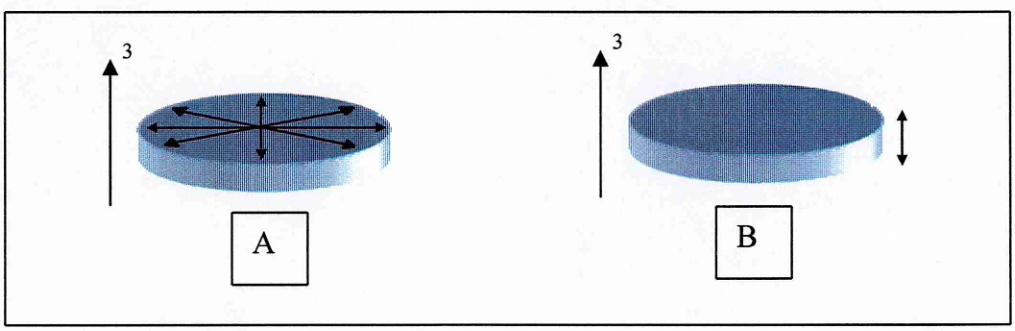

Figure 1.9: Representation of the radial vibrations (A) and thickness vibrations (B).

The main categories of ferroelectric materials are represented in Figure 1.10, classified on the basis of the structure of the unit cell. For each class a prototype member is also indicated.

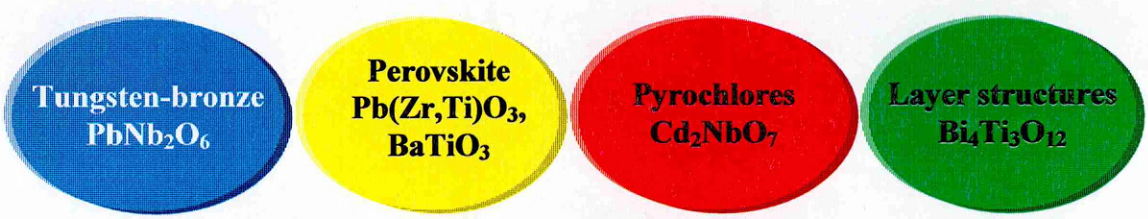

Figure 1.10: Principal families of piezoelectric materials classified in base of their crystalline structure. For each family a representative compound is also indicated.

Of all these classes, the perovskite one represents by far the most important category for piezoelectric applications. The layer structures are gaining increasing importance for memory applications, although the piezoelectric coefficient is not as high as that of the perovskite materials.

A summary of the piezoelectric coefficient d_{33} for a typical compound of each class is presented in Table 1-III. In the table is also indicated the Curie temperature (T_C), which gives an indication of the maximum temperature of use of the material (see next paragraph).

Compound	d_{33} (pC/N)	T_C (°C)
PZTA	268	315
$PbNb_2O_6$	73	570
$CdNb_2O_7$	5	-88
$BaTiO_3$	190	130
$Bi_4Ti_3O_{12}$	20	675

Table 1-III: Piezoelectric coefficient and Curie temperature of some piezoelectric materials. PZTA is a commercial composition of PZT[15].

1.2.2. Perovskite and PZT

Although barium titanate was the first piezoceramic to be commercially developed, the solid solutions between $PbTiO_3$ and $PbZrO_3$ (generally indicated as PZT) show the highest value of piezoelectric coefficients and represent the most used piezoelectric ceramics.

The name "perovskite" is given to those materials whose structures are similar to the one of the mineral Perovskite: $CaTiO_3$. The unit cell of this structure, generally indicated with ABO_3, consists of a corner-linked network of oxygen octahedra with the B cations in the middle of the octahedral cages and the A-cations situated in the interstices created by them. In the case of PZT the A sites are occupied by lead, whereas in the B sites there are Zr or Ti (Figure 1.11A).

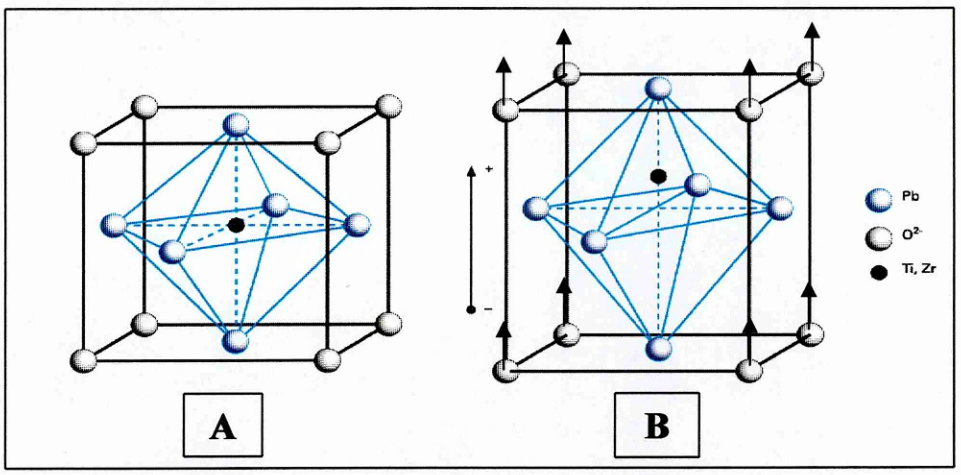

Figure 1.11: Representation of the perovskite structure of PZT. A) Structure above T_c; B) ferroelectric phase (in this case tetragonal) below T_c.

The great polarizability, and consequently the piezoelectricity, of this material is due mainly to the $(Ti/Zr)O_6$ octahedra that influence the electric behaviour of the entire cell. The small ionic radius of Ti^{4+} and Zr^{4+} (0.605 and 0.72Å respectively)[17] compared with the one of oxygen (1.40Å) allows easy movements of the B cations inside the octahedra, leading in such a way, to the formation of an internal dipole. The B ion is generally a transition metal with a closed shell (s^2p^6). The high electronic polarizability of the whole oxygen octahedron is due to a large number of possible hybridized orbitals with energy sufficiently closed and composed of the d, p and s orbitals of the B-cation. In particular, as the energy level of the d-orbitals of the B-cation gets closer to the one of the 2p orbitals of oxygen, the intensity of the covalent bond becomes larger with a consequent enhancing of the ferroelectric behaviour[18]. In addition, ions of the electronic structure [Xe] $6s^2$ (like Pb^{2+}) have the tendency to form asymmetrical partially covalent bonds. Their high electronic polarizability is due to the unshared pair of $6s^2$ electrons which is stereochemically active. When ions of this nature are introduced into the A-site of the perovskite lattice, they favour a distortion of the structure from cubic to the symmetry that stabilises a ferroelectric or antiferroelectric state.

The cubic cell of Figure 1.11A is stable only above the Curie temperature; below it the structure changes either to a tetragonal, monoclinic, orthorhombic or rhombohedral form depending on the composition of the system. In Figure 1.11B the unit cell below the Curie temperature is shown. The phase diagram of this system can be seen in Figure 1.12. From the figure it is clear that the border between the two

possible phases is almost independent of the temperature. In this region, called the morphotropic phase boundary (MPB), the piezoelectric coefficient and dielectric constant achieve their highest values, due to the simultaneous presence of multiple possible phases. In this situation the material presents more possible orientation for the domains and hence a more effective alignment along the applied field is possible during the poling process. It has been recently discovered, that a monoclinic phase may bridge the rhombohedral and tetragonal phases at the morphotropic phase boundary[19]. Glazer[20] pointed out the possibility that this monoclinic phase represents a key point to understand the real nature of the phase transitions in PZT and some of its unexplained anomalies. He showed that, if we consider the compounds at microscopic level (that is in terms of unit cell) and we focused on the role of lead, it is possible to describe all the systems of solid solutions as if it was always monoclinic at microscopic level but with a different long-range order: monoclinic-rhombohedral long range order in the side of $PbZrO_3$, monoclinic-monoclinic long-range order at the previously called MPB and monoclinic-tetragonal long range order at high concentration of $PbTiO_3$. The usual phase diagram for PZT could then be the consequence of the macroscopic scale generally involved when studying the system with techniques like XRD or electron and neutron diffraction. These techniques would be able to detect only the long range order present in the materials as a consequence of twinning effects.

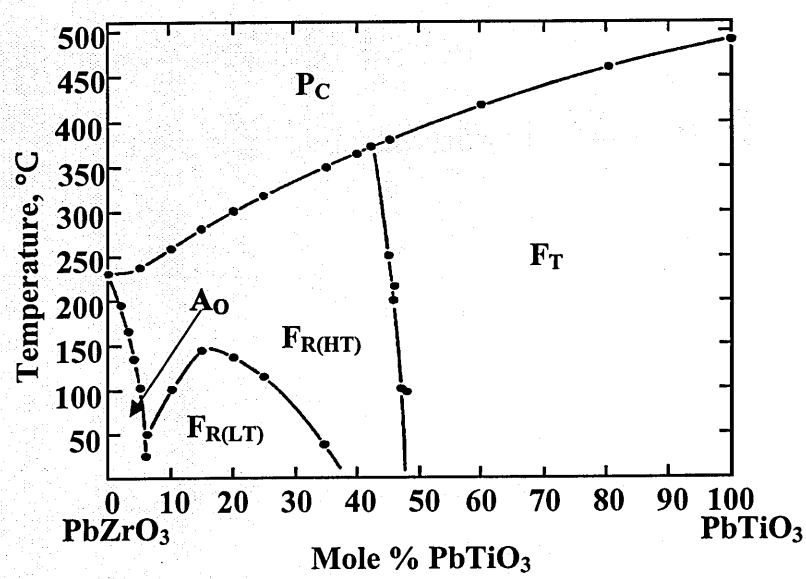

Figure 1.12: Phase Diagram of PZT, indicating the high temperature paralelectric cubic phase (P_C) ; the low temperature ferroelectric rombohedral ($F_{R(LT)}$) and tetragonal phases (F_T), and the high temperature ferroelectric rhombohedral one ($F_{R(HT)}$)[15].

1.3. LEAD-FREE PIEZOELECTRIC CERAMICS

Increased awareness of public health issues has pushed the research toward more environmental friendly materials. Unfortunately, the properties of the piezoelectric ceramics present at the moment in the market are not comparable to the ones of the lead-based compounds. Apart from a lower piezo-response, these non-Pb piezoelectric materials present several drawbacks such as for example, narrow temperature range of stability ($BaTiO_3$) and difficult processing (alkaline niobates). The most promising compounds are the ones of bismuth. Two of them have been chosen in this project to assess their potential for development of new lead-free materials and are examined in detail in the next chapter.

Here a summary of the other two major classes of lead-free ceramics is presented to provide a more complete view of the systems available at the present.

1.3.1. Barium Titanate ($BaTiO_3$)

Barium titanate was the first piezoceramic to find commercial application in 1947[21] and it is still used in some piezoelectric applications, although it has been generally superseded by PZT.

$BaTiO_3$ is characterized by several phase transitions (Figure 1.13) all accompanied by changes in the electrical and mechanical properties that compromise the stability of the material for a wide range of temperature. This characteristic and the low Curie temperature (130 °C) have limited the uses of this material to the applications (like sonar) in which it is possible to take advantage of its relatively high coupling coefficient [15] while accepting a narrow temperature range of operation.

The properties of $BaTiO_3$ have been deeply analysed from the time of its discovery and several types of doping have been developed to enhance its properties, in particular to move the phase transition away from the working temperature and to reduce the dielectric loss at high frequency[15].

Barium titanate is probably the best studied piezoelectric material.

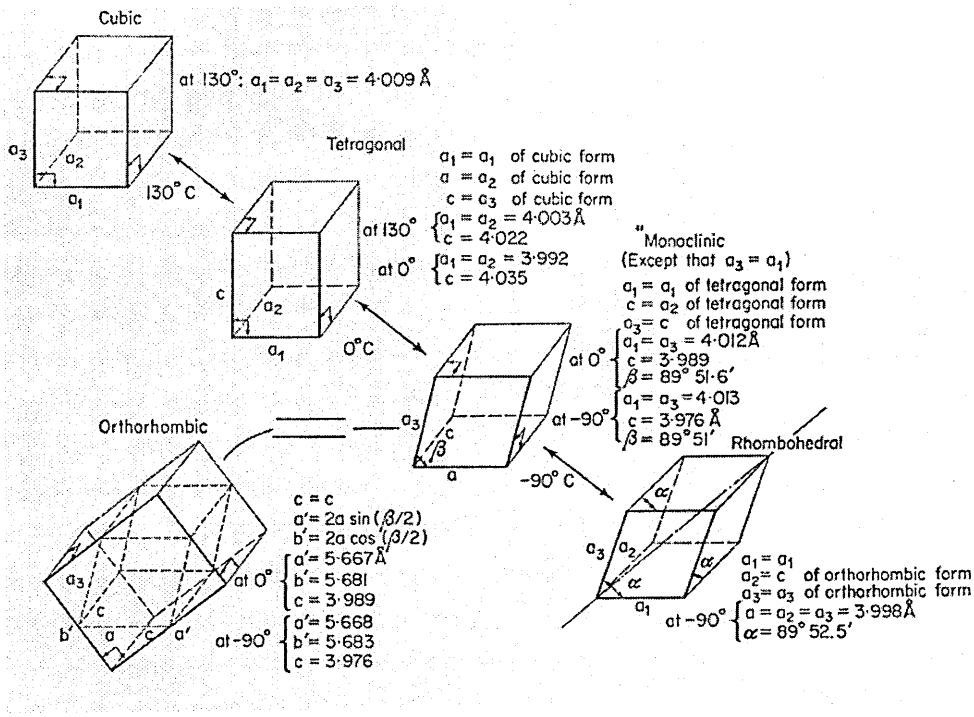

Figure 1.13: Evolution of the phases with temperature for barium titanate[3].

1.3.2. $\underline{(K,Na)NbO_3}$

Although potassium niobate ceramics exhibit low piezoelectric coefficients, it has been shown that when coupled with $NaNbO_3$, it gives rise to a solid solution where values of d_{33} can easily reach 80pC/N[22].

The low dielectric constant and high electromechanical coupling coefficients make these ceramics suitable for accelerometers or sensors operating at temperature up to 400°C[23,24] (the Curie temperature of $Na_{0.5}K_{0.5}NbO_3$ is 420°C[22]). In addition they do not contain any harmful components and could therefore be employed in biomedical applications.

Unfortunately, up to now, only hot-pressing has been able to give ceramics with a reasonable density[25]. Furthermore, slight changes in stoichiometry (due to alkaline oxides volatilization) can cause formations of extra phases. Some of these are highly hygroscopic and lead to ceramic disintegration on exposure to air.

1.4. BISMUTH-BASED LEAD-FREE CERAMICS

Among the known piezoelectric materials without lead, great importance has been placed on the ones based on bismuth. Since the electron shell of Bi^{3+} is similar to the one of Pb^{2+}, it can be expected to exhibit similar properties.
Bismuth compounds crystallize mainly in two structures:

- ✓ Perovskite
- ✓ Layer structure (known as Aurivillius compounds)

In the following paragraphs, these structures will be discussed with particular attention to the two compounds $Na_{0.5}Bi_{0.5}TiO_3$ (for the perovskite family) and $Bi_4Ti_3O_{12}$ (for the Aurivillius compounds) that represent the key materials in this study.

1.4.1. Perovskites: $Na_{1/2}Bi_{1/2}TiO_3$

The most important among the bismuth containing ferroelectric perovskites is $(Na_{1/2}Bi_{1/2})TiO_3$ (NBT), where sodium and bismuth share the A-site of the perovskite structure and titanium is in the B-site[26,27]. The A-site substituted perovskites are quite rare if compared with the analogue B-site substituted compounds. Apart from NBT only $Ag_{0.5}Bi_{0.5}TiO_3$, $K_{0.5}Bi_{0.5}TiO_3$, $Ag_{0.5}Nd_{0.5}TiO_3$ and $La_{0.5}Sr_{0.5}MnO_3$[28] are known. NBT presents a series of very interesting electrical and structural properties linked to this substitution. In particular its structure is so peculiar that, despite its discovery in 1960 by Smolenskii[26], only very recently has its phase evolution with temperature been clearly identified[29]. The peculiarity of this compound is stressed by the evolution of its phases on cooling: from cubic paraelectric ($Pm\bar{3}m$) to tetragonal (P4bm) at 540° and from tetragonal to rhombohedral (R3c) at 255°C, with regions of coexistence of phase between 500 and 540° (cubic and tetragonal) and 300-320° (rhombohedral and tetragonal). In addition an abrupt change in the dielectric properties has been noticed at 200°C. The nature of this transition has not been yet

clearly understood[30]. Some authors[31,32] attributed this change in properties to a ferroelectric → ferroelastic transition whereas Pronin et al. considered a ferroelectric-antiferroelectric transition[33]. More recently Roleder et al.[34] showed that the piezoelectric properties of NBT measured at room temperature, although changing above 200°C, do not disappear contradicting in this way the hypothesis of Pronin. In Figure 1.14 a schematic representation of the phase evolution of NBT with temperature is given.

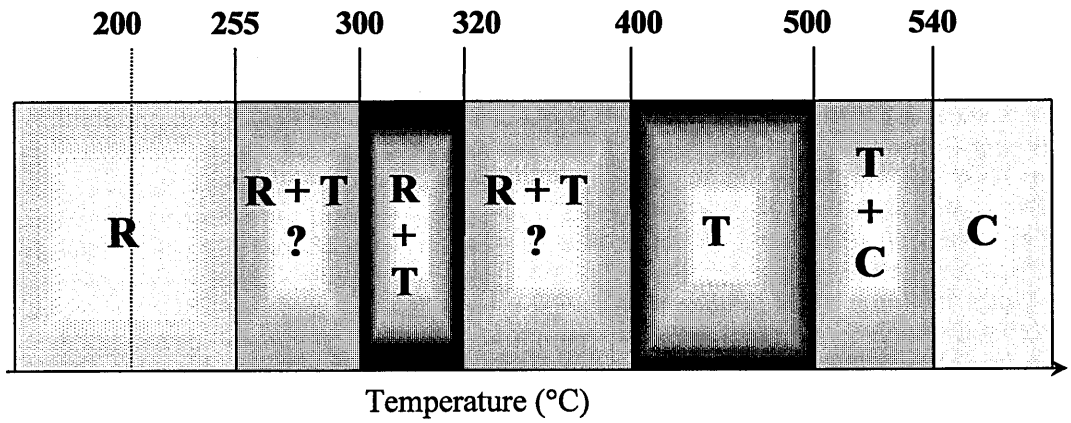

Figure 1.14: Phase evolution of NBT with temperature. R=Rhombohedral, T= Tetragonal, C= Cubic. The question mark indicates regions of uncertainty of the phase diagram. The dotted line at 200°C represents the probable ferroelectric-antiferroelectric transition.

It has also been proved that the diffuse phase transition in NBT (Figure 1.15), that for this reason is often considered a relaxor[35,36], is due to the presence of polar regions in the range of coexistence of tetragonal and rhombohedric phase. These polar regions become stable at T < 280°C constituting the nuclei of the low temperature ferroelectric phase[37,38].

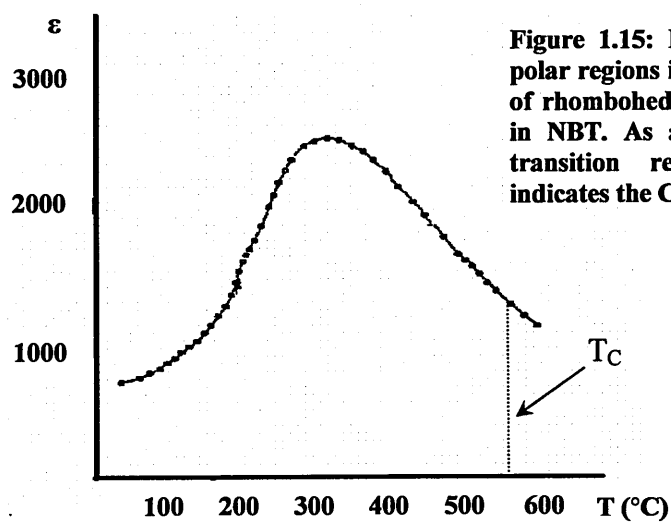

Figure 1.15: Effect of the presence of polar regions in the range of coexistence of rhombohedral and tetragonal phases in NBT. As a consequence the phase transition results very broad. T_C indicates the Curie temperature.

Discovered in 1960 by Smolenskii et al.[26],NBT is considered to be a key component for the realisation of lead-free piezoelectric ceramics[39], because it is strongly ferroelectric with a Curie temperature of 320°C and a residual polarisation of 38 $\mu C/cm^2$ [40]. Nevertheless, it is characterised by a high value of coercive field (73 kV/m), due to the high conductivity, which hinders the poling process and the development of good piezoelectric properties[41].

To improve the properties of the system it is possible to substitute the sodium or bismuth by rare earth elements (Nd^{3+}, La^{3+} and Sm^{3+}) or $Nb^{5+}$for Ti^{4+} in the B-site. In doing so, the value of d_{33} reaches 100 pC/N (for NBT d_{33}= 70 pC/N[42]). Doping the system with lanthanum increases the value to 92 pC/N[43].

The strong ferroelectric behaviour of the solid solutions based on NBT is mainly due to the role of bismuth ion in the perovskite A-site. For this reason it has proved useful to couple the system with other bismuth compounds to have a constant amount of active ions. Solid solutions of the type $Na_{0.5}Bi_{0.5}TiO_3 - Bi^{3+}Me^{3+}O_3$ (Me= Sc, Fe, Mn, Cr and Co) have been produced: the d_{33} in this case increases up to 75 pC/N[44,45].

Another way to improve the piezoelectric properties of the sodium bismuth titanate is to exploit its structure (rhombohedral at room temperature) to form solid solutions with perovskite compounds of tetragonal structure in the attempt to form a MPB tetragonal-rhombohedric resembling the one present in PZT. For this reason NBT has been coupled with the following systems (all tetragonal at room temperature)[46,47,48,49,50]:

$K_{0.5}Bi_{0.5}TiO_3$[51]

$BaTiO_3$

$SrTiO_3$

$CaTiO_3$

$NaNbO_3$[52]

$KNbO_3$

Among these, the best properties are exhibited by the solid solution NBT-$BaTiO_3$, with a d_{33} at the MPB of 125 pC/N[41] which is the highest value ever found in a lead-

free ceramic. This system presents a MPB similar to the one of PZT as well as an antiferroelectric state below the Curie temperature (≈ 250 °C) (Figure 1.16).

Further enhancement of the piezoelectric properties is achieved by adding to the composition at the morphotropic phase boundary $(Bi_{1/2}Na_{1/2})_{0.94}Ba_{0.06}TiO_3$, CeO_2 (d_{33} = 152 pC/N)[53] or at $(Bi_{1/2}Na_{1/2})_{0.92}Ba_{0.08}TiO_3$, Nb_2O_5 (d_{33}= 149 pC/N)[54]. Combinations of the previous compounds have also been investigated: the system obtained by the coupling of NBT- $BaTiO_3$ and $NaNbO_3$ leads to d_{33}=110 pC/N and k_t= 0.51[55].

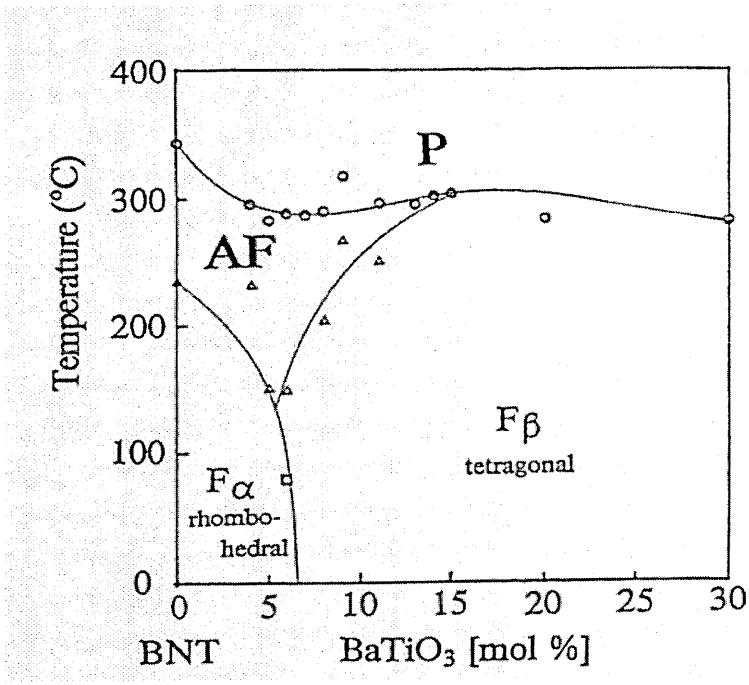

Figure 1.16: Phase Diagram of the sodium bismuth titanate-barium titanate system, for high concentration of NBT. It is clear the presence of an MPB similar to the one of the PZT system[41].

1.4.2. Aurivillius Compounds

1.4.2.1. Crystal Structure

Discovered by Bengt Aurivillius in 1949[56] these mixed oxide layered compounds have the general formula

$$(Bi_2O_2)^{2+}(A_{m-1}B_mO_{3m+1})^{2-}$$

where A can be mono-,di- or trivalent ions or a mixture of them, B is a transition element (Fe^{III}, Ti^{IV}, Nb^{V}, Ta^{V}, W^{VI} for example), and m represents the number of perovskite units sandwiched between $(Bi_2O_2)^{2+}$ layers and can have a value from 1 to 8 [57,58,59,60]. The structure presents a stack of m perovskite-like units, of nominal composition $MeRO_3$, between fluorite-like layers of bismuth oxide along the c-axis. This layer structure induces a platelike morphology with the $(Bi_2O_2)^{2+}$ layers parallel to the plane of the platelets. In the paraelectric form these compounds are tetragonal or more frequently pseudo-tetragonal (slightly orthorhombic distortion $b_o/a_o \approx 1.007$[61]). The structure is represented in Figure 1.17 for the compounds with m = 2,3,4.

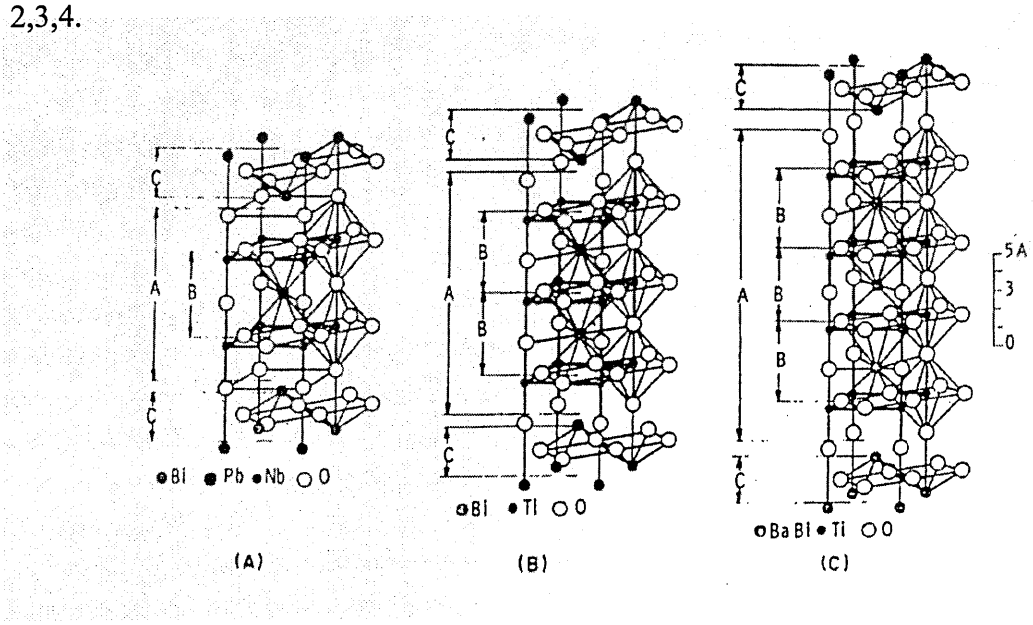

Figure 1.17: Representation of the paraelectric crystal structure of Aurivillius compounds. A) m=2, B) m=3 and C) m=4. In each figure A represents the perovskite part of the cell composed by different number of perovskite blocks (B), whereas C indicates the bismuthyl layers[61].

The $(Bi_2O_2)^{2+}$ layers can be seen as a planar square net layer of oxygens with Bi in positions above and below the net, forming square pyramids of BiO_4; the stereoactive lone pair of Bi^{3+} is pointing along the c-direction away from the layer of oxygen atoms. The non-bonding interaction between this lone pair and the neighbouring oxygen anions prevents the bismuthyl layer from moving closer to the top of the perovskite layer. In this type of structure the bismuth cations can occupy two sites that are in different bonding environments:

a) In the $(Bi_2O_2)^{2+}$ layer, it is bonded rather anisotropically
b) In the perovskite block, it is in a cuboctahedral isotropic environment

These two situations lead to a different behaviour of the bismuth towards substitution[62]: in contrast to the perovskite subunits, which exhibit a great variability in the metal cation substitution, the bismuth oxide layers are considered essentially invulnerable to it. The latter behaviour seems to be due to the stereochemical influence of the lone pair of Bi^{3+} in stabilising the $(Bi_2O_2)^{2+}$ sheets. The potential candidates for this substitution are then limited to Pb^{2+}, Sb^{3+}, Te^{4+} and La^{3+} that form similar pyramidal layers. On the other hand, the B-site of the perovskite block is somehow less flexible than that usually found in "conventional" perovskites. Ti^{4+} can be replace by 3,4,5 and 6 cations but only if their size lies in the range 0.62Å (Mo^{6+}) – 0.69 Å (Nb^{5+}). Larger cations like Zr^{4+}, Sn^{4+} and Hf^{4+} are not tolerated[63]. The c parameter of the paraelectric unit cell depends on the number of perovskite units increasing with m[64] (Figure 1.18).

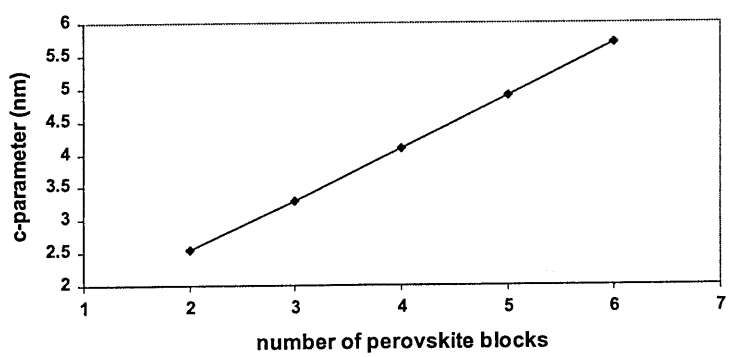

Figure 1.18: Trend of the c-parameter of the paraelectric cubic cell with the number of perovskite blocks. The two parameters are strongly correlated.

The continuous extension of the R-O-R chains along the c-axis is interrupted not only by the presence of bismuth oxide layers but also by the translation of the perovskite units in the plane perpendicular to the c-axis (Figure 1.19)[65].

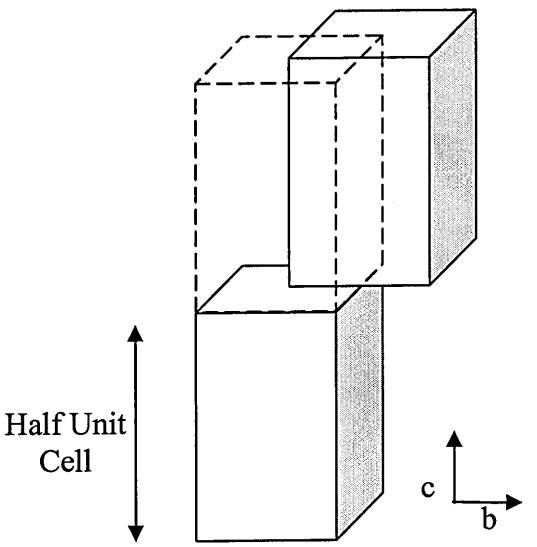

Figure 1.19: Translation of the unit cell of the Aurivillius compounds in the a-b plane.

A useful way to visualise the structures of these compounds, and in particular the number of perovskite blocks involved, is illustrated for some Aurivillius compounds in the following[66]:

m = 1	Bi_2WO_6	$\rightarrow (Bi_2O_3) \cdot 1(\square WO_3)$
m = 2	$BiTiNbO_9$	$\rightarrow (Bi_2O_3) \cdot 2(Bi_{1/2}\square_{1/2}Ti_{1/2}Nb_{1/2}WO_3)$
m = 3	$Bi_4Ti_3O_{12}$	$\rightarrow (Bi_2O_3) \cdot 3(Bi_{2/3}\square_{1/3}TiO_3)$
m = 4	$BaBi_4Ti_4O_{15}$	$\rightarrow (Bi_2O_3) \cdot 4(Ba_{1/4}Bi_{2/4}\square_{1/4}TiO_3)$
m = 5	$Ba_2Bi_4Ti_5O_{18}$	$\rightarrow (Bi_2O_3) \cdot 5(Ba_{2/5}Bi_{2/5}\square_{1/5}TiO_3)$
m = 6	$Pb_3Bi_4Ti_6O_{21}$	$\rightarrow (Bi_2O_3) \cdot 6(Ba_{3/6}Bi_{2/6}\square_{1/6}TiO_3)$
m = 7	$Pb_4Bi_4Ti_7O_{24}$	$\rightarrow (Bi_2O_3) \cdot 7(Pb_{4/7}Bi_{2/7}\square_{1/7}TiO_3)$
m = 8	$Bi_9Ti_3Fe_5O_{27}$	$\rightarrow (Bi_2O_3) \cdot 8(\square_{1/8}Bi_{7/8}Fe_{5/8}Ti_{3/8}O_3)$

Writing the formulae in this way stresses also the presence of unoccupied site in the A position (represented by the symbol □) of the perovskite block. This give rise to the creation of compensating oxygen vacancies that plays an important role in the conductivity of the material. Besides, such unoccupied sites introduce strains in the

lattice leading to a less stable material. As the number of perovskite slabs increases, the number of unoccupied sites reduces, lowering the conductivity of the material and increasing its stability.

An important factor that determines the stability of the perovskite compounds is the tolerance factor t, defined as

$$t = \frac{(\bar{r}_A + r_O)}{\sqrt{2} \cdot (\bar{r}_B + r_O)} \qquad \textbf{Equation 1.14}$$

Where $\bar{r}_A$ represents the mean radius of the ions in the A-site, $\bar{r}_B$ the one for the B-site and r_O the value of the radius of the oxygen ion. For the perovskite layer of the Aurivillius compounds, it is considered to be between 0.86 and 0.97[67] i.e. a narrower range with respect the perovskite structure $(0.77\text{-}1.01)^3$.

Moreover, the valence of the cationic part of the perovskite (C.V.) depends on the number of layers (m) according to the relation C.V. = 6m.

1.4.2.2. Ferroelectricity

These compounds are often classified as displacive ferroelectrics, because the phase transition from non-polar to polar is accompanied by the displacement of certain atoms from their higher-temperature high symmetry positions. In contrast to the conventional displacive ferroelectrics, however, their ferroelectric structures can not be described as deriving from the paraelectric one with only one polar mode. Instead several modes need to be taken into account to justify the motion of the cations in the cell as well as the tilting of the octahedra present in the room temperature structures[68]. As a consequence the distortion of the basal plane of the cell (Figure 1.20) transforms the prototype structure in the Fmmm orthorhombic with Bravais lattice of A-type (m even) or B-type (m odd)[61], while subsequent variations can further lower the symmetry, as examined in details for $Bi_4Ti_3O_{12}$.

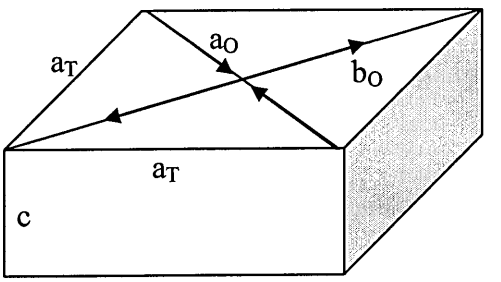

Figure 1.20: Mechanism of distortion of the cell from the tetragonal paraelectric (parameters a_T, c) to orthorhombic (a_O,b_O,c).

The Aurivillius phases are characterised by high values of residual polarization and coercive field, with all the dielectric (and consequently piezoelectric) properties strongly anisotropic with peak values in the a-b plane. Basically the major component of the spontaneous polarisation in these compounds is due to the large a-axis displacement of the Bi^{3+} in the perovskite A site with respect to the chains of corner-connected octahedra or vice versa. A small contribution arises from a displacement of the Ti away from the centre of the oxygen octahedra[58]. The low temperature structure is completed by a tilting of the octahedra of the perovskite blocks as shown in Figure 1.21[69].

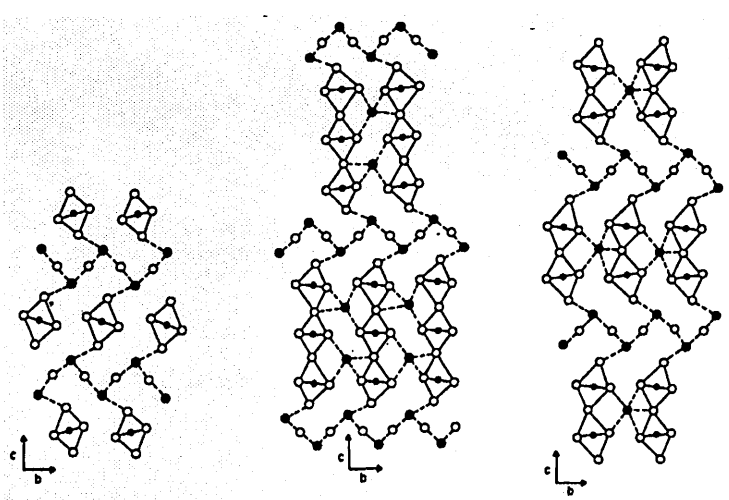

Figure 1.21: Structure of the Aurivillius phases below the Curie temperature that stress the presence of tilted octahedra in the perovskite block. It is also indicated the fifth bond of the bismuth in the bismuthyl layer with the apex oxygen of the perovskite block responsible of the tilting[30].

The tilting is a consequence of the formation of a Bi-O bond between bismuth in the bismuth oxide layer and the apex oxygen of the perovskite block (Figure 1.21). This fifth Bi-O bond is one of the main characteristics of the phase transition and can be justify considering the electronic configuration of the atoms involved[62]. The outer shell of oxygen of valence 2- is $2p^4$. So to reach the inert gas configuration it needs 2 electrons that, in the case of the oxygen of the $Bi_2O_2^{2+}$ block, can come from only the neighbour bismuth atom. The latter forms four of these bonds adopting a pyramidal configuration. If each oxygen gains two electrons from bismuth, the latter would be left in the unstable 2+ state. To reach the stable 3+ state, bismuth then forms the additional bond, introducing the tilting along a of Figure 1.20. This additional fifth Bi-O bond is also responsible for the different symmetry of the odd and even compounds in the ferroelectric state. The two symmetries (B2cb for m odd and A21am for m even) are the only ones that allow the formation of the bond without causing a distortion of the oxygen octahedra. These distortions would shorten the O-O bonds leading to an energetically unstable strained structure[70].

The symmetry differences between the two kinds of compounds are reflected in the behaviour of the polarisation: in the case of odd compounds (and $Bi_4Ti_3O_{12}$ in particular), other than the high value of polarisation along the a-axis there is also a component along the c axis. In this case, the resulting polarisation is tilted with respect to the a-b plane (of an angle of about 4° in the case of $Bi_4Ti_3O_{12}$)[71].

In Table 1-IV the piezoelectric properties of some Aurivillius compounds are summarised. The compounds 2 and 3 corresponds to a regular intergrowth of one half the unit cell of an m=3 member structure and one half the unit cell of an m=4 (or 2) member structure[72].

These compounds represent a subgroup of the Aurivillius family formed by recurrent intergrowth of perovskite blocks of the Aurivillius phases. The general formulae of these compounds can then be written as[73]

$$(Bi_2O_2)^{2+}(A_{n-1}B_nO_{3n-1})^{2-}\,(Bi_2O_2)^{2+}(A_{m-1}B_mO_{3m-1})^{2-} \Rightarrow Bi_4A_{m+n-2}B_{m+n}O_{3(m+n)-2}$$

Where m and n are the number of perovskite layers that form the intergrowth[74].

	Compound	m	T_C (°C)	d_{33} (pC/N)
1	$Bi_4Ti_3O_{12}$	3	675	6
2	$BaBi_8Ti_7O_{27}$	3+4	500	7.5
	$CaBi_8Ti_7O_{27}$		750	7.4
	$SrBi_8Ti_7O_{27}$		580	8
3	$Bi_7Ti_4NbO_{21}$	3+2	675	8
4	$BaBi_4Ti_4O_{15}$	4	395	12
	$SrBi_4Ti_4O_{15}$		485	15
5	$Sr_2Bi_4Ti_5O_{18}$	5	285	25

Table 1-IV: Electrical properties of some Aurivillius compounds[63].

A useful representation of this kind of intergrowth is given in Figure 1.22.

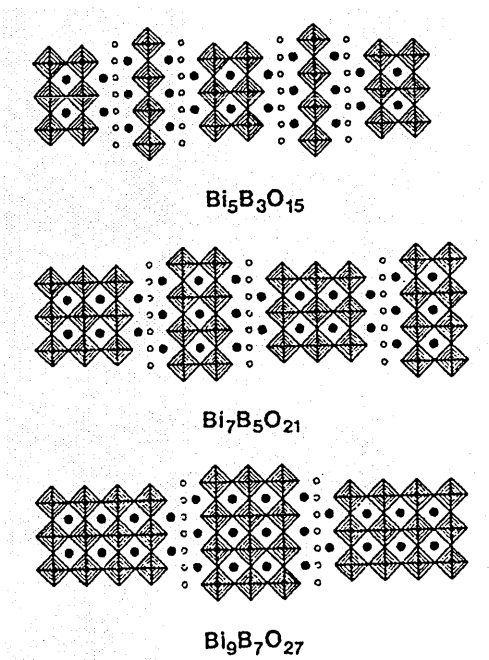

Figure 1.22: Schematic representation of some compounds of the homologous series of intergrowth structure. A and Bi ions are represented as filled circles, whereas oxygen in the bismuth oxide with open circles[73].

In Figure 1.22 the first three members of this family formed by the intergrowth of m=1 and m=2 ($Bi_5B_3O_{15}$), m=2 and m=3 ($Bi_7B_5O_{21}$) and m=3 with m=4 ($Bi_9B_7O_{27}$) are represented. To identify these compounds it is not only necessary to indicate the thickness of the fragment involved, but also their alternation scheme. For the same

kind of intergrowth there could be, in fact more than one possible arrangement as indicated in Figure 1.23 in the case of a $Bi_5B_3O_{15}$.

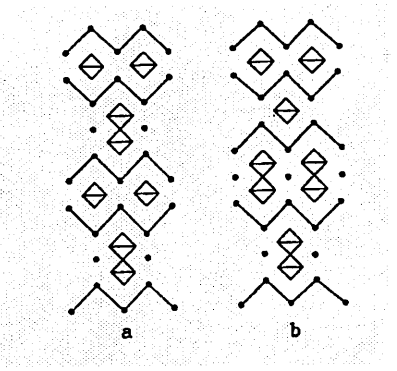

Figure 1.23: Two possible intergrowth for the $Bi_5B_3O_{15}$ type of compounds. a) 1212 and b) 1122[73].

For these compounds a system of identification has been developed using a sequence of numbers whose digits represent the entity of the fragments involved and the sequence of numbers indicates the alternation scheme. In this way the compounds of Figure 1.23 are identified as a) 1212, b) 1122[75]. The formation of this type of structure is thought to derive only from long-range interactions arising from elastic forces[76]. Of interest is the fact that the interface between the two fragments is formed by a Bi_2O_2 layer that is compressed in respect of the usual dimension found in the Aurivillius compounds[77].

From the number of variables involved in the structure of these compounds (fragments of different thickness, chemical composition and different alternation schemes) there could be in principle more mixed-layered compounds than ordinary ones. Nevertheless not many of them are known and only very few of them have been studied in detail: $M^{II}Bi_8Ti_7O_{27}$[72,73] (whit M^{II} = Ca, Sr, Ba and Pb) and $Bi_7Ti_4NbO_{21}$[78,79] are probably the best known members. Very recently Boullay et al.[80] showed that the properties of these compounds are strictly related to those of the fragment end-members that seem to behave independently in the structure.

1.4.2.3. Ferroelectric fatigue

The phenomenon of ferroelectric fatigue is generally defined as the loss of switchable polarisation by repeated polarisation reversal[81]. In general this problem is considered in relation to the loss of information in ferroelectric random access memories (FeRAMs). In the conventional dynamic random access memory (DRAM) the binary information is stored in terms of the sign of the store charge in a capacitor. To maintain this information it is necessary to compensate for charge reduction due to leakage currents. In this type of memory a voltage must, therefore, be continually applied[82].

In FeRAM, the dielectric material of the capacitor is replaced with a thin film of ferroelectric material. The information is then stored in the polarisation states of the ferroelectric thin film: the two spontaneous polarisations under zero electric field can be used as "0" and "1" digital states[83]. For this kind of application it is then important that the ferroelectric material used presents Pr high enough to be detected and which does not change under repetitive read/write cycles. Unfortunately the commonly used PZT has been proven to suffer severe degradation problems especially when coupled with simple metallic electrodes like Pt. The amount of switchable polarisation is completely suppressed after 10^8 cycles of reading and writing[84,85]. To explain this effect three causes have been proposed[86]:

1. Fatigue is due to the migration of oxygen vacancies and the formation of defect planes near the interface electrode-thin film[87]. Various mechanisms have been invoked to justify this model. Among them, the effect of 90° domains and induced strain, the pinning of domains induced by migration of oxygen vacancies, charge injection of electrons from the cathode, conversion of Ti^{4+} to Ti^{3+} and the formation of interfacial layers between metal electrodes and ferroelectric materials.
2. Entrapped charges injected from the electrodes to the film block the domain nucleation at the electrode-thin film interface and so suppress the switching of the polarisation.
3. The growth of a passive dead-layer at the electrode-thin film interface is responsible for the appearance of fatigue.

All these different models equally explain the ferroelectric fatigue and it is possible that the mechanisms coexist to an extent that depends on the nature of the material and electrode considered.

Aurivillius compounds are thought to be promising materials for FRAM applications. In particular $SrBi_2Ta_2O_9$ (SBT, a layer compounds with m=2) and modified $Bi_4Ti_3O_{12}$ show no ferroelectric fatigue even in the presence of pure metal electrodes[88,89]. The fatigue in these materials seems to be strongly related to the presence in the structure of oxygen vacancies. In particular, it has been proven that the fatigue-free behaviour of SBT is due to the effect of the Bi_2O_2 layers. Their net electrical charges compensate for space charges near the electrodes self-regulating their position in the lattice[90]. XPS analysis showed that oxygen vacancies are located near the Bi ions of the Bi_2O_2 layers. The polarization in Aurivillius compounds is mainly due to the rotations, distortions and relative ions displacements within the perovskite blocks, vacancies in the bismuthyl layers do not compromise it. On the other hand, in BIT oxygen vacancies can be induced both in the bismuthyl layers and in the pseudo-perovskite block[91]. The latter are thought to be responsible for the degradation in polarization observed in undoped BIT.

1.4.2.4. Oriented Ceramics

Aurivillius compounds present high anisotropic plate-like morphology induced by the layered structure of their unit cell. They are important candidates for piezoelectric and pyroelectric applications. However, in randomly oriented polycrystalline ceramics, their morphology limits the final density and also hinders the poling due to the limited number of orientations available to the spontaneous polarisation[92]. For these reasons, many techniques have been used to develop grain oriented ceramics to improve the properties of these compounds. These techniques exploit the anisotropy of the material to obtain ceramics with high densities and large degrees of grain orientation in which the ferroelectric and piezoelectric properties approach the single-crystal values. The effect of texturing on the values of d_{33} for some Aurivillius compounds is shown in Table 1-V. The analysis of the table highlights the great improvement achievable when the ceramic is composed by oriented grains.

Textured ceramics where initially produced using hot-forging[93,94], hot pressing[95,96], or shearing induced alignment of the grains by tape casting followed by pressureless sintering[97,98]. Although these techniques can produce textured ceramics, they are expensive and not always able to give fully dense specimens. In addition, technological complications limit their use to relatively simple systems[99].

Composition	Texture percentage	d_{33} (pC/N)	Degree of Enhancement
$Bi_4Ti_3O_{12}$	> 98%	30	77% of xtal
$(Pb,K)_{0.4}Ba_{0.6}Nb_2O_6$	> 50%	120	50% of polyxtal
$CaBi_4Ti_4O_{15}$	83-100%	45	200% of polyxtal
$Sr_{0.53}Ba_{0.47}Nb_2O_6$	90%	78	87% of xtal
$Na_{0.475}Ca_{0.05}Bi_{4.475}Ti_4O_{15}$	86-93%	44	238% of polyxtal

Table 1-V: Effect of texturing on the piezoelectric properties of Aurivillius Compounds. xtal = single crystal, polyxtal= polycristalline material.

Recently, the template grain growth (TGG) technique has been reported to represent a valid method to produce textured ceramics[100,101]. In this process a small percentage of anisometric grains (called templates) are aligned in a matrix of fine grains by means of a shear process (i.e. tape casting or extrusion) and sintered to produce a dense ceramic. If there is crystallographic match between the template particles and the final particles and if the right driving force is present, during the thermal treatment of the green ceramics the template particles grow at the expense of the finer matrix increasing the volume fraction of textured material within the ceramic[98]. Grain boundaries have higher internal energy than the grains. Hence if more grains are present the energy of the system is increased. To reduce this energy the large templates tend to consume the small matrix grains during sintering via an Ostwald ripening process[101]. The matrix grains oriented parallel to the templates form low-energy grain boundaries and for this reason are not easily consumed. On the contrary, if the angle of misalignment between template and matrix grain is high, the grain boundary between the two possesses high energy and the matrix grain will be readily consumed. At the end of the ripening process, the ceramic will be very dense with grains oriented in the same direction of the templates. The usual steps in this process

are: the production of the templates (molten salt synthesis is the process normally used), the mixing and dispersion of the templates with the fine powder of the matrix, the alignment by tape casting, and the final pressureless sintering.
In the following paragraph the attention will be focused on the prototype compounds of this family, bismuth titanate. This compound is the most studied and well known, and for this reason is an optimum candidate to study the characteristic features of this family.

1.4.2.5. Bismuth Titanate ($Bi_4Ti_3O_{12}$)

Bismuth titanate $Bi_3Ti_4O_{12}$ (BIT), is the prototype compounds for the Aurivillius family. In accord with the general formula for this family, it is composed of three perovskite blocks sandwiched between bismuthyl layers. It can be described as being formed by two unit cells of hypothetical perovskite structure $BiTiO_3$ inserted between $(Bi_2O_2)^{2+}$ layers, or as $Bi_2Ti_3O_{10}^{2-}$ slabs regularly interleaved with the bismuth oxide layers.
The $Bi_2Ti_3O_{10}^{2-}$ units are formed by three layers of oxygen octahedra (with Ti ion in the centre) linked through corners forming O-Ti-O linear chains. Bi occupies the space formed by the oxygen octahedra. The two kinds of layers are separated by the lone pair of bismuth in the bismuthyl layer. The electrons, pointing in the c direction towards the perovskite block, form a long bond with the apex oxygen of the TiO_6 octahedra. Consequently, the bismuth oxide layer can not move close to the perovskite block[102].
BIT is a displacive ferroelectric: its room temperature structure can be seen as being derived from a high symmetry parent structure (I4/mmm) by the displacement of certain atoms from their high temperature equilibrium positions[59]. So, as the temperature reduces, there is a change from a non polar to a polar structure. Nistor et al.[102] showed that the displacements of ions from their equilibrium positions are due to the lone pair of the bismuth ions. To decrease the interaction between the lone pair and the ions in the lattice the latter move apart, inducing distortions and rotations as described in the following section. The final structure can be obtained by combining the various displacement modes.

Considering the octahedral shape of the oxygen in the perovskite layer as virtually insensitive to variations of temperature, three types of displacement modes are induced. They are thought to be responsible for the change in symmetry from the paraelectric phase and as a consequence for the ferroelectricity in BIT[59,103]:

1. **Shifts along the a direction relative to a stationary [001] chains of Bi cations** (Figure 1.24): a quite rigid shift of the Ti_3O_{10} part of the perovskite slab (Oct), a motion in the opposite direction of the Ti with respect to the oxygen octahedra (B) and a rigid motion of the oxygen ion within the $(Bi_2O_2)^{2+}$ layer (O_t). In this way the I4/mmm parent structure becomes F2mm.

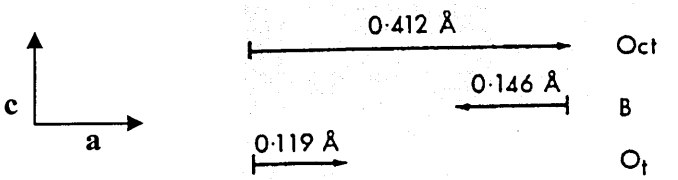

Figure 1.24: Schematic representation of the F2mm atomic displacement mode. Oct = oxygen octahedra, B = Ti^{4+}, Ot = bismuthyl layer[59].

2. **Alternating rotations of octahedra about axes parallel to a** (Figure 1.25): the symmetry of the parent structure changes to Bmab. The oxygen atoms forming the octahedra are constrained to move in the **b** or **c** directions; inducing, in this way, an octahedral expansion.

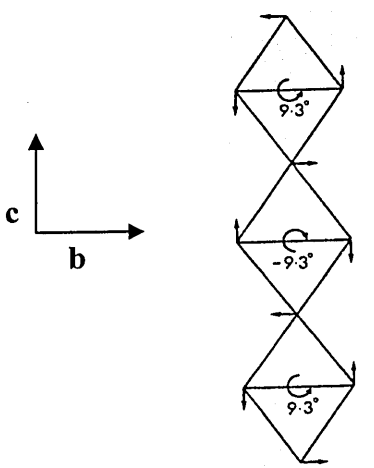

Figure 1.25: Schematic representation of the Bmab atomic displacement. The oxygen shifts are exaggerated by a factor of three[59].

3. **Rotation of TiO_6 octahedra about axes parallel to c**. The symmetry requirements for this mode lead to two different types of possible rotation: one in which the central octahedron of each perovskite slab does not rotate (Bbab symmetry, Figure 1.26.a), and the other with the three octahedra rotating in the same direction (Bbam symmetry, Figure 1.26.b). The angles resulting from these two modes (9.2, 6.5 and -5.8°) imply a unit-cell volume reduction linked with this kind of rotation.

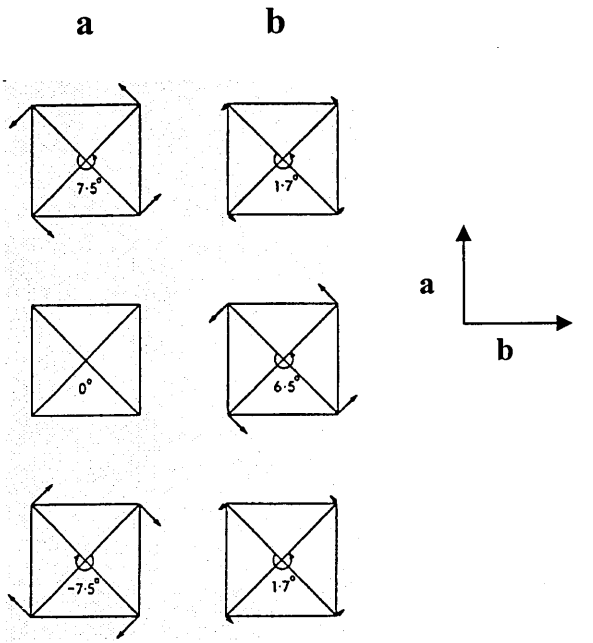

Figure 1.26: Schematic representation of the atomic displacement pattern of the Abab mode (a) and Bbam mode (b). Atom shifts are exaggerated of a factor of three[59].

These three kinds of displacement are responsible for the two components of the spontaneous polarisation present in BIT: one along the **c** direction (Ps = 4-5 $\mu C/cm^2$) and the other, much stronger (Ps = 50 $\mu C/cm^2$), in the **a** direction. This value of polarisation is two times larger than the one of the classical ferroelectric $BaTiO_3$. As a consequence, the total polarisation vector makes an angle of about 4.5 degree with the a-b plane [104]. Dorrian et al. showed[105] that the component along **c** of the polarisation can be reversed independently of the main component (that lies along **a**) and can be

destroyed when 1 or 2% of bismuth is replaced by a rare-earth ion. They attributed this disruption to a cooperative electronic effect between the lone pair electrons of neighbouring bismuth ions and the ions of the perovskite blocks. Dorrian suggested that the bismuth ions are able to reorient in an applied field with the lone pair located in an orbital extending toward the more distant neighbour. Considering that the eight active bismuth ions per unit cell reorient themselves in a parallel way, he calculated a value of Ps along **c** of 5 $\mu C/cm^2$: this value is remarkably close to the experimental value supporting the hypothesis.

In summary, the major component of the large spontaneous polarisation of BIT is due to the large a-axis displacement of the Bi^{3+} ions in the perovskite A site, with respect to the chains of corner-connect octahedra or vice versa, with a small contribution arising from a displacement of the Ti away from the centre of the oxygen octahedra. The idealised parent structure of the paraelectric phase (I4/mmm a = 3.86Å, c = 33.29 Å) is then transformed, by this movement, via an intermediate phase of symmetry Fmmm in the ferroelectric B1a1. The latter is an extremely subtle monoclinic distortion of an essentially orthorhombic structure of symmetry B2cb. The monoclinic distortion is so small that it can only be detected by the change in orientation of the optical indicatrix. For this reason at room temperature $Bi_4Ti_3O_{12}$ is generally considered to be orthorhombic[64].

Knowing the direction of the polarisation vector and the point symmetry of the paraelectric state, it is possible to derive the orientation of domain wall in every ferroelectric crystal[106]. There are eight possible directions for the polarisation vector in BIT[106]. As a consequence a relatively high number of domains are possible, as shown in Figure 1.27.

For a displacive ferroelectric the fundamental properties are the transition temperature from a paraelectric to a ferroelectric state (T_C), the spontaneous polarisation (P_S) and the atomic displacement Δz. A relationship between them is established by means of the following empirical equations[107,108]

$$Tc = 865.76 - 47.17\ (Ps) \qquad \textbf{Equation 1.15}$$

$$Tc = 1.23\ 10^4\ \Delta z^{1.62} \qquad \textbf{Equation 1.16}$$

Assuming T_C = 675°C the values for the spontaneous polarisation and the displacement, (4.22μC/cm^2 and 0.17 A.U.) respectively can be obtained. The value of the polarisation is in good agreement with the experimental value for the polarisation along **c**. In contrast with the other family of ferroelectrics, bismuth titanate shows a linear dependence of T_C against Ps.

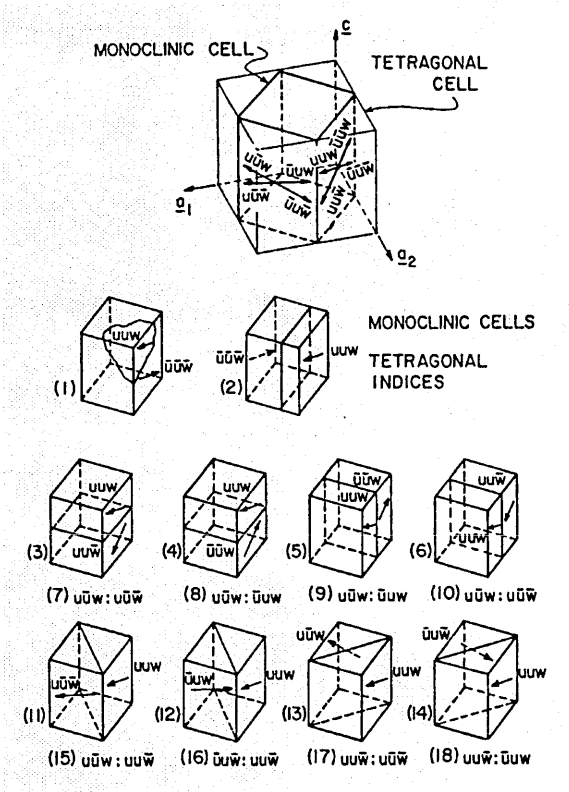

Figure 1.27: Domain wall possibility in BIT illustrated in "monoclinic cell". The uvw indices represent the polarization directions in the tetragonal paraelectric state[106].

Bismuth titanate is a candidate for high temperature piezoelectric applications and memory devices due to its high Curie temperature, the stability of its longitudinal piezoelectric modulus over broad temperature (20-600°C) and pressure (0-300 MPa) ranges, and its low aging rate[109]. Moreover the possibility of switching Ps independently in the c direction, with resultant change in the birefringence and tilt of the optical indicatrix in the a-c plane, makes BIT suitable for electro-optic devices[110]. Nevertheless $Bi_3Ti_4O_{12}$ is difficult to polarise because of its high conductivity, which amounts to 10^{-10}–10^{-11} S/m at room temperature and increases sharply with increasing temperature. At the temperature generally used for the poling of BIT (200°C) the

value is so high (10^{-5} S/m) that the longitudinal piezoelectric coefficient does not exceed $6 \cdot 10^{-12}$ C/N[57]. Moreover, BIT contains unstable Ti and Bi ions. These ions are responsible for the fatigue problems in BIT. As already mentioned, two accredited mechanisms to explain fatigue invoke the effect of electronic charge trapping at domains walls and of oxygen vacancies in pinning the domains. The oxidation of Ti^{4+} to Ti^{3+} changes the amount of charge at the domain walls so increasing the clamping effect on the domain and hindering the domain switching. On the other hand, evaporation of Bi during sintering causes an increase in the oxygen vacancies, one the three effects outlined on paragraph 1.4.2.3, which is thought responsible for fatigue.
For these reasons, several attempts have been made to improve its characteristics by reducing its conductivity. This is important for two reasons: attainment of a high enough field to polarise the material and maintenance of efficiency at high temperature.
Consistent with the structure of the material, the conductivity of BIT presents a high anisotropy that increases with temperature and reaches a maximum near the transition temperature. The mechanism of conduction seems to be electronic p-type, caused by hole compensation of cation vacancies. A $Bi^{3+} \rightarrow Bi^{5+}$ hopping through the $(Bi_2O_2)^{2+}$ layer or through the perovskite layer could explain the directionality of the conductivity. This is influenced also by oxygen vacancies in the $(Bi_2O_2)^{2+}$ layers [111].
According to the nature of p-type conductor of BIT, an increase in resistivity can be obtained through the addition of donor dopants or reduction in the amount of Bi in the system, whereas, the substitution of the instable Bi and Ti ions drastically reduces the problems of fatigue. For the nature of the crystalline structure, the substitution in BIT take place almost exclusively in the perovskite block; only the isoelectronic Te^{4+}, La^{3+} and Pb^{2+} are able to enter the bismuth oxide layers to some extent[62]. Armstrong and Newnham[112] showed that bismuth titanate can be substituted in the A-site with di- or tri-valent cations in the range 1.1-1.3 Å, while cations with radius between 0.58 and 0.65Å can replace the B-site of the perovskite block. The main dopants used to modify bismuth titanate are elements of the V and VI groups, i.e., Nb Ta, Sb, W, V, Mo. All these elements reduce the conductivity of BIT; the only exceptions are vanadium and molybdenum that do not replace titanium in the lattice. The maximum reduction is realised with Nb and Ta: 3-4 orders of magnitude greater than BIT

undoped and two order greater than Sb doped BIT[60]. The decrease in conductivity leads to an enhancement of the piezoelectric coefficient: d_{33} change from about 6 pC/N of BIT undoped, to 22 pC/N for the Nb^{5+} doping[113,114], 21 pC/N for the Ta^{6+} doping[115], 19 pC/N for W^{6+} doping[116,117] and Sb^{5+} doping [87]. This difference in piezoelectric modulus is due to the difference of electronegativity of the substituent ion. Antimony and tungsten are more electronegative than niobium and tantalum. Therefore they form stronger covalent bonds in bismuth titanate increasing in this way its ferroelasticity. In the ferroelastic effect, the domains are reoriented by internal strain caused by an externally applied stress. In particular compressive stress will switch the polar orientations perpendicular to the stress and tensile stress in a parallel direction. Covalent bonds are generally shorter than ionic ones[118], so their formation will induce distortions on the BO_6 octahedra of the perovskite blocks and consequently induce strains inside the material[119]. These strains can induce pinning of the 90° domains reducing in this way the alignment in the poling direction and, as a consequence, the piezoelectric response. In the same way the dielectric constant is strongly influenced by the substitution, passing from 20000 (value at T_c) for BIT to 15000 for BIT with Nb and 7000 for BIT with Sb[60]. The substitution in the A-site of the perovskite structure involves a lowering in T_c proportional to the percentage of substitution[60,109]. Wolfe et al[120] showed that in the case of rare earth substituted bismuth titanate, T_c decreases linearly with the rare earth concentration and that it is affected also by the radius of the substitute ion. They used the one-dimensional model, shown in Figure 1.28, to explain this dependence. The main idea is based on the difference in size and electronic configuration of the rare earth ions compared with the one of bismuth.

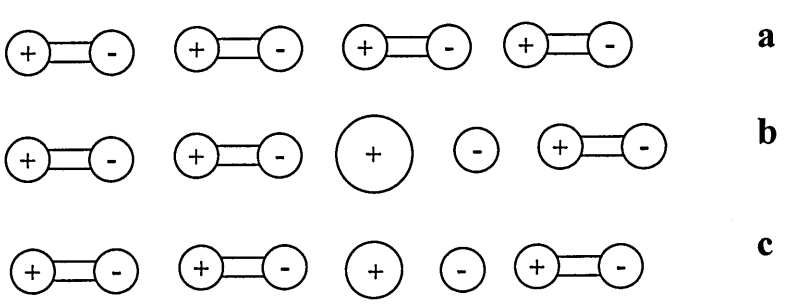

Figure 1.28: One-dimensional model of bismuth and oxygen atoms in bismuth titanate showing the effect of rare earth substitution[120].

The figure shows a polar chain that is representative of the bismuth and oxygen atoms in BIT (Figure 1.28a). The substitution of a rare earth ion for bismuth (Figure 1.28b) has mainly two effects:

- ✓ It weakens the ferroelectric interaction of the bismuth atoms reducing their number in the chain (compositional dependence)
- ✓ Its large effective size pushes apart the bismuth atoms (radius effect)

These two effects contribute to a lowering of the Curie temperature of bismuth titanate. When the radius of the substituted ion approaches that of bismuth, the radius effect vanishes and T_C is dependant only on the amount of substituting atoms. Because of its electron lone pair and consequent non-spherical configuration, bismuth prefers an asymmetric arrangement of oxygen neighbours whereas the almost spherical shape of rare earth ions is more suitable for a symmetric environment. As a consequence, the rare earths will enter the lattice in the perovskite units leaving untouched the bismuthyl layers. The maximum amount of substitution will then be limited by the Bi_2O_2 layers. Multiple-ion substitutions of Bi^{3+}/Ti^{4+} by a combination of divalent metal ion and a penta-valent ion such BaNb, PbNb and SrNb, lower the T_C[121,122]. Of particular interest is the doping of BIT with lanthanum. It has been reported that this substitution leads to an essentially fatigue-free material with good ferroelectric properties[123]. The substitution with lanthanum for bismuth in the perovskite blocks enhances the rotation of TiO_6 octahedra in the a-b plane greatly increasing the ferroelectric response of BIT[124]. This effect is enhanced even further using a lanthanide of smaller ionic radius. Kojima et al[123] showed that Nd-substitued BIT presents values of remanent polarization compatible with those of the commercial PZT used for FeRAM applications.

The properties of these materials are enhanced further when using techniques that allow the formation of grain-oriented ceramics and, consequently, an alignment of the axes of the crystals that enable easier poling[92, 125,126].

1.4.3. Coupling between BIT and a perovskite

Among all the possibilities, it is interesting to examine the structural changes and the electrical characteristics of the systems formed by BIT with perovskites. Currently there has been no systematic approach to this particular coupling, but only rather limited studies about particular compounds. The papers in the literature generally refer to single compounds without considering them as a part of the Aurivillius family. The few studies concerning the family as a whole present the structural implications of an increased amount of perovskite block without a systematic analysis of the consequence to the electric and piezoelectric properties. Subbarao published some of the most comprehensive reviews about this family[127,128]. His studies are part of the rare attempts to uniformly consider the electric properties among the family in the light of the crystal structure. Subbarao, however, does not consider the properties as functions of an increasing amount of perovskite end member. Instead only the role of the A- (or B-) site cation on the properties of a specific Aurivillius compound is considered.

Probably, the only studies that consider the evolution of the properties along a $Bi_4Ti_3O_{12}$- n(ABO_3) series are those published in the 1960's by Ismailzade. In two different papers he studied the structural evolution of the $Bi_4Ti_3O_{12}$- n($BaTiO_3$)[129] and $Bi_4Ti_3O_{12}$- n($BiFeO_3$)[130]. These early studies however reported indications only of the possible implications of the structure on the Curie temperature and did not consider any other electrical properties.

In the following paragraphs the more studied compounds are presented in a very short review. They will be represented in ternary structural diagrams of the constituent oxides for a better visualisation.

The systems studied are:

1. $Bi_3Ti_4O_{12} - M^{2+}TiO_3$ with M^{2+} = Ba, Ca, Pb, Sr;
2. $Bi_3Ti_4O_{12} - BiFeO_3$;
3. $Bi_3Ti_4O_{12} - (NaBi)_{1/2}TiO_3$.

1.4.3.1. $Bi_3Ti_4O_{12} - M^{2+}TiO_3$ with M^{2+} = Ba, Ca, Pb, Sr

The most deeply studied system is $xPbTiO_3$-yBIT[131]. In the phase diagram in Figure 1.29 the evolution of the system from a layer structure with 3 perovskite layers (BIT), to the pure perovskite $PbTiO_3$ is shown. An increasing amount of $PbTiO_3$ corresponds to an increasing number of perovskite units in the layer structure (Table 1-VI). Pb and Ti atoms of the lead titanate progressively enter the $(Bi_2O_2)^{2+}$ layers leading to more perovskite units and causing eventually the collapse of the layered structure to a perovskite one.

From the diagram it is clear that as m increases, the amount of PbO necessary for passing from a compound with m to one of m+1 decreases, so the structure become more susceptible to rapid changes. Compounds with m>6 could be the result of a very fine intergrowth of members with different numbers of m instead of proper compounds[63,132]. As already mentioned, periodic intergrowth of Aurivillius phases are common. These compounds could be seen as pure by a long-range analysis but at a local level would be seen as the results of intergrowth. So, increases in $PbTiO_3$ correspond to a progressive destruction of the bismuthyl layer in a more or less ordered way.

	Composition	(x):(y) value	m value (perovskite units)
1	$Bi_4Ti_3O_{12}$	0:1	3
2	$PbBi_{12}Ti_{10}O_{39}$	1:3	3 and 4
3	$PbBi_8Ti_7O_{27}$	1:2	3 and 4
4	$PbBi_4Ti_4O_{15}$	1:1	4
5	$Pb_2Bi_4Ti_5O_{18}$	2:1	5
6	$Pb_3Bi_4Ti_6O_{21}$	3:1	6
7	$Pb_4Bi_4Ti_{27}O_{24}$	4:1	7
8	$PbTiO_3$	1:0	∞

Table 1-VI: Possible compounds in the $Bi_4Ti_3O_{12}$-$PbTiO_3$ system.

The compounds 2 and 3 correspond to a regular intergrowth of one half the unit cell of an m = 3 member structure and one half the unit cell of an m = 4 member structure[133].

Measurements made on single crystals had shown that, when considering systems with integer values of m, the remanent polarisation increases with the number of octahedra in the perovskite block[134].

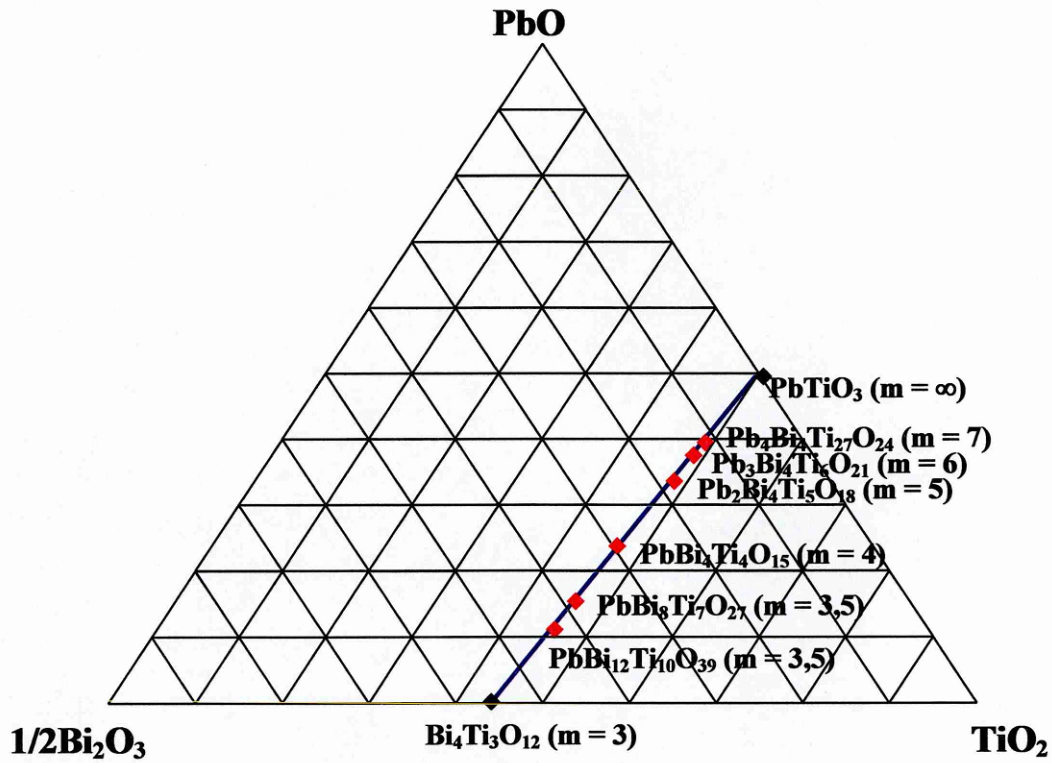

Figure 1.29: PbO-Bi_2O_3-TiO_2 phase diagram with the compounds studied in literature.

For the systems formed with the other M^{2+} members there is information only on the compounds belonging to the three classes (Figure 1.30) (M^{2+} = Ba, Ca, Sr)

- $M^{2+}Bi_8Ti_7O_{27}$ ⇨ $Bi_3Ti_4O_{12} - M^{2+}Bi_4Ti_4O_{15}$
- $M^{2+}Bi_4Ti_4O_{15}$ ⇨ $Bi_3Ti_4O_{12} - M^{2+}TiO_3$
- $M^{2+}{}_2Bi_4Ti_5O_{18}$ ⇨ $Bi_3Ti_4O_{12} - 2M^{2+}TiO_3$[135,136]

The lattice parameters and the piezoelectric coefficient of the compounds of Ba, and Sr increase with the number of perovskite blocks. Contrary to this, the highest Curie temperatures are obtained in the compounds with the minimum thickness of perovskite layers, with a monotonic trend from the lowest number of m until the pure perovskite.

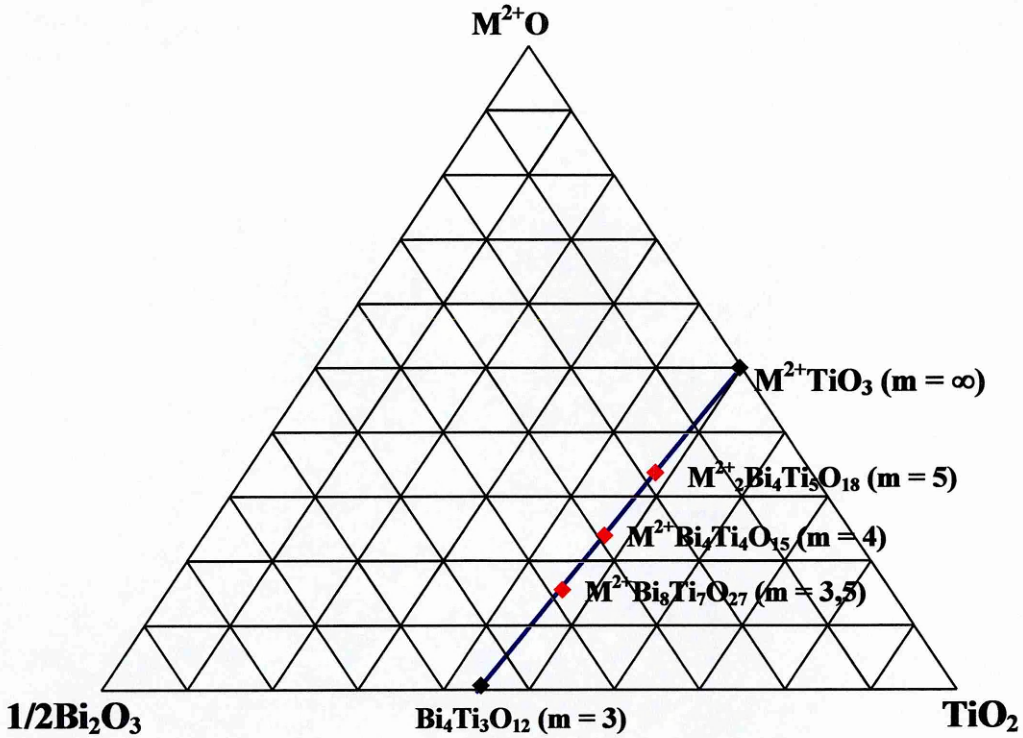

Figure 1.30: $M^{2+}O$-Bi_2O_3-TiO_2 phase diagram with the compounds studied in literature.

The compounds of lead exhibit a nonmonotonic behaviour, probably associated with the special role played by the electron shell and high electronic polarisability of Pb. The variation of T_C in these compounds is summarised in Figure 1.31[137]. Among compounds of the same number of m, the Curie temperature decreases with increasing cationic radius of M^{2+}.

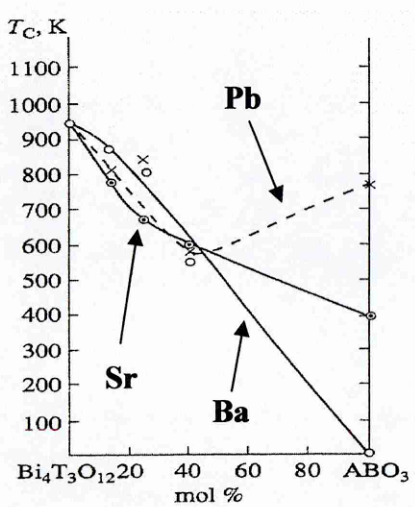

Figure 1.31: Curie temperature vs. concentration of non-bismuth ions in the perovskite block of BIT-nABO_3 compounds[137].

1.4.3.2. $Bi_3Ti_4O_{12} - BiFeO_3$

The compounds of this system have also been studied for their magnetic properties[138,139,140]. The phase diagram is presented in Figure 1.32. The conductivity increases with the perovskite layers and for this reason several kinds of doping have been used[141].

By increasing the amount of ferrite units, both the number of perovskite blocks and the content of iron in the perovskite layer rises, although the bismuth content remains at 100%. The Curie temperatures increases with the amount of iron up to the one of the ferrite[137].

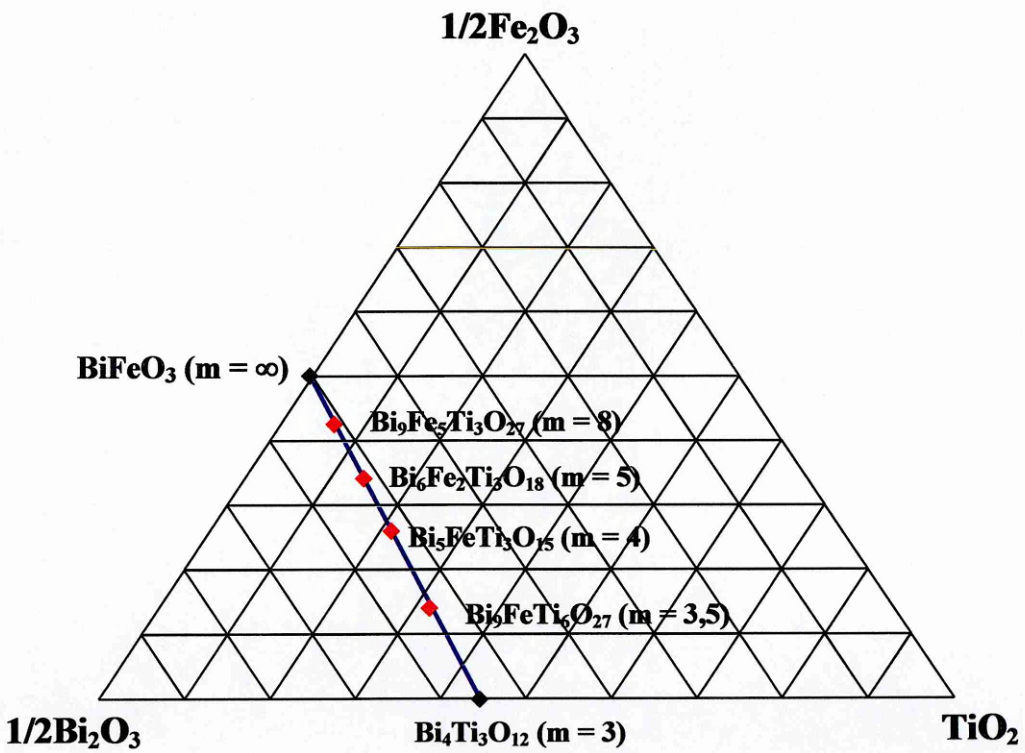

Figure 1.32: Fe_2O_3-Bi_2O_3-TiO_2 phase diagram with the compounds studied in literature.

1.4.3.3. $Bi_3Ti_4O_{12} - (NaBi)_{1/2}TiO_3$.

Only two compound of this system have been studied, $Na_{0.5}Bi_{8.5}Ti_7O_{27}$ (m = 3,5) and $Na_{0.5}Bi_{4.5}Ti_4O_{15}$ (m = 4) (Figure 1.33). Compared to the previous systems the different charge of Na_2O leads to a narrower area for the formation of the solid solutions.
$Na_{0.5}Bi_{4.5}Ti_4O_{15}$ has a Curie temperature of 655°C with a peak of the dielectric constant of 1600 and a d_{33} of 10 pC/N[39]. Nevertheless, doping the system with calcium and adding small proportions of manganese, causes the rise of this value to 21 pC/N and k_{33} of 0.36-0.40. This represents an excellent value for these kinds of compounds[142].

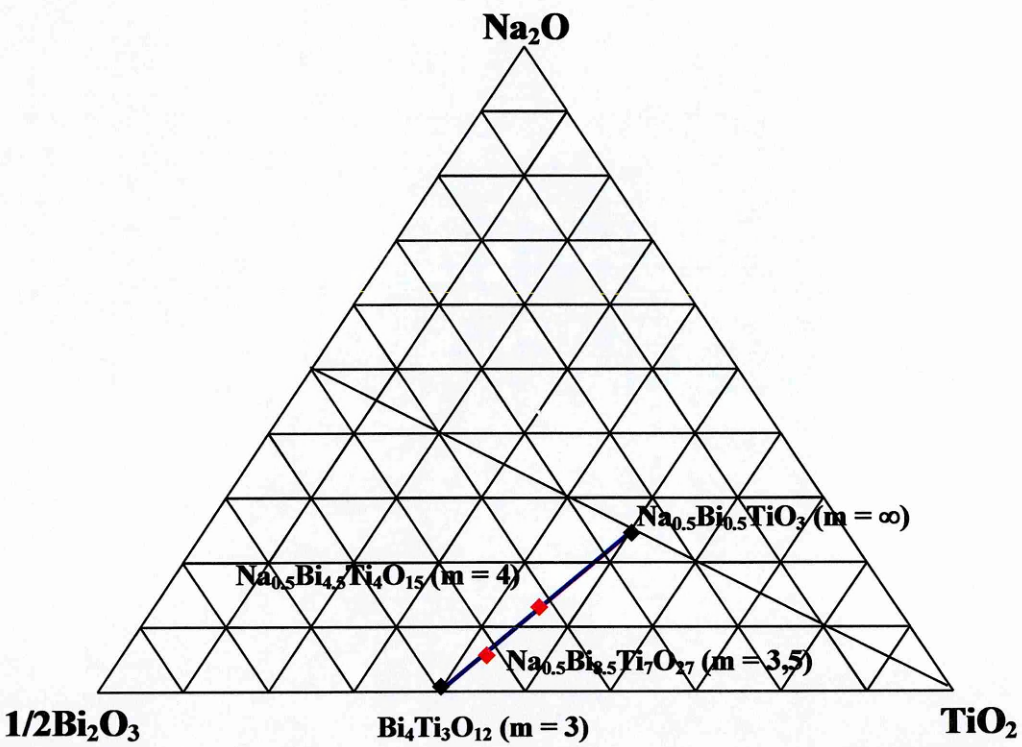

Figure 1.33: Na_2O-Bi_2O_3-TiO_2 phase diagram with the compounds studied in literature.

It is important to notice that all the values reported here are for samples obtained via the conventional ceramic route. Considering the layer structure of these materials, the properties are improved using techniques, such hot forging and hot pressing, which allow to produce oriented ceramics.

2. EXPERIMENTAL

2.1. CERAMICS PRODUCTION AND CHARACTERISATION

The main steps involved in the production and characterisation of a piezoelectric ceramic specimen are shown in Figure 2.1. They are grouped in three subsections representing the principal stages of the process. In the following paragraphs all steps will be analysed and the experimental conditions used for the project will be indicated.

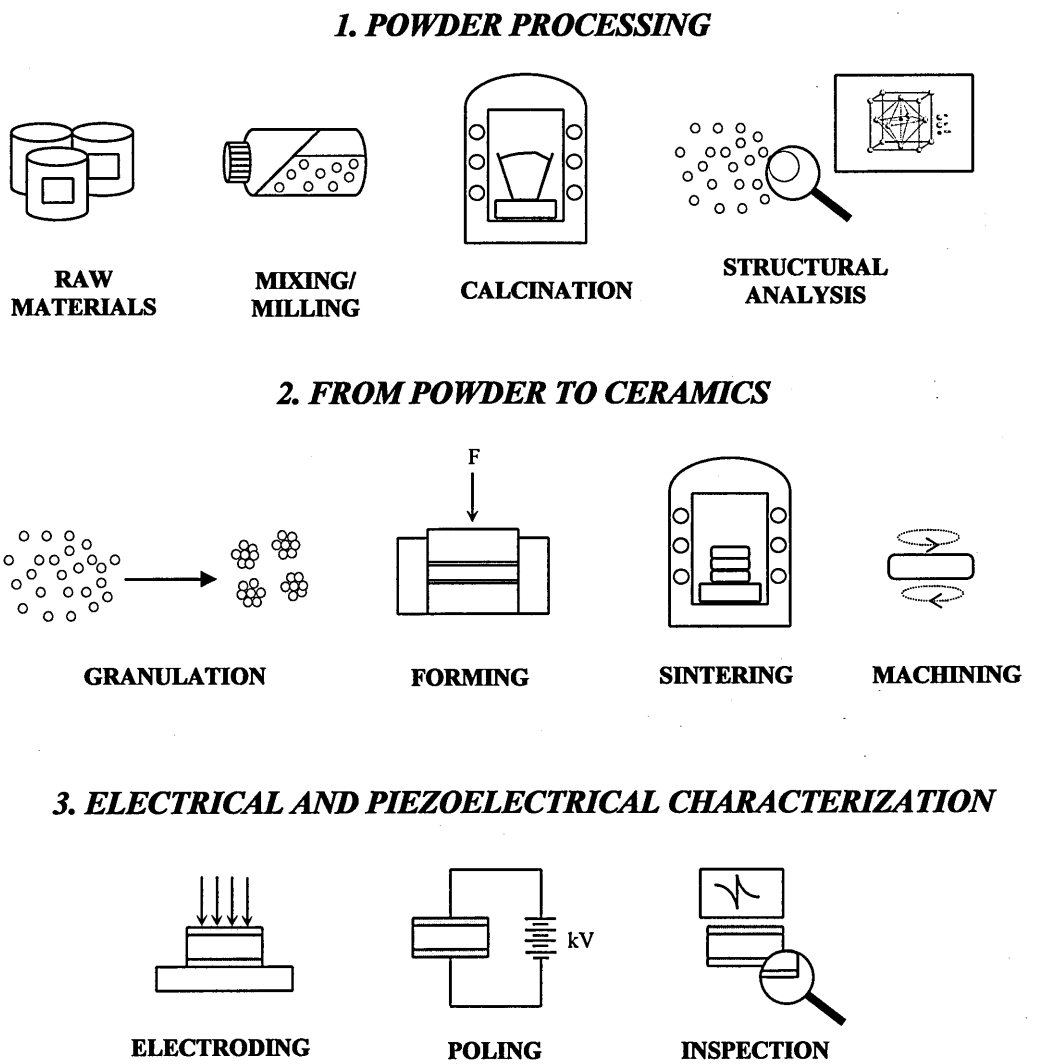

Figure 2.1: Schematic representation of the ceramic process and characterization.

2.1.1. Powder processing

2.1.1.1. Mixing

The raw materials, in the form of metal oxides and carbonates, were mixed in stoichiometric proportions required for the desired composition. The mixture was milled for 24 hours in polyethylene jars with ZrO_2 media. This process is necessary to obtain a uniform mixing of the reagents prior to calcination.

2.1.1.1.1. Experimental Conditions

NBT-BIT-BT

Eighty five systems of the general formula $Ba_yNa_{0.5x}Bi_{(4-3.5x-4y)}Ti_{(3-2x-2y)}O_{3(4-3x-3y)}$ with $x + y + z = 1$ were prepared in order to study the NBT-BIT-BT phase diagram. Their exact formulae and labels are reported in Appendix A. The raw materials used are shown in Table 2-I. The use of carbonates instead of oxides is preferred because during calcination the release of CO_2 leads to finer, and as a consequence, more reactive particles.

Reagent	Purity	Company
Na_2CO_3	99.5 %	Aldrich
$BaCO_3$	99+ %	Aldrich
Bi_2O_3	99.9 % < 10μm	Aldrich
TiO_2	99+ % (anastase)	Aldrich

Table 2-I: Raw materials used for the production of powders in the NBT-BIT-BT system.

BMT

The reagents used to obtain Bi_2MgTiO_6 are presented in Table 2-II. Following the study of this compound, several other compositions of the general formula $Mg_yBi_{2x}Ti_{(1-x-y)}O_{2+x-y}$ ($x + y + z = 1$) were made with the same raw materials. Their formulae are reported in section 3.3.1.2.1.

Reagent	Purity	Company
$(MgCO_3)_4Mg(OH)_25H_2O$	99 %	Aldrich
Bi_2O_3	99.9 % < 10μm	Aldrich
TiO_2	99+ % (anastase)	Aldrich

Table 2-II: reagent used to make the powders in the BMT system.

2.1.1.2. Calcination

In this process the precursors react to form the system of interest at elevated temperature. In order for chemical reactions to take place in condensed phases, atoms must be able to move around in the crystalline solid in a diffusive process. As with all the diffusion processes, calcination is thermally activated: it is necessary to supply to the atoms enough energy to overcome the activation energy for moving from one site to another.

2.1.1.2.1. Experimental Conditions

NBT - BIT - BT

The powders were calcined in saturated zirconia crucibles to limit the loss of bismuth and sodium (see section 3.1) using the arrangement of Figure 2.2.

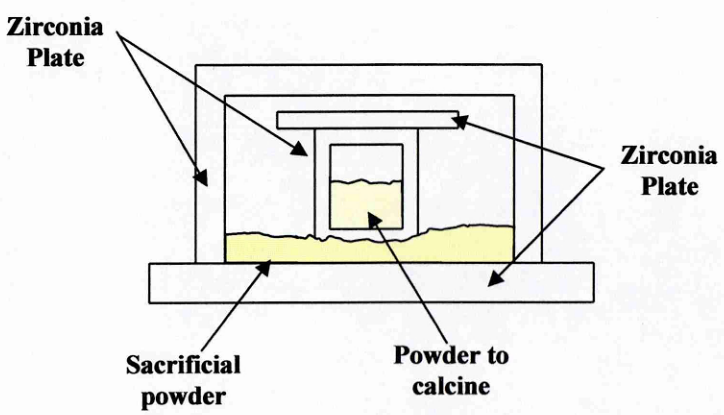

Figure 2.2: Arrangement for calcination.

In this arrangement, the zirconia crucible with the powder for calcination is put on a bed of sacrificial powder of BIT or NBT. The choice depends whether the powder to

calcine contains sodium or not. In the latter case it is necessary to prevent not only the volatilisation of bismuth but also of sodium. For this reason a sacrificial layer of NBT is more beneficial. The crucible is closed with a zirconia lid and the system is sealed with a zirconia crucible placed upside down on a zirconia plate.
The powders were calcined at 850°C and 1150°C for 4 hours following the heating programs of Table 2-III.

Step	Operation
1	Heating 2°C/min up to 600 °C
2	Dwelling 1h at 600 °C
3	Heating 5°C/min to 850 °C
4	Dwelling 4h at 850 °C
	(Dwelling 4h at 1150 °C)

Table 2-III: Calcination program for the powder of the NBT-BIT-BT system. Two different calcination temperatures has been used: 850 °C and 1150 °C (final step).

The intermediate step at 600 °C was done to prevent the eutectic melt of $Bi_{12}TiO_{20}$ (an intermediate phase that forms at low temperature) and Bi_2O_3 that occurs at 795 °C as suggested by Shulman et al[143].

BMT system

MgO has low reactivity in the $Pb(Mg_{1/3}Nb_{2/3})O_3$ system[144]. For this reason the compounds of compositions $Mg_yBi_{2x}Ti_{(1-x-y)}O_{2+x-y}$ were made in two steps:

1. synthesis of $MgTiO_3$;
2. reaction of $MgTiO_3$ with the right amount of Bi_2O_3 and TiO_2 to obtain the right composition.

The process that was used for Bi_2MgTiO_6 is shown in Figure 2.3. The same conditions have been used for the other compositions made. The heating program was similar to

the one used in the previous system, but with a final dwelling time of two hours at 900 °C.

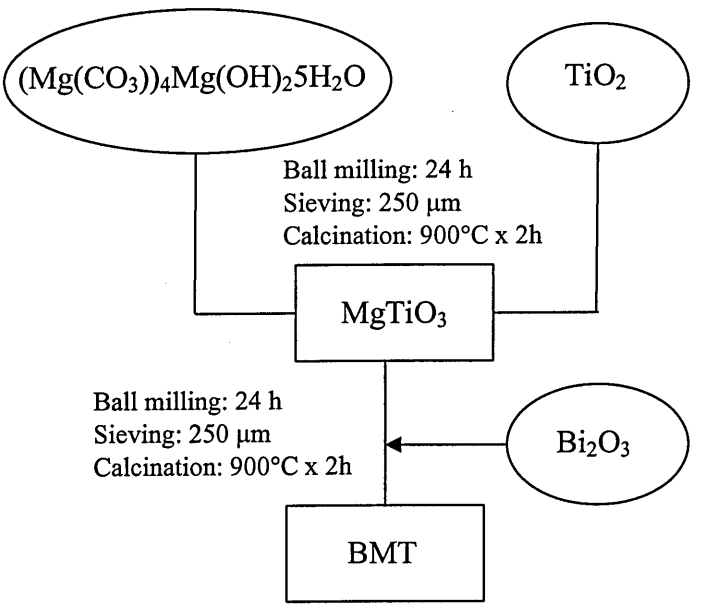

Figure 2.3: Schematic representation of the process used to obtain powder in the BMT system, with the experimental conditions and the pre-reaction step to produce magnesium titanate.

2.1.2. Structural and morphological analysis

The structure of the calcined powders was examined by XRD analysis with a diffractometer (Siemens D5005, CuKα) in a theta/two theta configuration. For each composition, three spectra were recorded:

1. wide: 5-60° (2θ); step 0.02 s; 2 s each step;
2. low angle 1: 2-20°(2θ); step 0.02; 20 s each step;
3. low angle 2: 5-15° (2θ); step 0.02 s; 20 s each step.

To help in the identification of the phases involved, some of the diffraction patterns were simulated using the crystallographic software "Crystallographica"[145]. The data on atoms positions, occupancy and temperature factors were taken from the

Daresbury Crystallographic database[146]. The unit cell parameters of the pure phase were refined using a least square program compiled in Mathcad (see Appendix B). These refinements used all peaks that were possible to identify unequivocally.
Morphology was checked on powders and ceramics coated with a conductive Au/Cr layer using scanning electron microscopy (XFEG ABT-55 or Cambridge Stereoscan 250) coupled with EDX analysis. The ceramics samples were previously polished and thermally etched at temperatures that were generally 100°C less than the ones used in sintering.

2.1.3. Thermal analysis

Differential thermal analyses (DTA, Staton Red croft STA 780) were performed on selected powders of the two systems to analyze their thermal evolution and to choose a more appropriate sintering temperature. The analyses were made in air (air flow 55cm^3/min at a heating rate of 5°C/min) with alumina as standard.

2.2. FROM POWDERS TO CERAMICS

2.2.1. Consolidation or forming

The powder prepared is formed into a shape similar to that desired by the so-called forming process. The sample obtained is called "green". Compaction relies on an external source to deform the powders into a high density component that approaches the final geometry desired. In this process, binders are widely used to impart to the green body the necessary strength for handling. They are polymer molecules or colloids that adsorb on the particles surface and promote inter-particle bridging.

Several forming methods are in use[147]; the selection of which one to use depends on the nature of the powder and on the desired shape of the final product. The ceramic samples for the piezoelectric characterisation are generally made in form of a disc because this shape is technologically easy to obtain. In this project the pellets were shaped by uniaxial pressing coupled with cold isostatic pressing (CIP).

Conventional uniaxial powder compaction is performed applying a pressure along one axis in a hard mould of the type shown in Figure 2.4.

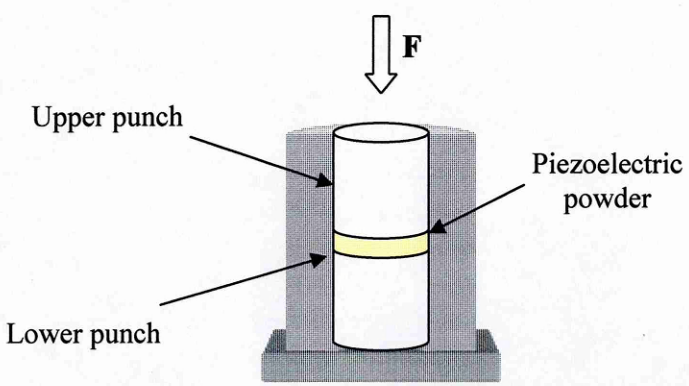

Figure 2.4: Uniaxial pressing apparatus.

In the press used for this project, the pressure is applied only by the upper punch and for this reason the main drawback of this simple technique is the formation of a gradient of density along the thickness of the pellet.

To overcome this problem the pellets preformed in the uniaxial die have been re-pressed isostatically. In cold isostatic pressing (CIP) the samples are sealed inside a plastic bag under vacuum, and immersed into a fluid chamber (containing a mixture of water and oil) which is pressurised by an external hydraulic system (Figure 2.5). In this way the pressure is uniformly applied throughout the pellet.

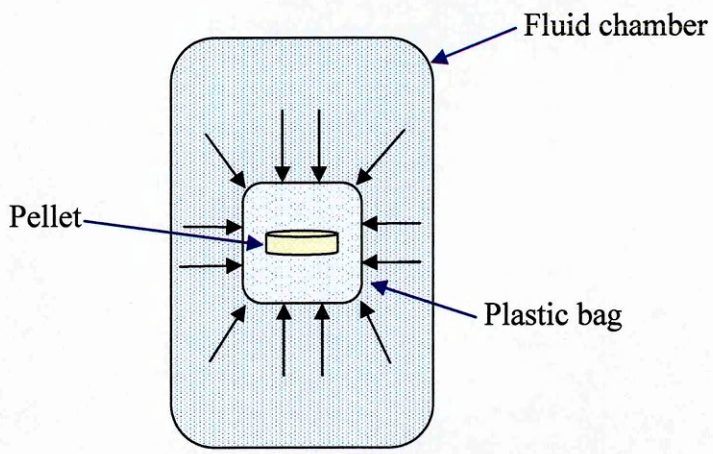

Figure 2.5: Schematic representation of a cold isostatic press (CIP).

2.2.1.1. Experimental Conditions

The powders were granulated with 2% in weight of polyvinyl alcohol (PVA) that act as a binder. They were ball-milled for 6h in polyethylene jars with zirconia media, then dried and sieved at 250μm. 9 grams of powders for each sample were then uniaxially pressed (50 MPa) using a 28 mm diameter mould and the pellet obtained repressed isostatically (150 MPa).

2.2.2. Sintering

During sintering, the particles of the green body bond together by atomic motions to eliminate the porosity and to form a ceramic sample of high density and mechanical strength. Like calcination, sintering is a thermally activated process: the driving force

for the densification is the decrease in the free energy associated with the high surface area of the powder.

Before firing, the green body is composed of individual grains separated by porosity with a density between 25 and 60% of the theoretical value. For maximising strength and electrical properties, it is beneficial to eliminate as much porosity as possible.

Changes that occur during the firing process are related to[148]:

- ✓ Changes in grain size and shape;
- ✓ Changes in pore shape;
- ✓ Changes in pore size;
- ✓ Changes in sample size.

The sintering process is illustrated in Figure 2.6. An increase in temperature, increases diffusional motions of atoms at the contact points between particles. These grow into necks in the early stage of sintering and evolve in grain boundaries that replace the solid-vapour interfaces. In the intermediate stage, the pore geometry is irregular and the pores are located at grain boundary intersections. As sintering progresses, the pore geometry approaches a cylindrical shape where the densification occurs by decreasing the pore radius. In the last stage of the process, the interaction between pores and grain boundary can lead to the formation of porosity inside the grain (called closed porosity) that limits the final density of the ceramic body.

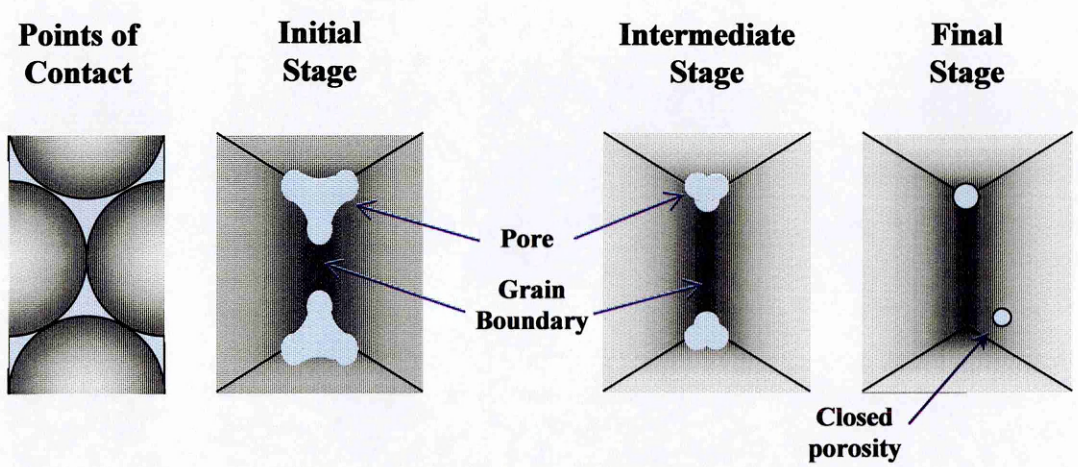

Figure 2.6: Stages of the sintering process.

2.2.2.1. Experimental conditions

The green bodies coming from the forming stage were sintered following the conditions of Table 2.IV with the arrangement shown in Figure 2.7.

System	Step	Operation
BMT	1	Heating at 2°C/min up to 700°C
	2	Dwelling at 700°C for 15 min
	3	Heating at 2°C/min up to 970°C
	4	Dwelling at 970°C x 2h
	5	Cooling at 3°C/min to room temperature
NBT-BIT-BT	1	Heating at 2°C/min up to 750°C
	2	Dwelling at 750°C for 15 min
	3	Heating at 2°C/min up to 970°C
	4	Dwelling at 970°C x 2h
	5	Cooling at 3°C/min to room temperature

Table 2-IV: Condition of sintering for the two different systems. The step 2 is the burn out of the binder.

The dwelling step 2 was carried out to burn out the binder present in the samples.

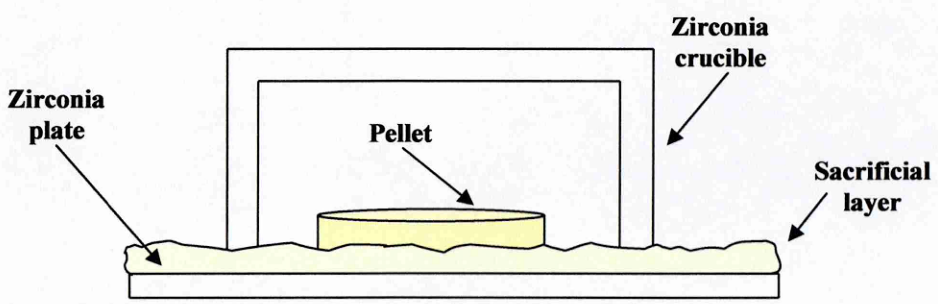

Figure 2.7: Arrangement for sintering. Depending on the nature of the pellet the sacrificial layer can be NBT of BIT.

The pellet during sintering is lying in a sacrificial layer to avoid the problems of losses from evaporation of sodium and bismuth. As already seen for calcination the sacrificial layer can be BIT or NBT depending on the composition of the sample to densify: BIT for the BMT system or in the compounds of the BIT-BT series; NBT for a generic composition in the BIT-NBT-BT system away from the BIT-BT baseline of the phase diagram. The zirconia plate and crucible were conditioned as explained in section 3.1 to limit any possible loss of Na or Bi.

2.3. ELECTRICAL AND PIEZOELECTRIC CHARACTERIZATION

2.3.1. Machining and Electroding

To obtain scientifically valid results piezoelectric constants must be determined under particular conditions and with a specimen of strictly controlled shape and dimensions. In particular, for disc-shaped samples the standards[149] impose a ratio diameter/thickness > 20 even if a ratio over 10 is normally accepted. The thickness of the pellets was therefore reduced from approximately 2 mm to 1mm, with an average diameter of 25mm, to satisfy this requirement.

Reducing the sample thickness also assists accurate dielectric and piezoelectric measurements as the material is less affected by Bi and Na evaporation. It has been demonstrated[150] that the properties of an NBT pellet change along the thickness due to the evaporation of the oxides of these cations. The evaporation causes a depletion of bismuth and sodium from the surface exposed to the air that is only partially counterbalanced by the Bi/Na atmosphere and the effect of the direct contact with the sacrificial powder which acts as sink of ions that can flow to the pellet from the bottom face. These diffusion processes are regulated by the Fick's Law. Consequence of this flow of atoms **in** the pellet from the sacrificial layer and **out** of the pellet from the face exposed to air is the formation of a gradient of composition along the thickness as shown in Figure 2.8.

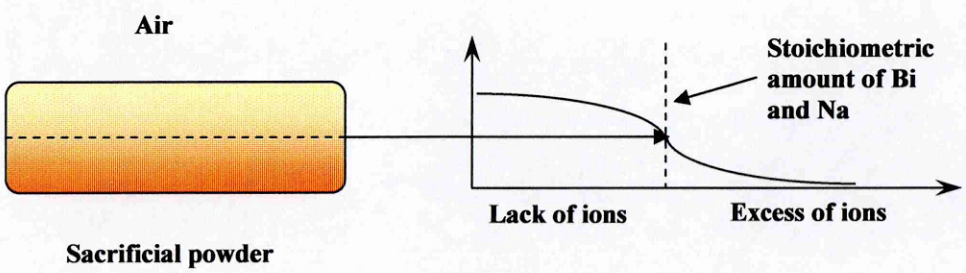

Figure 2.8: Compositional fluctuation along the thickness of a pellet due to evaporation of ions from the face exposed to air and injection from the sacrificial layer. The core of the pellet should be relatively uneffected by these variation retaining the right composition.

As a result of this opposite flows inside the pellet, its core should be the part less affected by fluctuation of composition and then to retain the predicted stoichiometry of the system. The reduction in thickness was made grinding symmetrically both faces of the disc to obtain its core.

To measure its electrical and piezoelectric properties, the ceramic sample needs to be electroded. The gold electrodes (100μm thick) were deposited by evaporation (Edwards A4A0) on the planar faces of the disks previously covered with a chromium seed layer (20μm thick) that helps the adhesion of gold on the surface of the ceramic.

2.3.2. Electrical measurements

2.3.2.1. Dielectric constant and dielectric loss

The electroded pellet is considered to behave like a parallel plate capacitor. The capacitance of the dielectric can then be put in relation with its dielectric constant through the relation[151]:

$$C = \frac{\varepsilon_0 \varepsilon A}{t} \qquad \textbf{Equation 2.1}$$

Where

C = capacitance of the dielectric (F)

ε_0 = permittivity of free space

ε = dielectric constant

A = area of the pellet (m^2)

t = thickness of the pellet (m)

By measuring the capacitance of the pellet it is then possible to calculate the dielectric constant of the material examined.

The dielectric loss can be defined as the energy converted into heat in a dielectric material when this is subjected to a change in the electric field.

If a sinusoidal voltage V (=$V_0 \sin\omega t$) is applied to a perfect capacitor, the current flowing in it is $V_0 \omega \cos\omega t$ and lead V by 90° (Figure 2.9A). In a real dielectric the rotation of the dipoles and electrical conduction in the material result in a loss of energy as heat so that the two quantities are no longer 90° out of phase but 90°-δ (Figure 2.9B).

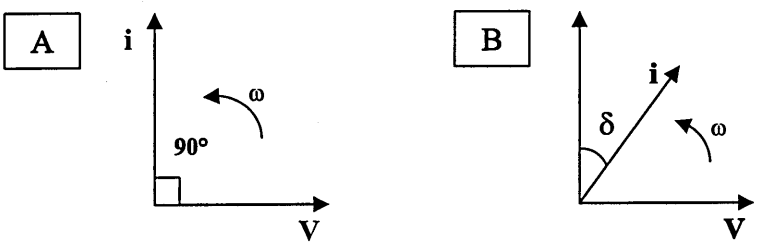

Figure 2.9: Phasor diagram for A) an ideal capacitor B) a real lossy capacitor.

The time average power loss is then

$$\bar{P} = \frac{1}{T}\int_0^t VIdt = \frac{1}{T}\int_0^t V_0 \sin\omega t I_0 \cos(\omega t - \delta)dt = \frac{1}{2}V_0 I_0 \sin\delta \qquad \textbf{Equation 2.2}$$

Generally δ is small enough to assume $\sin\delta \cong \tan\delta$; the latter is called the dissipation factor and expresses the fraction of capacitive current and voltage dissipated as heat. The dielectric loss can also be expressed as ratio at a particular frequency between the real and imaginary part of the capacitance of the capacitor. A large loss means big dielectric absorption, so a capacitor made by a lossy dielectric (as all the real materials are) presents a change of capacitance with frequency. Dielectric materials need to have a reasonably stable capacitance with frequency to be technologically applicable. As the rate of deterioration in capacitance is directly linked to the loss tangent, a smaller loss tangent leads to a smaller change in capacitance with frequency of the capacitor.
Dielectric constant and dielectric loss were measured:

1. At room temperature at two different frequencies (1kHz and 33Hz) using a Genrad 1689 RLC Digibridge with an applied voltage of 0.5V.

2. As function of the temperature in the range 25-300°C at 5 different frequencies (0.5, 1, 10, 100, 1000 kHz) using an HP Electrometer (HP4192ALF) and a computer controlled rig connected as shown in Figure 2.10.

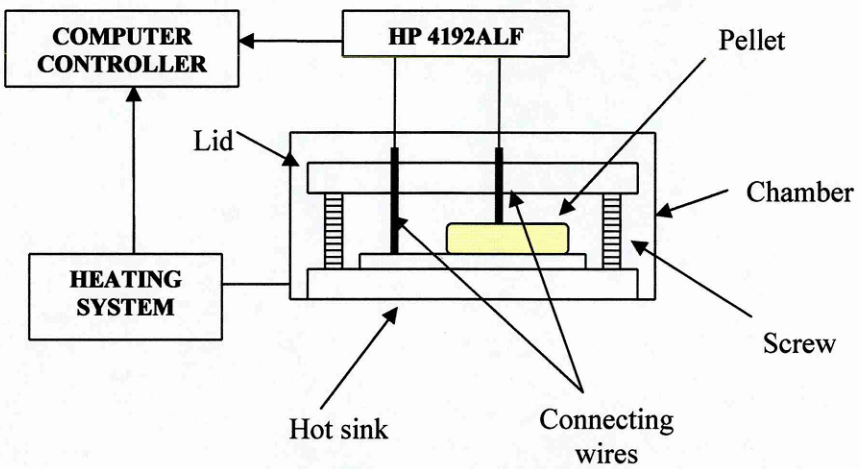

Figure 2.10: Schematic of the apparatus used for capacitance measurements.

2.3.2.2. Resistivity

The current "i" flowing through the thickness "h" of a disk when a voltage "V" is applied on its surface area "A", is linked to the resistivity "ρ" of the material through the following equation

$$i = \frac{A\ V}{\rho \cdot h} \qquad \textbf{Equation 2.3}$$

If the dimensions of the pellet are known, it is then possible to calculate the resistivity of the material by measuring the current flowing through it when a known voltage is applied. The DC resistivity was measured as function of the temperature using a Kethley 6517 electrometer and a computer controlled rig with the assembly shown in Figure 2.11. The computer controls a thermoelectric heater-cooler (Peltier control of Figure 2.11) used to ramp the temperature of the specimen within the range 15-65°C

under vacuum: the system is kept at a fixed temperature for 10 minutes to ensure equilibrium conditions before each measurements.

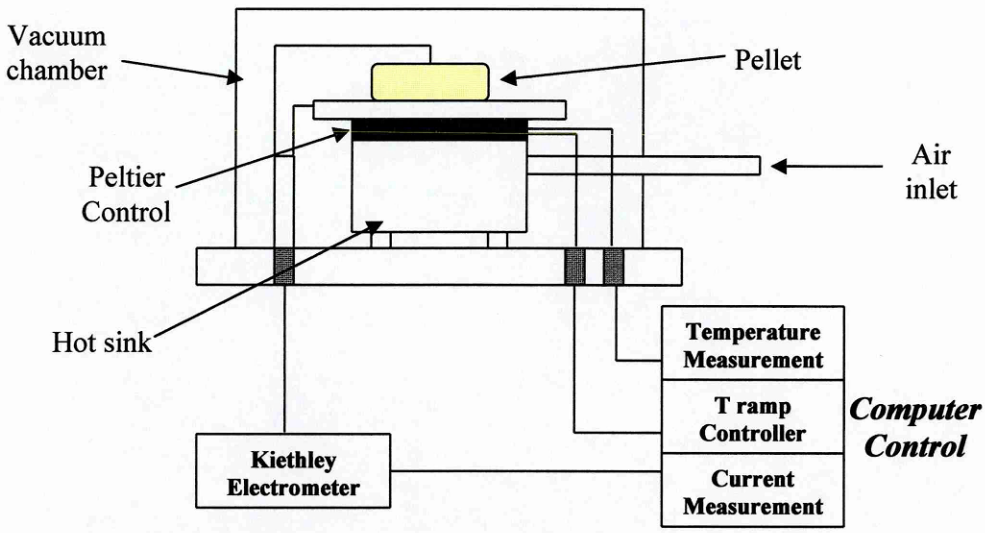

Figure 2.11: Apparatus for resistivity measurements.

The typical heating program used and current behaviour recorded are shown in Figure 2.12.

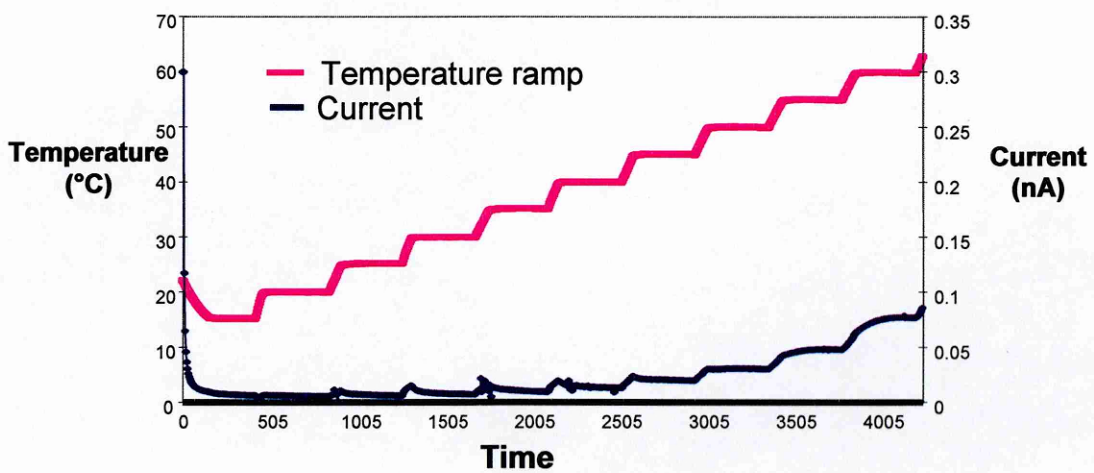

Figure 2.12: Heating ramp and current trend of a typical resistivity measurement.

For the range of resistivity values expected, the voltage imposed to the sample, was in the range 2-15V.

2.3.3. Piezoelectric measurements

2.3.3.1. Poling

A ceramic sample needs to be poled to exhibit piezoelectric behaviour. In other words it is necessary to apply an external electric field to align the polar axes. In this way the material develops a permanent dipole moment.

From the hysteresis loop obtained by plotting polarisation against electric field (Figure 2.13), it is evident that the value of the field to apply to have the best polarisation is that corresponding to the spontaneous polarisation (P_S). For values below this, there is only a partial poling of the ceramic leading to lower piezoelectric properties. For higher values there is an increased probability of electrical breakdown.

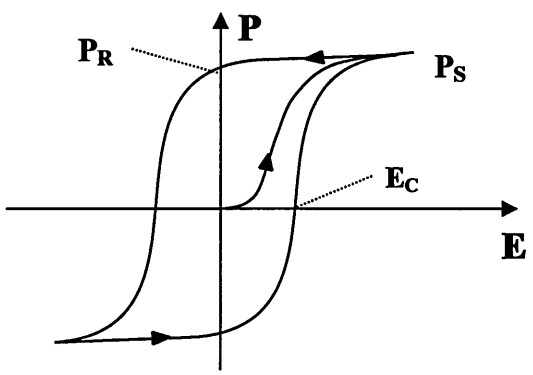

Figure 2.13: Hysteresis loop of a ferroelectric ceramic. E_C=coercive field, P_R=remanent polarisation, P_S=spontaneous polarisation.

In the poling process, the pellet was immersed in a stirred silicon oil bath and heated to 120°C. The voltage was then applied for a fixed time and left on until the system had cooled to room temperature to avoid depoling due to the high temperature. The values of voltage and time at 120°C used are presented in Table 2-V.

System	Voltage (kV/mm)	Time (min)
NBT-BIT-NBT	4	15
BMT	4	30

Table 2-V: Experimental parameters of the poling process.

The complete poling apparatus is shown in Figure 2.14.

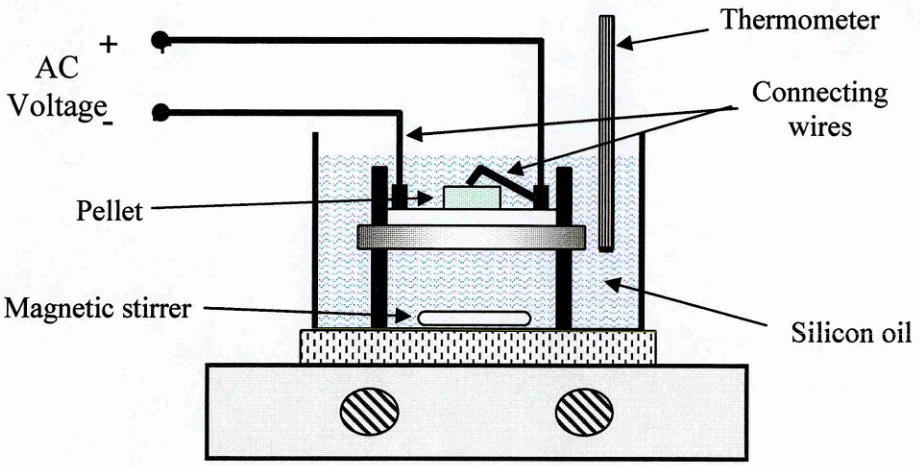

Figure 2.14: Poling apparatus.

2.3.3.2. Hysteresis loop

The hysteresis measurements were performed using an RT 66A Standardised Ferroelectric Test System operating in the virtual ground mode. This mode uses a circuit evolution of the well known Sawyer-Tower circuit of Figure 2.15[152].

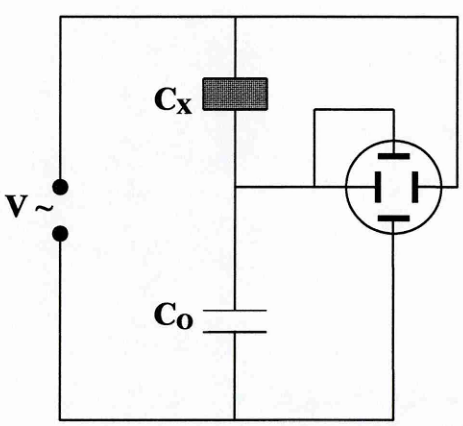

Figure 2.15: Sawyer-Tower circuit.

The voltage lying across the ceramic C_X is put on the horizontal plates of an oscilloscope, plotting in this way a quantity which is proportional to the field lying across the material. The linear capacitor C_0 is connected in series with the crystal,

therefore the voltage across it is proportional to the polarisation of the sample. This voltage is represented on the vertical plates of the oscilloscope.

The virtual ground mode reduces the effect of the parasitic elements present in the Sawyer-Tower arrangement. It measures the charge stored in the ferroelectric sample by integrating the current required to maintain one terminal of the sample at zero volts, hence the term "virtual" ground. The equivalent circuit is shown in Figure 2.16.

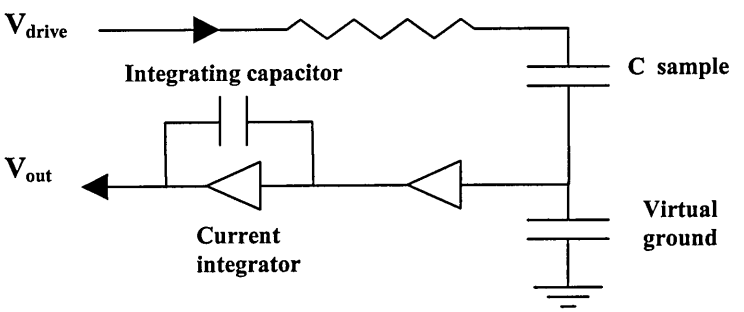

Figure 2.16: Virtual ground mode for ferroelectric hysteresis measurements.

2.3.3.3. Piezoelectric coefficients

The piezoelectric coefficients can be determined through three different sets of experimental conditions:

1. In static conditions;
2. In quasi-static conditions;
3. Under an alternating field (resonance-antiresonance method).

In the following paragraphs all these methods will be briefly analysed.

2.3.3.3.1. Static Conditions

In static conditions, the piezoelectric coefficients are obtained with an electrometer measuring the polarisation charges appearing in a material subjected to a load. The application of a constant stress under conditions of zero electric field can be expressed by Equation 2.4[153].

$$D_i = d_{ip} \cdot T_p \qquad \textbf{Equation 2.4}$$

Where D_i is the dielectric displacement in the direction "i", d_{ip} the piezoelectric coefficient and T_p the stress applied along the "p" direction.
Using a plate-shape sample and considering the application of uniaxial stress perpendicular to the major surfaces, the previous turns into

$$D_3 = d_{33} \cdot T_3 \qquad \textbf{Equation 2.5}$$

This equation shows that applying a simple tensile or compressive stress on the major surfaces of an electroded disc and measuring the voltage produced, it is possible to calculate the value of d_{33}.
The major problems of this technique are:

- Pure uniaxial stress is not easy to ensure, due to friction;
- Some of the charge generated by the application (or removal) of the stress can leak off before the measurement;
- Pyroelectric effect can cause drift as the temperature of the specimen changes.

2.3.3.3.2. Quasistatic Conditions

Alternating signals can eliminate the influence of the pyroelectric effect, so an improvement of the previous technique considers the application of an alternating stress or electric field to the sample. As long as the frequency of the signal applied is less than that of the fundamental resonance frequency of the sample, Equation 2.5 is still valid and the results are more accurate than those obtained with a static technique. The quasistatic principle is applied by the Berlincourt d_{33}-meter, used in this project.

2.3.3.3.3. Resonance-Antiresonance Method

Values of elastic, piezoelectric and dielectric constant can be obtained by analysing the resonance behaviour of a suitably shaped specimen subjected to a sinusoidal electric field. Under these conditions the piezoelectric component changes its dimensions as a function of frequency: that is it vibrates.

In particular, near its mechanical resonance frequency (dependant on its shape, dimension and composition) the amplitude of the oscillation is bigger than in static conditions due to an amplification phenomenon of the oscillations. The last harmonics of the wave just finished is perfectly in phase and of the same sign as the following one: they overlap generating a big amplification of the signal.

As a first approximation the behaviour of a piezoelectric material close to its fundamental resonance can be represented with the circuit in Figure 2.17.

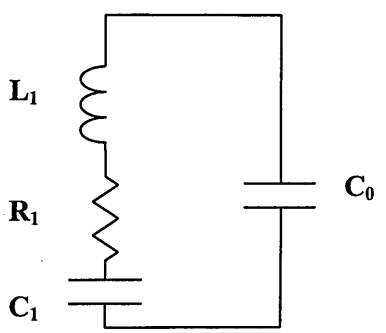

Figure 2.17: Equivalent circuit for a piezoelectric material.

Each element of the circuit represents a quantity characteristic of the material. More precisely, L_1 is the mass of the resonator, C_1 its elasticity, R_1 the mechanical dissipation and C_0 represents the capacity of the piezoelectric material at low frequency.

For two values of characteristic frequencies the reactance of this circuit is zero: they are called the resonance and antiresonance frequency.

The method basically consists of measuring the electrical impedance of the sample as a function of frequency: the values at resonance and antiresonance frequencies allow to resolve the component of the equivalent circuit and (using the appropriate mathematical models) calculate the parameters of the piezoelectric material.

Figure 2.18 reports the characteristic behaviour of log|Z| as a function of frequency for a disk-shape piezoelectric material. The resonance frequency corresponds to the smaller value of log|Z| , whereas the antiresonance is the one for which it is at a maximum.

At low frequency (Figure 2.18A) there is the resonance corresponding to the pure radial mode of the disk. This vibration decreases with frequency and disappears completely for frequencies near 1MHz. In Figure 2.18B can be notice the presence of several overtones of this mode.

For higher values another resonance effect appears due to the thickness mode (Figure 2.18B); the two vibrations are distinct in frequency and do not interfere with each other. This is important as each vibration's mode allows the user to calculate different piezoelectric and elastic coefficients. For this reason the modes must be kept pure.

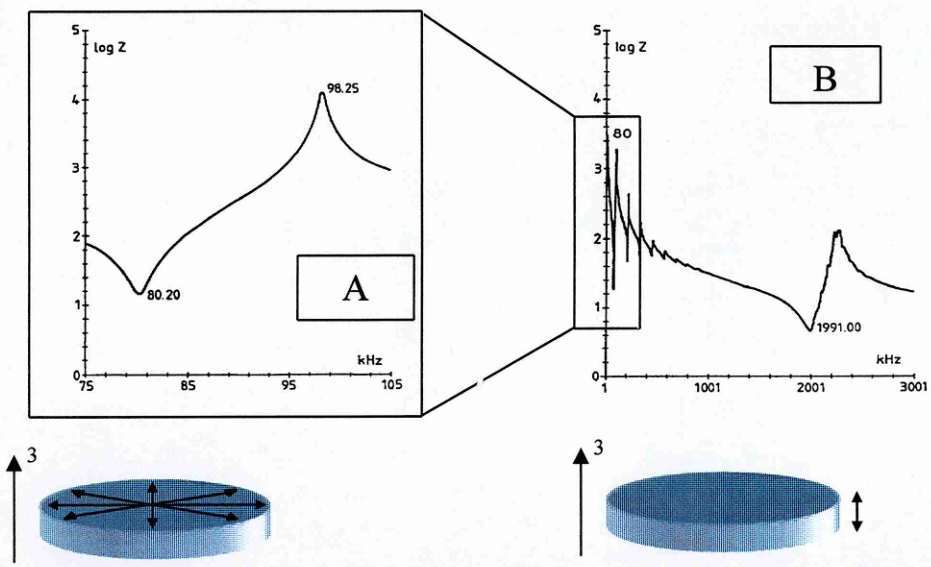

Figure 2.18: Resonance behaviour of a disk-shaped piezoelectric material. A) Detail of the low-frequency radial mode B) complete spectrum of resonance behaviour, at frequency around 2MHz appears the thickness mode of the disk.

The range of frequencies corresponding to the different resonances depends on the mechanical and electrical characteristics of the material and on its geometrical dimensions. In general the values of frequency are inversely proportional to the relative length of the vibration mode considered. For the disc morphology in Figure

2.18, the planar vibration is at lower frequencies than the thickness vibration because it is associated to a longer geometrical dimension.

For a complete characterisation of a piezoelectric ceramic, it is necessary to produce it in different shapes to isolate and enhance the different vibrational modes responsible for all the piezo-elastic coefficients. For a disc-shaped specimen, there are two possible vibration modes: planar and thickness. These two modes provide d_{31}, d_{33}, c^E_{33}, c^E_{13}, σ_p, s^E_{11}, s^E_{12}, k_p, k_{31} and k_t of the material analysed.

Generally the planar mode is the one used for calculations, because it is simpler to interpret. By extrapolating the value of frequency at resonance (fr), antiresonance (fa) and at the resonance for the first overtone ($fr^{(2)}$) it is possible to determine the piezoelectric coefficients using the following set of equations[153]:

$$k_p = \left[2.51 \cdot \frac{f_a - f_r}{f_r} - \left(\frac{f_a - f_r}{f_r} \right)^2 \right]^{\frac{1}{2}} \qquad \textbf{Equation 2.6}$$

$$\sigma_p = 0.35 - \left(\frac{f_r^{(2)}}{f_r} - 2.59625 \right) \cdot 1.4628 \qquad \textbf{Equation 2.7}$$

$$s^E_{11} \cdot \left(1 - \sigma^2_p\right) = \frac{\eta^2_1}{\rho \cdot (2 f_r \pi a)^2} \qquad \textbf{Equation 2.8}$$

where

$$\eta_1 = 2.07951 - \left(\frac{f_r^{(2)}}{f_r} - 2.59625 \right) \cdot 0.89702 \qquad \textbf{Equation 2.9}$$

"a" is the radius of the disk and "σ_p" is the Poisson ratio.

Finally from the following equation

$$k^2_{31} = \frac{k^2_p \left(1 - \sigma_p\right)}{2} \qquad \textbf{Equation 2.10}$$

and remembering the relation between the coupling factor and the piezoelectric coefficient the measure of the "free" dielectric constant (ε^{T}_{33}) at a frequency lower than the one of resonance allows to calculate d_{31} using Equation 2.11.

$$k^2_{31} = \frac{d^2_{31}}{s^E_{11}\varepsilon^T_{33}} \rightarrow d_{31} = k_{31}\sqrt{s^E_{11} \cdot \varepsilon^T_{33}} \qquad \text{Equation 2.11}$$

With this method the complete piezoelectric behaviour can be calculated with reasonable accuracy by measuring only a few of its properties.

A complete structural and electro-piezoelectrical analysis is crucial to study a new material. If the relationships between structure and electrical properties are known, the material can be tailored to match the requirements needed for a specific application by only changing its composition. In the following chapters the results of these studies will be reported and analysed. Particular attention will be paid on obtaining trends in structural-electrical property relations.

3. RESULTS AND DISCUSSION

This section presents the work done and the results are interpreted on the base of the current knowledge. The nature of the project leads naturally to split it into two different sub-sections that consider the main parts of the project:

1. NBT-BIT BT system
2. BMT system

These sections follow an introduction in which preliminary work done on the plates and crucibles used during the project is presented.
These sub-sections can be considered as self-consistent. They will be summarised in the Final Remarks and Future work section where the links and possible implications of these studies will be also presented.

3.1. PRELIMINARY WORK

The mayor problem in the synthesis of bismuth-based ceramics comes from the relatively high vapour pressure and therefore volatilisation of Bi_2O_3 and (in the case of NBT-based materials) Na_2O. The loss of these components changes the stoichiometry of the systems and, consequently, the material properties[154,155]. The phenomenon is well known for $Pb(Ti,Zr)O_3$ ceramics in which the high volatilisation of PbO causes abrupt lowering of density and of piezoelectric properties[156,157,158]. The melting point of the two volatile oxides is comparable (825°C for Bi_2O_3 and 886°C for PbO) and accounts for the similarity in behaviour of the two cations.

The oxides of bismuth and sodium are not only lost in the air but also in the sides of crucibles and plates used in the ceramic synthesis. These oxides can enter the sides of the zirconia or alumina of which the crucibles are generally made. A study using NBT powder on crucibles of these two materials was done to determine the loss due to the "crucible effect". Eight successive calcinations were carried out in the attempt to saturate their crystalline lattice: four at 850°C for 4 hours and four at 1150°C for 4 hours. The NBT powder was renewed after each calcinations and the crucibles carefully weighed before and after each treatment, following a strictly controlled procedure (showed in Table 3.I). The heating program was the one presented in section 2.1.1.2 and each crucible was weighed ten times to ensure reproducible results.

Step	Operation
1	Weigh empty crucible (T_{room})
2	Weigh full crucible (T_{room})
3	Calcination
4	Weigh full crucible after calcination (T_{room})
5	Clean empty crucible (water + ultrasonic bath)
6	Dry empty crucible at 80°C for 2h
7	Cool down to room temperature

Table 3-I: Standard procedure for the saturation of crucibles.

The results of the saturation steps on the weights of the two different crucibles are presented in Figure 3.1.

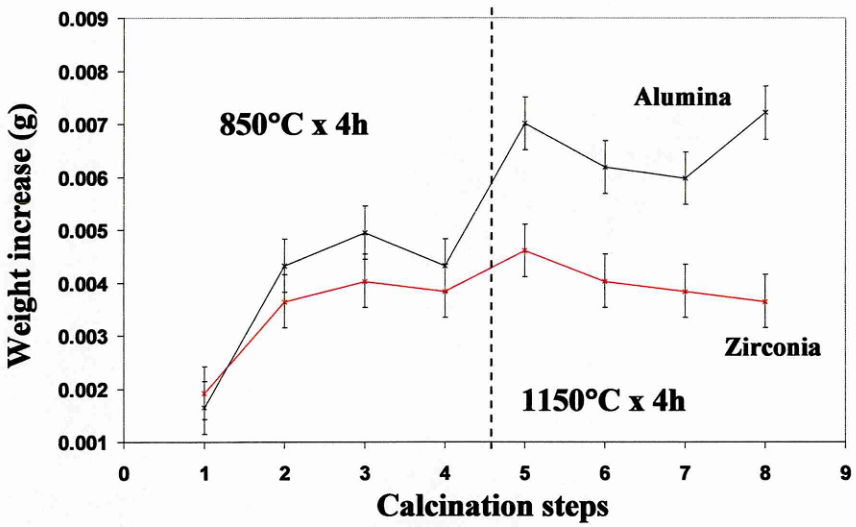

Figure 3.1: Weight increase as a function of the number of calcination steps for an alumina and zirconia crucible. The errors are calculated as standard deviation of ten measurements.

The weight of the alumina crucible is increasing even after five calcinations, whereas the one of zirconia is almost constant. Looking at the data, the zirconia crucible can be considered saturated, whereas the alumina one seems able to accommodate further cations in its lattice. The reactivity of the two materials toward Na_2O can explain this different behaviour. Na_2O can react with Al_2O_3 to form the well known Naβalumina ($NaAlO_2$). In the case of alumina, the cations enter the lattice as interstitial ions and react with the crucible to form a new compound.

The "crucible effect" was analysed also considering its influence on the structure of the NBT powder used for the saturation. In Figure 3.2A and B the diffractograms of the powder calcined in alumina and zirconia crucible as functions of the calcination steps are presented.

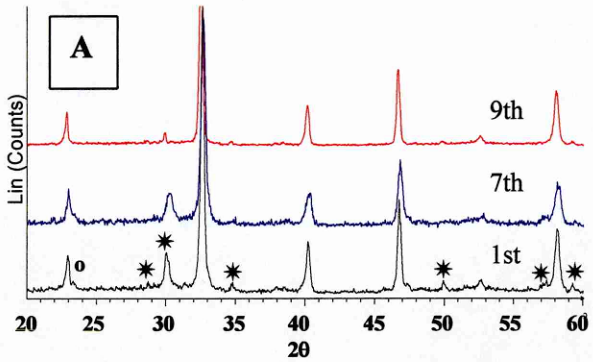

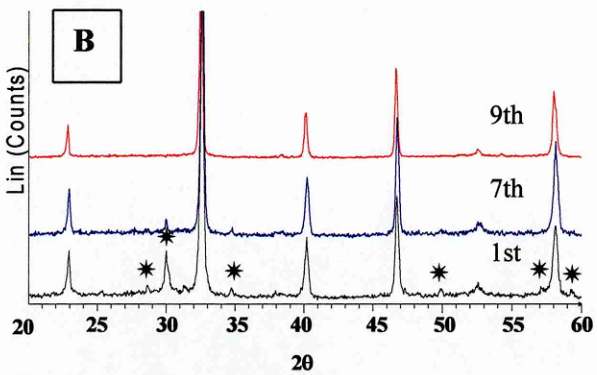

Figure 3.2: Effect of the number of calcination steps on the structure of the calcined NBT. The star indicates the peaks of the parasitic pyrochlore phase whereas the "o" is due to the double-side tape used to mount the powders. A) alumina crucible, B) zirconia crucible.

The patterns show the presence of two phases: NBT and $Bi_2Ti_2O_7$ (a pyrochlore phase that is formed in deficiency of sodium). The NBT powder calcined in zirconia crucible (conditioned with eight calcinations) does not present any secondary phase. In the powder calcined in alumina crucible the intensity of the strongest peak (4 4 4) of $Bi_2Ti_2O_7$, is reduced by 61%, but still present. These data show that conditioning the crucibles and using zirconia instead of alumina prevents the appearance of second phases due to the evaporation of bismuth and sodium oxides.

Following these results only zirconia crucibles and plates were used in this project. Each of them was saturated with nine calcination treatments of 1150°C for 4 hours. Two different sets of equipment were used. One (saturated with NBT powder) was used to produce ceramics containing sodium; the other (saturated with BIT powder) was used for all the systems in which sodium was not present (such as the BMT or the BIT-BT series). The use of zirconia tools requires a careful design of the heating and cooling programs. Zirconia is well known to be sensitive to thermal shock. Its monoclinic crystal structure changes above 950°C to tetragonal with a corresponding shrinkage of greater than one percent. The heating and cooling programs for

calcination and sintering must take this change into account. Hence the rates of increasing or decreasing of temperature were set reasonably slow to avoid any risk of thermal shock.

3.2. $Na_{1/2}Bi_{1/2}TiO_3 - Bi_4Ti_3O_{12} - BaTiO_3$ System

3.2.1. STRUCTURAL ANALYSIS

3.2.1.1. Powder Synthesis and Characterisation

In general, the analysis of a phase diagram implies that all the various compositions considered must be synthesised at the same values of temperature and pressure. The choice of the temperature and time of calcination is then crucial: if it is too low it would result in incomplete reaction while if it is too high it would cause excessive loss of bismuth and sodium.

A very broad range of temperatures and times have been used in the literature to synthesise the compounds belonging to the Aurivillius family. Even for the same compound, several sets of conditions are available as shown in Table 3.II for $SrBi_4Ti_4O_{15}$.

Temperature (°C)	Time at maximum temperature (h)
900[159]	4
850[160]	24
800[161]	2
1000[162]	2

Table 3-II: Calcination conditions found in the literature for $SrBi_4Ti_4O_{15}$.

The phase diagram for this system describes several kinds of compounds that potentially need a very broad range of temperatures and dwell times to be formed. The need to explore the possibility of new compounds in the system leads the choice of temperature and dwelling time high enough to ensure their formation.

A first set of calcinations were carried out at 850°C for four hours on compositions of the BIT-NBT and BIT-BT series. These conditions are, on average, the most quoted in the literature to make ceramics of the Aurivillius family. The two series were chosen to test the efficiency of the calcination parameters. In the $Bi_4Ti_3O_{12}$-

$Na_{1/2}Bi_{1/2}TiO_3$-$BaTiO_3$ system only the compounds of these series have been previously studied. However this has not been done in a systematic manner. If the chosen temperature and dwell time are the right ones, they should be able to promote the formation of, at least, the compounds already known.

In Figure 3.3 the X-ray diffractograms of the compounds of the NBT-BIT series are shown.

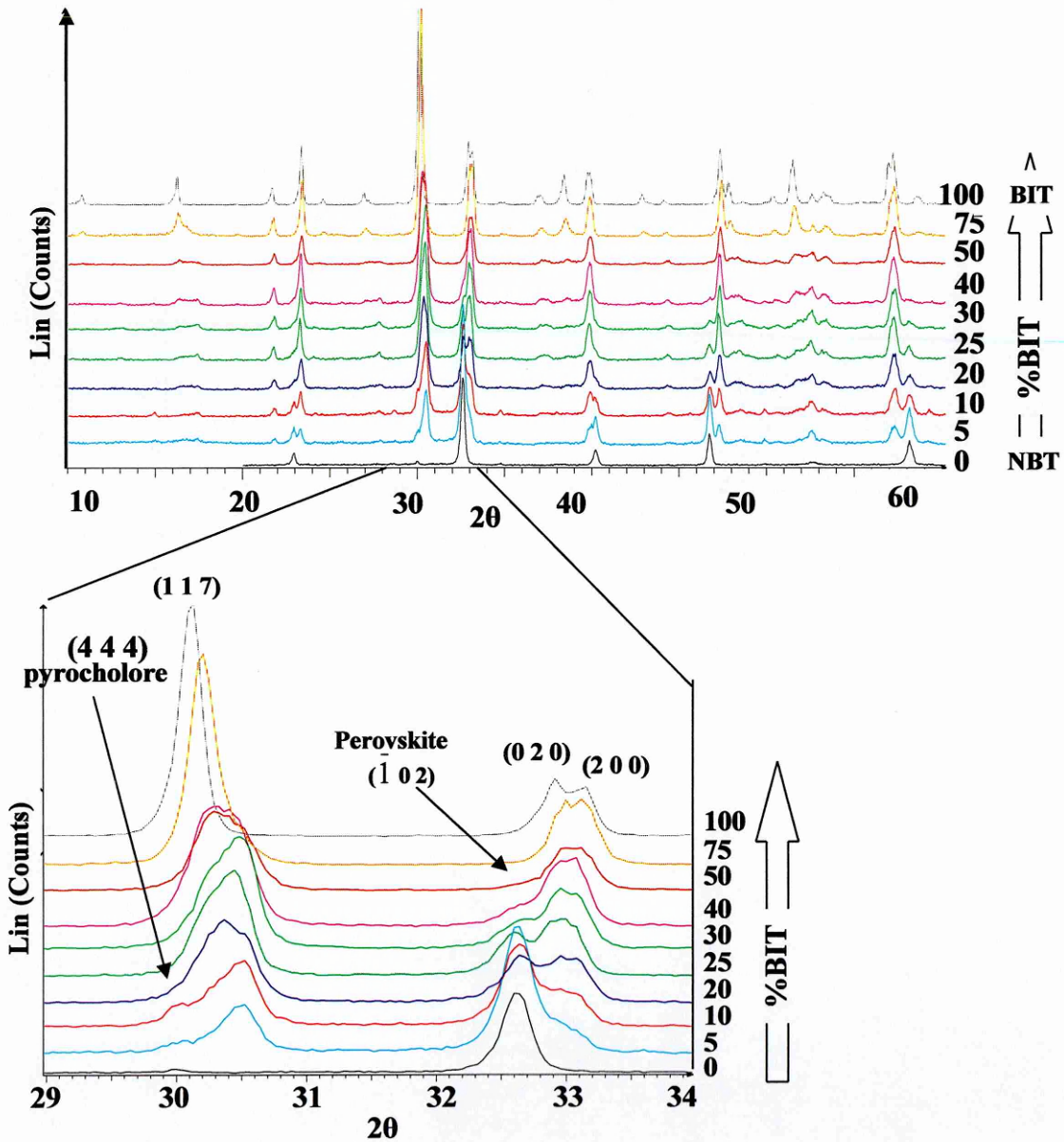

Figure 3.3: XRD analyses of compounds of the NBT-BIT series calcined at 850 C for 4h. In the inset is highlighted that NBT starts to be present at 50%mol in BIT.

The inset in the figure clarifies the evolution of the series for an increasing amount of perovskite end member. NBT already starts to appear at 50% in BIT and is present

throughout the rest of the series. It is interesting to notice that at high concentrations of sodium bismuth titanate there is also pyrocholore present, probably due to the dissociation of part of the NBT. The composition at which NBT starts to appear (50BIT, $Na_{0.5}Bi_{4.5}Ti_4O_{15}$, m=4) is one of the two known in this series and clearly is not obtainable as a pure phase with the calcination conditions used. Figure 3.4 shows that at 850°C the expected m=4 compound coexists with BIT.

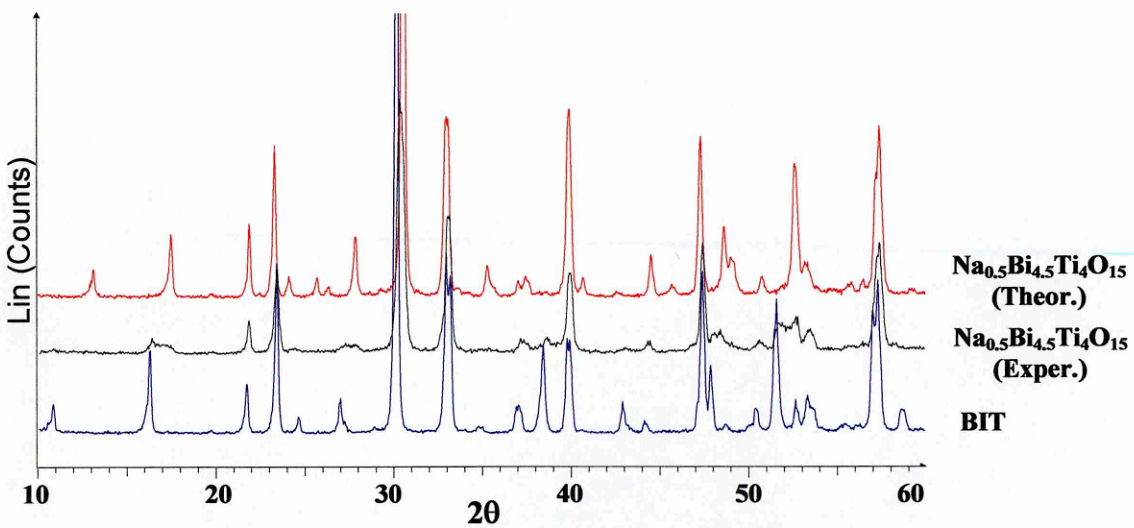

Figure 3.4: Comparison between the X-ray diffractograms of $Na_{0.5}Bi_{4.5}Ti_4O_{15}$ obtained at 850C for 4 h, (Exper.), its expected structure (Theor.), and BIT.

All the compounds made in this series were mixed phase with different proportions of $Na_{0.5}Bi_{4.5}Ti_4O_{15}$ and $Bi_4Ti_3O_{12}$. No pure compounds, other than BIT, can be detected in the series.

The situation is even worse when the BT-BIT series is considered (Figure 3.5).

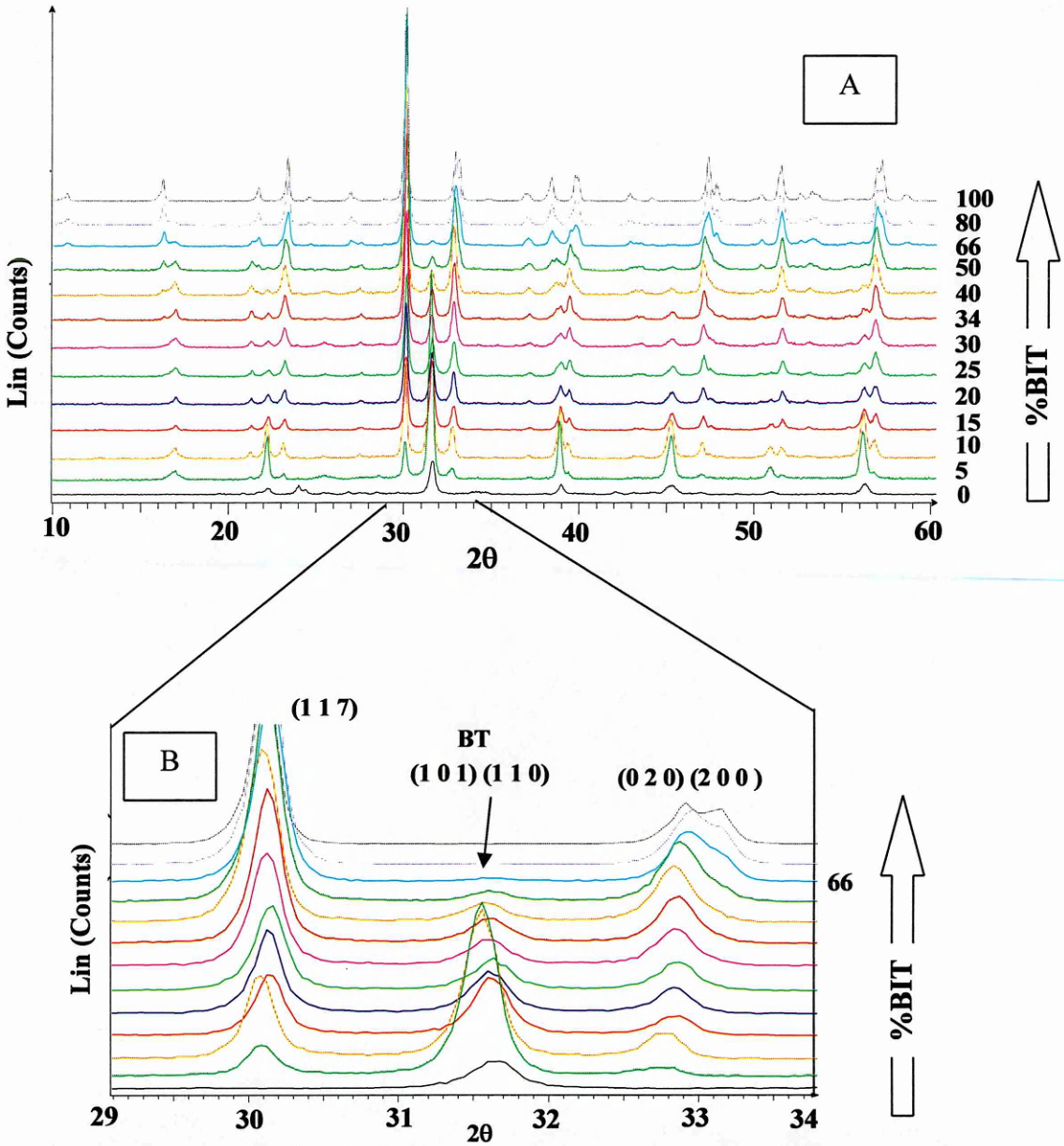

Figure 3.5: XRD analyses of the compounds of the BT-BIT series calcined at 850C for 4h (A) Detail of the XRD analyses that shows that the perovskite end-member starts to appear at 66%mol in BIT (B).

The perovskite end member starts to appear at a concentration of 66%mol BIT (Figure 3.5B) all the compounds in this series are mixtures as in the NBT-BIT series. Three compounds have been previously identified in the BIT-BT system. They correspond to the compositions 66BITBT ($Ba_2BiTi_7O_{27}$, m=3.5), 50BITBT ($BaBi_4Ti_4O_{15}$, m=4) and 34BITBT ($Ba_2Bi_4Ti_5O_{18}$, m=5) and their diffractograms are shown in more detail

in Figure 3.6, Figure 3.7 and Figure 3.8. None of these compounds (labelled in light blue) presents the structure expected from the literature data.

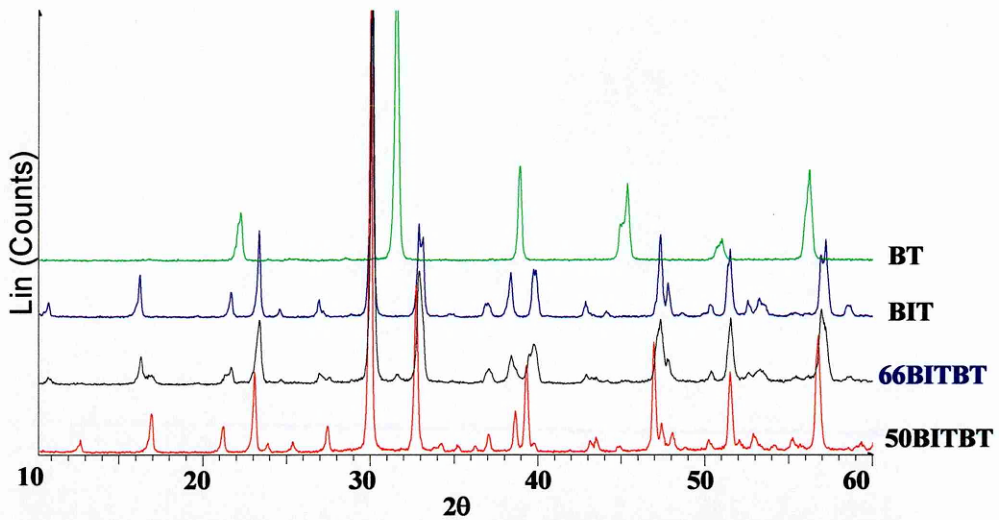

Figure 3.6: Comparison of the XRD analyses of $BaBi_8Ti_7O_{27}$ (66BITBT) at 850C x 4h, BIT, BT and 50BITBT (m=4). The diffractogram of 66BITBT is clearly formed by a mixture of BIT, BT and 50BITBT.

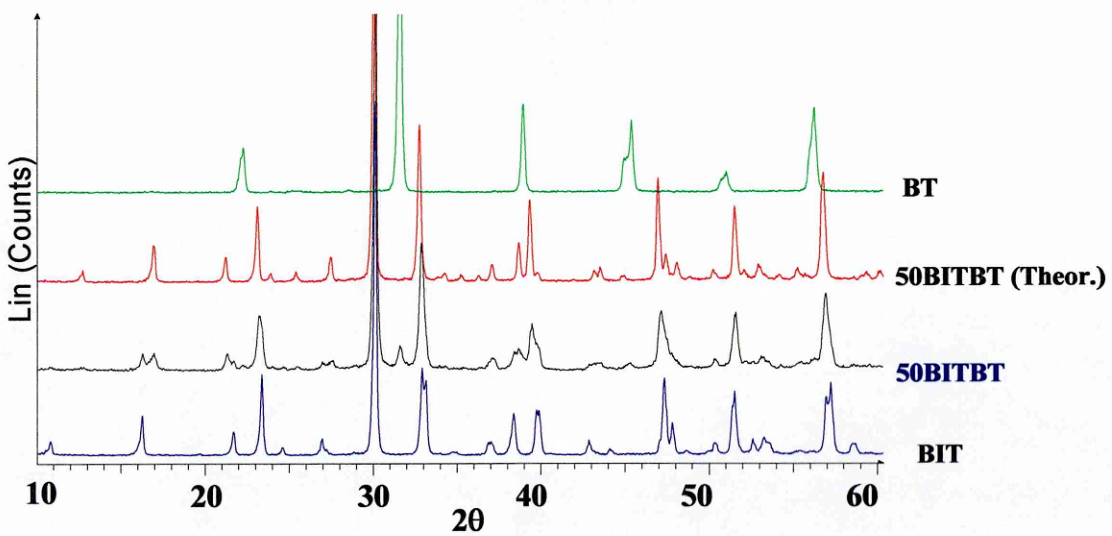

Figure 3.7: XRD analysis of $BaBi_4Ti_4O_{15}$ (50BITBT) calcined at 850C for 4h. The diffractogram is compared with the one expected (50BITBT(Theor.)) and those of BIT and BT. All these phases are present in the diffractogram of 50BITBT.

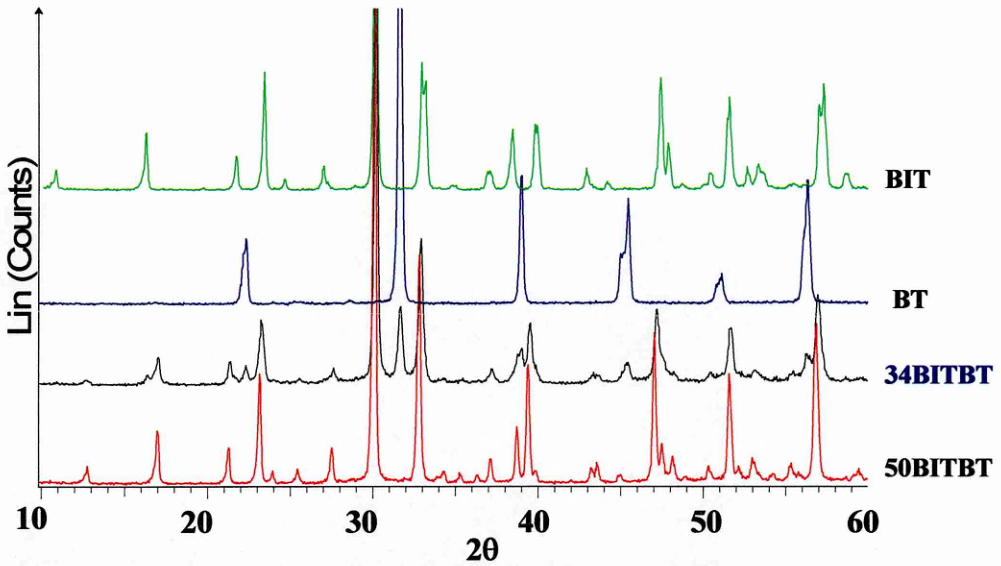

Figure 3.8: XRD analysis of $Ba_2Bi_4Ti_5O_{18}$ calcined at 850C for 4h. The diffractogram is compared with the ones of BIT, BT and 50BITBT. Also in this case the system is formed by a mixture of Bi_4Ti_3O12, $BaTiO_3$ and $BaBi_4Ti_4O_{15}$.

The diffraction analyses reveal that all the compositions are formed by a mixture of BIT, the m=4 compound of the series ($BaBi_4Ti_4O_{15}$) and barium titanate. The amount of barium titanate second phase, increases with the number of perovskite blocks as expected by stoichiometry. The calcination conditions are not strong enough to obtain barium titanate, as shown in Figure 3.9. The figure shows that, in the diffractogram of BT, the raw materials are still present.

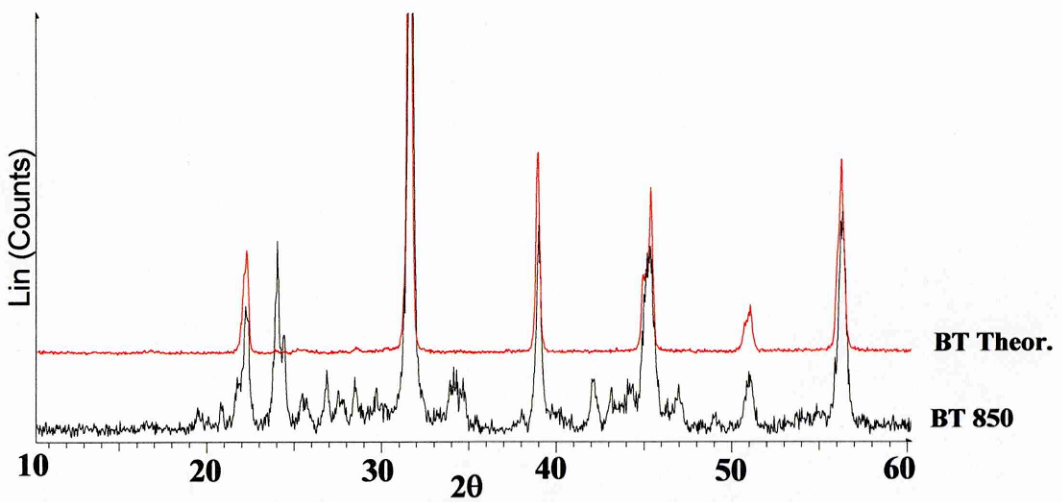

Figure 3.9: Diffractogram of BT calcined at 850C for 4h. compared with the one expected for barium titanate (BT Theor). The extra peaks in the difractogram below are due to residual of the raw materials.

The previous analyses showed that the conditions that have been chosen initially, although consistent with the one in literature, are inadequate to study the NBT-BIT-BT system as a whole. A further attempt at 950°C for 4h reduced the presence of the perovskite partner in the various compositions, but did not lead to the formation of pure compounds. Finally it was decided to calcine the powder at 1150°C for 4 hours. The major concern in using such a high temperature was the increased loss of Bi and Na from the powder. To limit as much as possible the problem, the arrangement of Figure 2.2 was designed. In principle, these severe conditions, should assure the driving force for the formation of all the possible compounds in the phase diagram, including the intergrowth ones that are generally more refractory and difficult to synthesise.

The XRD analyses on the known compositions of the system obtained at 1150°C for 4 hours revealed that they are all pure phases (Figure 3.10), and their structures are consistent with the ones found in literature.

The absence of $Bi_2Ti_2O_7$ indicates that the assembly used to calcine the powders, in conjunction with the saturation of the crucibles and plates used, effectively balance the evaporation of Na_2O and Bi_2O_3. The weight loss from the powders was measured to be below 1% in all the systems considered, confirming the previous assertion.

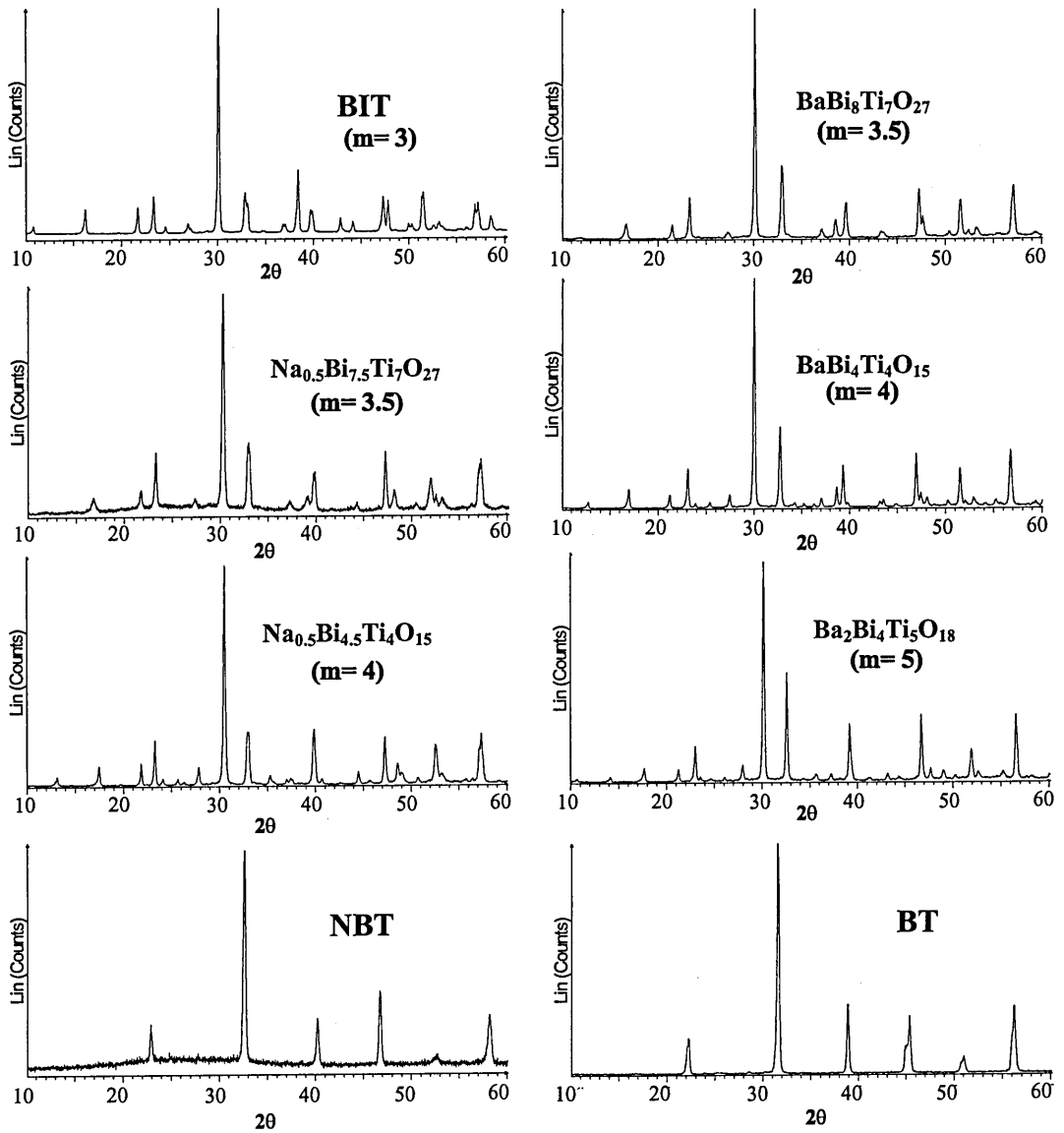

Figure 3.10: Diffractograms of all the known compounds of the BIT-BT-NBT system. They show that all the compounds are obtained as pure phases. These structures are consistent with those of the literature.

3.2.1.2. Powder Morphology

The SEM pictures taken of the powders show the plate-like morphology typical of the Aurivillius compounds as shown in Figure 3.11 for $BaBi_4Ti_4O_{15}$. The inset shows also that the severe calcination conditions promote the pre-sintering of the particles. This phenomenon could influence the subsequent steps of any ceramic production, leading

to low density samples with poorer electrical and piezoelectric properties than those generally found in the literature.

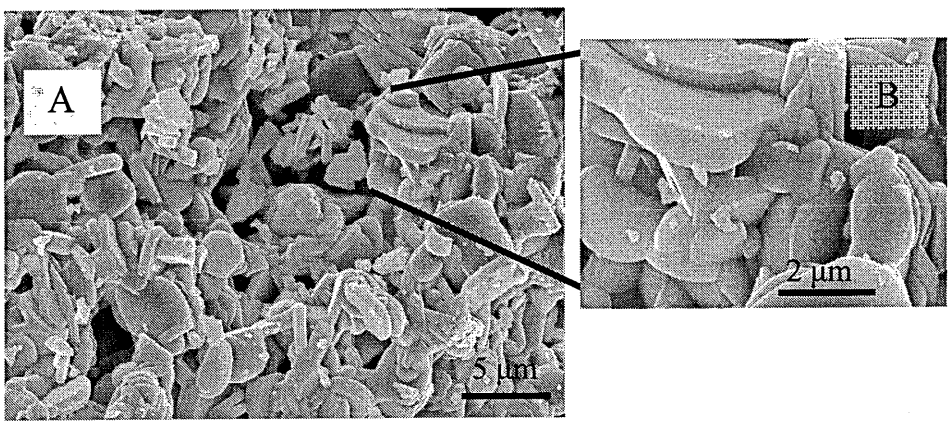

Figure 3.11: SEM micrographs for $BaBi_4Ti_4O_{15}$. In A) the platelike morphology of the powder is presented. The severe calcination conditions lead to strong pre-sintering of the particles (B).

The effect of the calcination temperature is particularly drastic in the case of BIT. Figure 3.12 shows that the temperature is so high as to promote both sintering and abnormal grain growth, resulting in particle of more than 60µm.

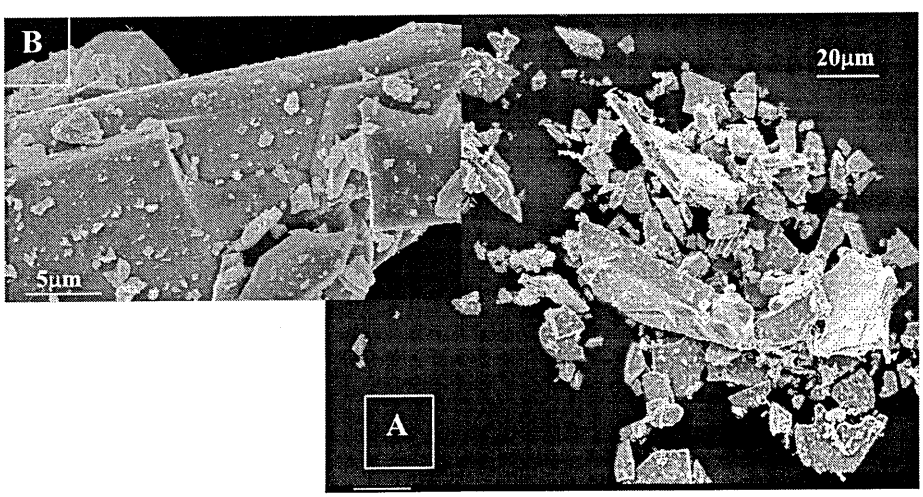

Figure 3.12: SEM micrograph for BIT. A) The calcine conditions lead to strong pre-sintering of the particles and abnormal particle growth (B).

The Aurivillius compounds' morphology differs strongly from that of a typical perovskite compound such as barium titanate (Figure 3.13) and makes it easy to differentiate between the two different types of phase.

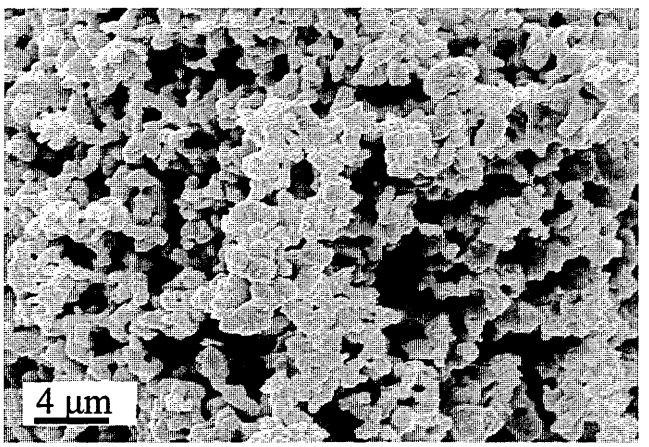

Figure 3.13: SEM micrograph of barium titanate. The morphology of the powder is extremely different from the one of the Aurivillius compounds.

For this reason, SEM analysis was a useful tool, complementary to XRD analysis, to detect the presence of second phases. In Figure 3.14 is presented an example in which the presence of the two different type of compound can be seen easily.

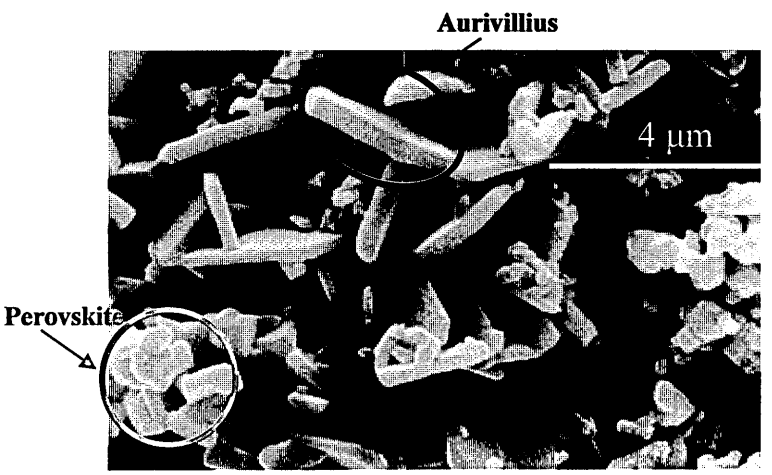

Figure 3.14: The difference in morphology between perovskite and Aurivillius compounds makes it easy to spot mixtures of the two from SEM micrographs.

Generally the number of perovskite blocks (m) does not influence the morphology of the powders, although m influences the c-parameters of the unit cells of the

compounds. The pictures of the compounds belonging to the BIT-BT series presented in Figure 3.15 show, in fact, no appreciable difference in morphology or particle size.

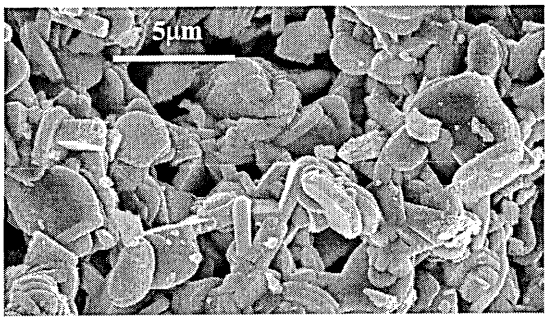

$BaBi_8Ti_7O_{27}$
(m=3.5)

$BaBi_4Ti_4O_{15}$
(m=4)

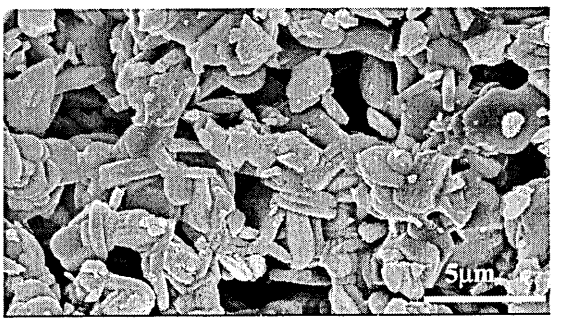

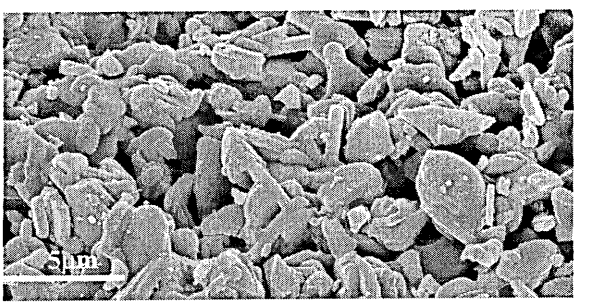

$Ba_2Bi_4Ti_5O_{18}$
(m=5)

Figure 3.15: SEM micrographs of the pure phases in the BT-BIT system. There is no appreciable difference in morphology or dimension of the particles among the three.

On the other hand, there is a distinct difference between compounds belonging to the BIT-NBT series and the one of the BIT-BT series. It is worth remembering that the compounds of barium require higher calcination temperatures and therefore are less affected by pre-sintering and grain-growth processes. The different behaviour can be clearly seen comparing the micrographs of the two compounds with m=4 (Figure 3.16).

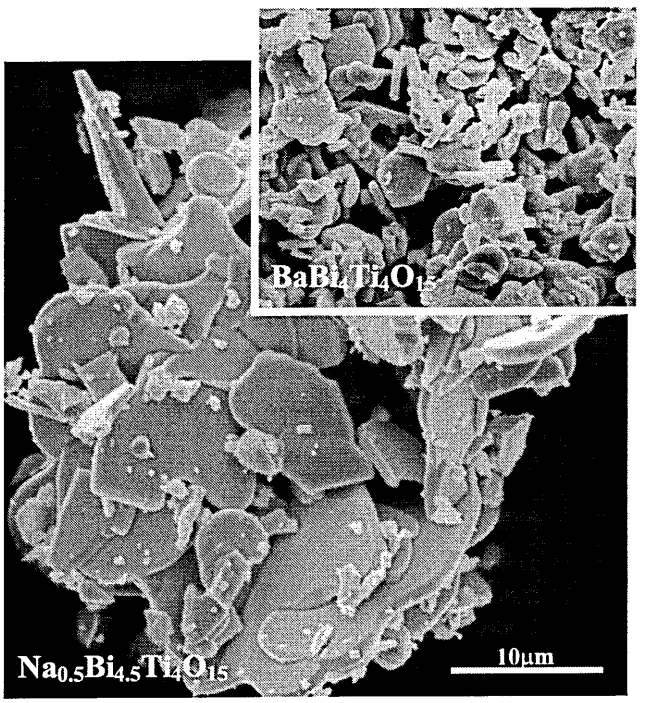

Figure 3.16: Comparison between the particles of $Na_{0.5}Bi_{4.5}Ti_4O_{15}$ and $BaBi_4Ti_4O_{15}$. Both compounds are m=4. The magnification is the same for both micrographs and highlights the big difference in particle size between them.

The particles of $Na_{0.5}Bi_{4.5}Ti_4O_{15}$ are considerably bigger than the ones of $BaBi_4Ti_4O_{15}$ (in the inset). The compounds of NBT are more sensitive to the temperature as can be seen from the SEM of the m=5 compounds (Figure 3.17). The progressive increase in NBT causes a corresponding increase in the particle size of the system under analysis (in this case $(1-x)Ba_2Bi_4Ti_5O_{18} + xNa_{0.5}Bi_{0.5}TiO_3$).

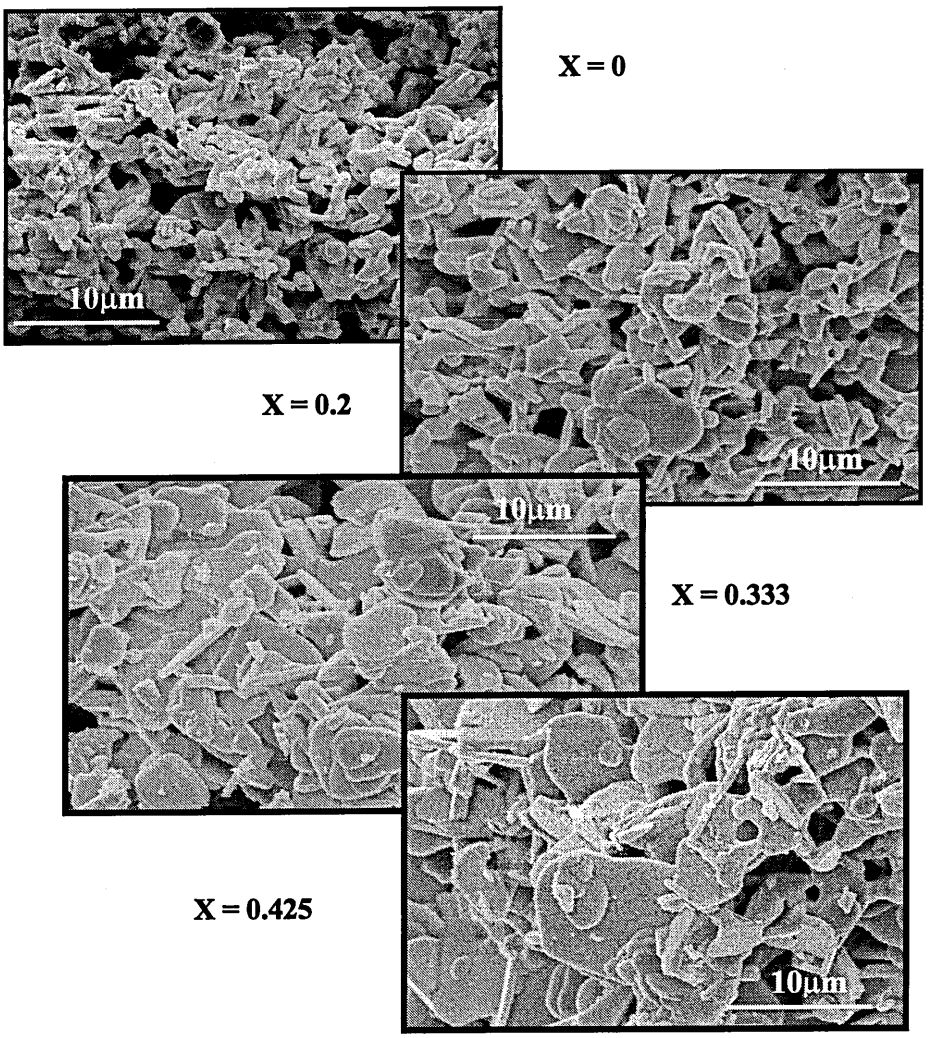

Figure 3.17: SEM micrographs of the m=5 series. The particle size increases with x as consequence of the low calcination temperature needed for NBT compounds.

3.2.1.3. Mechanism of formation of Aurivillius compounds

The analysis of the diffractograms as a function of temperature of calcination (850°, 950° and 1150°C) has suggested a mechanism for the formation of the Aurivillius compounds. Each compound of the family is a multistep process that starts with the formation of BIT and the perovskite end-member that then react together at higher temperatures to give the expected Aurivillius compound. The mechanism is shown as following for $BaBi_4Ti_4O_{15}$ (m=4).

1. $2Bi_2O_3 + 4TiO_2 + BaO \rightarrow Bi_4Ti_3O_{12} + BaTiO_3$

Figure 3.7 showed the diffractogram of the system calcined at 850°C. The system is composed by BIT, BT and $BaBi_4Ti_4O_{15}$. At this temperature the two end members previously formed have already start to react to form $BaBi_4Ti_4O_{15}$.

2. $Bi_4Ti_3O_{12} + BaTiO_3 \rightarrow BaBi_4Ti_4O_{15}$

Figure 3.10 showed the same raw materials calcined at 1150°C. At this temperature $BaBi_4Ti_4O_{15}$ is completely formed.

A similar mechanism has been proposed by Lu et al.[154] for the formation of $SrBi_4Ti_4O_{15}$.

In the case of compounds with m=5 (like $Ba_2Bi_4Ti_5O_{18}$ for instance) the process requires an additional step in which $BaBi_4Ti_4O_{15}$ reacts with another molecule of barium titanate to form the final compounds.

1. $2Bi_2O_3 + 2BaO + 5TiO_2 \rightarrow Bi_4Ti_3O_{12} + 2BaTiO_3$
2. $Bi_4Ti_3O_{12} + 2BaTiO_3 \rightarrow BaBi_4Ti_4O_{15} + BaTiO_3$
3. $BaBi_4Ti_4O_{15} + BaTiO_3 \rightarrow Ba_2Bi_4Ti_5O_{18}$

For a generic compound of m perovskite blocks, the proposed mechanism forecasts n+1 steps (where n is the number of perovskite end member moles necessary for stoichiometry, i.e. n = m-3). First BIT and the perovskite end member are formed. In the following step the molecules of $ATiO_3$ (where A is a 2+ cation or a combination of cations to give 2+ valence) are progressively consumed to give Aurivillius compounds of increasing number of perovskite blocks. The entire process is presented in the following sequence.

1. $2Bi_2O_3 + (3+n)TiO_2 + nAO \rightarrow Bi_4Ti_3O_{12} + nATiO_3$
2. $Bi_4Ti_3O_{12} + nATiO_3 \rightarrow ABi_4Ti_4O_{15} + (n-1)ATiO_3$
3. $ABi_4Ti_4O_{15} + (n-1)ATiO3 \rightarrow A_2Bi_4Ti_5O_{18} + (n-2)ATiO_3$

.....

n+1. $A_{n-1}Bi_4Ti_{(2+n)}O_{(9+3n)} + ATiO_3 \rightarrow A_nBi_4Ti_{(3+n)}O_{(12+3n)}$

It is clear that compounds with a high number of perovskite blocks require a higher number of formation steps and, as a consequence, higher calcination temperature. With this in mind it is possible to explain also the low reactivity of intergrowth compounds. $BaBi_8Ti_7O_{27}$ (m= 3.5) for example is the result of the intergrowth of BIT and $BaBi_4Ti_4O_{15}$. Following the previous mechanism, first the two parent compounds are formed which then react together to form the intergrowth at higher temperature.
This mechanism suggests also that the temperature chosen for the calcination could not be high enough to promote the formation of compound with more than five perovskite blocks. However the DTA analysis on one compound of the series (30BIT, Figure 3.18) shows that at temperature around 1175°C it starts to melt. Temperatures higher than 1150°C are therefore not possible for this system.

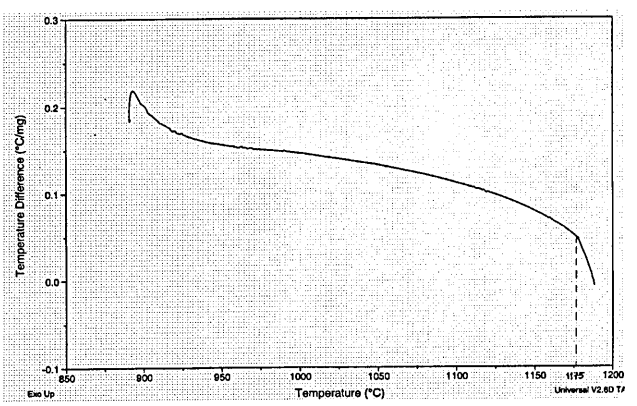

Figure 3.18: DTA analysis for 30BIT. The compound starts to melt at around 1175 C. Calcination temperatures higher than this value are therefore not possible for the NBT-BIT-BT system.

3.2.1.4. Phase Diagram

Based on the previous results on the NBT-BIT and BT-BIT series, the powders of all the successive compositions were calcined at 1150°C for 4 hours.
At this point it is important to stress the crucial role played by the low angle analyses on the study of the phase diagram. These analyses were essential to determine the nature and number of the compounds involved. In the region below $2\theta = 20°$, the only peaks present are the ones from the (0 0 ℓ)-type planes of the Aurivillius-type

structure. These reflections can be considered to provide the fingerprints of the phase present. The structures of these layer compounds differ primarily in the thicknesses of the perovskite blocks and consequently in the c-parameter of the cell. For this reason, although the diffractograms of these compounds can be quite complex overall, the analysis of the low angle region (0-20° of 2θ) is relatively easy and gives unequivocal identification of the phase present. So, while the wide angle diffractogram (5-60°) was necessary to verify the presence of a perovskite phase, the scan between 2 and 20° allowed the determination of the nature and number of Aurivillius phases in the system under analysis. The situation can be clearly understood from the example given in Figure 3.19. This refers to the evolution of $BaBi_4Ti_4O_{15}$ (m=4) when an increasing amount of $Na_{1/2}Bi_{1/2}TiO_3$ (NBT) is added. The wide scan (A) shows the presence of a perovskite, but is not enough to identify the Aurivillius compounds present. The scan between 2 and 20° (B) clearly shows the presence of a mixture of Aurivillius phases with m=4 and m=5. In this case, the low-angle analysis showed how an increasing amount of NBT causes the appearance of a second phase corresponding to m=5 (♣) that becomes predominant at the end of the series, where the amount of NBT is 80%mol.

Sometimes, the (0 0 ℓ) peaks are so weak that even the 2-20° scan did not allow the complete identification of the phases present. In these cases a scan between 5 and 15° was essential. Figure 3.20 are shows the diffractograms of the region near $Bi_4Ti_3O_{12}$, taken between 2 and 20° (A) and the successive refinement between 5 and 15° (B). Although the first scan gives an idea of the situation, the nature of the Aurivillius compounds is unequivocally clarified only in (B): a narrower scan range highlights how the system passes through the formation of compounds and mixtures of compounds with increasing values of m for increasing amounts of perovskite.

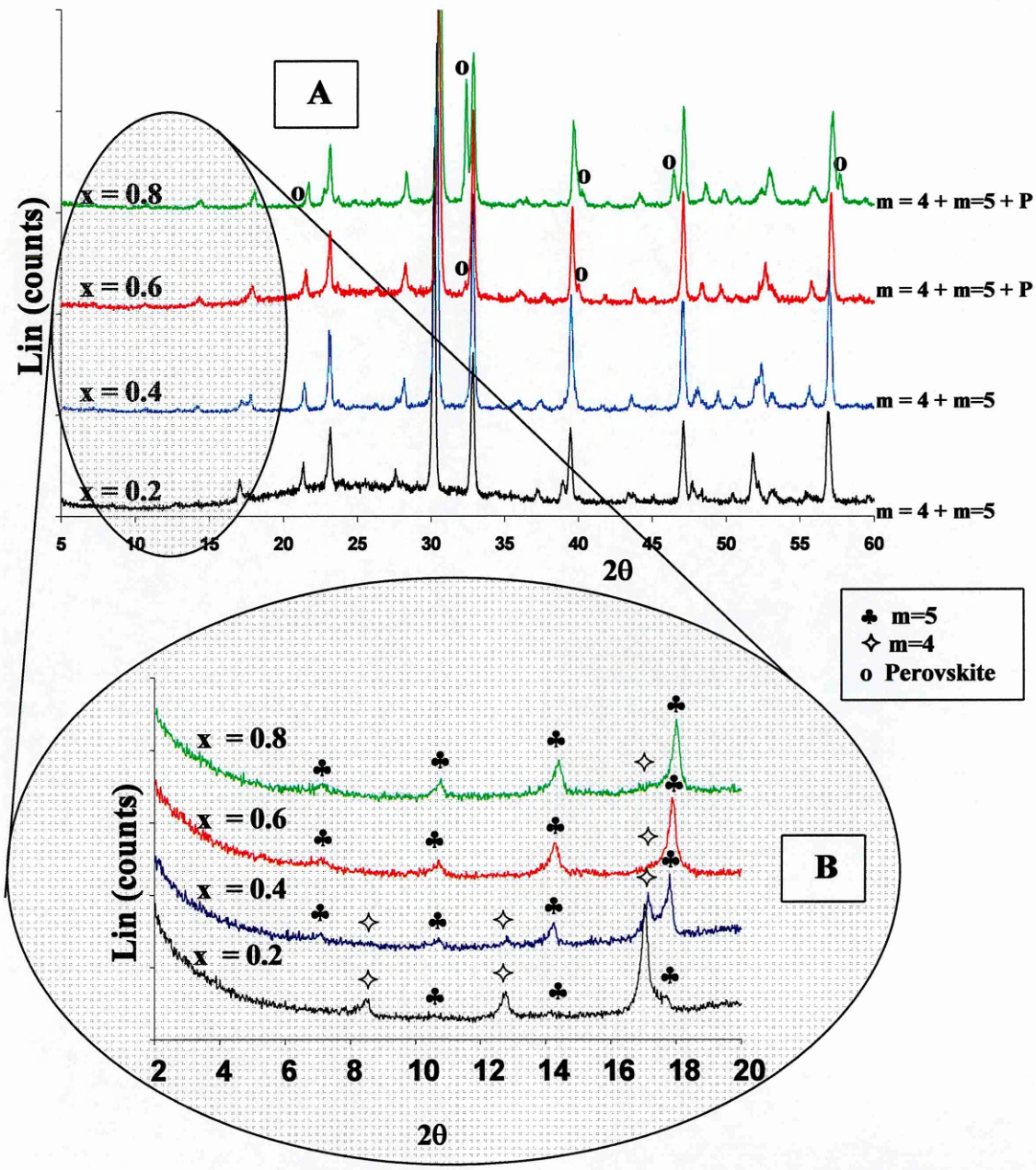

Figure 3.19: Importance of low angle XRD scan to identify Aurivillius compounds. The diffractograms are the ones of the (1-x)$BaBi_4Ti_4O_{15}$ - x $Na_{0.5}Bi_{0.5}TiO_3$ system. The wide scan (A) shows the presence of perovskite second phase (P) but is unable to specify the nature of the layer compounds present. The low angle analysis (B) shows the exact number and nature of these compounds in each of the spectra.

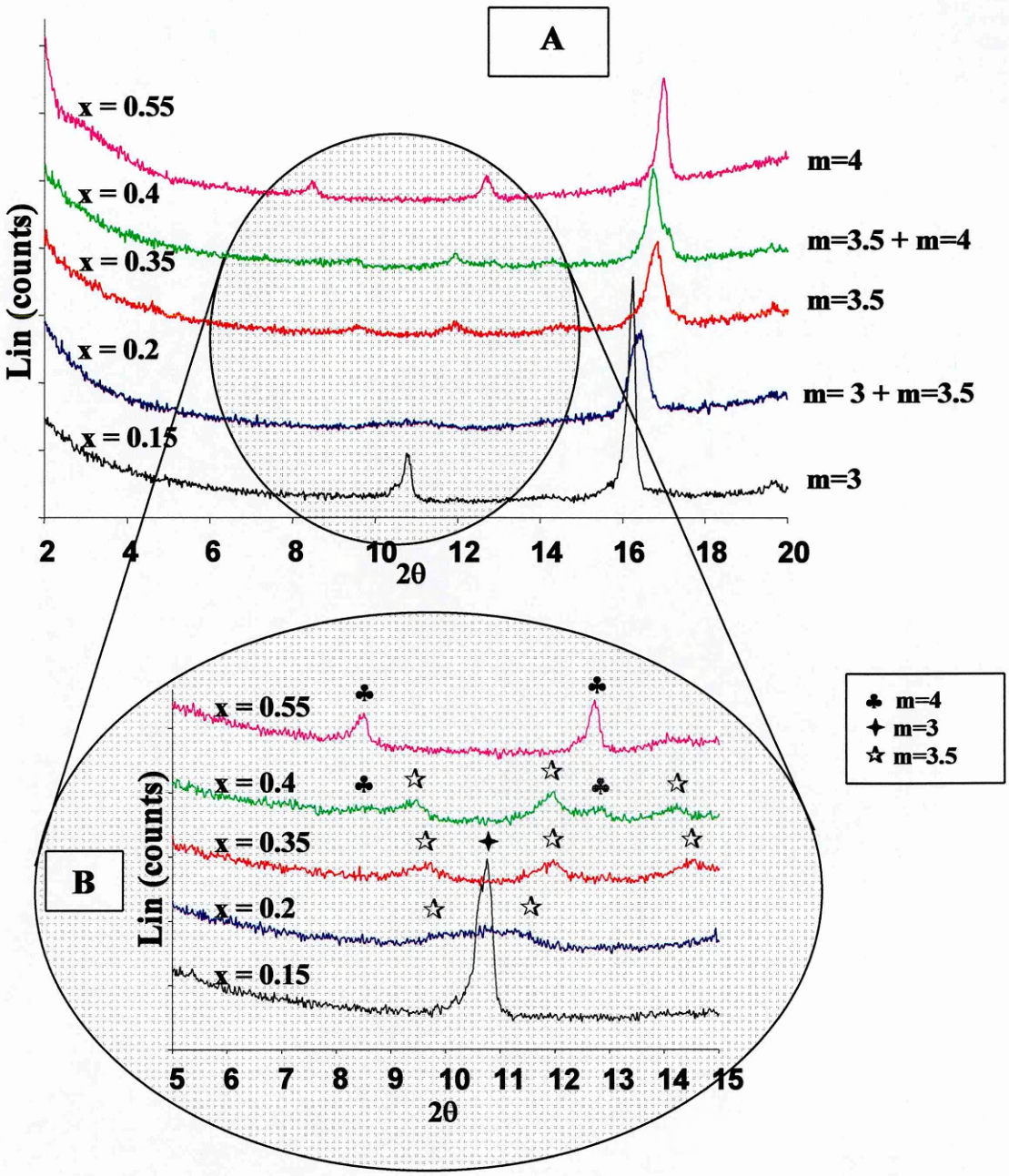

Figure 3.20: Importance of the 5-15° scan for the study of the NBT-BIT-BT phase diagram. Although the 2-20 scan (A) gives information about the structure of compounds involved, the refinement between 5 and 15 (B) allows their exact identification. The diffractograms are the ones of the (1-x)$Bi_4Ti_3O_{12}$ – x$(Na_{0.25}Ba_{0.5}Bi_{0.25})TiO_3$ series.

The systematic XRD analyses of the 85 different compositions made led to the sketch of the possible phase diagram of Figure 3.21.

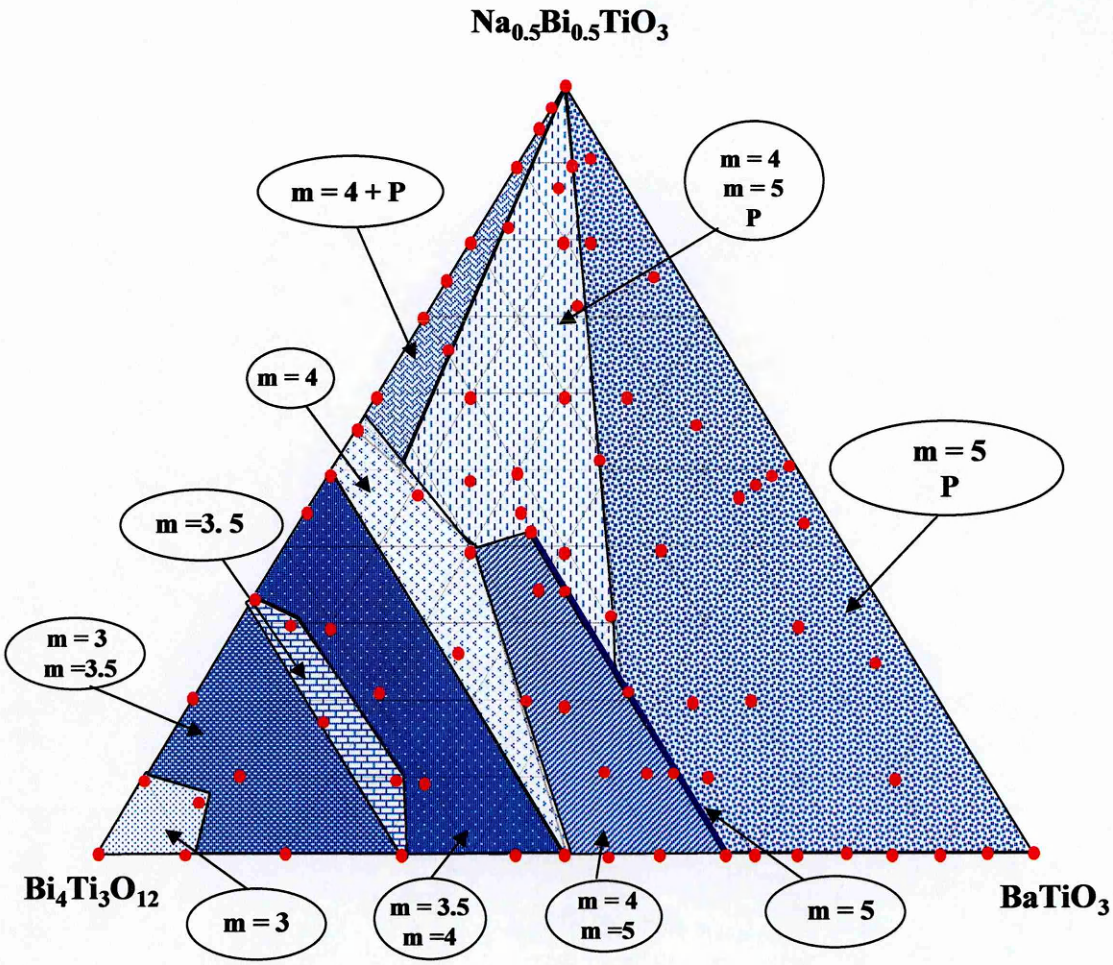

Figure 3.21: Final Phase Diagram of the NBT-BIT-BT system. P = perovskite, m = number of perovskite blocks of the Aurivillius phase present. The red dots represent the systems analysed.

The system is characterised by several multiphase regions. The perovskite structures start to appear at values of $BaTiO_3$ > 65%mol and $Bi_{1/2}Na_{1/2}TiO_3$ > 50%mol. Below these values only Aurivillius compounds are present. No compounds with more than m=5 were found. As expected, adding a perovskite (BT or NBT, m=∞) to an Aurivillius compound with m=3 (BIT) leads to the formation of compounds with increased values of m. Addition of $BaTiO_3$ results in a structure that is more versatile and able to form compounds with more perovskite blocks than $Na_{1/2}Bi_{1/2}TiO_3$.

Pure perovskite structures were obtained only along the NBT-BT line: when a layer compound (even at low concentration) is added to the system, it is rejected, forming a second phase. The possibility of obtaining pure perovskite compounds away from the

stoichiometric compositions of BT and NBT was tested, in particular making three compositions close to the pure perovskite line:

1) 2%mol of BIT in NBT;
2) 2%mol of BIT in BT;
3) 2%mol of BIT in the perovskite formed by 50%mol NBT and 50%mol BT.

The diffractograms are shown in Figures 3.22A), B) and C) respectively. Each spectrum is compared respectively to the one of a pure perovskite and with the Aurivillius compound most likely to be present.

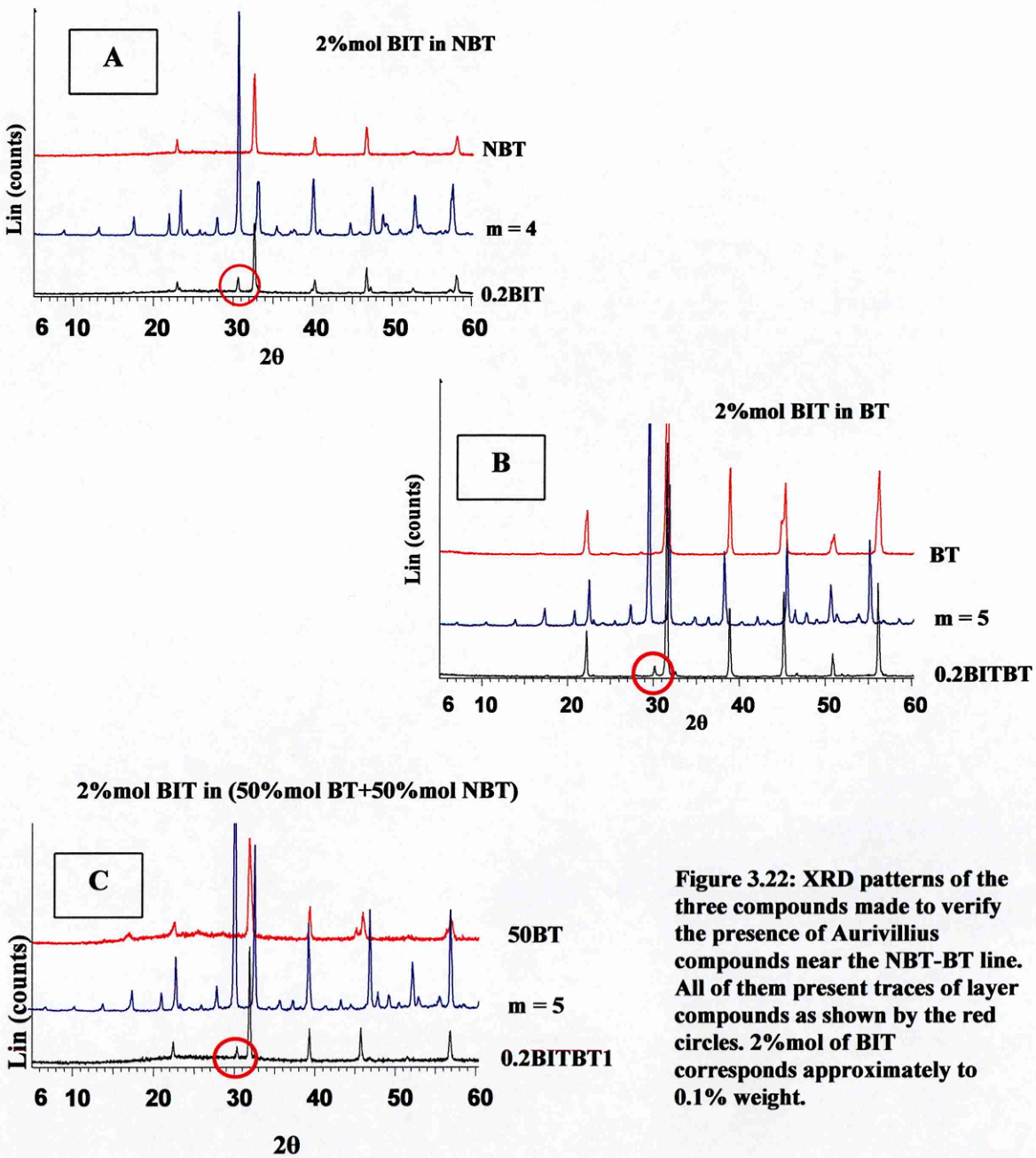

Figure 3.22: XRD patterns of the three compounds made to verify the presence of Aurivillius compounds near the NBT-BT line. All of them present traces of layer compounds as shown by the red circles. 2%mol of BIT corresponds approximately to 0.1% weight.

Each of the spectra shows an extra peak at $2\theta \approx 30°$ typical of an Aurivillius compound. This shows that is impossible to obtain pure perovskite compounds at concentrations of BIT larger than 2%mol.

Particularly interesting is the line, deep in the phase diagram, where all the compounds are of Aurivillius type with m=5. Table 3.III reports the labelling system adopted for the four compositions examined in this region.

Composition	χ_{BIT}	χ_{NBT}	χ_{BT}	Label
$Na_{0.2125}Ba_{0.25875}Bi_{1.4775}Ti_{1.6325}O_{5.84625}$	0.316	0.425	0.259	55BITBT0.7
$Na_{0.1665}Ba_{0.333}Bi_{1.5025}Ti_{1.668}O_{6.006}$	0.334	0.333	0.333	50BT0.5
$Na_{0.1}Ba_{0.48}Bi_{1.38}Ti_{1.64}O_{5.88}$	0.320	0.200	0.480	40BITBT0.7
$Ba_{0.66}Bi_{1.36}Ti_{1.68}O_{6.06}$ ($Ba_2Bi_4Ti_5O_{18}$)	0.340	-	0.660	34BITBT

Table 3-III: Compositions and labelling system for the compounds of the m=5 line.

The XRD analyses on these compositions are shown in Figures 3.23 and 3.24, where the diffractograms are compared also with the ones of BT and NBT. The low angle scans, shown in Figure 3.24, stress the five-blocks-nature of all these layer compounds. On the other hand, the results presented in Figure 3.23 exclude the possibility of traces of perovskite-second phases. In Figure 3.23B) the wide scan is shown in detail between 29 and 34° (2θ). The most intense peak of the perovskite compounds is generally found in this range of angles. However, no trace of this peak can be found in the diffractograms shown.

It is important to stress that all these compounds are novel compositions and not the result of doping of well known compounds. Besides, the high number of m suggests that this series could show piezoelectric properties at least comparable with that of the well known compound $Ba_2Bi_4Ti_5O_{18}$ ($d_{33} \approx 20pC/N$)[163].

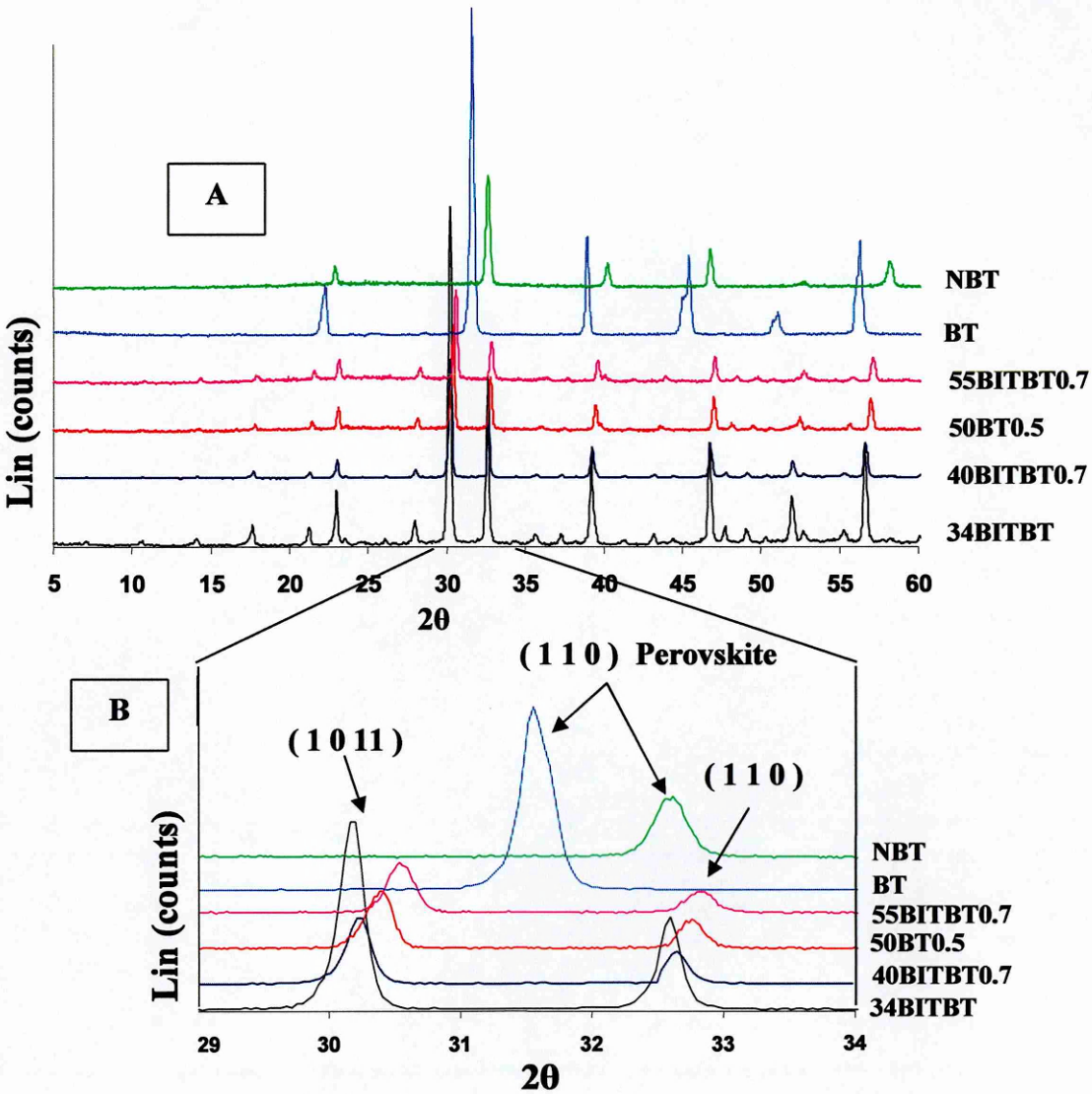

Figure 3.23: Diffractograms of the compounds belonging of the m=5 line of the NBT-BIT-BT phase diagram (A). The detail in B) shows the absence of perovskitic second phases in the compounds examined.

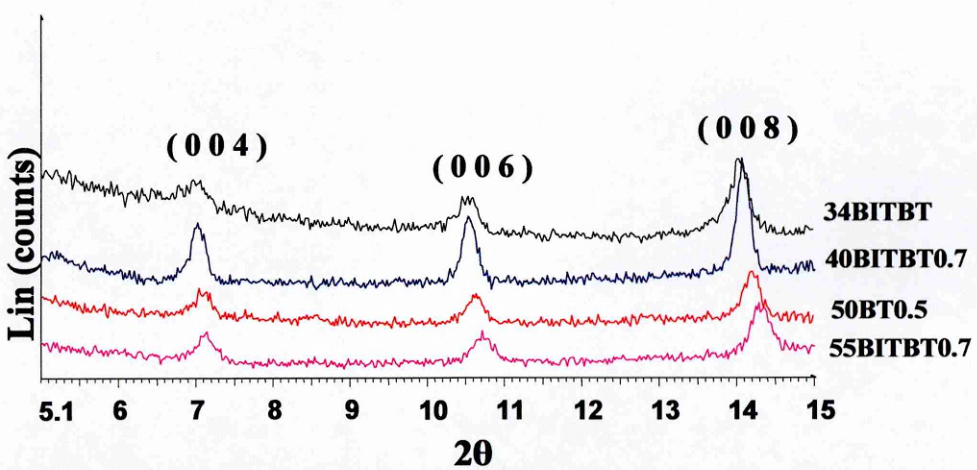

Figure 3.24: Low angle XRD analysis of the compounds of Figure 23. All of them have an essential m=5 layer structure.

3.2.1.5. Phase Diagram and Stoichiometry

The monophasic regions of the NBT-BIT-BT system form parallel lines in the phase diagram indicating that, at least up to 50%mol BIT, it is not the nature of the A-site cation of the perovskite partner that influences the structure of the Aurivillius compound but rather the molar ratios of the end-members. These regions are also parallel to the base line BT-NBT as would be expected for stoichiometry in these compounds.

The combination of $Bi_4Ti_3O_{12}$ with either perovskites has the effect of diminishing the amount of Bi^{3+} in the perovskite blocks of the Aurivillius compounds, with a corresponding increase in m. This can be clearly seen from the following equations in which the formulae of BIT and two compounds with m=4 are expanded to highlight the two different layers and the number of m

$$\left.\begin{aligned} Bi_4Ti_3O_{12} &= Bi_2O_2^{2+}3\cdot(Bi_{2/3}TiO_3)^{2-} \\ Bi_4Ti_3O_{12} + BaTiO_3 &= Bi_2O_2^{2+}4\cdot(Bi_{2/4}Ba_{1/4}TiO_3)^{2-} \\ Bi_4Ti_3O_{12} + Na_{1/2}Bi_{1/2}TiO_3 &= Bi_2O_2^{2+}4\cdot(Bi_{5/8}Na_{1/8}TiO_3)^{2-} \end{aligned}\right\} \; m = 4$$

The substitution of Bi^{3+} with cations of lower valency is compensated by negative charges on the substitution site as clarified using the Kröger-Vink notation for the substitution

$$Bi^{3+} \xrightarrow{Ba^{2+}} Ba'_{Bi}$$
$$Bi^{3+} \xrightarrow{Na^{+}} Na''_{Bi}$$

Supposing that the number of perovskite blocks is conditioned by these charged sites, it is possible to explain the trend in the monophasic regions. The charge of the sites in the BT-BIT series is half the one in the BIT-NBT series but the sites are double in concentration; as a consequence, the compounds with increasing m are formed at exactly the same amount of the perovskite partner.

The nature of the A-site cations starts to play a vital role at a high percentage of perovskite and this is the reason why the m=5 region (the blue line of figure 3.21) does not reach the BIT-NBT base line. Although there is a difference in ionic radius

between the A-site of BT and NBT (Na^+=1.17Å, Ba^{2+}=1.42Å)[131,164], the A site cation dimensions cannot be the only parameter to influence the evolution of phases along the BIT-NBT series. It is well known that when BIT is coupled with $PbTiO_3$ it is possible to obtain compounds with m up to 8[165] even though Pb^{2+} has a radius (1.2 Å) very similar to Na^+. This implies that there is a relationship between the structure of the Aurivillius compounds and the electronic structure of the cations involved (like Bi^{3+}, Pb^{2+} has a lone electron pair). Note that for m=3, 3.5 and 4 compounds there are regions of non-stoichiometric but single phase compounds when the compositions move away from the BIT-BT and BIT-NBT lines. These only occur on the "high perovskite" side of the lines. This implies that these structures are quite stable and tolerant of non-stoichiometry. The m=5 compounds, however, only exist on the stoichiometric line running through the composition $Ba_2Bi_4Ti_5O_{18}$ parallel to the BT-NBT line. This implies that the m=5 structure is probably only just stable in this system and this is why the structure is the most sensitive to the precise electronic structure or nature of the A-cation.

In Table 3.IV are summarised the data for all the compositions of the pure phases spotted in the phase diagram. They are grouped by number of perovskite blocks and their formula is normalised to the stoichiometry amount of titanium. In the Aurivillius compounds the perovskite blocks are the ones affected by vacancies, whereas the Bi_2O_2 layers are basically insensitive to any substitution. In the former, the A-site is unstable while the B-site is considerably more stable. The systems are then expected to balance the possible non-stoichiometry by introducing vacancies in the A-site and oxygen vacancies, leaving the B-site predominantly untouched. It is therefore preferable to refer all the compositions to the most stable cation, Ti.

Table 3.IV shows the labels and the normalised formulae of each compound and the effect of non-stoichiometry on the A-site of the perovskite block. The stoichiometric compounds of barium have been chosen as reference. In the calculation of the vacancies it has been assumed that sodium and the excess in bismuth are going to substitute barium in the A-site and that the electro-neutrality of the composition is balanced by oxygen vacancies. In the case of compounds with m=3 the reference is BIT so the calculations are made considering the substitution of bismuth in the A-site by Ba and Na.

Formula	Label	m	Ba	V''_{Ba}	Na'_{Ba}	$Bi^{\bullet}_{Ba}$	$V^{\bullet\bullet}_{O}$	% A-Vac	% O Vac
$Ba_2Bi_4Ti_5O_{18}$	34BITBT	5	2	-	-	-	-	-	-
$Ba_{1.42}Na_{0.3}Bi_{4.28}Ti_5O_{17.99}$	40BITBT0.7	5	1.42	-	0.3	0.28	0.02	-	-0.1
$Ba_{1.04}Na_{0.52}Bi_{4.42}Ti_5O_{17.93}$	50BT0.5	5	1.04	0.02	0.52	0.42	0.07	-0.5	-0.4
$Ba_{0.79}Na_{0.64}Bi_{4.54}Ti_5O_{17.93}$	55BITBT0.7	5	0.79	0.03	0.64	0.54	0.07	-0.75	-0.4
$BaBi_4Ti_5O_{15}$	50BITBT	4	1	-	-	-	-	-	-
$Ba_{0.56}Na_{0.28}Bi_{4.11}Ti_4O_{14.875}$	50BT1	4	0.56	0.05	0.28	0.11	0.125	-1.7	-0.8
$Ba_{0.355}Na_{0.385}Bi_{4.22}Ti_4O_{14.875}$	70BITBT2	4	0.35	0.04	0.38	0.22	0.125	-2	-0.8
$Na_{0.5}Bi_{4.5}Ti_4O_{15}$	50BIT	4	-	-	0.5	0.5	-	-	-
$Na_{0.58}Bi_{4.37}Ti_4O_{14.84}$	45BIT	4	-	0.05	0.58	0.37	0.16	-1.7	-1.1
$BaBi_8Ti_7O_{27}$	66BITBT	3.5	1	-	-	-	-	-	-
$Ba_{0.84}Na_{0.15}Bi_{7.96}Ti_7O_{26.85}$	70BITBT2	3.5	0.84	0.01	0.15	0.04	0.15	-0.7	-0.5
$Ba_{0.51}Na_{0.26}Bi_{8.22}Ti_7O_{26.97}$	50BT2.5	3.5	0.51	0.01	0.26	0.22	0.03	-0.1	-0.1
$Ba_{0.15}Na_{0.46}Bi_{8.37}Ti_5O_{26.93}$	70BIT1	3.5	0.15	0.02	0.46	0.37	0.07	-0.3	-0.3
$Na_{0.5}Bi_{8.5}Ti_7O_{27}$	66BIT	3.5	-	-	0.5	0.5	-	-	-
Formula	Label	m	Bi	V'''_{Bi}	Ba'_{Bi}	Na''_{Bi}	$V^{\bullet\bullet}_{O}$	% A-Vac	% O Vac
$Bi_4Ti_3O_2$	BIT	3	2	-	-	-	-	-	-
$Ba_{0.08}Na_{0.04}Bi_{3.83}Ti_5O_{11.89}$	90BITBIT	3	1.86	0.03	0.11	-	0.11	-1.5	-0.9
$Ba_{0.08}Na_{0.04}Bi_{3.83}Ti_3O_{11.85}$	50BT4	3	1.83	0.05	0.08	0.04	0.15	-2.5	-1.25
$Na_{0.054}Bi_{3.91}Ti_3O_{11.89}$	90BIT	3	1.91	0.04	-	0.05	0.11	-1.8	-0.9

Table 3-IV: Composition and nature of the vacancies of the pure phases identified in the NBT-BIT-BT system. The pure phases of the BT-BIT series are considered as reference model. %A-vac = percentage of A-site vacancies in respect of the BT-BIT pure compound of equal m. %O-vac = percentage of oxygen vacancies. BIT is the model for the m=3 compounds.

The first thing to emerge from this table is the flexibility of this class of compounds. They can form pure phases even with quite defective stoichiometry. This is due to the ability of the structure to "adapt" itself to overcome the repulsions induced by defects. For doing so the compound can tilt the octahedra of the perovskite blocks and/or change the distance between the latter and the bismuthyl layers.

The percentage of vacancies as a function of m gives an idea of the adaptability of the structure. In Figure 3.25 the amount of A-site and oxygen vacancies are plotted against m for the pure phase of the series $xBi_4Ti_3O_{12}$–$(1-x)[0.5(BaTiO_3)+0.5(Na_{0.5}Bi_{0.5}TiO_3)]$.

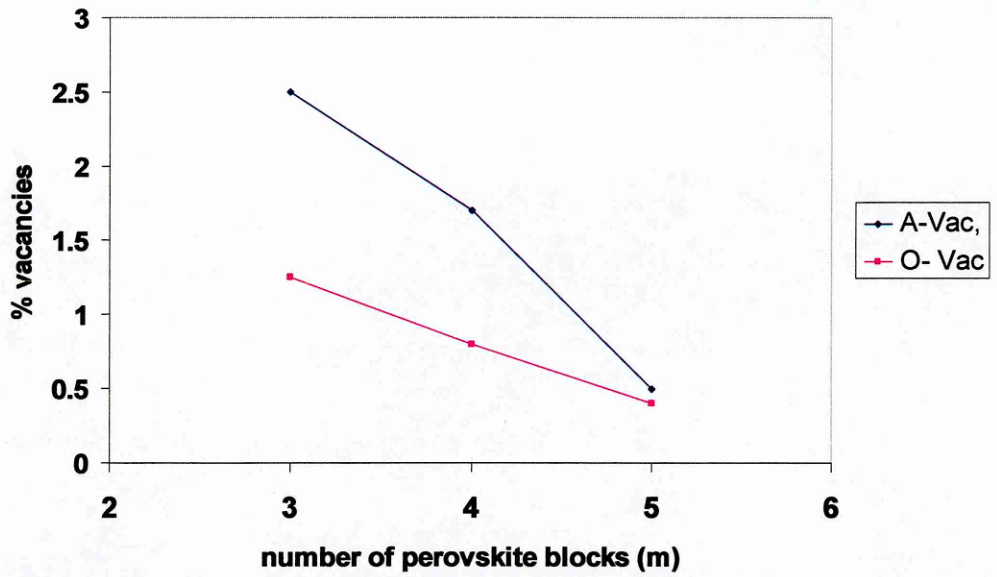

Figure 3.25: Number of A-site vacancies and oxygen vacancies as a function of the number of perovskite blocks.

The graph shows that the higher is m, the lower is the number of vacancies that the structure is able to tolerate. The number of vacancies is related to the flexibility of the structure: a high number of vacancies indicates a higher ability of the structure to withstand changes in stoichiometry before collapsing. The low amount of vacancies allowed by compounds with five perovskite blocks, can explain why these structure exist in a very narrow range of compositions. The low flexibility of the compound is the reason why small changes in stoichiometry cause the partial collapsing of the structure with consequent appearance of a second phase. Figure 3.25 shows also that the number of A-vacancies goes to zero before m=6. This could explain why in this series structure with m>5 are not possible.

3.2.1.6. Stability of the Aurivillius compounds

It would be of great importance to determine the conditions under which the compounds in the system can form and be stable. If general criteria of stability can be established, then it is possible to predict if a composition will be stable in the system under exam. To study the relation between structure and stability for Aurivillius

compounds of the system, the attention was focused again on the two main series BIT-BT and BIT-NBT. The main goal in analysing the phases of these two series is to understand why coupling BIT with NBT and BT does not lead to the same number of compounds. Containing perovskite blocks, the Aurivillius compounds can be considered to be subjected to the similar criteria of formation and stability as those governing the perovskite structures. Classically, a compound needs to satisfy two main requirements to crystallise in perovskite form. First, the bonds between oxygen ions and other cations must have a strong ionic character, and second the ionic radius of the cations should be within certain values. The ionicity of a bond can be deduced by the difference in electronegativity between the ions involved. Large electronegativity difference means a strong ionic bond. In particular, using the values of electronegativity defined by Pauling, the ionic component of the bond between oxygen (O) and a cation (A) can be expressed with the following equation[166]:

$$\%P_{AO} = [1-\exp(-1/4(\Delta E_{A-O})^2)]x100 \qquad \textbf{Equation 3.1}$$

where ΔE_{A-O} is the electronegativity difference between the two ions (i.e. $\Delta E_{A-O} = E_A - E_O$) The bonds to be considered in the BIT-BT-NBT system and the percentage of ionicity are presented in Table 3-V.

Bond	ΔE_{A-O}	$\%P_{AO}$
Ti-O	2.0	63
Bi-O	1.6	47
Ba-O	2.6	81
Na-O	2.6	81

Table 3-V: Electronegativity and percentage of ionicity for the M-O bonds of the NBT-BIT-BT system.

This table clarifies why the polarity of the bond cannot be considered as a criterion to determine the stability of the compounds in the system. The various compounds of the phase diagram differ only in the nature of the cations in the A-site of the perovskite block (i.e. sodium, barium or a mixture of the two). Na-O and Ba-O bonds, however,

present the same percentage of ionicity and therefore the latter cannot be used as criteria to explain the different behaviour of the two series considered.

The second (and more commonly used) factor considered to determine the stability of a perovskite compound is its tolerance factor (t). This factor gives a criterion for the formation of perovskites derived on purely geometrical consideration, and it is defined, by the equation (see paragraph 1.4.2.1):

$$t = \frac{\overline{r_A} + r_O}{\sqrt{2}\left(\overline{r_B} + r_O\right)}$$

Where $\overline{r_A}$ and $\overline{r_B}$ are the mean radii of the A- and B-site of the perovskite cell respectively, and r_O is the radius of the oxygen atoms. This relation is derived from a "hard spheres" model of ions in contact and represents an ideal cubic perovskite when "t" is equal to one[167]. It has been found that a tetragonal, rhombohedral or orthorhombic perovskite will form if $0.81 < t < 1.01$. When the tolerance factor is less than the minimum value for a perovskite, the hexagonal ilmenite structure is usually formed, as in the case of $MgTiO_3$ for which $t = 0.75$.

Ismailzade showed that, considering t as indicator of stability, any Aurivillius compound with $0.86 \leq t \leq 0.97$ should be stable[168]. Following his criterion the tolerance factors of the compounds of the two series were calculated up to a hypothetical m=10 compound (m indicates the number of perovskite blocks sandwiched between bismuthyl layers). The results of these calculations are presented in Table 3-VI, in which the red font indicates compounds for which the value of tolerance factor is above the "permitted" 0.97.

From Table 3-VI it is clear that in the BIT-BT series compounds with up to m=7 should be possible (experimentally 5 is the maximum value of m for this series), whereas virtually any compound should exist in the NBT-BIT series (experimentally m reaches the maximum value of 4 for this series). The tolerance factor is not therefore an accurate criterion to determine the stability of Aurivillius compounds. All these calculations are based on a very simple "hard spheres" model that does not take into account the interactions between atoms, different kinds of layers in the layer

compounds, or the fact that the ions are not perfect and impenetrable spheres (their shape depends on their electronic structure).

A-member	B-member	Compound	m	A-radius	B-radius	t
$Bi_4Ti_3O_{12}$	$Na_{0.5}Bi_{0.5}TiO_3$	A + B	4	1.193	0.605	0.914
$Bi_4Ti_3O_{12}$	$Na_{0.5}Bi_{0.5}TiO_3$	A + 2B	5	1.19	0.605	0.913
$Bi_4Ti_3O_{12}$	$Na_{0.5}Bi_{0.5}TiO_3$	A + 3B	6	1.188	0.605	0.912
$Bi_4Ti_3O_{12}$	$Na_{0.5}Bi_{0.5}TiO_3$	A + 4B	7	1.186	0.605	0.912
$Bi_4Ti_3O_{12}$	$Na_{0.5}Bi_{0.5}TiO_3$	A + 5B	8	1.185	0.605	0.911
$Bi_4Ti_3O_{12}$	$Na_{0.5}Bi_{0.5}TiO_3$	A + 6B	9	1.185	0.605	0.911
$Bi_4Ti_3O_{12}$	$Na_{0.5}Bi_{0.5}TiO_3$	A + 7B	10	1.184	0.605	0.911
$Bi_4Ti_3O_{12}$	$BaTiO_3$	A + B	4	1.273	0.605	0.942
$Bi_4Ti_3O_{12}$	$BaTiO_3$	A + 2B	5	1.31	0.605	0.955
$Bi_4Ti_3O_{12}$	$BaTiO_3$	A + 3B	6	1.332	0.605	0.963
$Bi_4Ti_3O_{12}$	$BaTiO_3$	A + 4B	7	1.346	0.605	0.968
$Bi_4Ti_3O_{12}$	$BaTiO_3$	A + 5B	8	1.357	0.605	0.972
$Bi_4Ti_3O_{12}$	$BaTiO_3$	A + 6B	9	1.365	0.605	0.975
$Bi_4Ti_3O_{12}$	$BaTiO_3$	A + 7B	10	1.371	0.605	0.977

Table 3-VI: Tolerance factors calculations for hypothetical compounds of the NBT-BIT and BT-BIT series. The red font indicate values of tolerance factor outside the range of stability for Aurivillius compounds (0.86-1.01).

A better criterion was introduced by Kikuchi in 1979[165]. He exploited the idea of Kittel[169] that considered the Aurivillius compounds as infinitively adaptive structures in which the configurational entropy of the stacking layers can be neglected. Under this assumption, the free energy of these phases can be reduce to the elastic energy of a layer of composition A interacting with layers of composition B. Using this idea, Kikuchi proposed a method to determine the stability of Aurivillius compounds that considers the structural mismatch between Bi_2O_2 and perovskite layers. Using an elastic model for the structure, he showed that a useful criterion for the stability of layer compounds can be derived from the total strain energy caused by the different lateral dimension of the bismuthyl layer compared with the one of the perovskite block. He expressed the total strain energy with the Equation 3.2.

$$E = 0.5K_B\Delta V \qquad \textbf{Equation 3.2}$$

where

$$\Delta V = V_B'\left(1-\frac{a^2}{a_B'}\right)^2 + mKV_p'\left(1-\frac{a^2}{a_p'^2}\right)^2 \quad \textbf{Equation 3.3}$$

and

a_p' = lattice parameter of the unconstrained perovskite-like unit,

a_B' = lattice parameter of the unconstrained Bi_2O_2 unit,

$\underline{a}$ = pseudo-tetragonal lattice parameter of the layered compound,

m = number of perovskite layer in one structural unit,

V_B', V_p' = volumes of the unconstrained bismuthyl layer and perovskite-like unit respectively,

K_B = bulk modulus of the Bi_2O_2 unit,

K = ratio between the bulk moduli of the two different kind of layers.

Assuming K_B to be constant because it is not dependent on the composition of the perovskite-like layers, Kikuchi proved that almost all the stable Aurivillius compounds known at the time, have ΔV less than 0.4 $Å^3$. a'_p was calculated for a number of hypothetical compounds, using the formula suggested by Armstrong and Newnham[170], and used by Kikuchi himself

$$a_P' = 1.33r_B + 0.60r_A + 2.36 \quad \textbf{Equation 3.4}$$

where r_B and r_A are the atomic radii of the cations in the B and A site of the perovskite block respectively. The values of cationic radii are taken from the Shannon-Prewitt 'IR' scale[164], using VI coordinated values for B-site ions and VIII for the A-site. The radius of Bi^{3+} considered was 1.20 Å.

As shown in Equation 3.3 the model of Kikuchi needs a value for the a-parameter of the actual unit cell of the compound to calculate ΔV. In the case of hypothetical compounds this value is obviously unknown. As a consequence the trend of the a-parameter along the two series was determined by the x-ray analyses of the compounds using the least squares approach described in Appendix B. The parameters are reported in Table 3.VII for the two different series.

Compound	% mol BIT	m	a (Å)	c(Å)
34BTOBT	34	5	3.888(1)	50.075(1)
50BTOBT	50	4	3.866(1)	42.012(1)
66BTOBT	66	3.5	3.847(1)	37.198(1)
90BTOBT	90	3	3.840(1)	32.898(1)
Compound	**% mol BIT**	**m**	**a (Å)**	**c (Å)**
45BTO	45	4	3.842(1)	40.848(1)
50BTO	50	4	3.845(1)	40.775(1)
66BTO	66	3.5	3.843(1)	36.802(1)
90BTO	90	3	3.833(1)	32.742(1)

Table 3-VII: Cell constants for the compounds of the BT-BIT and BT-BIT obtained by XRD analysis.

The values of the "a" parameters were then plotted against the amount of BIT present in each composition to identify a possible trend (Figures 3.26 and 3.27). For the compounds that generally presents an orthorhombic distortion, a pseudo-tetragonal value of "a" was calculated with the following expression $a = (a_{orth} + b_{orth})/2\sqrt{2}$ where a_{orth} and b_{orth} are the values of the a- and b-parameter of the orthorhombic cell.

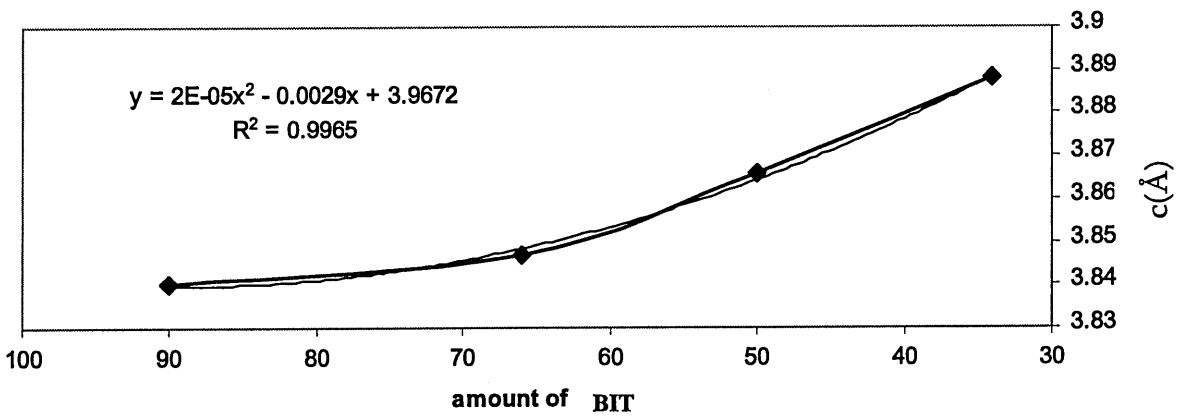

Figure 3.26: Trend of the a-parameter of the cell with the amount of BIT for compounds of the BT-BIT series. In the graph is also indicated the equation for the best fitting trend line.

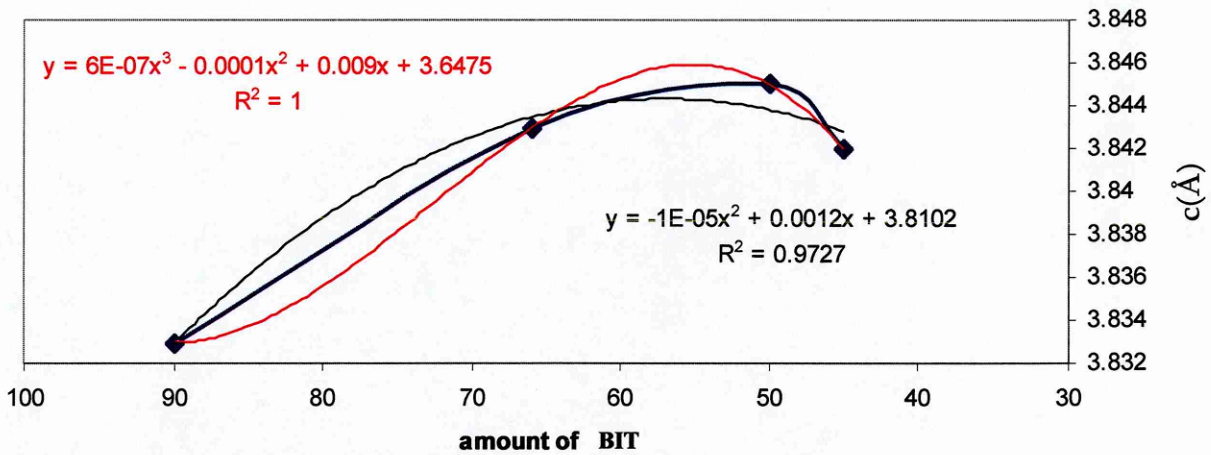

Figure 3.27: Trend of the a-parameter of the cell with the amount of BIT for the NBT-BIT series. The trend is been fitted this time with second order and third order equations (in the graph).

The BIT-BT series exhibits the predicted behaviour with an increase in the "a" parameter for a decreasing amount of BIT (and increasing m). The trend can be described by the quadratic equation $y = -1E\text{-}05x^2 + 0.0012x + 3.8102$ (Figure 3.27). By contrast, the BIT-NBT series exhibits a maximum a-parameter for the composition corresponding to 50% mol BIT, $BaBi_4Ti_4O_{15}$ m=4, and decreases for a lower amounts of the Aurivillius compounds. In this case, the behaviour is better described by a third order polynomial rather than by a second order one. However four points are not enough to ensure a good accuracy with a third order polynomial so care should be taken in considered this kind of trend line.

The different behaviour of the two series can be ascribed mainly to the different radii of the A-site cations of the two perovskite end-members. The radius of Ba^{2+} (1.42Å) is larger than that of Bi^{3+} (1.20Å). So when $BaTiO_3$ is coupled with BIT in increasing amounts, the a-parameter is expected to increase to accommodate the bigger A-site cation. On the other hand, the Na^+ has a smaller radius (1.16Å) than Bi^{3+}. It is maybe for this reason that the a-parameter increases up to a critical value corresponding to the composition at 50% in BIT but after it tends to shrink to better accommodate the smaller Na^+ that starts to be present in larger amounts and starts to influence the parameter.

Using the equation of the fitted trend-line, the a-parameter was calculated for the hypothetical compounds from m=5 to m=10 for the NBT-BIT series, and from m=6 to m=10 for the BT - BIT series (Table 3-VIII).

Compound	*% mol BIT*	*m*	*a (Å)*	*a third order (Å)*
34BITBT	34	5	3.839	3.83
25BITBT	25	6	3.833	3.831
20BITBT	20	7	3.83	3.831
17BITBT	17	8	3.827	3.832
14BITBT	14	9	3.825	3.832
12.5BITBT	12.5	10	3.823	3.833

NBT-BIT series

Compound	*% mol BIT*	*m*	*a (Å)*
25BITBT	25	6	3.907
20BITBT	20	7	3.917
17BITBT	17	8	3.923
14BITBT	14	9	3.93
12.5BITBT	12.5	10	3.934

BT-BIT series

Table 3-VIII: Prediction of the a-parameters of hypothetical compounds of the NBT-BIT-BT system.

These values were then used in the Kikuchi model calculations summarised in Table 3-IX. In this table, the first two columns indicate the nature of the cation present at the A-site of the perovskite block and the radius considered in the calculations, m indicates the number of perovskite blocks considered, K and ΔV are the parameters used in Equation 3.3. It is worth remembering that for the Kikuchi criteria only the compounds that present values of ΔV smaller than 0.4 $Å^3$ can be stable. The values in red are the ones of the compositions considered instable by the model. In the case of NBT-BIT the values are calculated using the a-parameters derived from the second grade interpolation line, and those from the third grade interpolation line (in italics).
It is clear that the model works very well for the BT-BIT series and is capable of predicting the impossibility of compounds with a number of perovskite blocks higher than 5 as shown by the experimental data. However, the model does not explain the behaviour of the NBT-BIT series. This is another confirmation that simple elastic considerations are not sufficient to justify the trend of stability along the Aurivillius

series and that it is necessary to also take in account the electronic structure of the ions involved. The electronic structure is extremely important in the case of Bi^{3+}, whose electron lone pair is known to strongly influence the properties of its compounds. The lack of any electronic considerations can therefore be particularly dramatic in the NBT-BIT solid solutions where bismuth is present also in the perovskite partner, strongly affecting the results as shown in the previous calculations.

A-site cation		B-site cation		m	a (Å)	a'p(Å)	K	ΔV(Å³)
Type	radius	type	Radius					
Na,Bi	1.193	Ti	0.605	4	3.849	3.88	0.566	**0.123**
Na,Bi	1.19	Ti	0.605	5	3.839	3.878	0.315	**0.102**
Na,Bi	1.188	Ti	0.605	6	3.833	3.877	0.214	**0.091**
Na,Bi	1.186	Ti	0.605	7	3.83	3.876	0.16	**0.083**
Na,Bi	1.185	Ti	0.605	8	3.827	3.876	0.128	**0.078**
Na,Bi	1.185	Ti	0.605	9	3.825	3.875	0.102	**0.073**
Na,Bi	1.184	Ti	0.605	10	3.823	3.875	0.087	**0.071**
Na,Bi	*1.19*	*Ti*	*0.605*	*5*	*3.83*	*3.878*	*0.218*	***0.086***
Na,Bi	*1.188*	*Ti*	*0.605*	*6*	*3.831*	*3.877*	*0.191*	***0.086***
Na,Bi	*1.186*	*Ti*	*0.605*	*7*	*3.831*	*3.876*	*0.171*	***0.086***
Na,Bi	*1.185*	*Ti*	*0.605*	*8*	*3.832*	*3.876*	*0.155*	***0.087***
Na,Bi	*1.185*	*Ti*	*0.605*	*9*	*3.832*	*3.875*	*0.142*	***0.088***
Na,Bi	*1.184*	*Ti*	*0.605*	*10*	*3.833*	*3.875*	*0.132*	***0.088***
Ba	1.31	Ti	0.605	5	3.88	3.95	0.302	**0.305**
Ba	1.332	Ti	0.605	6	3.907	3.963	0.401	**0.427**
Ba	1.346	Ti	0.605	7	3.917	3.972	0.38	**0.485**
Ba	1.357	Ti	0.605	8	3.923	3.978	0.351	**0.527**
Ba	1.365	Ti	0.605	9	3.93	3.983	0.34	**0.567**
Ba	1.371	Ti	0.605	10	3.934	3.987	0.313	**0.592**

Table 3-IX: Kikuchi calculations for hyphotethical compounds of the two series examined. Red fonts indicate values not allowed by Kikuchi. Italics indicate values for the NBT-BIT series calculated from a-parameters oobtained by the 3rd order fitting line.

Wakiya et al. showed[171] that the perovskite $Pb(Zn_{1/3}Nb_{1/3})O_3$ is unstable due to the steric hindrance of the lone pair of Pb^{2+} that interacts with Zn^{2+} destabilising the structure. The compound can be stabilised by substituting the A-site to reduce the mutual interaction between the lone pair and the cations on the B-site. They used the

model of Figure 3.28 to explain the situation. In this figure the zinc, its first and second lead neighbours (indicated with the number 1 and 2) and the oxygen atoms are presented.

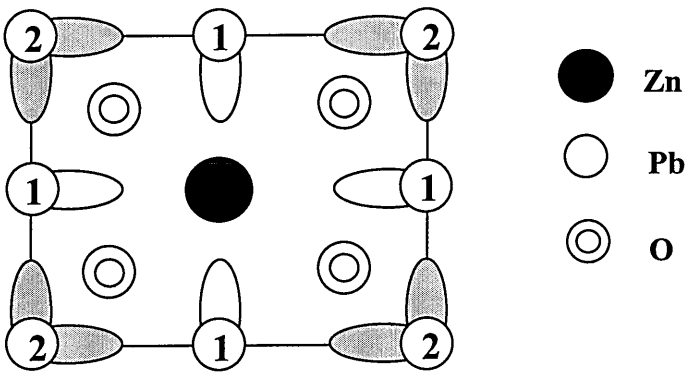

Figure 3.28: Wakiya model for PZN: 1 and 2 indicate the first and second Pb neighbour of the zinc cation. The protuberances represent the lone pair of lead[171].

The shape of the Pb^{2+} ion is non spherical due to the presence of the $(6s)^2$ lone pair that forms a protuberance. This interacts repulsively with the neighbouring cations so destabilising the structure. When Pb^{2+} is substituted with spherical cations like Ba^{2+} or K^{+}, the repulsive interaction is eliminated and the structure becomes considerably more stable. Bi^{3+} is isoelectronic with Pb^{2+} it presents the same lone pair but a smaller radius (1.42 Å for Pb^{2+}, 1.2 Å for Bi^{3+}). These two cations present similar behaviour as a consequence of their electronic similarity. It is therefore plausible that the lone pair of bismuth plays the same role of that of lead in destabilising the structure of the Aurivillius compounds. The steric hindrance of the lone pair of bismuth could explain the different behaviour of the two series considered in this work. For BIT-BT, the lone pair plays a secondary role because there is progressive substitution of the active Bi^{3+} with the spherical Ba^{2+} along the series causing the cell to become bigger, further decreasing the steric effect. The situation is completely different for the BIT-NBT series. First, the amount of Bi^{3+} substituted is less then in the previous series for the nature of the perovskite end member. Second, the cell start to shrink after 50%mol BIT making the destabilising effect, caused by the steric hindrance of the lone pair of bismuth, more dramatic. It is probably the combined effect of these two phenomena that limits the maximum number of perovskite blocks in the NBT-BIT series to four.
Another source of deviation from the model proposed by Kikuchi other than the electronic structure of the ions involved is represented by the tilting of the octahedra

in the perovskite blocks, a phenomenon that is well known to occur in the Aurivillius compounds[172,173]. This effect is probably less important than the electronic structure of the cations. The tilting of the various octahedra contributes to the lowering of the internal stress among the layers affecting the strain produced and, as a consequence, the model of Kikuchi. The balance of the forces that is the base of the Kikuchi model should include a term that counterbalances the decrease in strain in the perovskite layer with increasing m.

The steric effect of the lone pair of the bismuth ion could justify also the trend shown by the other pure phases found in the system. In Table 3-X the cell parameters of all these compounds are presented. The values of the cell parameters are the results of the least-squared approximation made on the XRD patterns of the compounds. The details of the formulae used for these calculations are presented in Appendix B. In the last column the Kikuchi ΔV values are presented.

Formula	Label	m	a (Å)	c (Å)	ΔV
$Ba_2Bi_4Ti_5O_{18}$	34BITBT	5	3.880(1)	50.075(1)	0.305
$Ba_{1.42}Na_{0.3}Bi_{4.28}Ti_5O_{17.98}$	40BITBT0.7	5	3.894(1)	50.133(1)	0.312
$Ba_{1.04}Na_{0.52}Bi_{4.42}Ti_5O_{17.93}$	50BT0.5	5	3.860(1)	49.124(1)	0.187
$Ba_{0.79}Na_{0.64}Bi_{4.54}Ti_5O_{17.93}$	55BITBT0.7	5	3.852(1)	49.668(1)	0.154
$BaBi_4Ti_5O_{15}$	50BITBT	4	3.866(1)	42.012(1)	0.226
$Ba_{0.56}Na_{0.28}Bi_{4.11}Ti_4O_{14.875}$	50BT1	4	3.850(1)	41.567(1)	0.142
$Ba_{0.355}Na_{0.385}Bi_{4.22}Ti_4O_{14.875}$	70BITBT2	4	3.850(1)	41.319(1)	0.104
$Na_{0.5}Bi_{4.5}Ti_4O_{15}$	50BIT	4	3.844(1)	40.941(1)	0.115
$Na_{0.58}Bi_{4.37}Ti_4O_{14.84}$	45BIT	4	3.845(1)	40.775(1)	0.117
$BaBi_8Ti_7O_{27}$	66BITBT	3.5	3.847(1)	37.198(1)	0.124
$Ba_{0.84}Na_{0.15}Bi_{7.96}Ti_7O_{26.85}$	70BITBT2	3.5	3.842(1)	37.026(1)	0.110
$Ba_{0.51}Na_{0.26}Bi_{8.22}Ti_7O_{26.97}$	50BT2.5	3.5	3.844(1)	37.232(1)	0.107
$Ba_{0.15}Na_{0.46}Bi_{8.37}Ti_5O_{26.93}$	70BIT1	3.5	3.845(1)	37.366(1)	0.099
$Na_{0.5}Bi_{8.5}Ti_7O_{27}$	66BIT	3.5	3.843(1)	36.802(1)	0.081
$Ba_{0.08}Na_{0.04}Bi_{3.83}Ti_5O_{11.89}$	90BITBT	3	3.840(1)	32.898(1)	0.13
$Bi_4Ti_3O_{12}$	BIT	3	3.839(1)	32.805(1)	0.106
$Ba_{0.08}Na_{0.04}Bi_{3.83}Ti_3O_{11.85}$	50BT4	3	3.833(1)	32.892(1)	0.084
$Na_{0.054}Bi_{3.91}Ti_3O_{11.89}$	90BIT	3	3.833(1)	32.742(1)	0.084

Table 3-X: Exact formulae, label, cell parameters and ΔV (Kikuchi) for each pure phase identified in the NBT-BIT-BT phase diagram.

All the compounds present values of ΔV well below the stability limit of 0.4Å^3 defined by Kikuchi as a maximum value for stable Aurivillius compounds and are therefore consistent with this theory.

Figure 3.29 shows the trend of the **c** parameter of the cell as a function of the amount of sodium bismuth titanate for the compositions given in Table 3-X. The three lines link compounds with the same number of perovskite blocks. As expected the cell becomes progressively thicker as the number of perovskite blocks is increased. It is also possible to notice that the parameter decreases slightly with the amount of NBT. This is because the dimensions of NBT are smaller than those of $BaTiO_3$.

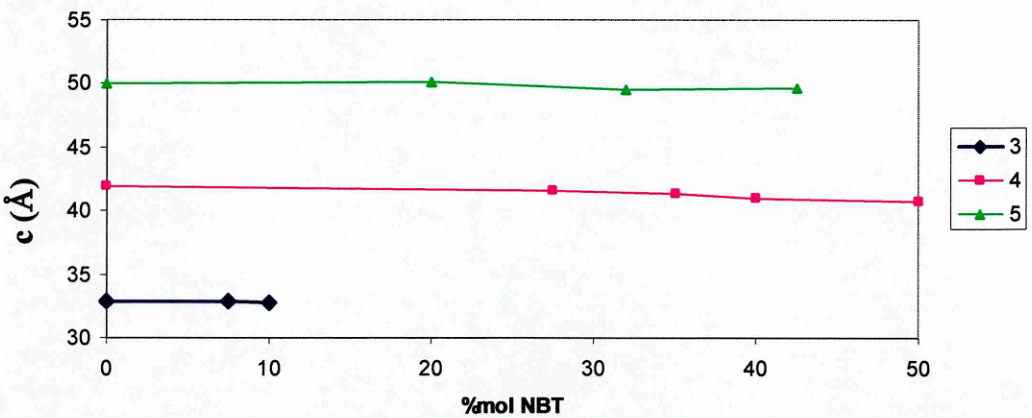

Figure 3.29: Trend of c-parameter as function of the amount of NBT for the compositions given in Table X. 3,4 and 5 indicate the number of perovskite blocks.

Far more interesting is the trend along the series of the a-parameter (Figure 3.30). Not surprisingly, the **a** parameter decreases with the amount of NBT in the compounds with m=3 and m=4. However, the behaviour is extremely interesting in the case of the compounds of the m=5 series. The decrease is so abrupt, that for the last compound of the series (corresponding to 42.5 mol%NBT), **a** drops to values similar to the ones of m=4 compounds. This fact could explain why the m=5 line in the phase diagram does not reach the NBT-BIT baseline. The shrinkage of the cell in conjunction with the increasing amount of NBT end member causes the cell to collapse (like in the NBT-BIT series) due to the steric effect of the bismuth lone pair.

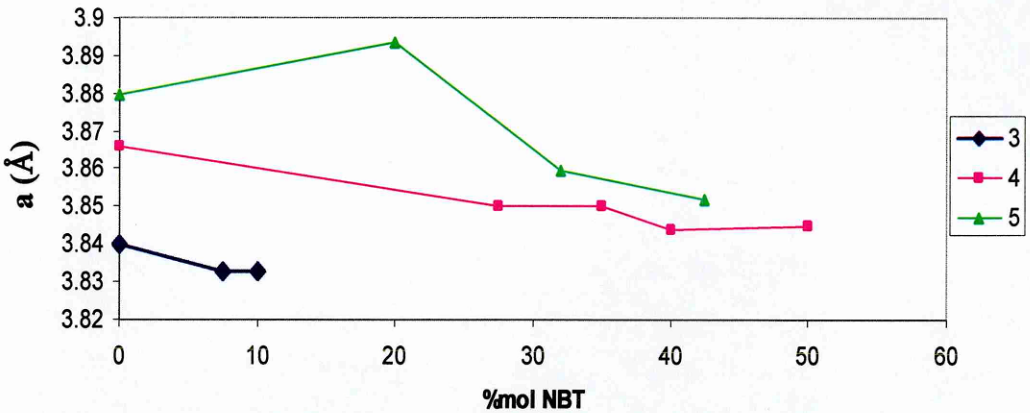

Figure 3.30: Trend of a-parameter of the unit cell of the pure phases given in Table X as function of the amount of NBT.

The compounds with m=3.5 have been excluded from the previous analyses. The intergrowth compounds are in fact generally quite complex and unpredictable as a consequence of their nature. The intergrowth can be ordered (343434 in this case) or completely random (334443434333 etc.) (section 1.4.2.2) affecting in this way the properties of the system. A discussion of these compounds has not been included in the general discussion due to the uncertain nature of the intergrowth.

3.2.2. FORMING AND SINTERING

The powders produced by calcination, were shaped and then sintered at 1165°C for 4 hours as described in the experimental section. The conditions of sintering were chosen after the examination of the DTA analysis on 30BIT (Figure 3.18). This composition was chosen because compounds of the BIT-NBT series are formed at lower temperatures than the compositions in which barium is present. As a consequence they also melt before the others. The melting point of this composition should then represent the minimum among all the compound of the system. From the DTA analysis the melting point was fixed at 1175°C. The sintering temperature must be lower than this value, to avoid melting, but higher than the 1150°C of calcination to give the driving force necessary to consolidate the ceramics. 1165°C was considered to be a good compromise between the two previous values of temperature.

Six pellets of each pure phase of the NBT-BIT and BT-BIT series were made and studied in an attempt to link the structural properties of the materials with the dielectric and piezoelectric ones. The measurements done on these samples showed good reproducibility with differences between samples obtained from different powder batches generally below 2%. This small difference confirmed that the process for the production of ceramics can be considered to be well established and reliable. In Table 3-XI the values of weight loss for the pellets of the pure phase analysed are reported. The data are presented with the errors calculated as standard deviation of 10 independent measurements; the errors on the weight loss (calculated using the error theory) are always below 0.05%. The weight loss of the samples examined is below 3%. Considering that the green body is formed by adding 2% weight of PVA to the powder, this values highlights the efficiency of the sintering apparatus in preventing the sodium and bismuth weight loss.

Composition	m	Weight green (g)	Weight sintered (g)	Weight loss (%)
45BIT	4	9.1960±0.0001	8.9800±0.0001	***2.3***
50BIT	4	8.4024±0.0002	8.1524±0.0001	***2.9***
66BIT	3.5	7.5395±0.0001	7.3431±0.0001	***2.6***
BIT	3	7.5825±0.0002	7.3550±0.0001	***3.0***
34BITBT	5	8.0962±0.0002	7.8249±0.0001	***2.7***
50BITBT	4	8.9700±0.0003	8.7188±0.0001	***2.8***
66BTIBT	3.5	7.9675±0.0001	7.7529±0.0001	***2.7***
BT	∞	8.6050±0.0001	8.3900±0.0001	***2.5***
NBT	∞	9.1820±0.0001	8.9157±0.0001	***2.9***

Table 3-XI: Weight loss for the pure compounds of the NBT-BIT and BT-BIT series during sintering at 1165°C.

Table 3-XII and Table 3-XIII on the other hand, show the data for shrinkage and density. The errors on the percentage shrinkage and density (calculated using the error theory) are of the order of 0.05%.

Comp.	M	Øg(cm)	Øs (cm)	% l. shr.	t_g (mm)	t_s (mm)	% t. shr.
45BIT	4	2.796±0.006	2.685±0.001	***2.3***	3.24±0.06	3.12±0.01	***3.7***
50BIT	4	3.008±0.002	2.855±0.003	***2.9***	2.27±0.03	2.15±0.01	***5.3***
66BIT	3.5	2.825±0.008	2.697±0.006	***2.6***	2.96±0.09	2.80±0.04	***5.4***
BIT	3	3.006±0.005	2.793±0.004	***3.0***	2.80±0.01	2.01±0.08	***8.8***
34BITBT	5	2.752±0.003	2.331±0.001	***2.7***	3.38±0.02	2.84±0.02	***16.0***
50BITBT	4	2.808±0.003	2.506±0.002	***2.8***	3.22±0.05	2.89±0.02	***10.2***
66BTIBT	3.5	2.786±0.004	2.563±0.003	***2.7***	2.76±0.05	2.48±0.05	***10.1***
BT	∞	2.826±0.009	2.590±0.006	***2.5***	3.96±0.06	3.23±0.05	***18.4***
NBT	∞	2.837±0.001	2.701±0.007	***2.9***	3.61±0.03	3.43±0.03	***5.0***

Table 3-XII: Values of shrinkage (in diameter and thickness) for all the pure phases of the NBT-BIT and BT-BIT series. Øg=diameter green, Øs=diameter sintered, t_g=thickness green, t_s=thickness sintered body, l. shr.=lateral shrinkage, t.shr.=thickness shrinkage.

These data reflect the morphology of the powders discussed in the previous paragraph.

The shrinkage (both lateral and in thickness) is definitely lower for the compounds of the NBT-BIT series. The thickness shrinkage is generally higher than the lateral one. The driving force for the ceramic consolidation is linked to the free energy of the surface of its particles. A definite volume can accommodate more small particles than big ones, and therefore pellets formed by smaller particles have bigger free area and higher free energy. The powders formed by small particle are more reactive during sintering and lead generally to higher values of shrinkage and density of the pellet. In section 3.2.1.3 it was pointed out that powders of the NBT-BIT series are generally formed by larger particles than the corresponding powder in the other series. This observation justifies the different percentage of shrinkage shown in Table 3-XII along the two series.

The different sintering behaviour is shown also by the values of density. The last column in Table 3-XIII indicates the variation in density from the green body to the sintered ceramics. A higher variation indicates higher reactivity of the powder and consequently higher densification activity of the sample. Compounds in which the perovskite end member is BT have values of variation up to five times higher than the compounds in which NBT is the perovskitic member.

The role of the perovskite is clear when comparing NBT with BT. Barium titanate is subjected to bigger values of shrinkage and a larger change of density than sodium bismuth titanate.

Composition	m	d_g g/cm^3	d_s g/cm^3	% inc in d	% theor d
45BIT	4	4.623	4.872	***5.4***	***66***
50BIT	4	5.209	5.477	***5.1***	***65***
66BIT	3.5	5.177	5.497	***6.2***	***70***
BIT	3	5.077	6.115	***20.4***	***78***
34BITBT	5	4.300	5.793	***34.7***	***80***
50BITBT	4	4.498	5.280	***17.4***	***79***
66BTIBT	3.5	4.737	5.789	***22.2***	***78***
BT	∞	3.464	4.304	***24.2***	***73***
NBT	∞	4.022	4.138	***2.8***	***69***

Table 3-XIII: Values of density of green body and sintered ceramic for the compounds of table XII. dg = green density, ds = sintered density, incr. in d. = increase in density passing from green to sintered. The last column represents the percentage of the theoretical density.

The sintered densities of the pellets are generally quite low, due to the strong pre-sintering phenomenon induced by the high calcination temperature. The pellets with compositions of the NBT series have densities around 65-70% of the theoretical value. Although more dense, pellets of the compounds of the other series have values not higher than 80%. Among the end-members, BIT exhibits a density 78% of the theoretical value whereas the perovskite end members have values of 73% for BT and only 69% for NBT. These values stress the big influence of the pre-sintering that occurs in calcination.

The low value of density is due to the presence of big pores as can be easily seen in the SEM picture in Figure 3.31. In this figure the surface and fracture micrograph of a pellet composed of the two perovskite end members are shown.

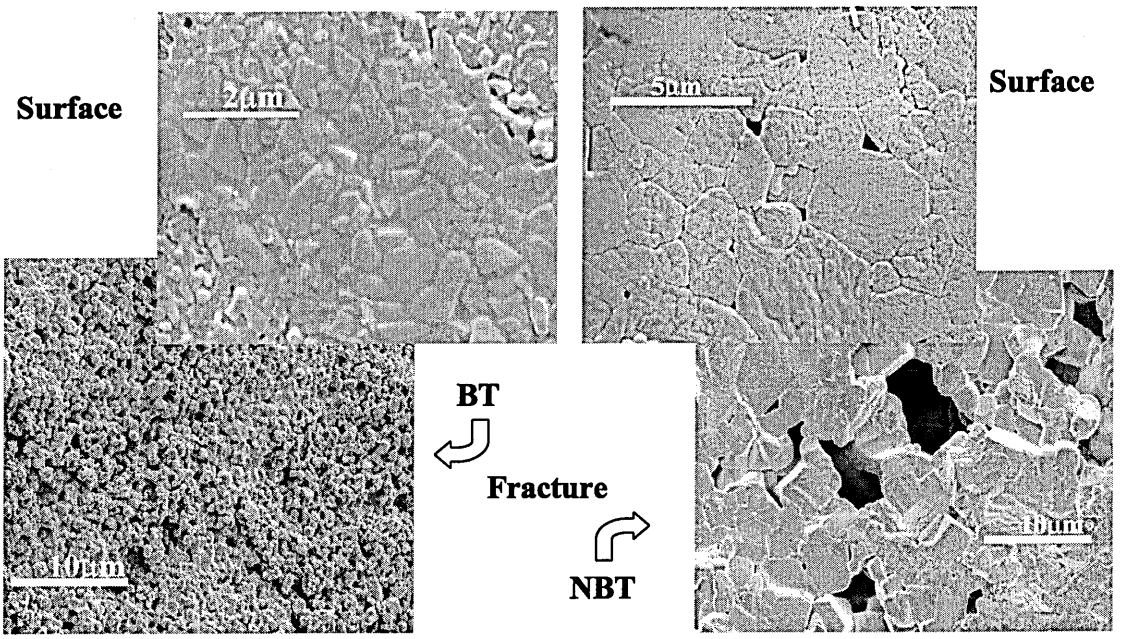

Figure 3.31: SEM micrographs of the polished and etched surface and fresh fracture of the two perovskite end members of the system: NBT and BT.

The porosity is very large in the case of NBT and gives reason for its poor density. Probably, the packing of the big agglomerates arising during calcination was so low to leave big holes that hindered the close contact between some of the particles necessary for the densification process. The severe calcination conditions are responsible also for the abnormal grain growth of NBT when compared with BT. Excess grain growth reduces the mechanical properties of the ceramic making it more subjected to mechanical failure.

The grain growth is particularly pronounced in BIT (Figure 3.32). In this case the grains reach dimensions of over 20μm, almost ten times bigger than is generally found in the literature for this material.

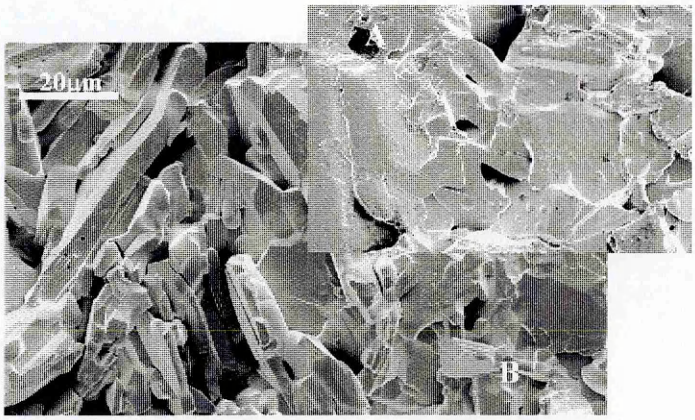

Figure 3.32: SEM micrographs of BIT fracture (A) and surface (B) . The two micrographs have the same magnification.

The platelike shape of the grains of these materials explains also the way in which the ceramics tend to densify. The major faces of the platelets possess the highest energy and as a consequence, they tend to reduce their energy forming stacks, as shown in Figure 3.33. When the particles are not parallel, there is the formation of large pores that are very difficult to eliminate.

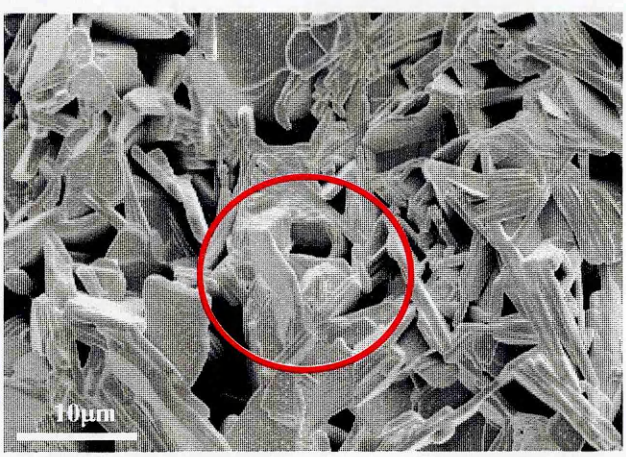

Figure 3.33: SEM micrographs that verify the mechanism of the densification of Aurivillius compounds. The platelike particles tend to form piles as shown in the red.

Figure 3.34 shows the SEM picture of the same compounds as shown in Figure 3.16. The difference in grain size is retained in the sintered body. This picture shows also the preferential "face to face" sintering of the platelets that hindered the final density of the compounds in the BIT-BT series.

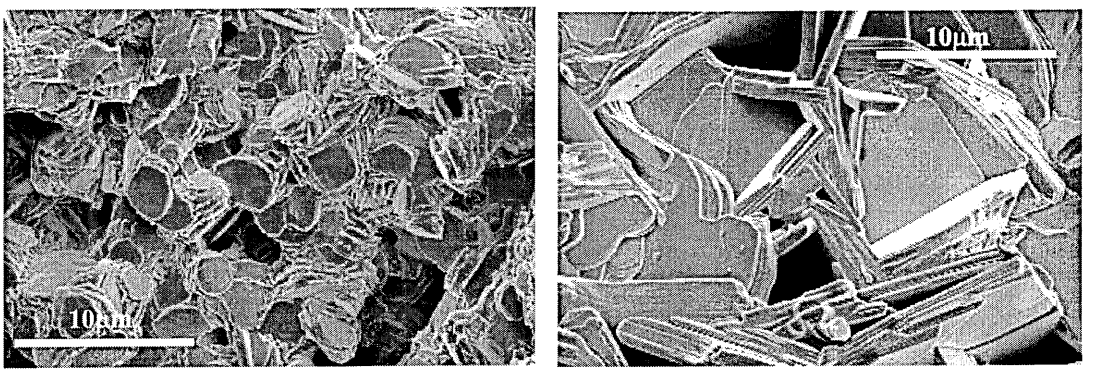

Figure 3.34: Comparison between ceramics of $BaBi_4Ti_4O_{15}$ (left) and $Na_{0.5}Bi_{4.5}Ti_4O_{15}$. The two compounds are the same of Figure 3.16.

The intergranular fracture showed by these pictures is typical of liquid-phase sintering. The phenomenon is well known in bismuth ceramics where Bi_2O_3 assists as a liquid phase in the densification process.

The structure of the two major faces of each pellet was checked by XRD: 1) as sintered; 2) after grinding and lapping. This was done to verify the influence of bismuth and sodium evaporation on the structure of the material and its evolution through the thickness of the pellet. The results of these analyses are reported in Figure 3.35 for BIT. The same behaviour was also observed for all the pellets of the different compositions made.

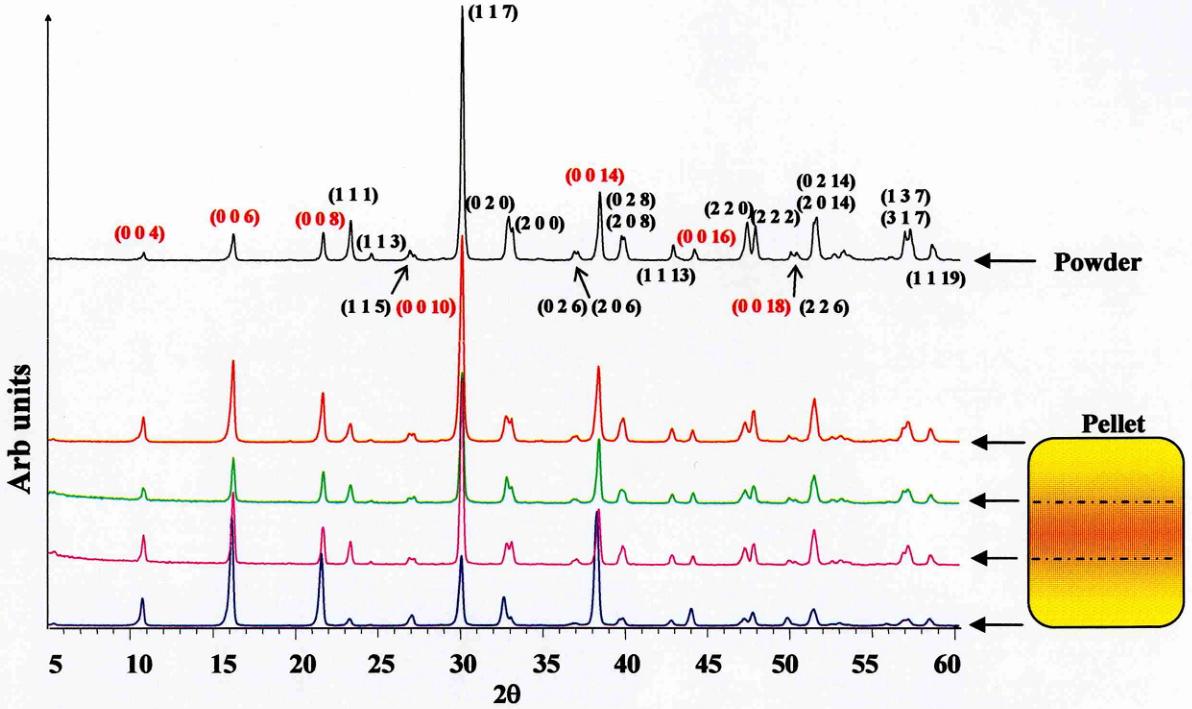

Figure 3.35: Effect of the sacrificial layer of powder on the structure of the sintered pellet.

The two faces of the sintered pellet are different. In the following discussion these notations will be used: "up" is the face exposed to the air, "down" is the one lying in the bed of sacrificial powder. The main difference between the diffractograms shown in Figure 3.35 is the marked c-orientation of the "down" face of the sintered pellet. The blue diffractogram is characterised by an increased intensity of the peaks corresponding to the (0 0 ℓ) planes. The orientation is so strong that the most intense peak is no longer the (1 1 7) (as in randomly oriented ceramics) but instead (0 0 6) and (0 0 14) peaks. A more systematic approach to determine the degree of orientation of materials was proposed by Lontgering[174]: the degree of c-orientation (%F) of the material can be determined by the XRD analysis using Equation 3.5.

$$\%F = \frac{P - P_0}{1 - P_0} \qquad \textbf{Equation 3.5}$$

where $P = \frac{\sum I(00\ell)}{\sum I(hk\ell)}$, $\sum I(00\ell)$ and $\sum I(hk\ell)$ are the sum of the intensities of the reflections in the sample. P_0 is the value of P for a random oriented powder. The results of these calculations are presented in Table 3.XIV.

Sample	P	%F
Random (Powder)	0.27	0
As sintered down	0.50	31.5
As sintered up	0.30	0.04
After grinding down	0.33	0.08
After grinding up	0.33	0.08

Table 3-XIV: Degree of orientation for the diffractograms of figure 3.36.

From the data of the table, it is clear the enhanced orientation of the face down of the pellet analysed just after sintering. The "up" face is basically randomly oriented as are the two faces of the sample after grinding. The higher value of orientation after grinding compared with the one of the pellet just sintered can be due to the grinding process itself. During grinding some of the particles not parallel of the surface could be removed more easily leaving a slight improvement in the orientation of the surface. Lu et al. showed[175] that when $SrBi_2Ta_2O_9$ (m=2) is sintered in presence of excess of Bi_2O_3, the liquid phase formed by the latter enhances anisotropic grain growth. In particular, in the grains with the a-b basal plane parallel to the mayor surface of the pellet. As a consequence, in presence of excess of bismuth oxide, $SrBi_2Ta_2O_9$ develops a strong c-orientation. In our case, the sacrificial powder used to limit Bi and Na acts as a source of Bi_2O_3. During sintering Bi_2O_3 melts and the liquid phase promotes the alignment of the platelets and the c-orientation of the face of the pellet lying over it. As expected, this phenomenon disappears after grinding leaving the two faces with the same degree of orientation.

3.2.3. ELECTRICAL MEASUREMENTS

3.2.3.1. Resistivity

Measurements of the resistivity as a function of temperature in the range 15-65°C for the composition corresponding to pure phases showed, among the Aurivillius compounds, the resistivity to increase as the number of perovskite blocks increases. The trend for the NBT-BIT and BT-BIT series is shown in Figure 3.36.

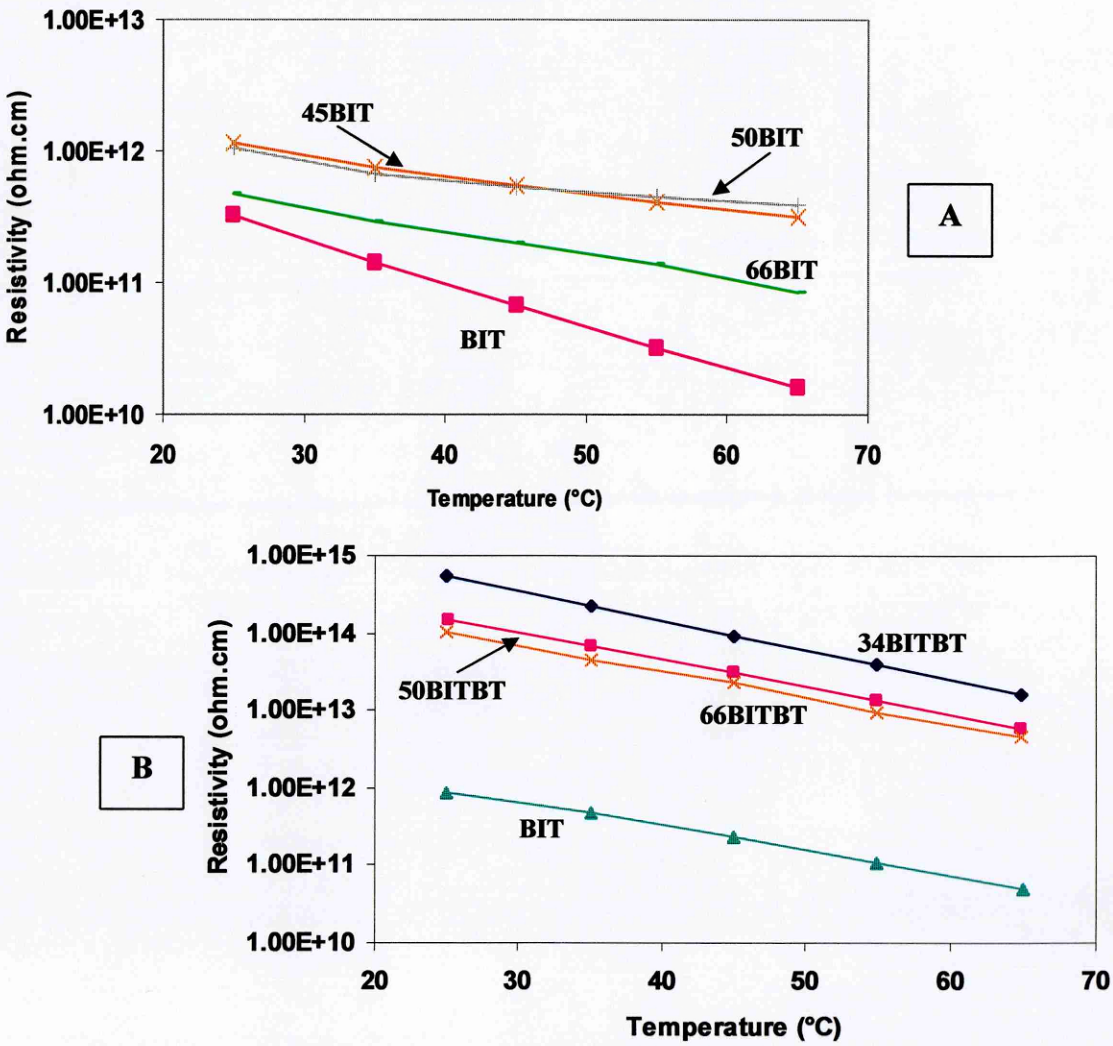

Figure 3.36: Trend of resistivity with temperature for the NBT-BIT series (A) and BT-BIT series (B).

This behaviour can be explained by considering the amount of vacancies present in each compound. In the following discussion the NBT-BIT will be considered, but the same considerations are valid for the compounds of BT-BIT. Using the notation first proposed by Srinivas and Jones[176], the formula of the Aurivillius compounds can be written in an alternative way to stress the number of perovskite blocks present:

$$Bi_4Ti_3O_{12} = Bi_2O_3 \cdot 3(Bi_{2/3}\square_{1/3}TiO_3)$$

$$Na_{0.5}Bi_{8.5}Ti_7O_{27} = 2\{Bi_2O_3 \cdot \tfrac{1}{2}[4\cdot(Na_{1/8}Bi_{5/8}\square_{1/4}TiO_3)\cdot 3(Bi_{2/3}\square_{1/3}TiO_3)]\}$$

$$Na_{0.5}Bi_{4.5}Ti_4O_{15} = Bi_2O_3 \cdot 4(Na_{1/8}Bi_{5/8}\square_{1/4}TiO_3)$$

The symbol "□" denotes an unoccupied site in the A-position of the perovskite block. This unoccupied site acts as an acceptor centres. As a consequence, the materials behave like a p-type semi-insulator, as already noticed by Shulman et al. for BIT[177] . The vacancies in the A-site of the perovskite blocks are also responsible for the creation of oxygen vacancies that are known to play a vital role in the conductivity of the oxide ferroelectrics. These can be seen by rewriting the previous compositions considering the effective charges of the vacancies

$$Bi_4Ti_3O_{12} = Bi_2O_3 \cdot 3(Bi_{2/3}\,V'''_{Bi_{1/3}}\,Ti\,O_{11/4}\,V^{\bullet\bullet}o_{1/4})$$

$$Na_{0.5}Bi_{8.5}Ti_7O_{27} = 2\{Bi_2O_3$$

$$\cdot\tfrac{1}{2}[4\cdot(Na_{1/8}Bi_{5/8}\,V'''_{Bi_{1/4}}\,Ti\,O_{45/16}\,V^{\bullet\bullet}o_{3/16})\cdot 3(Bi_{2/3}\,V'''_{Bi_{1/3}}\,Ti\,O_{11/4}\,V^{\bullet\bullet}o_{1/4})]\}$$

$$Na_{0.5}Bi_{4.5}Ti_4O_{15} = Bi_2O_3 \cdot 4(Na_{1/8}Bi_{5/8}\,V'''_{Bi_{1/4}}\,Ti\,O_{45/16}\,V^{\bullet\bullet}o_{3/16})$$

From these formulae it is easy to evaluate the numbers of vacancies for each compound of the Aurivillius series considered: the vacancies decrease with the number of perovskite blocks from 0.33 for $Bi_4Ti_3O_{12}$ (m=3) to 0.25 for $Na_{0.5}Bi_{4.5}Ti_4O_{15}$ (m=4) passing through 0.29 for $Na_{0.5}Bi_{8.5}Ti_7O_{27}$ (m=3.5). On the basis of this simple consideration, it is clear that the compound with more perovskite slabs should exhibit a higher resistivity.

The dependence of the conductivity (and consequently of the resistivity) on the temperature is described by Equation 3.6.

$$\sigma = \sigma_0 \exp\left(-\frac{E_A}{kT}\right) \qquad \textbf{Equation 3.6}$$

where σ_0 is a constant, k the Boltzmann's constant, E_A the activation energy of the conduction mechanism and T the absolute temperature. The lines obtained by plotting $\ln\sigma$ as a function of 1/T are called Arrhenius plots and allow E_A to be calculated. The Arrhenius plots for the compounds under examination are shown in Figure 3.37.

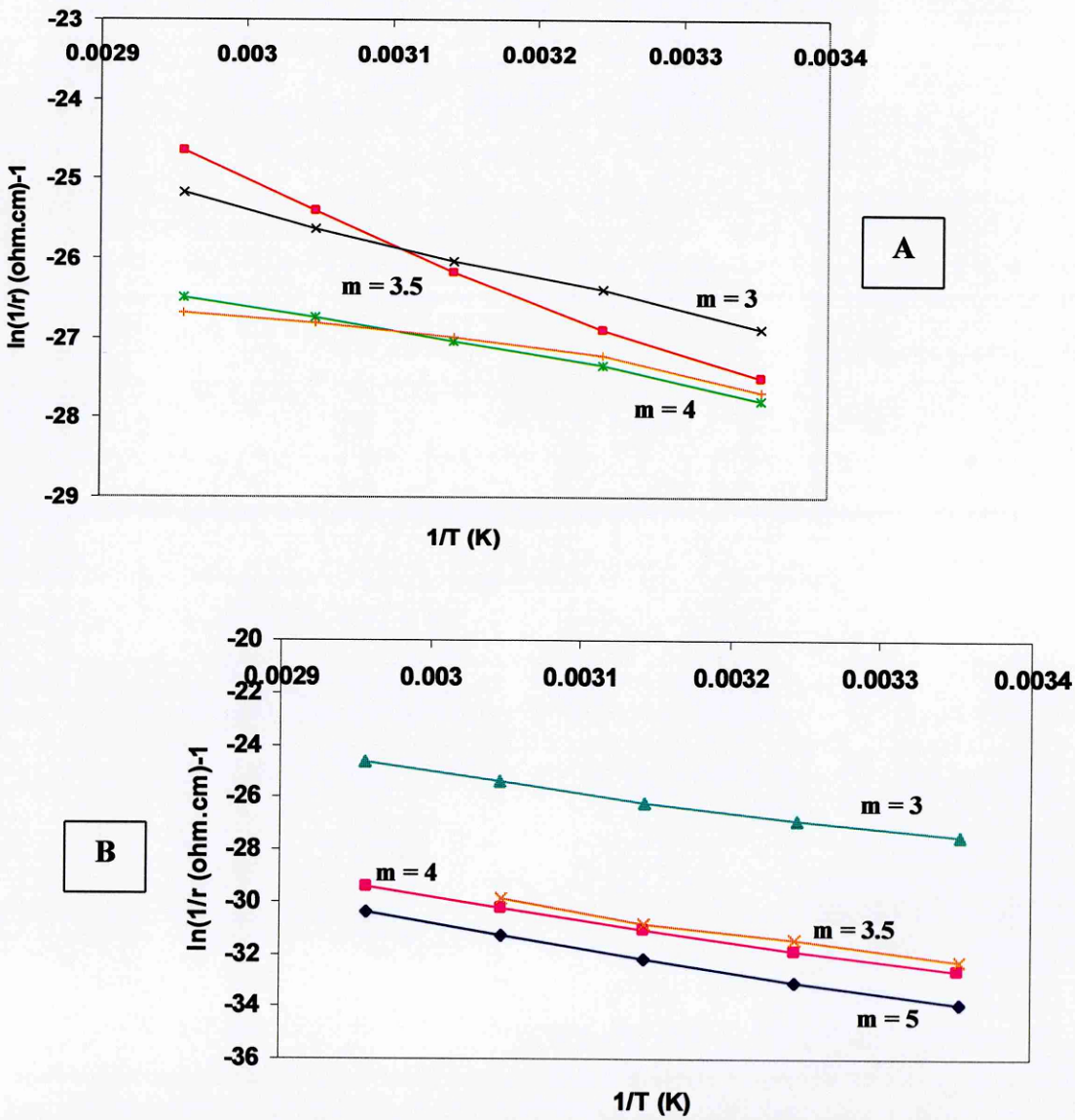

Figure 3.37: Arrhenius plots for the NBT-BIT series (A) and BT-BIT series (B).

Table 3-XV summarises the values of activation energies obtained. This time the trend in the two series is different. For NBT-BIT, the activation energy of the conductive mechanism reduces as the number of perovskite blocks increases; whereas for the compounds of the other series the activation energy is almost constant.

m	E_a NBT-BIT (eV)	E_a BT-BIT (eV)
3	1.25	1.25
3.5	0.80	1.29
4	0.56	1.31
5	-	1.27

Table 3-XV: Activation energy for the conduction mechanism of the systems of Figure 3.38.

For NBT-BIT, the behaviour is assumed to be due to the influence of the bismuth oxide layers which act as an insulator against charge transport[178]. In compounds with more perovskite blocks, the bismuthyl layers are further away from one another and their influence upon the conductivity is lower.

The different behaviour of barium compounds can be understood through a consideration of the mechanism of conduction in the Aurivillius compounds. The conductivity in this family is electronic p-type and is mainly due to the bismuth ions in the perovskite block (section 1.4.2.5). In the case of the BT-BIT series, not only do the A vacancies and O vacancies decrease with m but so do the number of active bismuth ions. The lowering of charge carriers is going to counterbalance the effect of the bismuthyl layers, giving essentially constant activation energy. The lower amount of charge carriers is also responsible for the higher value of resistivity shown by compounds belonging to the BT-BIT series when compared with the one of the homologous NBT-BIT series. A small role could also be played by the higher relative density of the pellets of the former compounds.

3.2.3.2. Permittivity

All the samples present a huge dielectric relaxation below 10 kHz confirmed also by a peak in the dielectric loss at the same frequency. The behaviour of the two quantities for the end member BIT is reported in Figure 3.38A) and B). The temperature activation of the polarization process is around 200-250°C for the Aurivillius compounds considered (except for BIT for which the phenomenon begins at 100°C) and the characteristic relaxation time is of the order of 10^{-2} to 10^{-3} s. All the compounds also show a big thermal hysteresis that decreases with the frequency, probably due to the reorientation of some of the domains present in the materials.

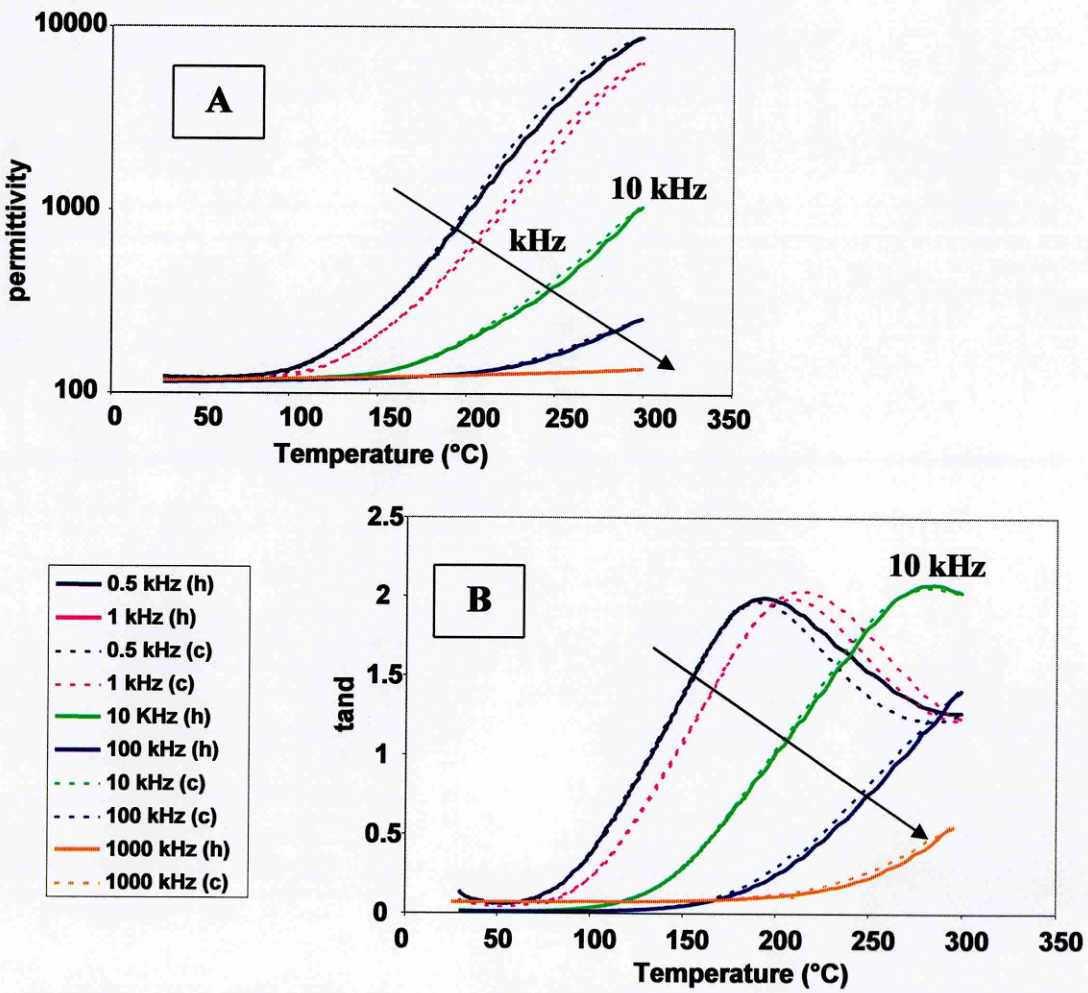

Figure 3.38: Trend of permittivity (A) and dielectric loss (B) as function of temperature and frequency for BIT.

This kind of behaviour has been reported before by Shulman et al.[177]. The brick-wall microstructure typical of the Aurivillius compounds and the tendency of the TiO_2-based compounds to reduce, suggests a thermally activated mechanism of interfacial polarisation of the grain conductivity that shifts the maximum of dielectric loss at higher temperature to higher frequencies. It is known[179] that this kind of mechanism of space-charge relaxation initiates at around 10 kHz, exactly the frequency observed. S. Ehara observed[180] that the relaxation of these compounds can be due to space charge accumulated on the surface of the crystals by a non-ohmic contact between the electrodes and the sample. For this reason the ohmic behaviour of the pellets were tested in the range 10-100V. The measurements of current flowing in the material as a consequence of an applied voltage were done in the apparatus of the experimental section (2.2.3). Each value was collected 10 min after the application of the voltage to allow the establishment of equilibrium conditions. The results are summarised in Figure 3.39.

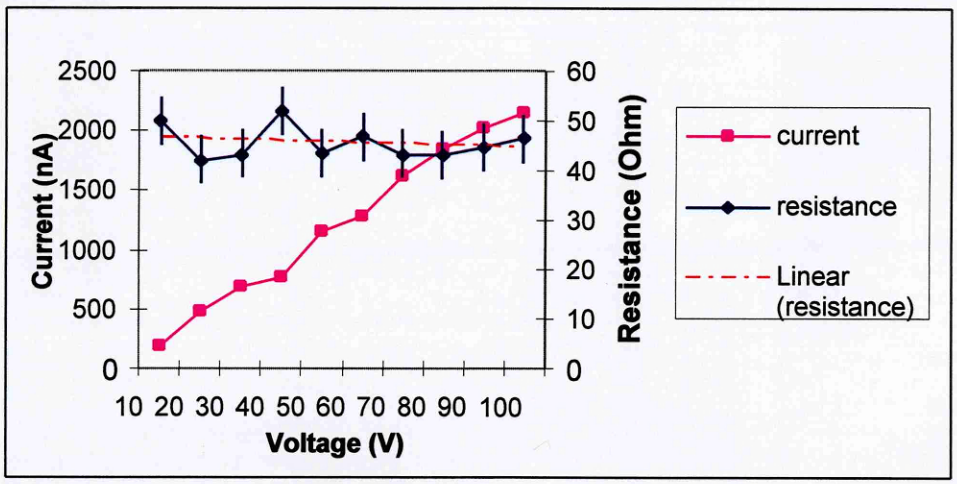

Figure 3.39: Ohmic behaviour of the BIT pellet.

The graph shows an acceptable ohmic behaviour with an average resistance of 45±3 Ohm. To test the effect of another electrode a new set of measurements was performed on pellets electroded with sputtered TiO_2/Pt. The results for BIT at 10 kHz are shown in Figure 3.40. In the figure the dielectric measurements conducted on two samples with Au/Cr and Pt/TiO_2 electrodes are shown. There is perfect agreement between the two set of measurements. The phenomena of relaxation that are shown by

the compounds of the system are due to interfacial polarisation of the grain conductivity. The trend below 100°C is due to the moisture adsorbed by pellet as a consequence of its porosity.

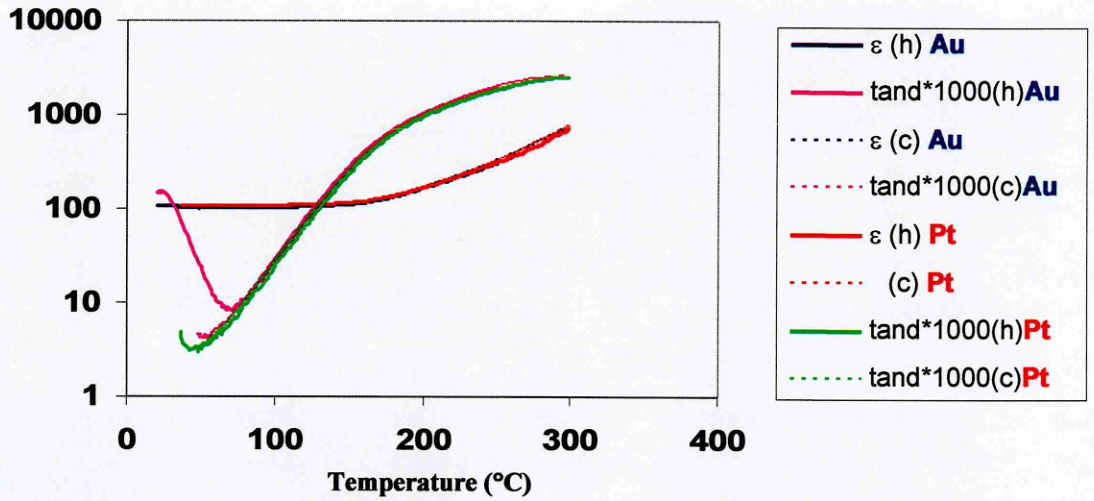

Figure 3.40: Effect of the nature of the electrode on the dielectric measurements on BIT.

Damjanovic et al. showed[181] that single phase Aurivillius ceramics may behave as basic Maxwell-Wagner units as a consequence of the high aspect ratio of its grains and high anisotropy of dielectric properties. The Maxwell-Wagner effect is related to the charge developing in the interfaces between two electrically heterogeneous materials. Such effect can lead to a huge relaxation of the dielectric properties especially in the radio frequency region[182]. The simplest case considers two materials with different values of dielectric constants and conductivities connected in series (Figure 3.41).

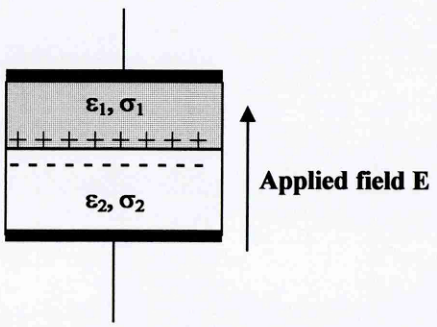

Figure 3.41: Maxwell-Wagner effect in a system formed by two capacitors (1,2) in series.

If the dielectric properties of the two materials are different, the charge carriers are not free to migrate inside material but are trapped within the interface between the two[183]. This phenomenon of space charge polarisation causes dispersion with frequency of the dielectric constant. For such a system the real and imaginary permittivity can be deduced by the expression of two capacitors in series with the knowledge of the relative permittivity (ε_1,ε_2), resistivity (ρ_1,ρ_2) and thickness of the two layers (d_1,d_2). The equations are frequency dependent and take the form of Debye equations[184] (Equations 3.7 and 3.8)

$$\varepsilon'(\omega) = \frac{\tau_1 + \tau_2 - \tau + \omega^2 \tau_1 \tau_2}{C_0 (R_1 + R_2)(1 + \omega^2 \tau_2)} \quad \textbf{Equation 3.7}$$

$$\varepsilon''(\omega) = \frac{1 - \omega^2 \tau_1 \tau_2 + \omega^2 \tau (\tau_1 + \tau_2)}{\omega C_0 (R_1 + R_2)(1 + \omega^2 \tau^2)} \quad \textbf{Equation 3.8}$$

where A is the area of the capacitor, τ a time constant, R resistance and C capacitance. No subscript indicates that the quantity is the one of the global system, whereas 1 and 2 indicate the two different materials. All these variables are linked by the following set of equations easily derived by the basic physics of capacitors[185].

$$\tau_1 = C_1 R_1,$$
$$\tau_2 = C_2 R_2,$$
$$\tau = \frac{\tau_1 R_2 + \tau_2 R_1}{R_1 + R_2}$$
$$C_0 = \frac{\varepsilon_0 A}{d},$$
$$C_1 = \frac{\varepsilon_1 A}{d_1},$$
$$C_2 = \frac{\varepsilon_2 A}{d_2}$$
$$R_1 = \rho_1 \frac{d_1}{A},$$
$$R_2 = \rho_2 \frac{d_2}{A}$$
$$d = d_1 + d_2$$

The grains in Aurivillius ceramics can form structures similar of the one in Figure 3.41. Figure 3.34 shows in fact the tendency of the Aurivillius to form stacks in sintering. Each of these groups of grains will exhibit Maxwell-Wagner relaxation. If we consider a non oriented ceramic, there will be several of these groups of grains, oriented in different ways and with different relaxation times. The ceramics will then give a response that is the result of the integration over all individual Maxwell-Wagner units. Such a model is beyond the scope of this work but is anyway important to realise that this approach could be used to model the relaxation phenomena observed in the Aurivillius compounds.

The relaxation is then linked to the brick-wall structure typical of the Aurivillius compounds. As a consequence, the phenomenon is not present in the perovskite end members as shown by the graphs in Figure 3.42A) and B) for NBT and BT respectively.

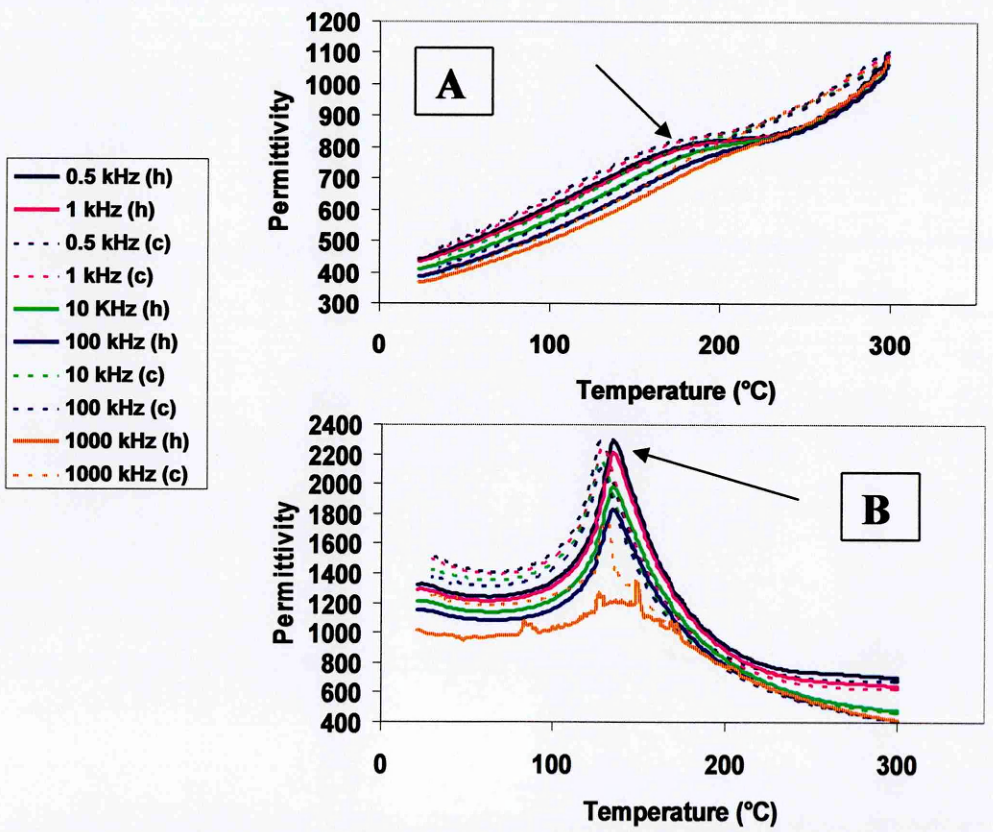

Figure 3.42: Permittivity as function of temperature and frequency for NBT (A) and BT (B). The arrows indicate the phase transition.

Both the members show large thermal hysteresis due to the rearrangement of domains inside the material. The permittivity anomaly at 200°C for NBT is the one not clearly understood as explained in section 1.4.1. On the other hand at 130°C, BT presents the permittivity peak due to the tetragonal-orthorhombic transition.

The relative permittivity in both series increases for an increasing number of the perovskite blocks as shown by Figure 3.43A) and B).

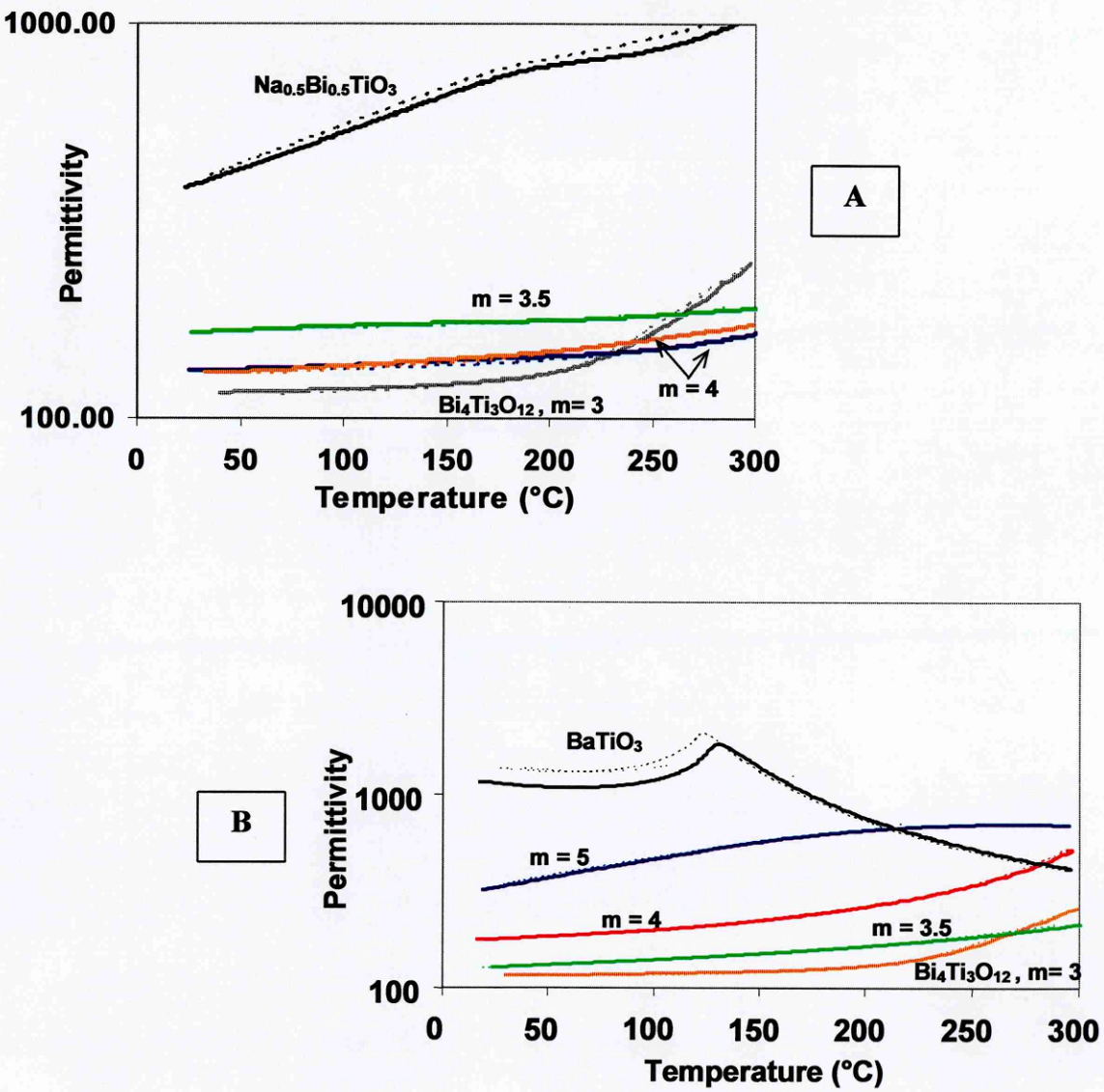

Figure 3.43: Relative permittivity as function of temperature and frequency for the NBT-BIT series (A) and BT-BIT series (B).

As explained earlier, intergrowth compounds do not always fit in a general trend due to the nature of the intergrowth itself. Probably for this reason the compound with

m=3.5 in the NBT-BIT series does not follow the same evolution as the homologue compound in the other series.

The relative permittivity of a material is linked to the internal strain of its unit cell. The higher the strain, the lower the possibility of the internal dipoles to reorient themselves under an external electric field, and as a consequence, the lower the relative permittivity exhibited by the material. The strain in Aurivillius compounds is related to two factors: 1) the A-site vacancies; 2) the formation of a strong bond between the Bi of the bismuthyl layers and the apex oxygen of the perovskite block that causes the tilting of the perovskite octahedra. Figure 3.44 shows the dependence of the A-site vacancies on the number of perovskite blocks as derived by the notation of Srinivas and James.

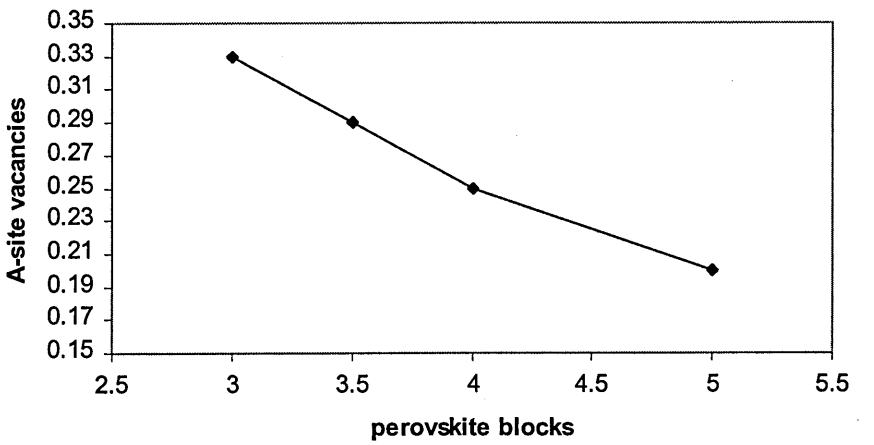

Figure 3.44: A-site vacancies as function of m in the Aurivillius compounds.

As noted previously, the number of vacancies decreases with an increase in number of perovskite blocks leading to progressively less strained system. On the other hand, the Bi-O bond become less strong as m increases as a consequence of the reduced influence of the bismuthyl layers. If this bond is weak, the octahedra are freer to move to decrease tension inside the structure and hence the material as a whole is less strained. The joint effect of these two phenomena, could account for the behaviour observed. It is important to note that the trend does not depend on the nature of the cations involved because it is observed in both the series examined.

Remembering the layered structure of the Aurivillius compounds, the relative permittivity of the unit cell could be obtained using the same model considered to

justify the relaxation phenomena. The unit cell can be considered as a capacitor formed by two materials of different permittivity: the bismuthyl layer and the perovskite blocks (Figure 3.45).

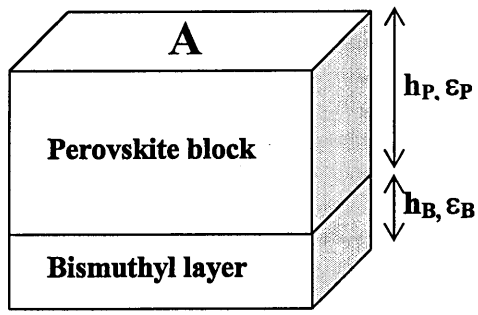

Figure 3.45: "Capacitors in series" model for the structure of a general Aurivillius compound,

As observed before, the dielectric behaviour of this system is described by the expression for a system of capacitors in series (Equation 3.9)

$$\frac{h}{A\varepsilon} = \frac{h_P}{A\varepsilon_P} + \frac{h_B}{A\varepsilon_B} \qquad \textbf{Equation 3.9}$$

where h_B and ε_B are the thickness and permittivity of the bismuthyl layer, h_P and ε_P the thickness and permittivity for the perovskite block and $h = h_B+h_P$. Rearranging the previous equation and considering $hp = m \cdot h'_P$ (the total thickness of the perovskite block is equal to m times the thickness of a single octahedra) it is possible to obtain an equation for the total permittivity in function of the number of perovskite blocks.

$$\varepsilon = \frac{mh'_P(\varepsilon_P\varepsilon_B) + h_B(\varepsilon_P\varepsilon_B)}{mh'_P + h_B} \qquad \textbf{Equation 3.10}$$

If it is assumed that the previous considerations about strain and the Bi-O bond are correct, it can be seen that in this equation is not only the thickness of the perovskite block that increases with m, but also the relative permittivity of the perovskite block (ε_P). As a consequence Equation 3.10 describes a function that increases with the number of perovskite blocks as confirmed experimentally.

3.2.3.3. *Piezoelectric Properties*

In Table 3.XVI the values of d_{33} coefficient measured with Berlincourt d_{33}-meter are reported.

Formula	Label	M	% BIT	d_{33} (pC/N)
$BaTiO_3$	BT	∞	0	118±2
$Ba_2Bi_4Ti_5O_{18}$	34BTIBT	5	34	12.5±0.7
$BaBi_4Ti_5O_{15}$	50BITBT	4	50	10.1±0.2
$BaBi_8Ti_7O_{27}$	66BITBT	3.5	66	8.9±0.3
$Na_{0.5}Bi_{0.5}TiO_3$	NBT	∞	0	40±3
$Na_{0.58}Bi_{4.37}Ti_4O_{14.84}$	45BIT	4	45	17.2±0.4
$Na_{0.5}Bi_{4.5}Ti_4O_{15}$	50BIT	4	50	14.9±0.5
$Na_{0.5}Bi_{8.5}Ti_7O_{27}$	66BIT	3.5	66	7.9±0.4
$Bi_4Ti_3O_{12}$	BIT	3	1	-

Table 3-XVI: Values of d_{33} for the NBT-BIT and BT-BIT series.

It was not possible to pole BIT as a consequence of his high conductivity at the temperature used (120°C) and for this reason no value of d_{33} is reported.

The d_{33} values decrease with the amount of bismuth titanate and the number of perovskite blocks for both the series, as expected. Observing the trend in the NBT-BIT series (Figure 3.46) it becomes clear the importance of examining the phase diagram in the attempt to find compounds with high m **and** with high percentage of perovskite end-member. 45BIT and 50BIT have in fact the same number of perovskite blocks, but the former has a higher amount of NBT in its composition. This difference is reflected in a higher piezoelectric coefficient. The graph shows a linear dependence of d_{33} upon the composition.

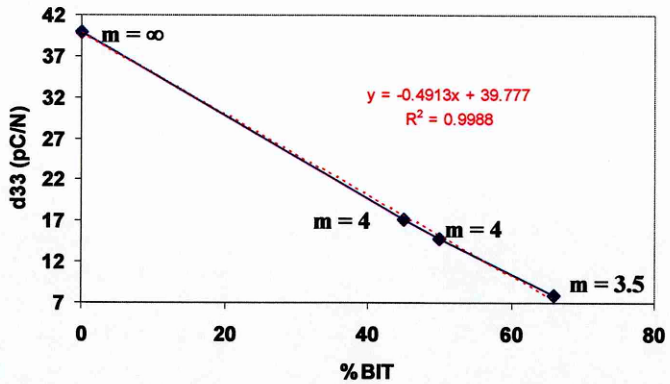

Figure 3.46: Trend of piezoelectric coefficient with amount of BIT for the NBT-BIT compounds.

The behaviour is slightly different in the other series. Although the trend is still linear among the Aurivillius compounds (Figure 3.47), there is a deviation from linearity if barium titanate is included. This behaviour is thought to be due to inefficient poling of the BT-BIT phases. In general, the BT compounds present higher relative permittivity and resistivity compared to the NBT ones. As a consequence the conditions used for the poling may not be strong enough to fully polarise the samples. The influence of this effect is higher for compounds with higher numbers of perovskite blocks because the dielectric properties increase with m.

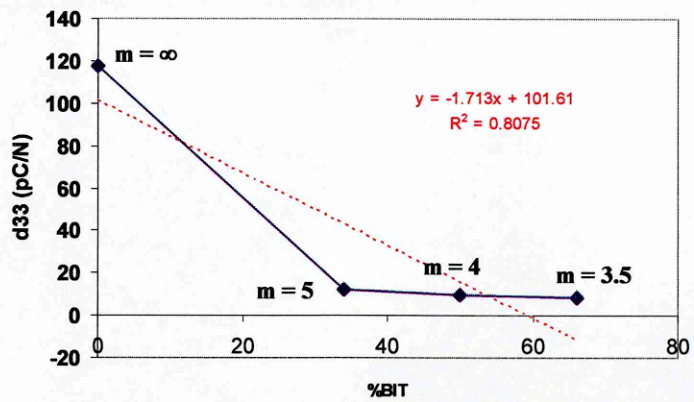

Figure 3.47: Trend of piezoelectric coefficient with the amount of BIT in the BT-BIT series.

The piezoelectric coefficients of the compounds examined are generally lower than the values found in literature (see Table 1-III). The situation is particularly bad in the case of the perovskite end members that present values up to 44% lower than the ones

generally considered for ceramics of these compounds. Table 3-XVII compares the two set of values.

Compound	d_{33}exp (pC/N)	d_{33}lit(pC/N)
$Na_{0.5}Bi_{0.5}TiO_3$	40	70
$BaTiO_3$	118	190

Table 3-XVII: Comparison between values of literature (d_{33}lit) and experimental values (d_{33}exp) for NBT and BT.

These low values are due to the low densities of the ceramics obtained as discussed in more detail in the next paragraph.

3.2.4. Final considerations about electrical and piezoelectrical properties

All the electrical and piezoelectrical properties of the pellets examined are lower than those generally found in literature. These differences are due to the quality of the ceramics obtained. The conditions necessary to produce the Aurivillius compounds are generally much more severe than the ones needed to produce perovskite compounds. In this work in particular, the ceramics have been made with the powder used to study the phase diagram. As a consequence the ceramic samples were of low density and consequently exhibited low electrical and piezoelectrical properties.

To verify that the lower density was the reason for the poorer properties, the same studies as conducted previously were performed on NBT ceramics obtained in optimised conditions. The pellets were made using the same conditions of calcination and sintering as generally used in literature to obtain dense ceramics. The powders were calcined at 800°C for 2 hours and the green body sintered at 1200 for two hours. These conditions gave ceramics samples with densities above 96% of the theoretical value.

Figure 3.48 shows the relative permittivity measurements for one of those pellet (A) compared with the same analysis done previously (B). As expected, the pellet of

higher density shows much higher values of relative permittivity retaining the same trend with temperature and frequency.

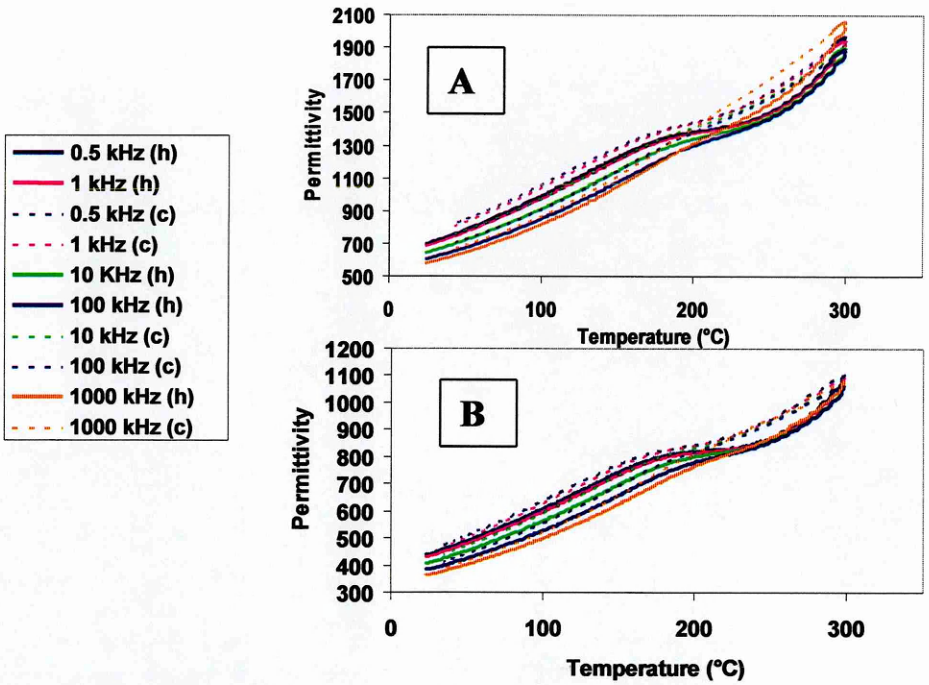

Figure 3.48: comparison between the dielectric constant as function of temperature and frequency for NBT: A) powder calcined at 800C x 2h, B) powder calcined at 1150C x 4h.

The same behaviour was exhibit by the resistivity and piezoelectric coefficient. In particular, d_{33} for this "optimised" pellet reached values of 79 pC/N. This value is higher than the best presented in the literature to date.

It is reasonable to assume that the discrepancies between the experimental and literature values for the Aurivillius compounds are due to the same effect. It is worth to remembering that all the ceramics made had densities between 60 and 80% of theoretical, which is very low. Nevertheless, although the values of resistivity, relative permittivity and piezoelectric coefficient are lower than expected, they are in the range of the ones found in literature. The compounds belonging to the same series, showed similar values of relative density, weight loss and shrinkage making it possible to compare their properties. The trends and behaviours found in this study can then be considered reliable although the absolute value of the quantities involved is conditioned by the density of the ceramic samples.

3.3. Bi_2MgTiO_3 (BMT) System

3.3.1. STRUCTURAL ANALYSIS

3.3.1.1. BMT: Powder Synthesis and Characterisation

3.3.1.1.1. Synthesis and preliminary analysis

This compound was made in the attempt to obtain a new perovskite. Figure 3.49 shows the comparison between the XRD pattern of the raw materials and the one of the system obtained. The raw materials certainly reacted but the diffractogram of the product is far more complicated than that of a simple perovskite.

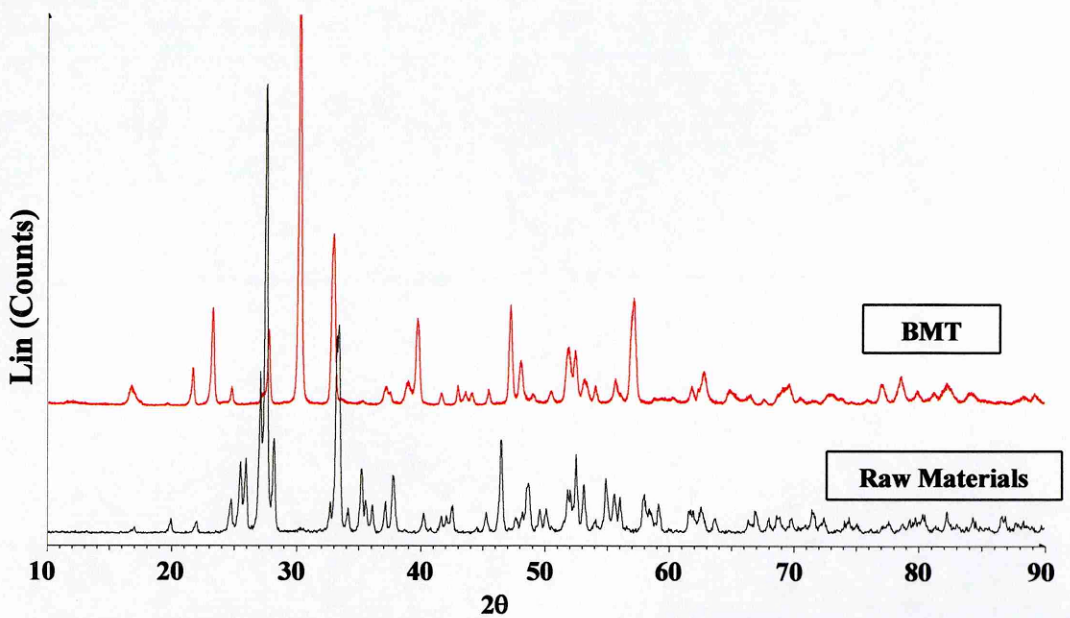

Figure 3.49: XRD diffractograms of the raw materials and final BMT system.

The calculation of the tolerance factor (0.98) revealed that this value is suitable for a perovskite compound

The SEM analysis on the powder showed the presence of a major phase of plate-like morphology (typical of layer compounds) and a secondary acicular one (Figure 3.50).

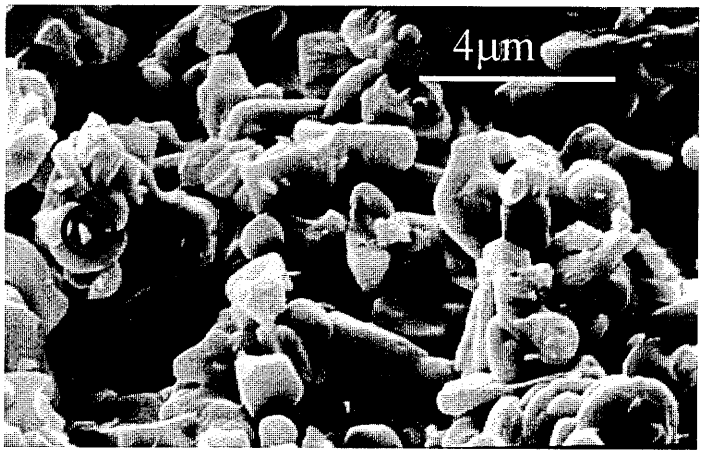

Figure 3.50: SEM micrograph of BMT. The system is formed by two phases: a platelike major one and a second one in form of needles (circle).

These data suggested a biphasic system in which one of the two phases is an Aurivillius compound. To check this possibility, some XRD simulations (Crystallographica) of known Aurivillius compounds were done. Figure 3.51 shows the one for $BaBi_4Ti_4O_{15}$. Several similarities can be seen between this diffractogram and the one of BMT. At least one of the two phases observed in the SEM micrograph of Figure 3.50 could be an Aurivillius compound.

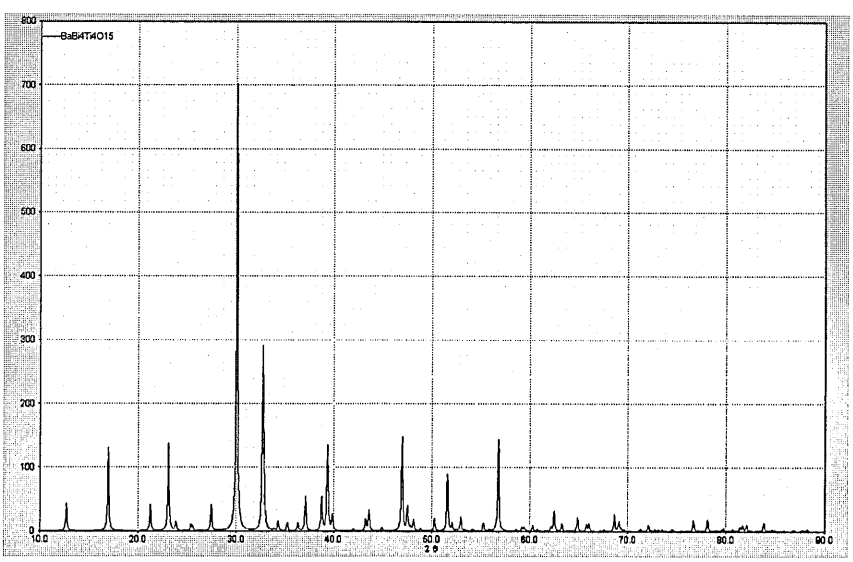

Figure 3.51: Crystallographica simulation of the XRD diffractogram of $BaBi_4Ti_4O_{15}$.

3.3.1.1.2. Evolution with the temperature

To understand the nature of the phases present and their mechanism of formation, a series of calcination were done in the range 500-800°C. The XRD analyses of the systems are presented in Figure 3.52.

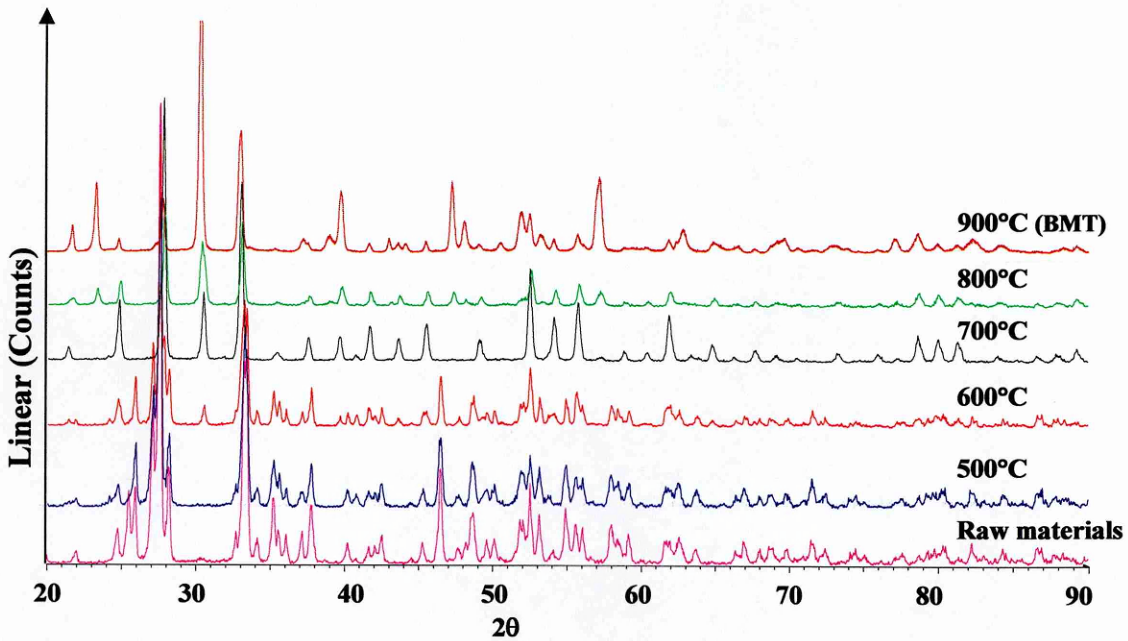

Figure 3.52: XRD diffractograms showing the phase evolution of BMT with temperature.

The raw materials start to react at 600°C to make a cubic phase (identified as $Bi_{12}TiO_{20}$) that is completely formed at 700°C. At 800°C the cubic phase changes its structure to the one of BMT. To check the stability of $Bi_{12}TiO_{20}$ the raw materials have been calcined at 700°C for 15 hours. The comparison between the diffraction pattern powder calcined for two and 15 hours (Figure 3.53) shows no differences; the cubic phase is clearly not a transient one.

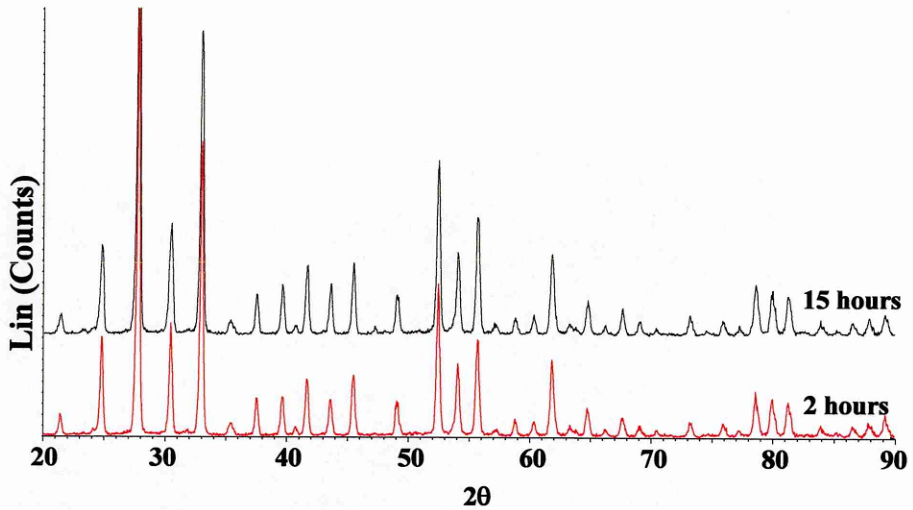

Figure 3.53: Effect of dwelling time on the structure of $Bi_{12}TiO_{20}$.

The phase evolution with the temperature can be also followed from the SEM micrographs of the powders. Figure 3.54 shows the micrograph of the system calcined at 600°C and the EDX analysis of the two different kinds of particles present.

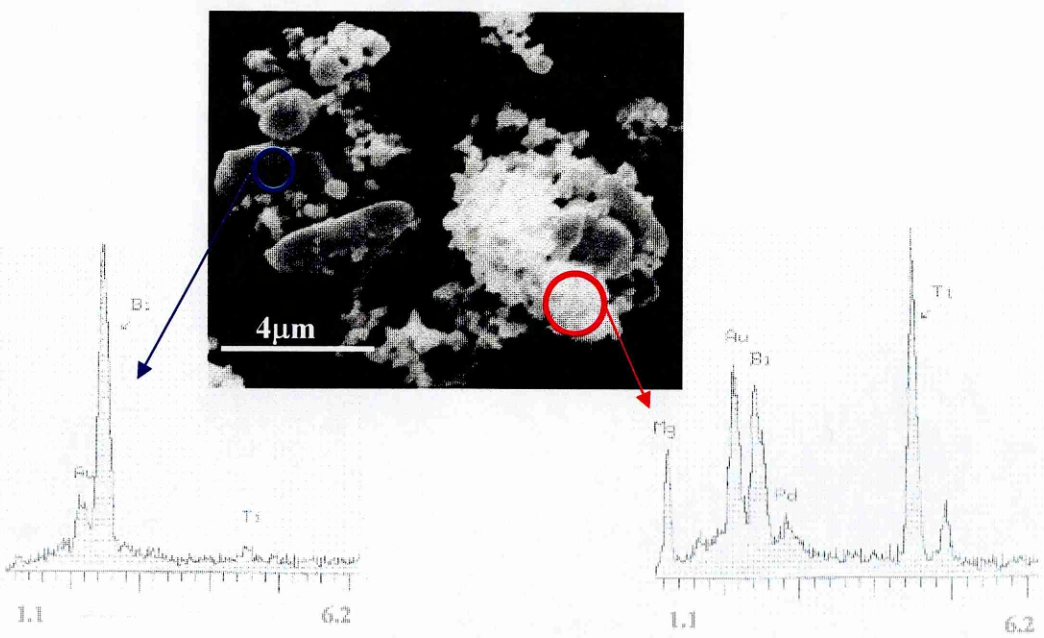

Figure 3.54: SEM micrographs of BMT powder calcined at 600°C. The EDX analyses of the two kind of particle present show that at this temperature bismuth and titanium react, whereas magnesium is not involved in the reaction.

figure). The second phase that can be seen in the micrograph is formed by the remaining Bi, Ti and by magnesium.

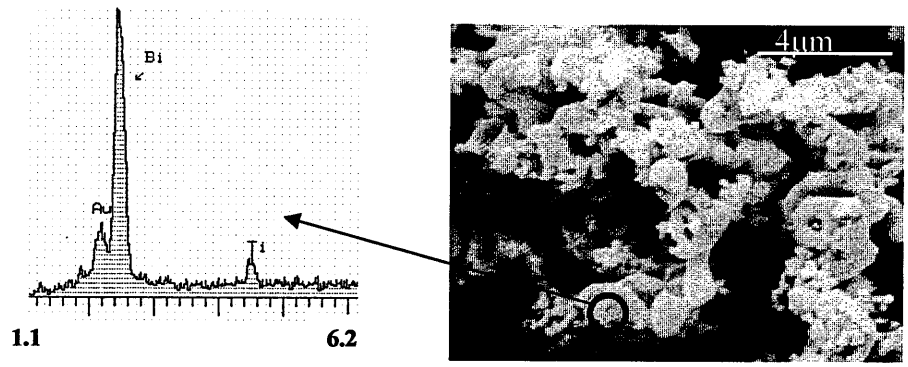

Figure 3.55: SEM micrograph showing the cubic $Bi_{12}TiO_{20}$ phase as stressed also by the EDX analysis. The second phase is constitued of all the materials and it is the same of Figure 3.54.

3.3.1.1.3. Importance of the pre-reaction

As presented in the experimental section (paragraph 3.1.1.2.1), BMT was synthesised in a two stages process. This process includes the pre-reaction of magnesium carbonate and titanium oxide to obtain magnesium titanate and the successive reaction between $MgTiO_3$ and Bi_2O_3 to give BMT. The formation of the cubic phase from Bi_2O_3 and $MgTiO_3$ seems to indicate that the pre-reaction performed to increase the reactivity of magnesium could be irrelevant. To check this possibility BMT was made starting directly from the oxides. The comparison of the diffractograms of the two systems is presented in Figure 3.56.

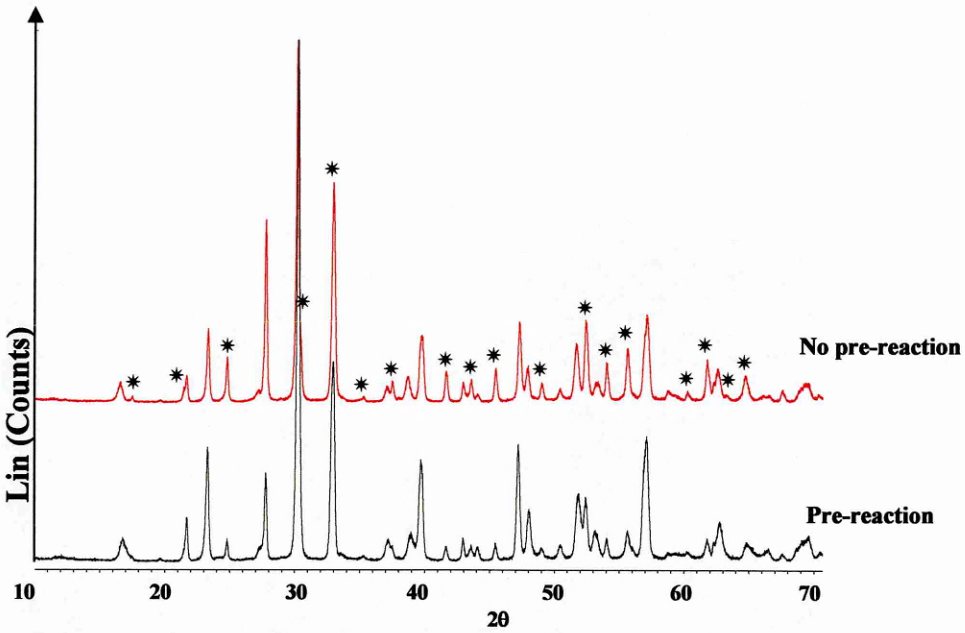

Figure 3.56: Effect of pre-reaction on the XRD diffractogram of BMT. When the raw materials are pure oxides (no pre-reaction), more $Bi_{12}TiO_{20}$ is formed (peaks indicated with the star).

The use of oxides as starting materials promotes the formation of a higher percentage of $Bi_{12}TiO_{20}$ but it does not change the biphasic structure of the system.

3.3.1.1.4. Structure and stoichiometry

These results suggested a reanalysis of BMT considering it as being formed by a mixture of $Bi_{12}TiO_{20}$ and a modified Aurivillius phase. Figure 3.57 shows the comparison between the diffractograms of BMT and its possible constituent phases.

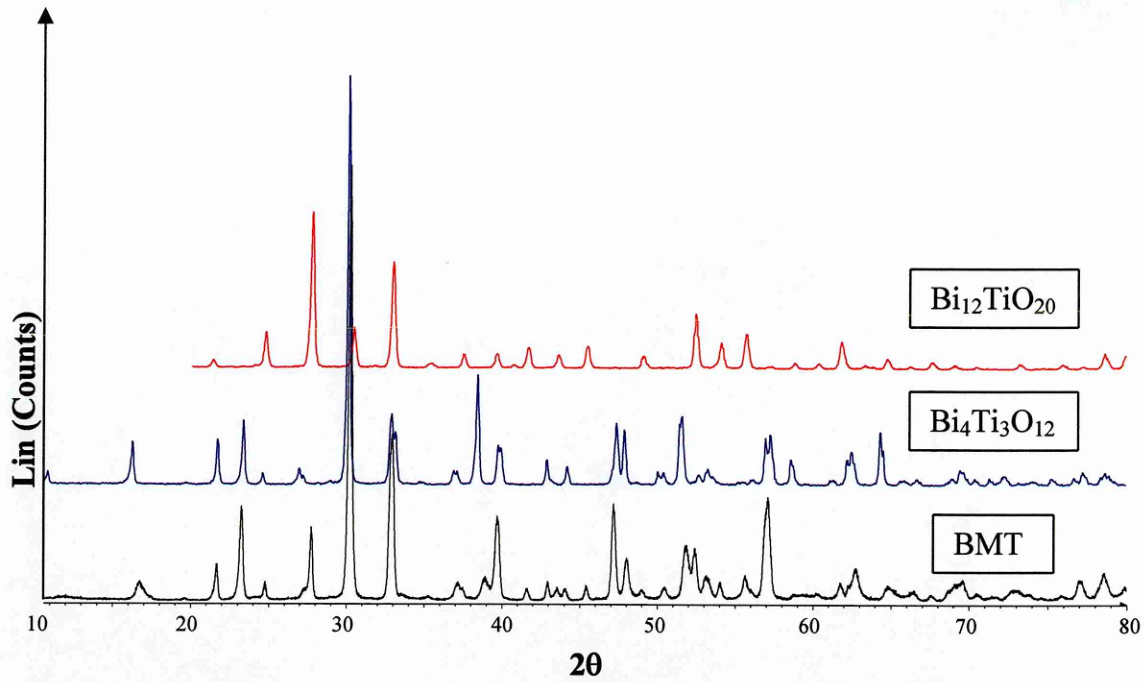

Figure 3.57: Comparison between XRD patterns of BMT and the two phases possibly present: BIT and $Bi_{12}TiO_{20}$.

Although the XRD patterns of $Bi_4Ti_3O_{12}$ matches quite well with the one of BMT, the studies conducted on the Aurivillius compounds of the NBT-BIT-BT system suggested that a low angles XRD analysis could have been useful to unequivocally determine the nature of the layer compound involved. The diffractograms of the Aurivillius compounds, in fact, differ mainly at low angles (peaks of the (0 0 ℓ) planes), whereas at angles higher than 20° the spectra are very similar. The XRD diffractograms in the range of 2θ 2-20° are shown in Figure 3.58. This comparison revealed a structure of the Aurivillius compound closer to the one of 66BITBT (m=3.5) than BIT (m=3). As introduced before (Paragraph 2.4.2.2) the intergrowth between m=3 and m=4 (indicated with m=3.5) is characterised by different levels of structural order determined by the sequence of 3 or 4 perovskite blocks. The breadth of the peaks of BMT in Figure 3.58 is probably indicative of strong disorder of the m=3.5 phase.

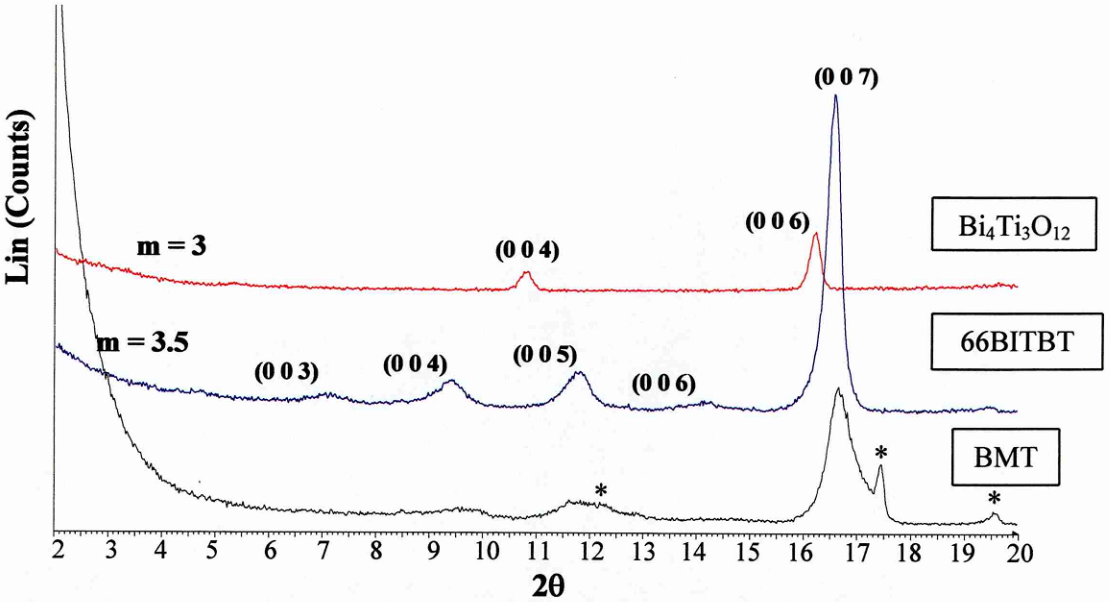

Figure 3.58: Low angle XRD diffractograms of BMT, BIT (m=3) and 66BITBT (m=3.5). The star indicates peaks of $Bi_{12}TiO_{20}$.

The diffractograms of Figure 3.59 show how the long range analysis would not be accurate enough to clarify the real structure of the main phase of BMT.

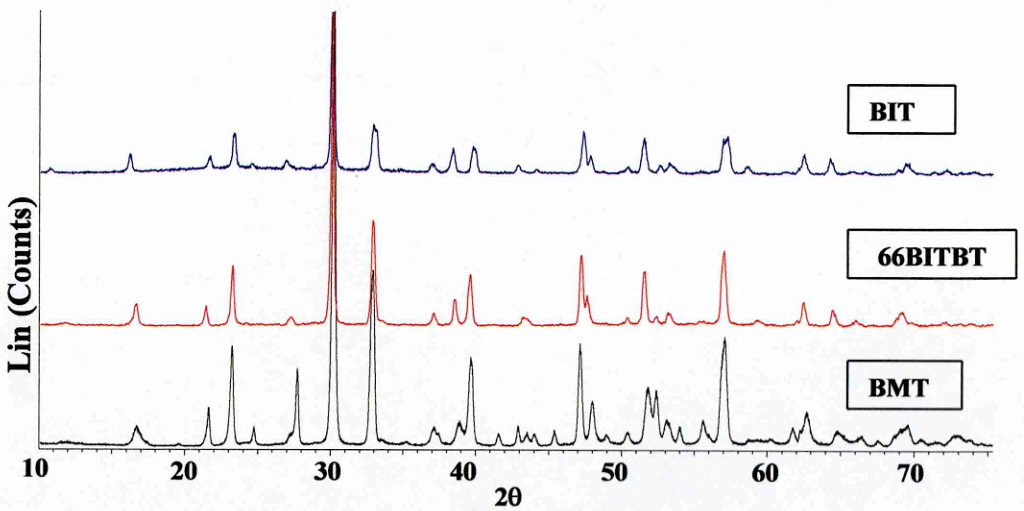

Figure 3.59: Long range XRD analyses of the two possible Aurivillius structure present (BIT, 66BITBT) and BMT.

The intergrowth between m=3 and m=4 (generally indicated as m=3.5) is known[186] to be present in the compounds derived from the coupling of $Bi_4Ti_3O_{12}$ with the $M^{II}TiO_3$

perovskites, where M^{II}=Ca, Sr, Ba and Pb, and it can be represented with the general formula

$$M^{II}Bi_8Ti_7O_{27} = (Bi_2O_2)_2^{2+} \cdot \left[(Bi_2Ti_3O_{10})^{2-} \cdot (M^{II}Bi_2Ti_4O_{12})^{2-}\right]$$

The radius of Mg^{2+} is too small to lead to a perovskite structure, magnesium titanate ($MgTiO_3$) crystallises in the ilmenite form[187]. The formation of an Aurivillius compound with m=3.5 in presence of magnesium seems to be established here for the first time.

It has been shown that the bismuthyl layers of the Aurivillius compounds are invulnerable to substitution except for cations that possess a lone pair like Bi^{3+} (Pb^{2+} and La^{3+})[188]. Magnesium is therefore expected to enter the lattice in the perovskite blocks. According to the formula presented above an m=3.5 compound of magnesium would be expected to give a compound of formula $MgBi_8Ti_7O_{27}$. Although the radius of Mg^{2+} (0.720Å) seems to suggests a B-site substitution (radius of Ti^{4+}=0.605 Å, radius of Bi^{3+}=1.2 Å), in bismuth perovskites it can enter both sites of the perovskite blocks[189]. Besides, the A-site of $MgBi_8Ti_7O_{27}$ is able to accept only 6% of magnesium, whereas from the EDX analysis 33% of the total cations in the lattice must be magnesium (Table 3.XIX). This cation probably enters the A and B sites of both m=3 and m=4 perovskite blocks.

	$MgBi_8Ti_7O_{27}$	**EDX**
Bi (%cations)	50	36
Mg (%cations)	6	33
Ti (% cations)	44	31

Table 3-XVIII: Cations percentages in the theoretical m=3.5 compound ($MgBi_8Ti_7O_{27}$) and the EDX analysis: Mg have to enter all the cations sites available to justify its high amount.

From this considerations the final composition of the Aurivillius phase of BMT has been fixed as

$$Mg(Bi_{5.76}Mg_{2.24})(Ti_{4.96}Mg_{2.04})O_{23.84}$$

3.3.1.2. *Effect of magnesium on properties of BMT*

3.3.1.2.1. *Structure*

The examination of the $MgO/Bi_2O_3/TiO_2$ phase diagram (Figure 3.60) revealed that the composition of the major phase found in the previous chapter lies very close to the line that joins $Bi_4Ti_3O_{12}$ to MgO. This observation suggested to change the direction of the research addressing it on the role of MgO on the properties of $Bi_4Ti_3O_{12}$. Six new systems of composition $(1-x)Bi_{3.74}Ti_{3.19}O_{12}+ xMgO$ (x = 0.1, 0.125, 0.175, 0.225, 0.275, 0.54 in the text indicated as BMT100x) were made and analysed. The composition BMT275 corresponds to the composition of the Aurivillius phase of BMT as determined by EDX.

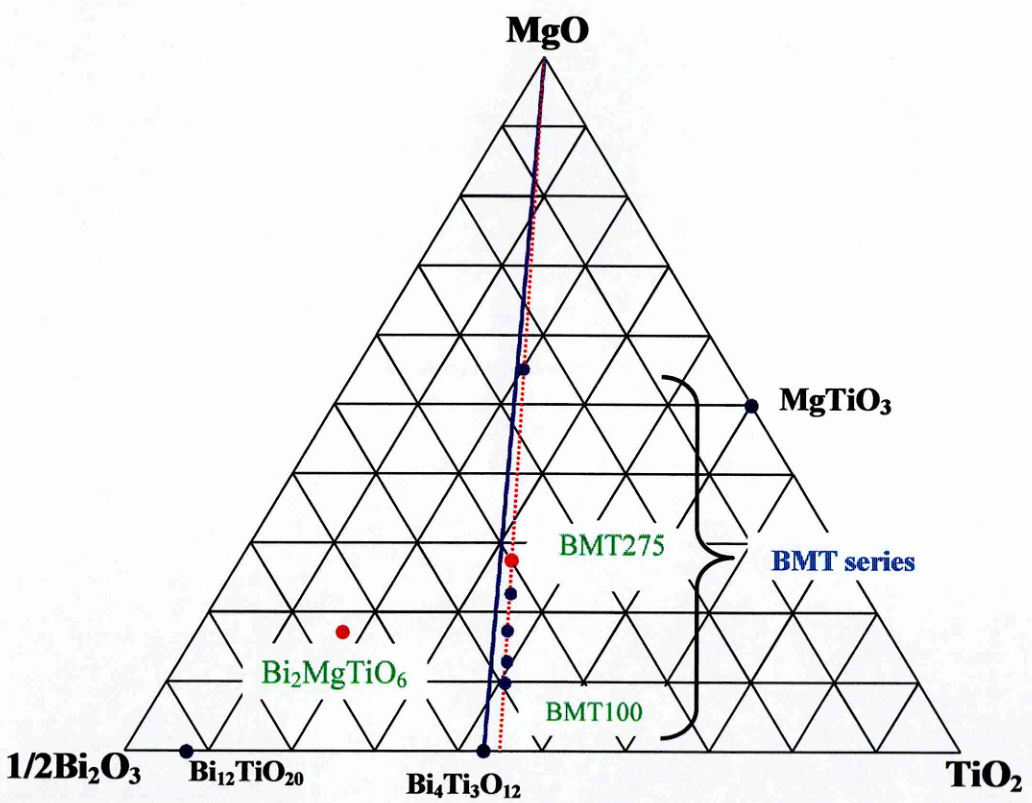

Figure 3.60: Phase diagram of the Bi_2O_3-MgO-TiO_2 system. The compositions involved in this study are also indicated.

The powders of all the compositions (as well as new batch of BIT) were calcined at 900°C for 2 hours. Figure 3.61 shows the diffractograms of the powders of the compounds after calcination. All the compositions have structures similar to the one

of BIT. The assumption was confirmed by the low range angle analyses (inset in Figure 3.61) that show only m=3 compounds. It is remarkable that even a content of 54%mol MgO does not seem to induce the formation of extra-phases.

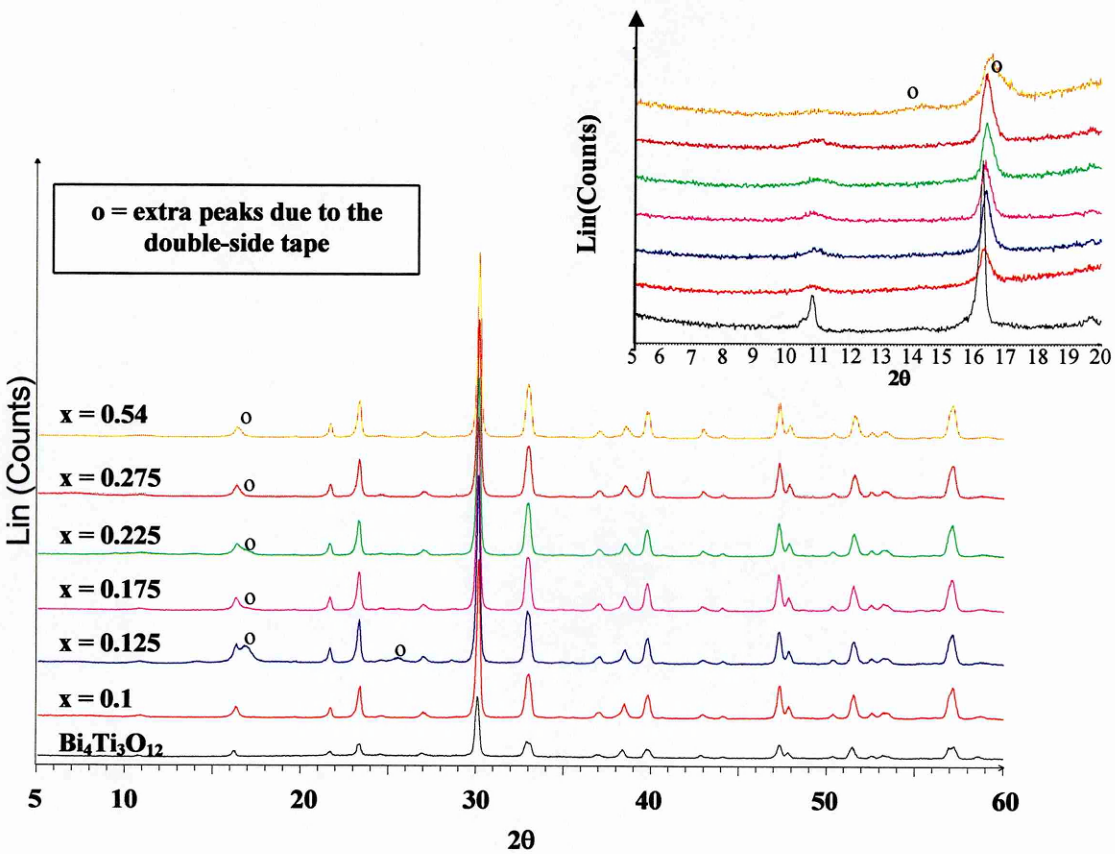

Figure 3.61: XRD analysis on the compound of the BMT series. The inset shows that the compounds are all Aurivillius with m=3.

The diffractograms of $Bi_4Ti_3O_{12}$ and the series end member ($Bi_{3.74}Ti_{3.19}O_{12}$ (x = 0)) are compared in Figure 3.62 and Figure 3.63. The wide angle range comparison (Figure 3.62) shows two diffractograms almost identical.

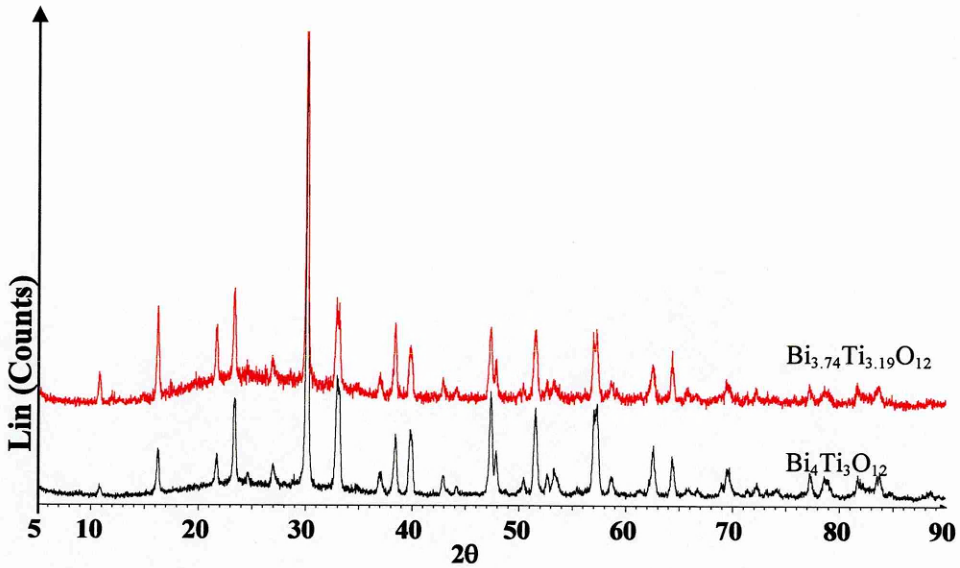

Figure 3.62: Comparison between the diffractograms of BIT and $Bi_{3.74}Ti_{3.19}O_{12}$ (BMT0).

However the low angle analysis reveals that $Bi_{3.74}Ti_{3.14}O_{12}$ is a mixture of an m=3 compound (probably an highly defective BIT) and the cubic phase $Bi_{12}TiO_{20}$ (Figure 3.63).

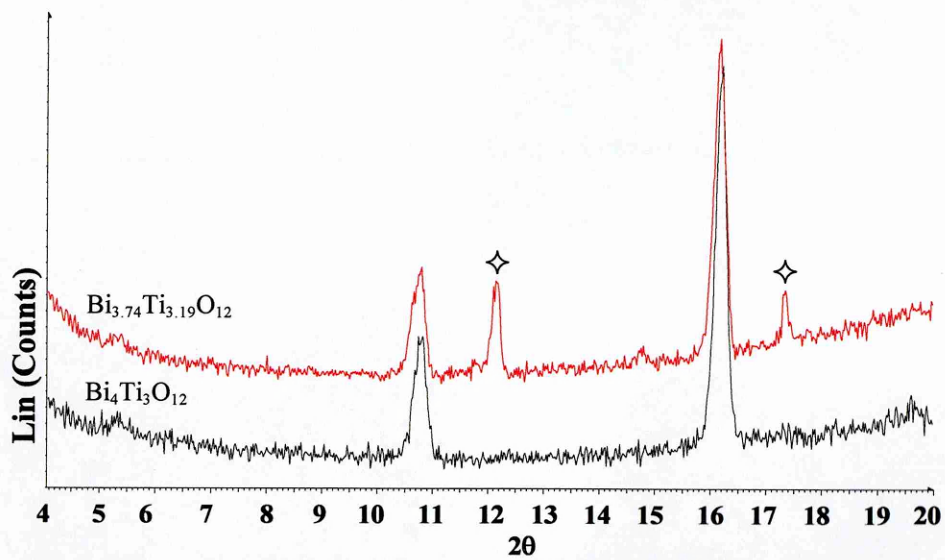

Figure 3.63: Low angle comparison between BMT0 and BIT. The star indicates peaks belonging to $Bi_{12}TiO_{20}$.

The introduction of magnesium suppresses the formation of the cubic second phase giving a monophasic systems. In the following discussion $Bi_{3.74}Ti_{3.19}O_{12}$ will not be considered as consequence of its biphasic nature

3.3.1.2.2. Powder morphology

The SEM micrographs of the powders confirmed that no secondary phase is present. Figure 3.64 shows the comparison between the two end members of the BMT series (BMT100 and BMT540) and BIT. The micrographs have the same magnification and show that the introduction of magnesium reduces the dimensions of the particles without changing their plate-like morphology. The same effect was observed by Tajima et al.[190] for PZT. They suggest that this effect is due to the diffusion of MgO on the crystal lattice of PZT. This diffusion process alters the surface and grain boundary energy of the material leading to smaller particles.

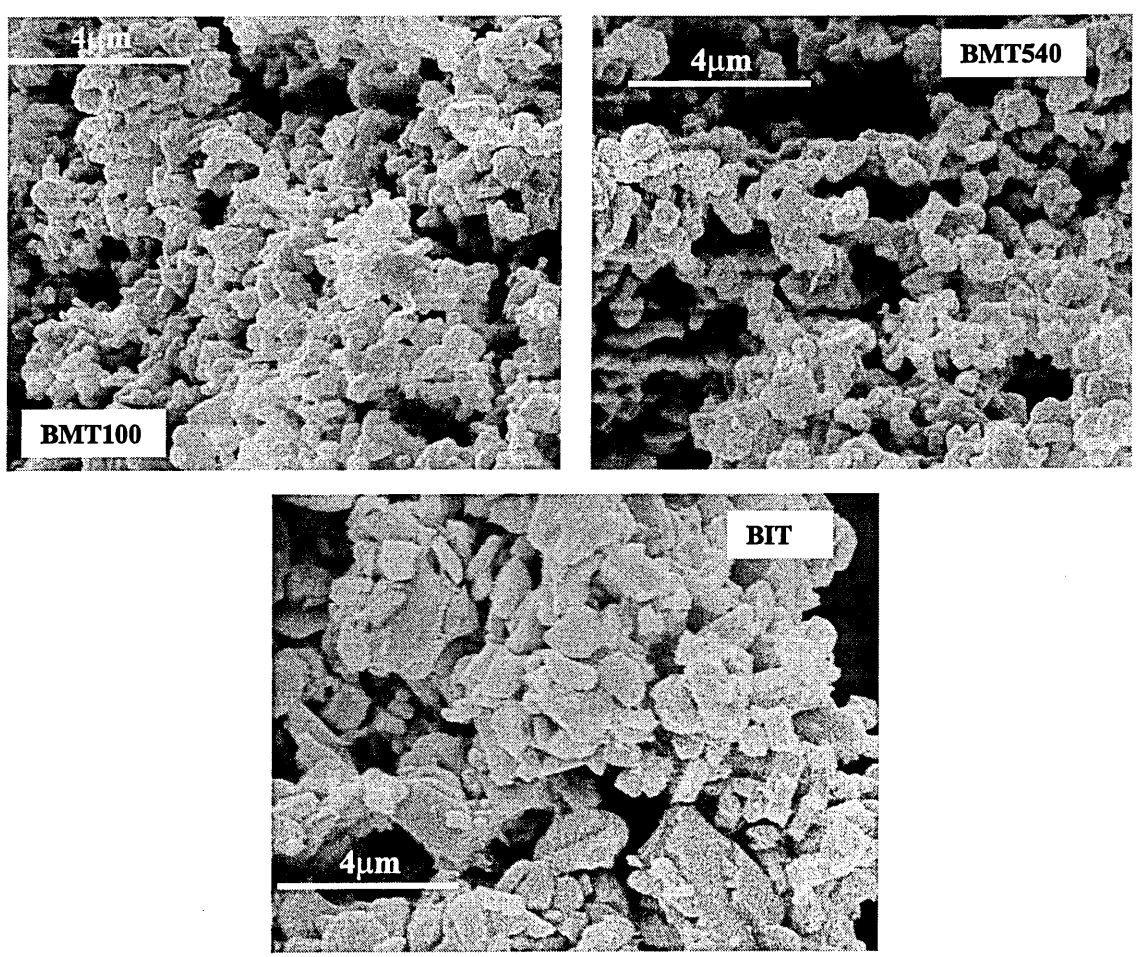

Figure 3.64: SEM micrographs of the two end member of the BMT series (BMT100 and BMT540) and BIT. BIT presents slightly bigger particles, whereas there is no difference in the two BMT compounds.

The dimensions of the particles seem to be independent of the content of magnesium. Figure 3.64 shows in fact that the particles of BMT100 and BMT540, end members of the series, have the same dimensions.

3.3.1.2.3. Cell parameters and stoichiometry

Examining the XRD patterns of Figure 3.61 a slight change in the position of the peaks along the series was noticed. The diffraction angles are determined only by the shape and size of the unit cell: a change in their position implies a change in the dimension of the unit cell. To appreciate the magnitude of this variation, the cell parameters of all the compositions were determined using the least-squares method. The peaks in the diffraction patterns were carefully indexed and the values of the planar spacing used to refine the cell-parameters according to the orthorhombic symmetry typical of BIT. The values obtained are presented in Table 3.XIX.

compound	a (Å)	b(Å)	c(Å)	orth dist
BTO	5.441(1)	5.418(1)	32.805(1)	1.0042
BMT100	5.425(1)	5.425(1)	32.697(1)	1.0000
BMT125	5.430(1)	5.431(1)	32.71(1)	0.9998
BMT175	5.431(1)	5.432(1)	32.729(1)	0.9998
BMT225	5.433(1)	5.433(1)	32.68(1)	1.0000
BMT275	5.429(1)	5.429(1)	32.693(1)	1.0000
BMT540	5.430(1)	5.430(1)	32.644(1)	1.0000

Table 3-XIX: Cell parameters and orthorhombic distortion of the compounds of the BMT series.

The addition of MgO decreases the a-parameter of the cell (Figure 3.65A) while increases the b-parameter leading to a transition from an orthorhombic to a tetragonal cell as shown by the value of orthorhombic distortion (Figure 3.65B).

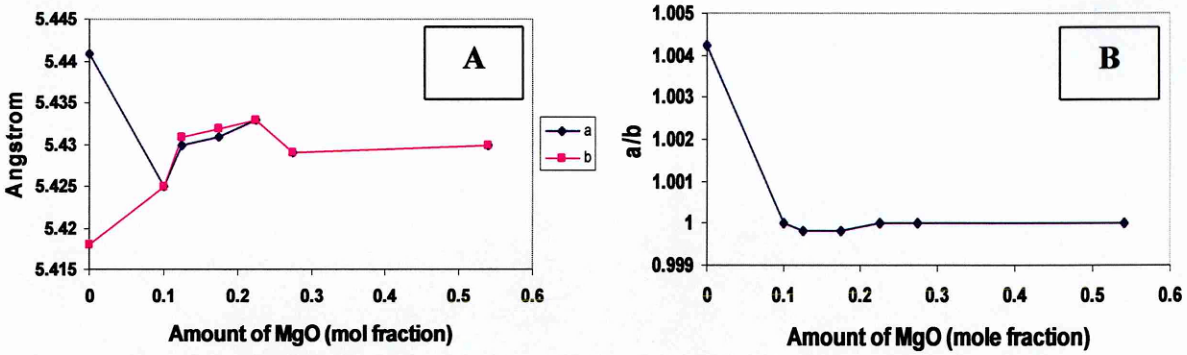

Figure 3.65: trend with composition of the a and parameters (A) and orthorhombic distortion (B) of the compounds of the BMT series.

The decreasing in orthorhombic distortion can be due to the substitution of bismuth by magnesium. Withers et al. [191] found the same phenomenon when divalent ions (like Pb^{2+} and Ba^{2+}) substitute bismuth in the A-site of the perovskite block in BIT. Hervoches et al.[192] showed that the main cause of the orthorhombic distortion in BIT is the strong underbonding of the bismuth ion in the perovskite blocks. In the optimum bonding condition the bond-valence sums of apparent valences (AV) of an atom are equal to its oxidation state. If the apparent valence of the atom is higher than its oxidation state the atom is said to be overbonded, whereas in the opposite case is said to be underbonded. In tetragonal BIT (structure above T_c) the bismuth of the perovskite block is strongly underbonded (AV= 2.38). The off-centre displacement of bismuth, together with the rotation and deformation of octahedra described in section 1.4.2.5, optimise the apparent valence and change the structure to the orthorhombic ferroelectric one. However, the apparent valence of a divalent cation that replaces bismuth in the A-site of the perovskite block will be higher than its oxidation state, i.e. the divalent cation will be overbonded. Any distortion away from the tetragonal structure will cause further overbonding and then a destabilising effect. For this reason the substitution of bismuth with divalent cations generally causes a decrease in the orthorhombic distortion. Rae et al.[193] reported the same effect in $Bi_2SrTa_2O_9$. The decrease in orthorhombic distortion is strong evidence that magnesium actually enters the A-site of the perovskite block in this series of compounds.

To analyse the effect of Mg on the stoichiometry of the systems, the formulae of all the systems was re-written taking into account the basic structure of an m=3 compound. Table 3.XX shows the labels and normalised formulae of the compounds

of the series, stressing the A-site vacancies in the perovskite block and the oxygen vacancies. Following the same considerations as for the NBT-BIT-BT system (paragraph 3.2.1.5), the formulae are normalised on the base of BIT (m =3) and with the stoichiometric amount of titanium as reference.

Label	Formula	V'''_{Bi}	Mg	$V^{\bullet\bullet}_{O}$
BIT	$Bi_4Ti_3O_{12}$	-	-	-
BMT100	$Bi_{3.52}Mg_{0.1}Ti_3O_{11.39}$	0.48	0.1	0.61
BMT125	$Bi_{3.52}Mg_{0.13}Ti_3O_{11.42}$	0.48	0.13	0.58
BMT175	$Bi_{3.52}Mg_{0.2}Ti_3O_{11.48}$	0.48	0.2	0.52
BMT225	$Bi_{3.52}Mg_{0.27}Ti_3O_{11.56}$	0.48	0.27	0.46
BMT275	$Bi_{3.52}Mg_{0.36}Ti_3O_{11.64}$	0.48	0.36	0.36
BMT540	$Bi_{3.52}Mg_{1.1}Ti_3O_{12.38}$	0.48	1.10	-0.38

Table 3-XX: Formulation and vacancies in the compounds of the BMT series.

Table 3.XX shows a deficiency of bismuth in comparison with BIT. The bismuth vacancies in Aurivillius compounds are generally introduced in the A-site of the perovskite blocks. Remembering that two of the bismuth ions of BIT are in the perovskite blocks of the unit cell, the compounds of the BMT series present almost 25% of the A-site of the perovskite blocks empty. The magnesium ion could potentially enter this site formally replacing bismuth and decreasing the bismuth vacancies. The filling of bismuth vacancies causes a consequent decrease in the number of the oxygen vacancies. For BMT540 the amount of magnesium is higher than the amount of bismuth vacancies available and it is possible that the magnesium ions start to replace titanium in the B-site. These formulae show also the extreme flexibility of the Aurivillius compounds that can stand a large number of vacancies without changing their fundamental structure.

The presence of magnesium affects also the c-parameter of the cell, decreasing its value (Figure 3.66). This reduction can be due to the substitution of bismuth with magnesium in the A-site of the perovskite blocks and the presence of oxygen vacancies. Another cause of the shrinkage of the cell along c can be found by analysing the structure of the Aurivillius compounds. The two kinds of layer (bismuthyl and perovskite) that form this family of compounds cannot get too close to

one another due to the electrostatic repulsion between the lone pairs of the bismuth ions that are present in each of them[194]. The substitution of bismuth with magnesium weakens this repulsion allowing the two layers to move closer. As a consequence the cell shrinks in the c-direction.

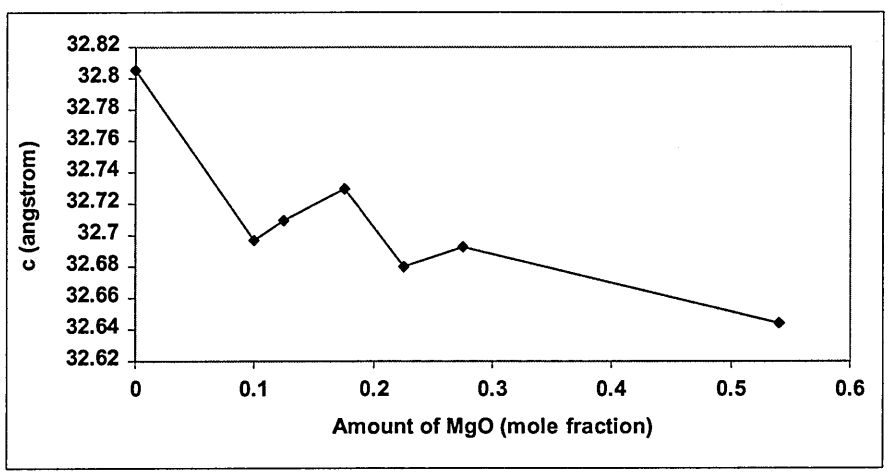

Figure 3.66: Trend of the c-parameter of the cell as a function of the amount of magnesium in the BMT series.

3.3.2. FORMING AND SINTERING

The temperature of sintering for the compounds of the BMT series was chosen after a thermal analysis on BMT (Figure 3.67).

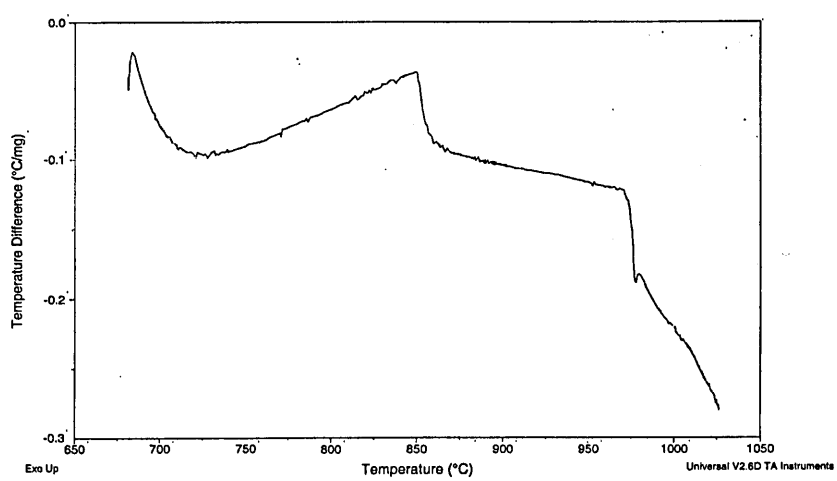

Figure 3.67: DTA analysis of BMT. Two thermal event can be seen: the formation of the Aurivillius phase at around 850°C and the melting point at 975°C.

Figure 3.67 shows the temperature evolution of BMT in the range 650-1125°C. Two thermal events can be seen: the formation of the Aurivillius phase at 850°C and the melting point of the compound at 975°C. All the pellets obtained using powders of the BMT systems were sintered at 950°C for two hours. To avoid any possible influence due to the furnace, the latter was carefully calibrated using the same program of heating of the pellet. An external thermocouple was used to compare the real temperature of the furnace with the one indicated on the display. The result of this analysis is shown in Figure 3.68.

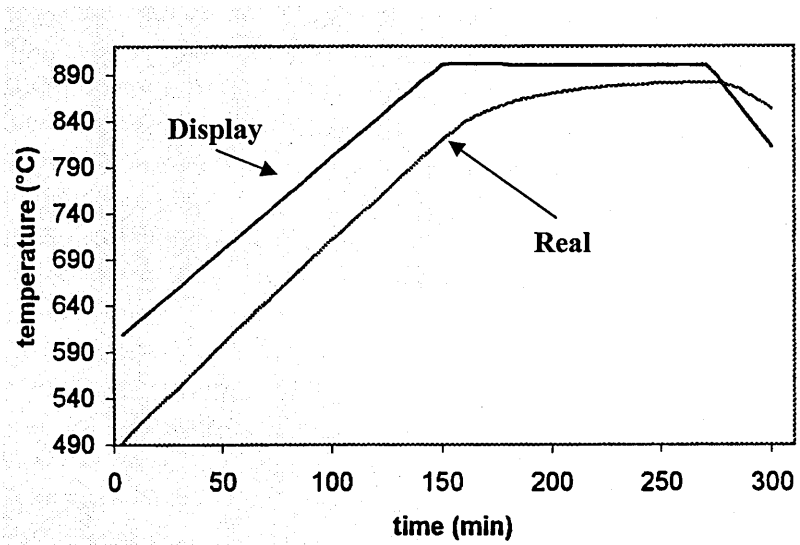

Figure 3.68: Calibration of the furnace for the BMT system. Display indicates the temperature shown by the display, Real the one of the external thermocouple.

The calibration was repeated in several area of the furnace and revealed a difference of 2°C from one area to another.

The c-orientation effect of the BIT sacrificial layer on the face down of the pellet, already noticed in the NBT-BIT-BT system, has also been found in these series, as shown in Figure 3.69 for BMT100.

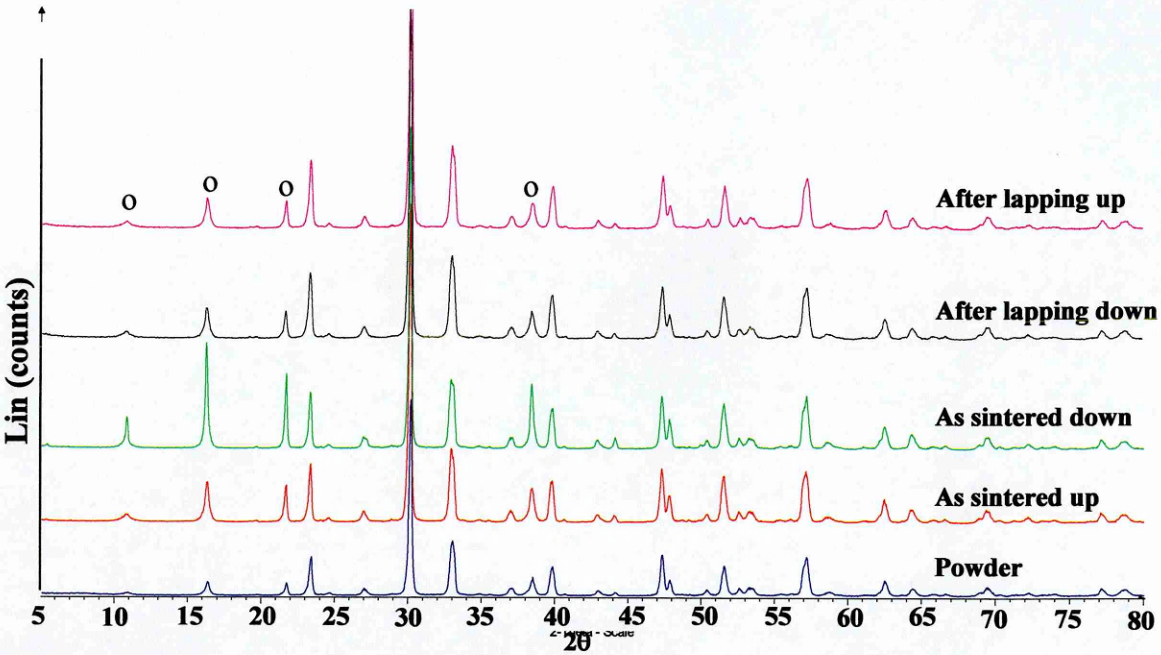

Figure 3.69: Effect of the sacrificial layer on the orientation of the particles. The face lying on the $Bi_3Ti_4O_{12}$ powder shows a high c-orientation (see Figure 3.35). After grinding the diffractograms are the same of the one of the powder. (o) peaks of the (0 0 *l*) planes.

The strong c-orientation also disappears after grinding (first two diffractograms on the top of Figure 3.69) in this case. It is important to notice that in the diffractogram of the sintered pellet there is no sign of a second phase. The crystallographic structure of the ceramic is the same as that of the powder.

Table 3-XXI reports the values of weight loss for the compounds of the series. The data are presented with the errors calculated as standard deviations of 10 independent measurements, whereas the errors on weight loss are always below 0.05%.

Composition	Weight green (g)	Weight sintered (g)	Weight loss (%)
BIT	8.7434±0.0001	8.5102±0.0002	**2.7**
BMT100	8.5297±0.0004	8.3062±0.0001	**2.6**
BMT125	8.0091±0.0001	7.7603±0.0001	**3.1**
BMT175	8.1102±0.0002	7.8482±0.0001	**3.2**
BMT225	8.0269±0.0002	7.7811±0.0001	**3.4**
BMT275	8.0963±0.0003	7.7269±0.0002	**4.6**
BMT540	7.8852±0.0005	7.3791±0.0001	**6.4**

Table 3-XXI: weight loss for the compounds of the BMT series.

The weight loss for BIT in this system is definitively lower than the one for BIT sintered at 1165°C as expected in consideration of the lower sintering temperature. Considering the addition of 2%weight of PVA as a binder, the weight loss is to be considered normal. The addition of magnesium increases the weight loss especially in the last two compounds of the BMT series. Saha et al.[195] showed that the addition of MgO as sintering aid of PMN increases the fluidity of the liquid phase (mainly PbO) responsible for the sintering. This increased fluidity allows the liquid phase to better penetrate the capillaries and improve densification, but also dramatically increases the weight loss of lead. This effect could be applicable also in the case of Aurivillius compounds where the liquid phase is composed by Bi_2O_3. It could be possible that part of the magnesium act as sintering aid in conjunction with bismuth oxide. This effect could explain the steady increase in weight loss along the series and the particularly high loss for BMT275 and BMT540.

In Table 3-XXII the data of lateral and thickness shrinkage are presented. Like in Table 3-XXI there is a sensible difference in the values for the last two compositions and the shrinkage is definitely lower for BIT.

Composition	$\varnothing_g$(cm)	$\varnothing_s$(cm)	%l. shr.	t_g (mm)	t_s (mm)	%t. shr
BIT	2.879±0.005	2.704±0.004	**6.1**	2.62±0.03	2.49±0.06	**5.0**
BMT100	2.799±0.003	2.314±0.002	**17.3**	3.31±0.02	2.73±0.03	**17.5**
BMT125	2.772±0.005	2.285±0.002	**17.5**	3.22±0.03	2.63±0.03	**18.3**
BMT175	2.781±0.004	2.287±0.004	**17.7**	3.25±0.04	2.67±0.04	**17.8**
BMT225	2.777±0.003	2.281±0.006	**17.8**	3.30±0.05	2.73±0.02	**17.3**
BMT275	2.766±0.002	2.242±0.003	**18.9**	3.55±0.05	2.85±0.05	**19.7**
BMT540	2.755±0.003	2.187±0.005	**20.6**	3.75±0.04	2.98±0.05	**20.5**

Table 3-XXII: values of lateral shrinkage (% l. shr.) and thickness shrinkage (%t. shr) for the compounds of the BMT series. $\varnothing_s$=diameter sintered body, $\varnothing_g$ = diameter green body, t_g = thickness green, t_s = thickness sintered body.

The errors in Table 3-XXII were calculated as in Table 3-XXI. The two kinds of shrinkage present similar values showing an almost isotropic decreasing of volume during sintering. The values of shrinkage are very high compared with the one found for the NBT-BIT system. It has been shown in section 3.3.1.2.2, that the particle sizes

of the compounds of the BMT series are smaller than BIT. This feature, in conjunction with the sintering aid effect of MgO introduced in the previous paragraph, could be responsible for the higher shrinkage of BMT compounds. This assumption is confirmed by the values of density presented in Table 3.XXIII. In this table are presented the green density (d_g) and two values of density of the sintered body. These values are derived in two different ways. The first ($d_s(G)$) is derived by pure geometrical considerations from the values of thickness, diameter and weight of the pellet. The second is determined by the Archimedes method. This method consists of weighing the ceramic pellet under two different conditions (i.e. water and air) by using the following equations.

$$\text{volume} = \frac{\text{dry weight} - \text{wet weight}}{\text{water density}} \qquad \textbf{Equation 3.11}$$

$$\text{density} = \frac{\text{dry weight}}{\text{volume}} \qquad \textbf{Equation 3.12}$$

From these two different values of density, or better, from the values of volume derived from them, the percentage of porosity in the pellet can be calculated (last column in Table 3.XXIII).

Composition	d_g (g/cm^3)	d_s (G) (g/cm^3)	d_s (A) (g/cm^3)	Δd(G) (%)	%porosity
BIT	5.126	5.952	6.704	16.1	10.8
BMT100	4.186	7.235	7.583	72.8	4.5
BMT125	4.121	7.195	7.446	74.6	3.4
BMT175	4.102	7.155	7.216	73.9	3.3
BMT225	4.031	6.975	7.197	73.0	3.1
BMT275	3.795	6.868	7.103	80.1	3.3
BMT540	3.527	6.592	6.816	86.9	3.3

Table 3-XXIII: density variations for the compounds of the BMT series. d_g= density green, $d_s(G)$= density sintered body calculated geometically,$d_s(A)$ = density sintered body calculated using the Archimede's method, Δd(G)= variation in geometrical density.

The pellets of the BMT series are definitely more dense than BIT, as shown by the lower values of porosity. It is possible that magnesium enters in the crystalline lattice

only partially and that part of it contributes to the densification of the pellet acting as sintering aid.

The high density of the pellets is shown also by the SEM micrographs of the polished surface (Figure 3.70A). There is no difference among the compounds of the series in the dimensions of the grains.

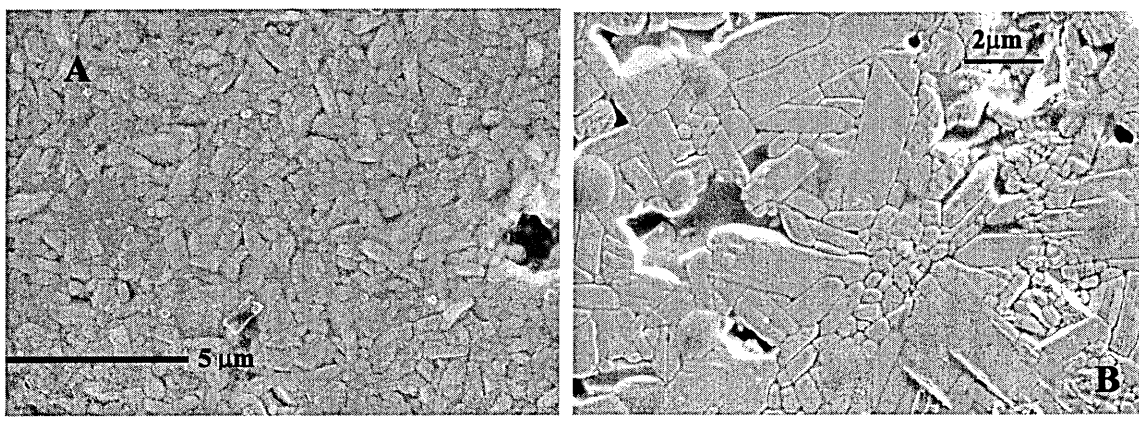

Figure 3.70: SEM micrograph of BMT125 (A) and BIT (B).

The grains of the compounds of the BMT series are smaller than the one of BIT (Figure 3.70B) with a considerably smaller aspect ratio, stressed also by the micrographs of the fractures (Figure 3.71)

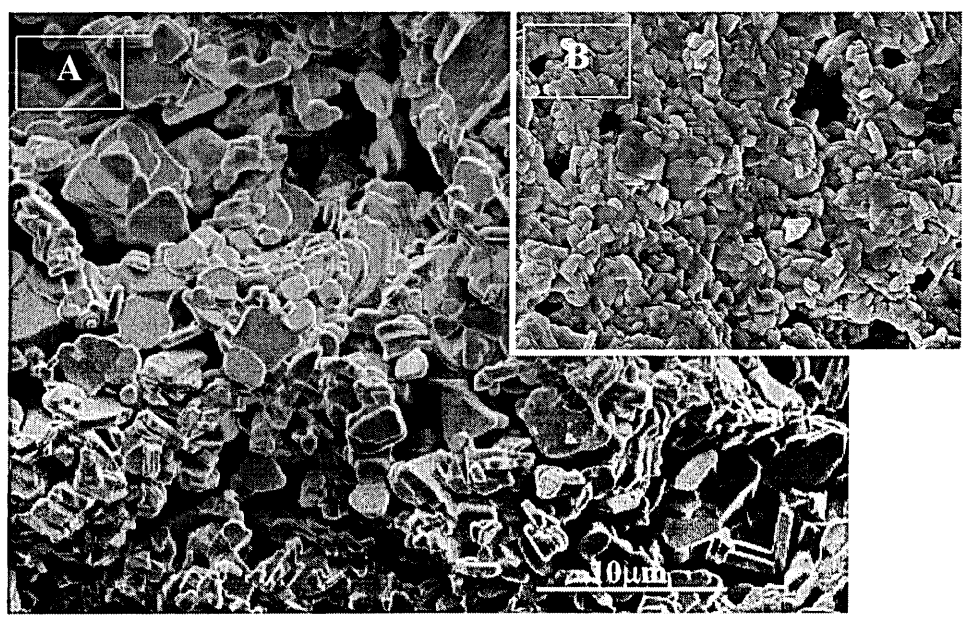

Figure 3.71: SEM micrographs of the fresh fracture of BIT (A) and BMT125 (B). The two micrographs have the same magnification.

The microstructure of the pellets was analysed by SEM after they had been thermally etched to better see the grain boundaries. The conditions used for this process (900°C x 30 min) were too strong and led to the appearance of extra phases. Figure 3.72 shows the etched surface of one of these pellets.

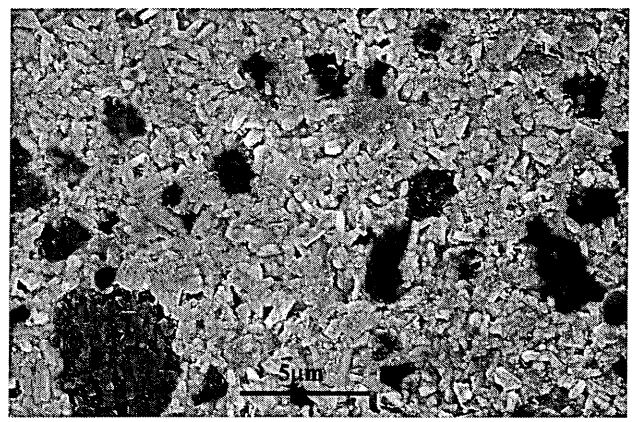

Figure 3.72: SEM picture of BMT125. The darker areas are regions reach in magnesium.

One possible explanation for this appearance can be found by analysing Figure 3.73.

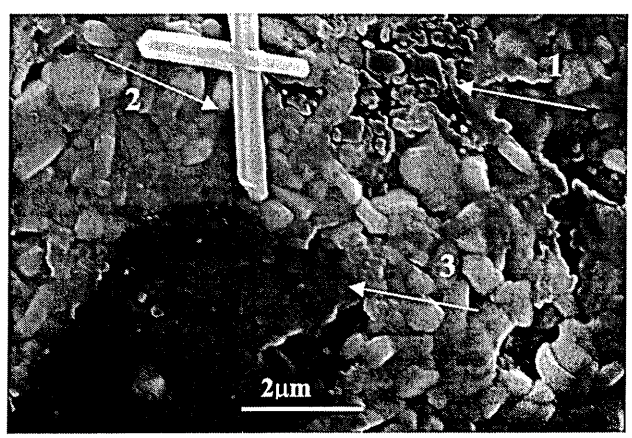

Figure 3.73: Effect of thermal etching on the microstructure of the BMT pellets. 1) morphology typical of a liquid phase (mainly Bi_2O_3);2) crystals of $Bi_2Ti_2O_7$ modified with Mg formed on the surface on the pellet; 3) magnesium rich phase (probably modified $MgTiO_3$).

During the thermal process Mg promotes the formation of Bi_2O_3 liquid phase, probably at the grain boundary. Figure 3.73.1 shows a detail in which a typical morphology of a liquid phase is presented. The formation of extra phases due to thermal etching in compounds with magnesium has been already observed by

Kolodiazhnyi et al.[196]. This extra liquid phase leads to the formation of crystals probably of $Bi_2Ti_2O_7$ modified with magnesium (Figure 3.73.2) and of grains reached in magnesium (Figure 3.73.3) that in a second stage densify to give bigger grains as shown in Figure 3.74. The EDX analysis on this magnesium rich phase revealed a bismuth substituted magnesium titanate.

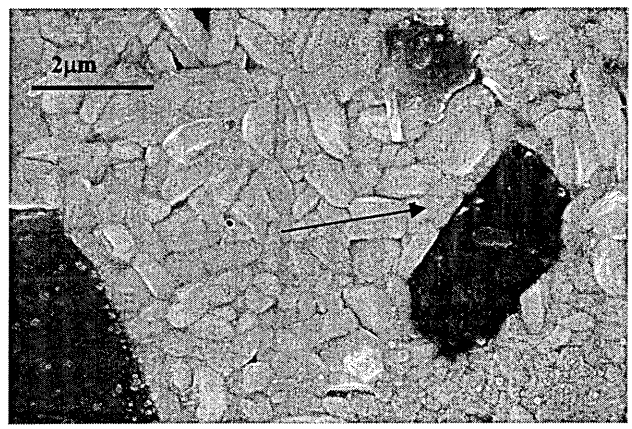

Figure 3.74: Final stage of the formation of big magnesium titanate grains due to the evaporation of bismuth. The arrow indicates the completely formed $MgTiO_3$ second phase.

The appearance of $Bi_2Ti_2O_7$ of this morphology has been already reported for other compounds as consequence of the evaporation of bismuth oxide[197,198]. In some of the pellets another extra-phase has been found (Figure 3.75).

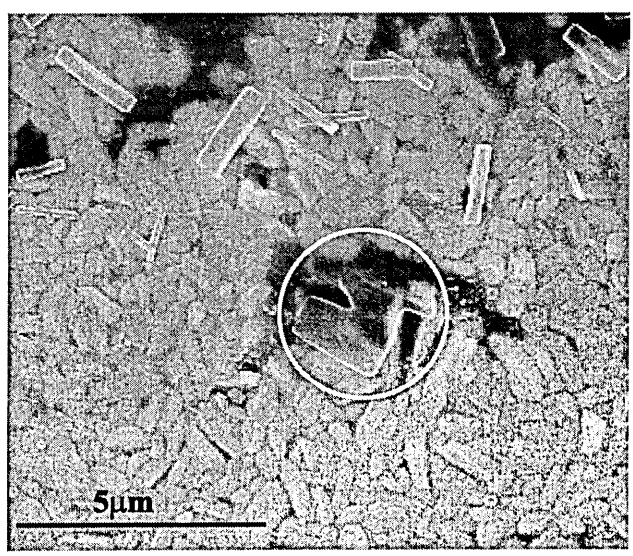

Figure 3.75: Effect of humidity on the surface of the pellet of BMT compounds. The magnesium reacts to form thin sheet of magnesium carbonate (in the circle).

This second phase, in shape of very thin sheet, has been identified as magnesium carbonate. It has been found for PMN containing MgO, that magnesium reacts with the atmospheric moisture on the surface of the ceramic to form $Mg(OH)_2$ that then reacts with the carbon dioxide of the atmosphere to form hydroxycarbonate[199]. The same effect could be involved in the formation of the extra phase of Figure 3.75.
All these extra phases must be due to the high temperature of etching used. Before the thermal treatment in fact, the XRD done on the pellets show a single phase (Figure 3.69 for BMT100). The micrograph done on the surface of BMT100 after etching (Figure 3.76) on the other hand, shows the presence of a large amount of modified magnesium titanate phase (darker grains) that would have been clearly visible in the XRD analysis. Moreover, even if the scattering factor of magnesium is much lower than the one of bismuth and titanium (almost one order of magnitude), the strongest peak of the compounds of magnesium and titanium is generally found around 25-27° (2θ) a region clear from peaks of the Aurivillius compounds.

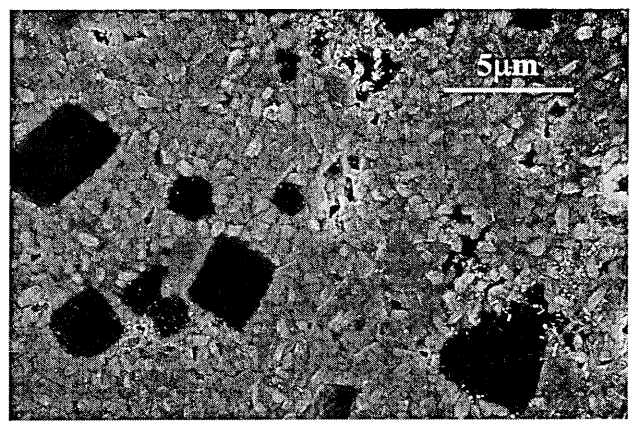

Figure 3.76: SEM micrograph of BMT1 after etching showing the presence of more than one phase.

It is important to point out that all the microstructural analyses have been done on the pellets after their electrical characterisation. In the following it will be assumed that the ceramics are all formed by a single phase of modified bismuth titanate, as found by the XRD analyses.

3.3.3. ELECTRICAL MEASUREMENTS

3.3.3.1. Resistivity

Figure 3.77 shows the comparison between the resistivity of BIT and the resistivity in the BMT series.

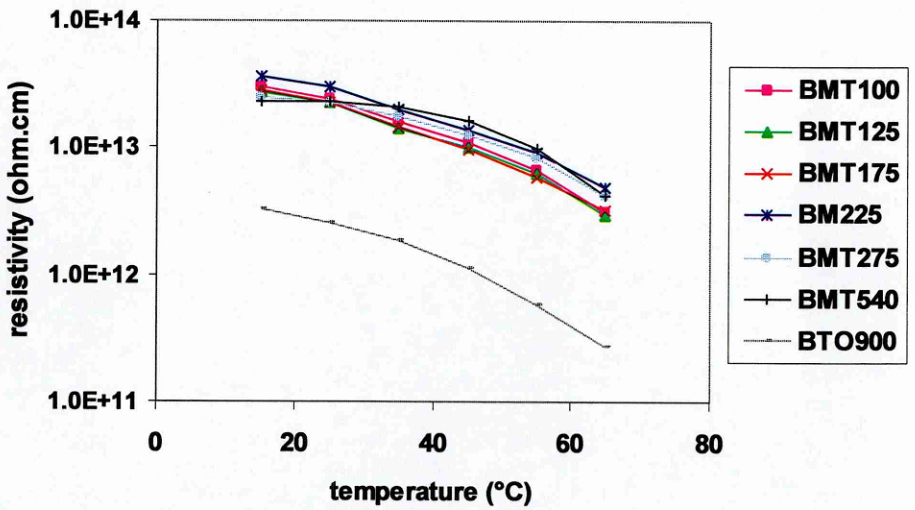

Figure 3.77: Trend of resistivity in function of temperature and composition along the BMT series.

The addition of magnesium increases the resistivity of BIT by more than one order of magnitude. The difference is higher at room temperature but it is appreciable over the whole range. This behaviour does not seem to be due to the effect of magnesium on the vacancies. The conductivity in BIT is of p-type and so it is increased by acceptor doping and bismuth vacancies. The stoichiometry of the compounds of the series (Table 3-XX) revealed much more bismuth vacancies and oxygen vacancies in these compounds than in BIT. In addition, magnesium is an acceptor dopant for BIT and should further decrease the resistivity. Villegas et al.[200] showed that the conductivity of Aurivillius compounds is closely related to the aspect ratio (length/thickness) of the platelets that form the ceramics. The conductivity of these layered compounds is highly anisotropic with values in the **a-b** plane higher than the ones along the **c**-axis. Therefore, the larger the aspect ratio of the platelets, the larger the contribution of the **a-b** planes and, as a consequence, the smaller the resistivity of the bismuth layer

ceramics. The ceramics of the BMT series have smaller aspect ratio than BIT as stressed in paragraph 3.3.2. This difference could account for the observed increase in resistivity.

Another effect could, however, explain the observed trend in resistivity. In the Aurivillius compounds, the conduction phenomena are mainly in the **a-b** plane, because they are blocked in the **c**-direction by the bismuthyl layers that act as barrier for the conduction[201]. The increased resistivity obtained adding magnesium, could be linked to the decreasing of the **c**-parameter along the series observed previously (Figure 3.65): the shrinkage of the unit cell draws up the two $Bi_2O_2^{2+}$ layers, enhancing in this way their repulsive action and consequently repressing the conduction. The influence of the **c**-parameter on the resistivity can be better seen by comparing its trend with the one of the resistivity at 35°C (Figure 3.78). The graph shows clearly that the decrease in **c** corresponds to a progressive increase in resistivity.

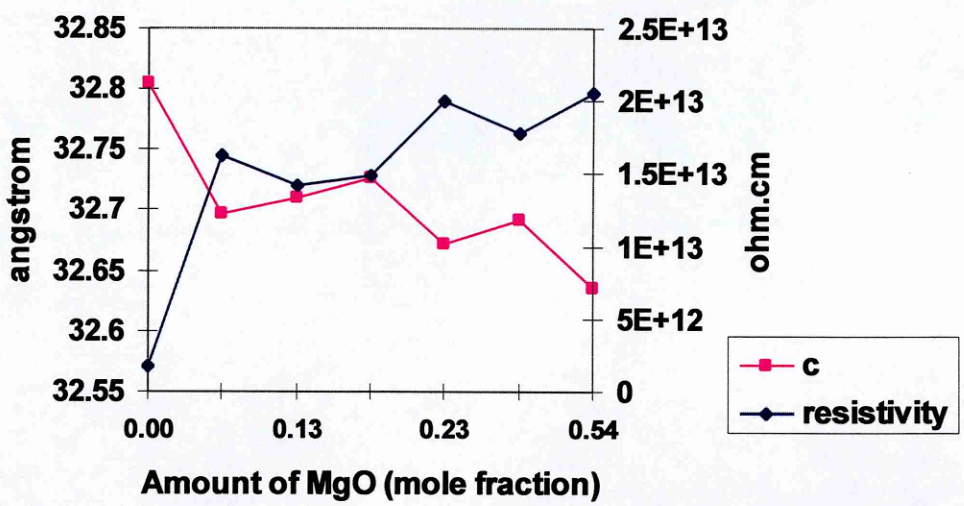

Figure 3.78: Trend with composition of resistivity and c-parameter for the compounds of the BMT series.

In Figure 3.79 the Arrhenius plots for the BMT series are presented.

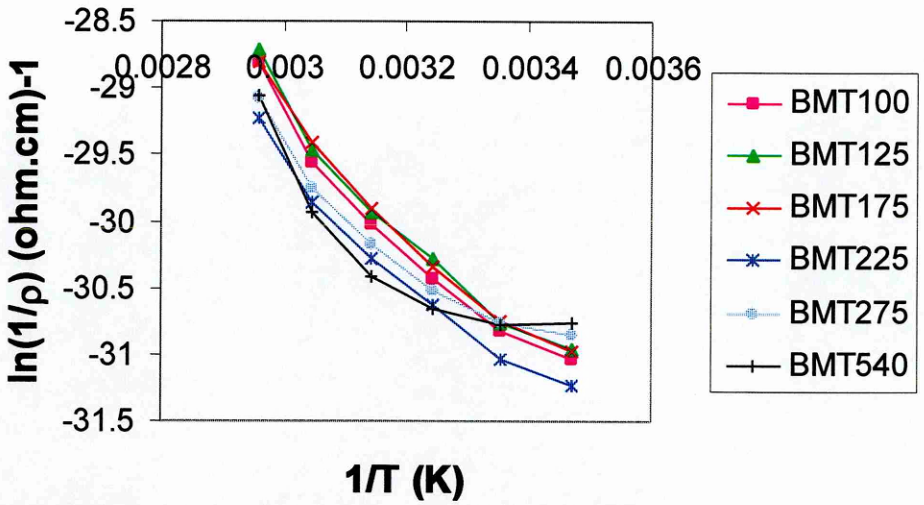

Figure 3.79: Arrhenius plots for the compounds of the BMT series.

From these data it seems that up to BMT175 the conduction is essentially intrinsic and the slope of the lines reflects the energy needed to create and move charge carriers in the materials. From BMT225 the plots are curves that can be considered as the result of an intrinsic conduction at high temperature and an extrinsic one at low temperature (Figure 3.80).

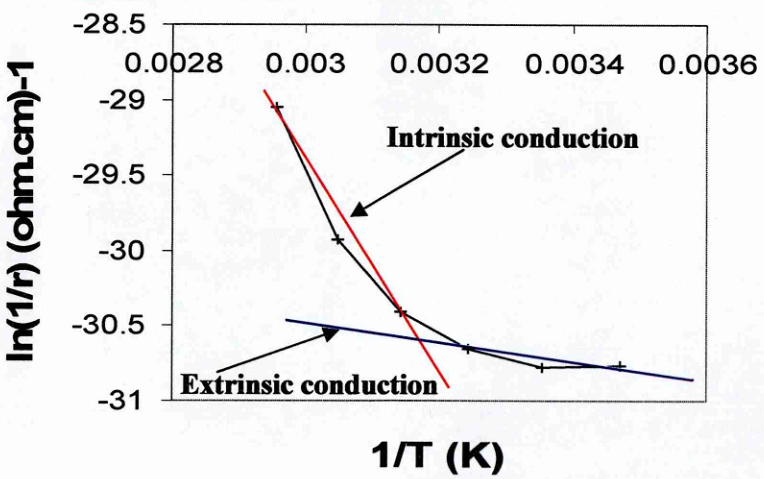

Figure 3.80: The two possible mechanisms of conduction in BMT540.

The slope of the line representing the extrinsic effect gives this time the energy needed only to move the vacancies created by the magnesium in the lattice. One

possibility is that for amount higher than 0.175%mol, magnesium does not fill the bismuth vacancies, but it starts to replace titanium on the perovskite B-site.

The values of activation energy for the compositions in which only intrinsic conduction is present are shown in Figure 3.81. There is a steep decrease in activation energy passing from BIT to BMT100, while after this it is almost constant.

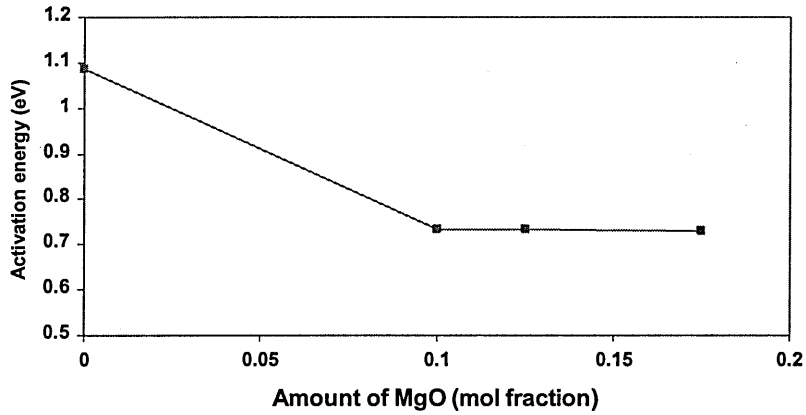

Figure 3.81: Activation energy for the compounds of the BMT series for which only intrinsic conduction seems to be involved.

The conduction process is more easily initiated in the BMT series compounds than in BIT. This phenomenon could be linked to the amount of bismuth vacancies present in the former. If it considered that along the series the resistivity increases, it is possible that this difference in activation energy is due to a change in conduction mechanism.

Along the series the bismuth vacancies are replaced with magnesium. The site is however still negatively charged and for this reason there is probably not a lot of difference in the activation energy. For the compounds where two conduction mechanism are thought to operate, the activation energy in the intrinsic region is almost comparable with the one of BIT, whereas is much lower in the extrinsic region.

3.3.3.2. *Permittivity and dielectric loss*

Figures 3.82 and 3.83 show the effect of magnesium on the dielectric properties of BIT.

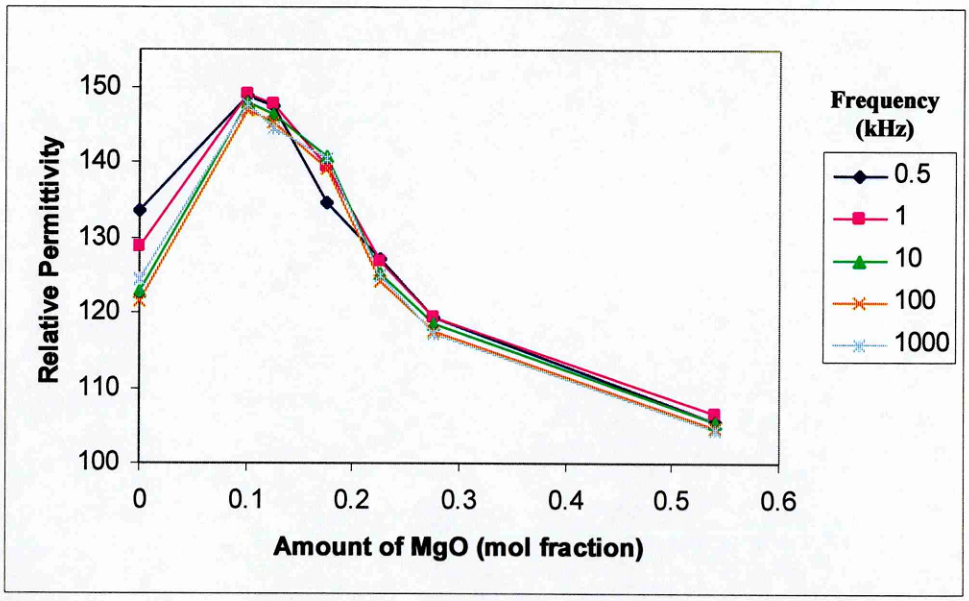

Figure 3.82: Trend of relative permittivity with composition and frequency for the BMT compounds.

The relative permittivity increases of a great extent passing from BIT to BMT100 and then steeply decreases with the increasing amount of magnesium. This behaviour is observable at each value of frequency.

It is well known for PZT[202] that acceptor dopants cause decrease in permittivity as a result of inhibition of the domain wall movement. The same effect might be expected for Mg that acts as acceptor for BIT. It has been assumed that the increase in permittivity passing from BIT to BMT100 is due to the increased density of the ceramics. After that, the magnesium starts to affect the dielectric constant gradually decreasing its value.

Acceptor dopants are well known to lower also the dielectric loss and the piezoelectric constant[15]. Figure 3.83 shows that this effect on the dielectric loss is present in the BMT series at each frequency.

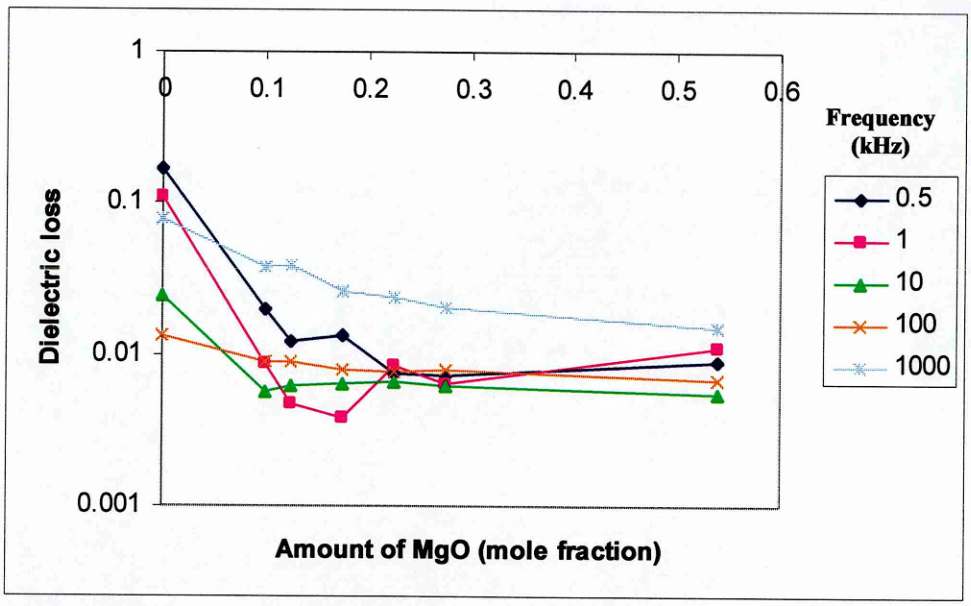

Figure 3.83: Variation of dielectric loss with composition and frequency along the BMT series.

The role in stabilising the domain wall of the system can be observed also considering the stability of the permittivity at 25°C in the range of frequency examined (Figure 3.84).

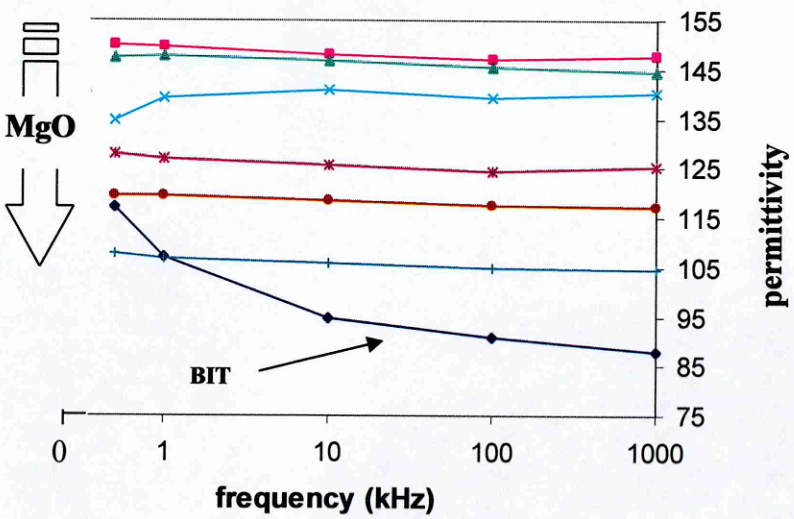

Figure 3.84: Increased stability of permittivity of the BMT compounds in the range of frequency 0.5-1000 kHz, in comparison of BIT.

The relaxation already noticed for BIT is strongly reduced in the compounds of magnesium. This effect can be due to the stabilising effect of magnesium on the domain walls but also to the different morphology of the grains in the BMT series ceramics. It has been mentioned in section 3.2.3.2 that the relaxation phenomena observed in BIT could be due to the tendency of the platelets of BIT to form stacks. These stacks behave like capacitors in series giving rise to Maxwell-Wagner relaxation phenomena. The ceramics of the BMT series are formed by platelets with much smaller aspect ratio. As a consequence they do not tend to form stacks as can be seen in Figure 3.71 and then they do not show Maxwell-Wagner relaxation.

The joint effect of morphology of the grains and effect of Mg on mobility of the domains walls could be responsible for the stabilisation of the dielectric constant.

The domain stabilisation induced by magnesium is also responsible for the elimination of the thermal hysteresis of the dielectric constant observed in BIT. In Figure 3.85 the comparison between BIT and BMT100 is shown. It is clear that for the compound of the BMT series there is no thermal hysteresis and the dielectric constant is not so spread in the range of frequencies considered.

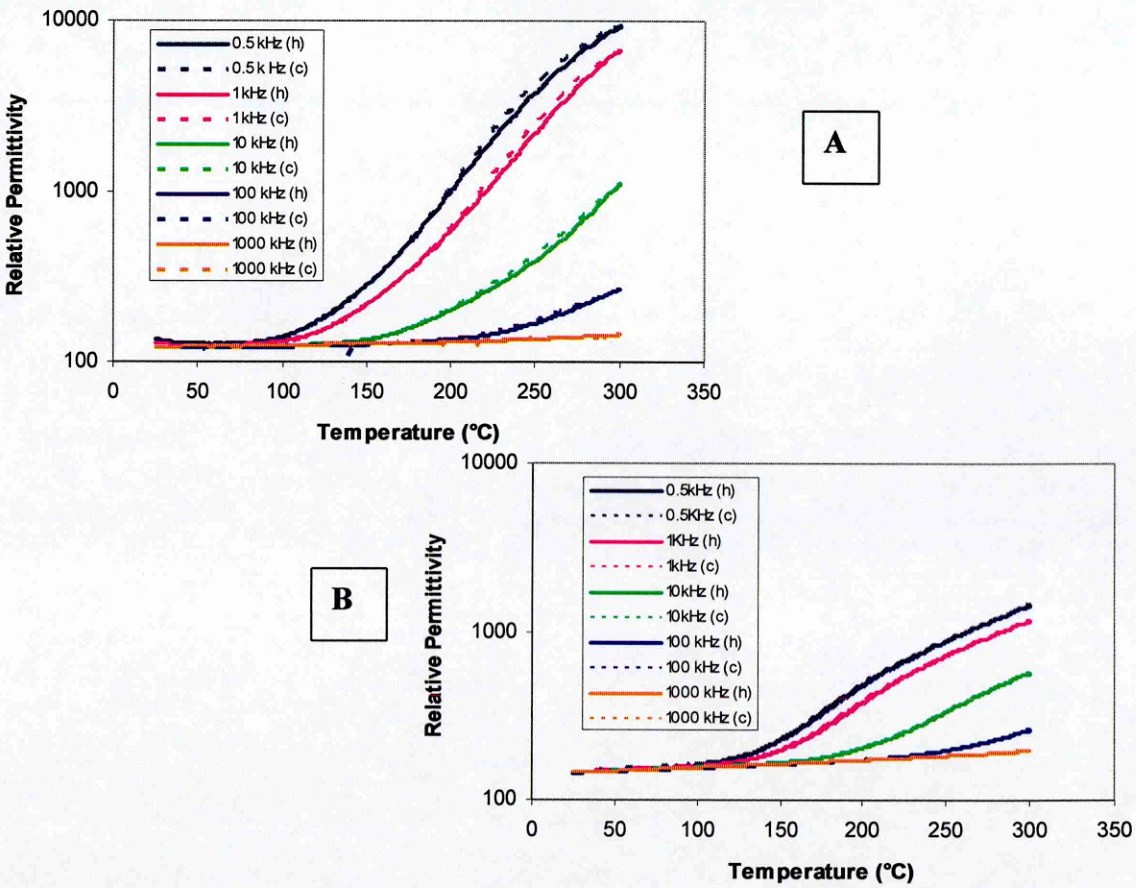

Figure 3.85: Effect of magnesium in stabilising the permittivity in the range of temperature examined. A) BIT, B) BMT1.

3.3.3.3. *Hysteresis Loops*

There is no sign of ferroelectric hysteresis in any of the compositions analysed before poling, but only a normal dielectric behaviour has shown in Figure 3.86 for BMT125.

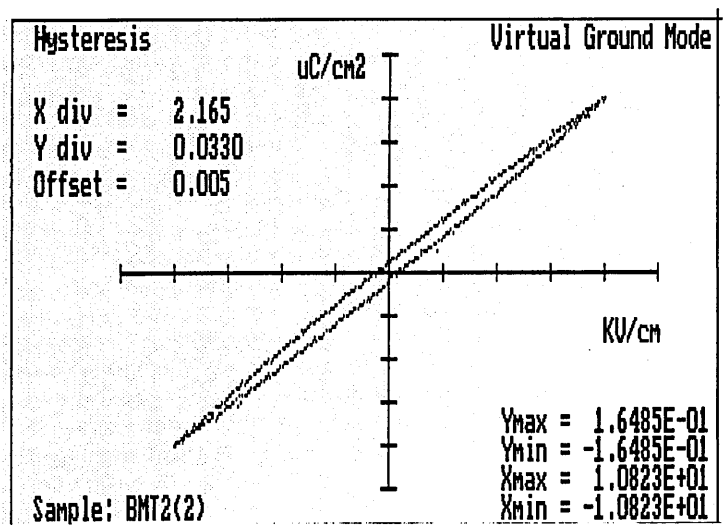

Figure 3.86: Hysteresis loop of BMT125.

This can be due to the fact that the maximum voltage applicable in the laboratories is not high enough to show hysteretic behaviour. On top of that, the inhibition of the wall movement by Mg has the consequence to increase the coercive field of these compounds in respect of the one of BIT.

3.3.3.4. *Piezoelectric Properties*

In Table 3.XXIV the piezoelectric coefficients for the compounds of the BMT series are reported. BIT does not show any piezoelectric activity due to the high conductivity observed at the temperature of poling.

Compound	d_{33} (pC/N)
BMT100	10.2±0.3
BMT125	9.3±0.4
BMT175	6.7±0.5
BMT225	5.0±0.4
BMT275	3.7±0.5
BMT540	2.5±0.5

Table 3-XXIV: Piezoelectric coefficient of the BMT series.

The value of d_{33} for BMT100 is almost double the one of BIT generally presented in the literature (6 pC/N). This increased value can be attributed to the higher density of the pellet and to the higher resistivity of this system. The decreasing of values along the series is the results of the acceptor role played by magnesium in the crystalline lattice, as already noticed in paragraph 3.3.3.1.

4. FINAL REMARKS AND FUTURE WORK

4.1. Final Remarks

The objectives of this thesis were to determine the structural and electrical relationships between perovskite and Aurivillius compounds and to investigate the possibility of obtaining a perovskite of formula Bi_2MgTiO_6.

A possible phase diagram of the $Na_{1/2}Bi_{1/2}TiO_3$-$Bi_4Ti_3O_{12}$-$BaTiO_3$ (NBT-BIT-BT) was derived. Although some regions need more work to be considered with certainty, the diagram obtained can be considered as a good indication of the behaviour of this system. The presence of several monophasic regions, indicates that the structure of the Aurivillius compounds is able to withstand a quite high level of non–stochiometry before collapsing. This structural flexibility also affects the electric and piezoelectric properties of these compounds and leads to compounds that are able "to adapt" their structure in response to changes of conditions. Examples of this "adaptation process" are the ability of the Aurivillius compounds to tilt and rotate the octahedra of the perovskite block to reduce the strain of the structure and the possibility to change the distance between bismuth layer and perovskite block as consequence of an increase (or decrease) of the repulsion force between them.

The structural analysis at three different reaction temperatures (850°C, 950°C and 1150°C) has allowed us to propose a multistep mechanism for the formation of these Aurivillius compounds. The number of steps has been found to be a function of the number of perovskite blocks. This mechanism could explain the reduced reactivity of compounds with high number of perovskite blocks and the particularly high temperatures needed to form intergrowth compounds.

The low angle X-ray analysis has been proved to be an essential tool to define the nature and number of Aurivillius compounds, whereas "a rule of thumb" has been applied to justify the stability of Aurivillius compounds.

The analysis of the dielectric and piezoelectric properties of the NBT- BIT and BT-BIT series showed the close link between the number of perovskite blocks and these properties. The results also showed that the piezoelectric properties of the Aurivillius compounds are "limited" by the $Bi_2O_2^{2+}$ layers, i.e. the higher is the ratio of the number of peroskite blocks to the number of bismuthyl layers in a compound, the

higher is its piezoelectric coefficient. When this ratio becomes equal to infinity, the structure is the one of a pure perovskite and d_{33} reaches its maximum value. In this respect it is possible that the higher is the piezoelectric activity of the perovskite partner of an Aurivillius compound, the stronger is the piezoelectric response of the latter.

The formula Bi_2MgTiO_6 does not correspond to a perovskite compounds but to a mixture of an Aurivillius compounds and cubic bismuth titanate. However this side of the project allowed us to discover that the addition of magnesium to $Bi_4Ti_3O_{12}$ greatly increases its dielectric constant (50%) and resistivity (almost two orders of magnitude) while at the same time decreasing the dielectric loss. As consequence of this, and of an increased density of the ceramics obtained, the piezoelectric coefficient of $Bi_4Ti_3O_{12}$ with 0.1% MgO is almost double the one presented in the literature (11 pC/N vs 6 pC/N).

The choice of study of compounds of bismuth was made because they represent the most valid alternatives to the lead based systems in ferroelectric and piezoelectric applications. Table 4.I shows the comparison between the piezoelectric coefficients d_{33} of some lead-based compounds and some lead-free ones.

Compound	d_{33} (pC/N)	Tc (°C)
PZT A	268	315
PZT B	480	220
$BaTiO_3$ (BT)	190	130
$Na_{1/2}Bi_{1/2}TiO_3$ (NBT)	79	320
NBT-BT (MPB)	125	250
BIT	6	675
BIT + 1%MgO	10	?

Table 4-I: Comparison of piezoelectric coefficient and Curie temperature of some piezoelectric compounds. The last row shows the value obtained in this work, the other values are from references 15,41 and 58.

The analysis of the data of Table 4.1I shows how bismuth compounds do not seem to be able at the present to replace lead-based systems to give the same level of piezoelectric efficiency.

However some conditions, other than the ban of lead from electronic components, could direct the choice to bismuth compounds:

- The necessity to operate at high temperature or pressure (for example in the automotive or aerospace industries). The compounds of bismuth have higher Curie temperatures and are much more stable materials under extreme conditions.
- The need to reduce aging and electrical fatigue (in ferroelectric memories for example). Lead compounds are strongly subjected to aging.

On the other hand, the results obtained on the piezoelectric coefficient of BIT doped with magnesium proved that the properties of bismuth compounds need to be studied more because they can be further improved.

4.2. Future Work

Main aspects of the project could be explored further. In particular

1. The phase diagram of the NBT-BIT–BT system needs to be studied in more detail, not only to clarify the exact position of the boundaries between the various regions and the particularly interesting region in the middle of it. In all this study the thermodynamic properties of the compounds have not been examined. A detailed thermal study (DTA, DSC, etc) would give the energies of formation and thermal parameters of the compounds involved. This further study could help to verify if the compositions obtained are thermodynamically stable and to give new light on the phase evolution of the system. These analyses could be coupled with XRD analyses performed live during the heating process.
2. The dielectric and piezoelectric examination should be extended to the non-stoichiometric compounds of the system. To examine the effect of non stoichiometry and verify the properties of the new phase found. Their exact

composition should be checked with techniques such as neutron diffraction that might allow us to study also the presence of oxygen vacancies. Their structures could be simulated accordingly.

3. The ceramics quality should be improved to give a clearer vision of the potentiality of these compounds. For this purpose the possibility of using techniques such as hot-pressing and hot forging could be explored.
4. The bismuth compounds have been thoroughly studied for memories applications. This implies the production of films. A new technique could be adopted taking into account the mechanism of formation of Aurivillius compounds. This could be a modification of the ComFi technology developed in Cranfield University by Dorey et al.[203] This modified sol-gel technique could take advantage of the fact that in the first stage of the mechanism of formation of Aurivillius compounds, the raw materials react to give the parent members. This step could be exploited in the fabrication of films. It could then be possible to deposit a first layer of barium titanate and then infiltrate it with a sol of $Bi_4Ti_3O_{12}$ in the right amounts. The firing of the whole system at the right temperature could lead to the formation of the Aurivillius compounds of the BT-BIT series. Thicker films could be produced using tape casting. The powder of BIT and BT produced by sol gel could be laminated by tape casting. The resulting system, in which the BIT particles act as texturing agents, fired at the right temperature should give the system of interest with, in addition, an improved c-orientation.
5. The structure of the compounds and the effect of the tilting and rotating of octahedra as well as of the distance between the two kinds of layer in the single compounds could be analysed with techniques like HRTEM. Their structural features could be then more carefully linked to the dielectric and piezoelectric properties.
6. Some of the properties of these compounds (stability, trend in permittivity and resistivity) have been justified considering the Aurivillius compounds as formed by two kind of layers interacting. These kind of "LEGO" approach could be used to examine the properties of other classes of layers compounds such as superconducting oxides or Ruddlesen-Popper phases. These classes

differ from the Aurivillius one only by the nature of one of the two kind of layers and should be suitable for this kind of analysis.

7. More work could be done to study the m=3.5 phases to verify the kind of order involved and its effect on the dielectric and piezoelectric properties.
8. The "capacitor in series" model could be used to model the relaxation processes in random oriented ceramics. While more work has to be done to understand the real nature of the conduction and loss of BIT in the presence of magnesium.
9. The role of $Bi_{12}TiO_{20}$ in inducing an m=3.5 structure on the Aurivillius phase of BMT also need further study. This phase appeared to be m=3.5 in the diffractogram of BMT. However when it is synthesised starting by the stoichiometric amount of raw materials, its structure presents 3 perovskite blocks.
10. A detailed study is needed to understand the real entity of the Mg doping and the exact formulae of the compounds of the BMT series.
11. The values of coercive field and remnant polarisation should be measured, reducing the thickness of the ceramic analysed or applying higher fields for the analysis. On top of that, it would be interesting to check the effect of magnesium on the Curie temperature, performing high temperature measurements of the dielectric constant.
12. The examination of the ac-resistivity in the systems could help in understanding the roles of the domains and domain walls in the dielectric properties of the compounds.
13. It would be possible to combine the two parts of this project studying a quaternary system formed by NBT-BIT-BT and MgO.

5. APPENDICES

5.1. APPENDIX A

Table 5.I shows the label, exact formula and the percentage in moles of the end members for each composition made in the NBT-BIT-BT system.

The general formula is $Ba_yNa_{0.5x}Bi_{(4-3.5x-4y)}Ti_{(3-2x-2y)}O_{3(4-3x-3y)}$ with $x_{(NBT)}$ = mol fraction NBT, $y_{(BT)}$ = mol fraction BT, $z_{(BIT)}$ = mol fraction BIT and x+y+z = 1.

Label	Formula	x (NBT)	y (BT)	z (BIT)
NBT	$Na_{0.5}Bi_{0.5}TiO_3$	1.000	0.000	0.000
BT	$BaTiO_3$	0.000	1.000	0.000
BIT	$Bi_4Ti_3O_{12}$	0.000	0.000	1.000
90BITBT	$Ba_{0.1}Bi_{3.6}Ti_{2.8}O_{11.1}$	0.000	0.100	0.900
80BITBT	$Ba_{0.2}Bi_{3.2}Ti_{2.6}O_{10.2}$	0.000	0.240	0.800
66BITBT	$Ba_{0.34}Bi_{2.64}Ti_{2.32}O_{8.94}$	0.000	0.340	0.660
55BITBT	$Ba_{0.45}Bi_{2.2}Ti_{2.1}O_{7.95}$	0.000	0.450	0.550
50BITBT	$Ba_{0.5}Bi_2Ti_2O_{7.5}$	0.000	0.500	0.500
45BITBT	$Ba_{0.65}Bi_{1.8}Ti_2O_{7.35}$	0.000	0.550	0.450
40BITBT	$Ba_{0.6}Bi_{1.6}Ti_{1.8}O_{6.6}$	0.000	0.600	0.400
34BITBT	$Ba_{0.66}Bi_{1.36}Ti_{1.68}O_{6.06}$	0.000	0.650	0.340
30BITBT	$Ba_{0.7}Bi_{1.2}Ti_{1.6}O_{5.7}$	0.000	0.700	0.350
25BITBT	$Ba_{0.75}Bi_1Ti_{1.5}O_{5.25}$	0.000	0.750	0.250
20BITBT	$Ba_{0.8}Bi_{0.8}Ti_{1.4}O_{4.8}$	0.000	0.800	0.200
15BITBT	$Ba_{0.85}Bi_{0.6}Ti_{1.3}O_{4.35}$	0.000	0.850	0.150
10BITBT	$Ba_{0.9}Bi_{0.4}Ti_{1.2}O_{3.9}$	0.000	0.900	0.100
5BITBT	$Ba_{0.95}Bi_{0.2}Ti_{1.1}O_{3.45}$	0.000	0.950	0.050
90BIT	$Na_{0.05}Bi_{3.65}Ti_{2.8}O_{11.1}$	0.100	0.900	0.000
80BIT	$Na_{0.1}Bi_{3.3}Ti_{2.6}O_{10.2}$	0.200	0.800	0.000
75BIT	$Na_{0.12}Bi_{3.125}Ti_{2.5}O_{9.75}$	0.250	0.750	0.000
66BIT	$Na_{0.17}Bi_{2.81}Ti_{2.32}O_{8.94}$	0.340	0.660	0.000
55BIT	$Na_{0.225}Bi_{2.425}Ti_{2.1}O_{7.95}$	0.450	0.550	0.000
50BIT	$Na_{0.25}Bi_{2.25}Ti_2O_{7.5}$	0.500	0.500	0.000
45BIT	$Na_{0.275}Bi_{2.075}Ti_{1.9}O_{7.05}$	0.650	0.450	0.000

Label	Formula	x (NBT)	y (BT)	z (BIT)
40BIT	$Na_{0.3}Bi_{1.9}Ti_{1.8}O_{6.6}$	0.600	0.400	0.000
30BIT	$Na_{0.35}Bi_{1.55}Ti_{1.6}O_{5.7}$	0.700	0.300	0.000
25BIT	$Na_{0.375}Bi_{1.375}Ti_{1.5}O_{5.25}$	0.750	0.250	0.000
20BIT	$Na_{0.4}Bi_{1.2}Ti_{1.4}O_{4.8}$	0.800	0.200	0.000
10BIT	$Na_{0.45}Bi_{0.85}Ti_{1.2}O_{3.9}$	0.900	0.100	0.000
5BIT	$Na_{0.475}Bi_{0.675}Ti_{1.1}O_{3.45}$	0.950	0.050	0.000
2.5BIT	$Na_{0.49}Bi_{0.59}Ti_{1.0}O_{3.32}$	0.975	0.025	0.000
50BITBT1	$Ba_{0.4}Na_{0.1}Bi_{1.7}Ti_{1.8}O_{6.6}$	0.200	0.400	0.400
50BITBT2	$Ba_{0.3}Na_{0.2}Bi_{1.4}Ti_{1.6}O_{5.7}$	0.400	0.300	0.300
50BITBT2.5	$Ba_{0.275}Na_{0.225}Bi_{1.325}Ti_{1.55}O_{5.475}$	0.450	0.275	0.275
50BITBT3	$Ba_{0.2}Na_{0.3}Bi_{1.1}Ti_{1.4}O_{4.8}$	0.600	0.200	0.200
50BITBT4	$Ba_{0.1}Na_{0.4}Bi_{0.8}Ti_{1.2}O_{3.9}$	0.800	0.100	0.100
50BITBT4.5	$Ba_{0.075}Na_{0.425}Bi_{0.725}Ti_{1.15}O_{3.675}$	0.850	0.075	0.075
34BITBT0.5	$Ba_{0.59}Na_{0.05}Bi_{1.3}Ti_{1.6}O_{5.75}$	0.100	0.594	0.306
34BITBT1	$Ba_{0.53}Na_{0.1}Bi_{1.19}Ti_{2.14}O_{7.25}$	0.200	0.528	0.275
34BITBT2	$Ba_{0.4}Na_{0.2}Bi_{1.02}Ti_{1.41}O_{4.84}$	0.400	0.396	0.204
34BITBT3	$Ba_{0.26}Na_{0.3}Bi_{0.84}Ti_{1.27}O_{4.22}$	0.600	0.264	0.136
34BITBT4	$Ba_{0.13}Na_{0.4}Bi_{0.67}Ti_{1.14}O_{3.61}$	0.800	0.132	0.068
50BIT1	$Ba_{0.2}Na_{0.2}Bi_{1.8}Ti_{1.8}O_{6.6}$	0.400	0.200	0.400
50BIT1.5	$Ba_{0.3}Na_{0.175}Bi_{1.575}Ti_{1.7}O_{6.15}$	0.350	0.300	0.350
50BIT2	$Ba_{0.4}Na_{0.15}Bi_{1.35}Ti_{1.6}O_{5.7}$	0.300	0.400	0.300
50BIT3	$Ba_{0.6}Na_{0.1}Bi_{0.9}Ti_{1.4}O_{4.8}$	0.200	0.600	0.200
50BIT4	$Ba_{0.8}Na_{0.05}Bi_{0.45}Ti_{1.2}O_{3.9}$	0.100	0.800	0.100
50BT	$Ba_{0.5}Na_{0.25}Bi_{0.25}TiO_3$	0.500	0.500	0.000
0.2BITBT1	$Ba_{0.5}Na_{0.245}Bi_{0.325}Ti_1O_{3.2}$	0.490	0.490	0.020
50BT0.5	$Ba_{0.3}Na_{0.2}Bi_{1.45}Ti_{1.6}O_{5.9}$	0.340	0.340	0.320
50BT1	$Ba_{0.3}Na_{0.135}Bi_{1.975}Ti_{1.9}O_{7.1}$	0.270	0.270	0.460
50BT2	$Ba_{0.2}Na_{0.1}Bi_{2.5}Ti_{2.2}O_{8.4}$	0.200	0.200	0.600
50BT2.5	$Ba_{0.2}Na_{0.085}Bi_{2.725}Ti_{2.3}O_{8.9}$	0.170	0.170	0.660
50BT3	$Ba_{0.1}Na_{0.05}Bi_{3.25}Ti_{2.6}O_{10.2}$	0.100	0.100	0.800
50BT4	$Ba_{0.1}Na_{0.035}Bi_{3.475}Ti_{2.7}O_{10.7}$	0.070	0.070	0.860

Label	Formula	x (NBT)	y (BT)	z (BIT)
5BITBT1	$Ba_{0.7125}Na_{0.125}Bi_{0.27}Ti_{1.1}O_{3.34}$	0.2500	0.7125	0.0375
5BITBT2	$Ba_{0.52}Na_{0.22}Bi_{1.33}Ti_{1.05}O_{3.25}$	0.4500	0.5225	0.0275
5BITBT3	$Ba_{0.48}Na_{0.24}Bi_{0.37}Ti_{1.06}O_{3.30}$	0.4835	0.4835	0.0330
5BITBT4	$Ba_{0.24}Na_{0.37}Bi_{0.42}Ti_{1.02}O_{3.11}$	0.7500	0.2375	0.0125
15BITBT1	$Ba_{0.595}Na_{0.15}Bi_{0.57}Ti_{1.21}O_{3.95}$	0.3000	0.5950	0.1125
15BITBT2	$Ba_{0.42}Na_{0.25}Bi_{0.55}Ti_{1.15}O_{3.67}$	0.5000	0.4250	0.0750
15BITBT3	$Ba_{0.3}Na_{0.32}Bi_{0.53}Ti_{1.11}O_{3.47}$	0.6500	0.2975	0.0250
15BITBT4	$Ba_{0.085}Na_{0.45}Bi_{0.51}Ti_{1.03}O_{3.13}$	0.9000	0.0850	0.0150
35BITBT1	$Ba_{0.58}Na_{0.05}Bi_{1.31}Ti_{1.63}O_{5.83}$	0.1000	0.5850	0.3150
40BITBT0.5	$Ba_{0.54}Na_{0.05}Bi_{1.49}Ti_{1.72}O_{6.24}$	0.1000	0.5400	0.3600
40BITBT0.7	$Ba_{0.47}Na_{0.1}Bi_{1.42}Ti_{1.66}O_{5.97}$	0.2000	0.4700	0.3300
40BITBT1	$Ba_{0.36}Na_{0.2}Bi_{1.16}Ti_{1.48}O_{5.16}$	0.4000	0.3600	0.2400
40BITBT1.5	$Ba_{0.3}Na_{0.25}Bi_{1.05}Ti_{1.4}O_{4.8}$	0.5000	0.2000	0.3000
40BITBT2	$Ba_{0.06}Na_{0.45}Bi_{0.61}Ti_{0.8}O_{3.36}$	0.9000	0.0600	0.0400
45BITBT1	$Ba_{0.58}Na_{0.05}Bi_{1.67}Ti_{1.9}O_{6.91}$	0.1000	0.4050	0.4050
45BITBT2	$Ba_{0.19}Na_{0.35}Bi_{0.89}Ti_{1.3}O_{4.3}$	0.7000	0.1650	0.1350
55BITBT0.5	$Ba_{0.36}Na_{0.1}Bi_{1.86}Ti_{1.88}O_{6.96}$	0.2000	0.3600	0.4400
55BITBT0.7	$Ba_{0.2}Na_{0.2}Bi_{1.8}Ti_{1.8}O_{6.6}$	0.4200	0.2600	0.3200
55BITBT1	$Ba_{0.247}Na_{0.22}Bi_{1.43}Ti_{1.6}O_{5.72}$	0.4500	0.2475	0.3025
65BITBT1	$Ba_{0.19}Na_{0.22}Bi_{1.65}Ti_{1.71}O_{6.22}$	0.4500	0.1925	0.3575
75BITBT1	$Ba_{0.14}Na_{0.22}Bi_{1.87}Ti_{1.82}O_{6.71}$	0.4500	0.1375	0.4125
70BITBT1	$Ba_{0.27}Na_{0.05}Bi_{2.57}Ti_{2.26}O_{8.67}$	0.1000	0.2700	0.6300
70BITBT2	$Ba_{0.19}Na_{0.18}Bi_{1.98}Ti_{1.9}O_{7.05}$	0.3600	0.1900	0.4500
70BITBT3	$Ba_{0.06}Na_{0.4}Bi_{0.96}Ti_{1.28}O_{4.26}$	0.8000	0.0600	0.1400
70BIT1	$Ba_{0.05}Na_{0.15}Bi_{2,75}Ti_{2.3}O_{8.85}$	0.3000	0.0500	0.6500
60BIT1	$Ba_{0.1}Na_{0.15}Bi_{2.55}Ti_{2.2}O_{8.4}$	0.3000	0.1000	0.6000
60BIT2	$Ba_{0.3}Na_{0.05}Bi_{2.45}Ti_{2.2}O_{8.4}$	0.1000	0.3000	0.6000
30BIT0.5	$Ba_{0.05}Na_{0.325}Bi_{1.525}Ti_{1.6}O_{5.7}$	0.6500	0.0500	0.3000
30BIT1	$Ba_{0.1}Na_{0.3}Bi_{1.5}Ti_{1.6}O_{5.7}$	0.6000	0.1000	0.2000
30BIT2	$Ba_{0.2}Na_{0.25}Bi_{1.45}Ti_{1.6}O_{5.7}$	0.5000	0.2000	0.3000

Table 5-I: formulae and labels for all the compounds of the NBT-BIT-BT system.

5.2. APPENDIX B

Example of mathcad spreadsheet for the calculation of the cell parameter using a least squares method.

Miller Indexes d spacing

h	k	l	d
0	0	8	4.09962
0	0	4	8.20811
0	0	6	5.46756
1	1	1	3.81385
1	1	3	3.62065
1	1	5	3.31368
0	0	10	3.27589
1	1	7	2.97040
2	0	0	2.72615
0	2	0	2.70754
0	0	14	2.34355
2	0	8	2.26684
1	1	13	2.10833
0	2	10	2.09250
0	0	16	2.04995
2	2	0	1.91896
2	2	2	1.90029
0	0	18	1.82191
2	2	6	1.81076
1	3	7	1.61625
3	1	7	1.60776
1	1	19	1.57446
1	1	21	1.44657

$n := \text{length}(d) - 1$

$$F(h,k,l,a,b,c) := a \cdot b \cdot \frac{c}{\sqrt{\left(h^2 \cdot b^2 \cdot c^2 + k^2 \cdot c^2 \cdot a^2 + l^2 \cdot a^2 \cdot b^2\right)}}$$

$i := 0..n$

$SSE(a,b,c) := \sum_i \left[\left(d_i - F\left(h_i, k_i, l_i, a, b, c\right) \right)^2 \right]$ Sum of squares to be minimised

$a := 5.4$ $b := 5.44$ $c := 32$ Initial guess for parameters

Given

$SSE(a,b,c) = 0$ $1 = 1$ $1 = 1$ Dummy equations

$\begin{bmatrix} a \\ b \\ c \end{bmatrix} := \text{minerr}(a,b,c)$

Plot data for fitted curve

$z \equiv 0, 0.1 .. 6$

$a = 5.441$

$b = 5.418$ Parameters for best fit

$c = 32.805$

$\frac{SSE(a,b,c)}{(n-2)} = 1.248 \cdot 10^{-5}$ Mean squared error

$P := \left(\overrightarrow{F(h,k,l,a,b,c)}\right)$

$m := \text{slope}(P,d)$ $m = 1.001$

$q := \text{intercept}(P,d)$ $q = -2.042 \cdot 10^{-3}$

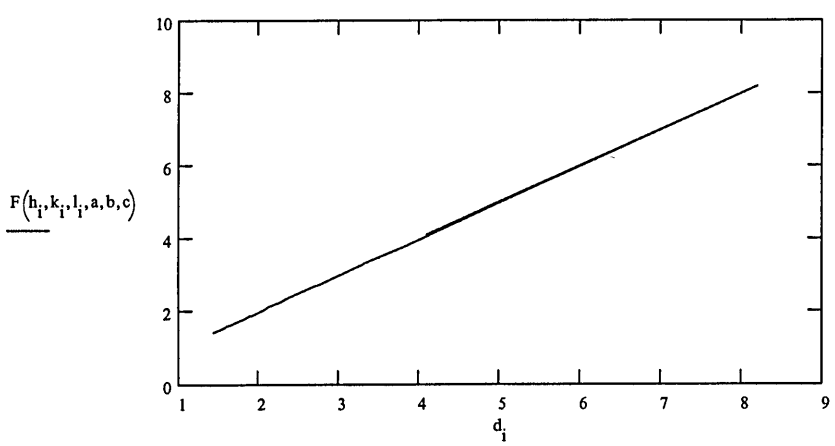

6. REFERENCES

[1] Global lead network: " The Global Dimensions of Lead Poisoning, An Initial Analysis" www.globalleadnet.org/pdf/Toxicity_of_Lead.pdf
[2] The United States Environment Agency: www.epa.gov/iris/subst/0277.htm#quaoral
[3] B. Jaffe, W. R. Cook Jr and H. Jaffe "Piezoelectric Ceramics" Academic Press London and New York (1971)
[4] W.P. Mason "Piezoelectricity, its history and applications" J. Acoust. Soc. Am. 70(6) 1561-1566 (1981)
[5] A. Ballato " Piezoelectricity: History and New Thrusts" IEE Ultrasonic Symposium (1996) 575
[6] S.L. Swartz, T.R. Shrout, T. Takenaka "Electronic Ceramics R&D in the US, Japan Part I: Patent History " Am. Ceram. Soc. Bull., 76, 759-65(1997)
[7] T. Abraham "US advanced Ceramics Growth Continues" Ceramic Industry 23-25 (2000)
[8] "Industries in Transitions" published by Business Communications & Co., May (2003)
[9] B.H. Park, B.S. Kang, S.D. Bu, T.W. Noh, J. Lee & W. Jo "Lanthanum-substituted Bismuth Titanate for use in non-volatile Memories" Nature, 401, 682-684(1999)
[10] S.L. Swartz, T.R. Shrout, T. Takenaka "Electronic Ceramics R&D in the U.S., Japan Part II, Japanese view" Am. Ceram. Bull. 76(8) 51-55 (1997)
[11] P.J.F. Le Fevre, "Applied Power Electronic Conference and Exposition, 2002, APEC 2002" 17th Annual IEEE, 1, 121-125(2002)
[12]World Semiconductor Council 2001: Lead-free white paper http://www.semiconductorcouncil.org/news/leadfree_wp.pdf
[13] C. Giacovazzo, H.L. Monaco, D. Viterbo, F. Scordari, G. Gilli, G. Zanotti, M. Catti "Fundamentals of Crystallography" Edited by C. Giacovazzo, Oxford Science Publications, IUCr, (1995)
[14] M.E. Lines and A.M. Glass "Principles and Applications of Ferroelectrics and Related Materials" Clarendon Press-Oxford (1979)
[15] A.J. Moulson and J.M. Herbert "Electroceramics- Materials, Properties, Applications" Chapman and Hall Editor, 1997
[16] J.F. Nye "Physical Properties of Crystal. Their Representation by Tensors and Matrices" Oxford Science Publishing, 2001
[17] R.D. Shannon and C.T. Prewitt "Effective Ionic Radii in Oxides and Fluorides" Acta Cryst., B25, 925-955 (1969)
[18] H. Miyazawa, E. Natori, S. Miyashita, T. Shimoda, F. Ishii and T. Oguchi "Electronic States of Perovskite-type oxides and Ferroelectricity" Jpn. J. Appl. Phys., 39, 5679-5682 (2000)
[19] B. Noheda, D.E. Cox, G. Shirane, J.A. Gonzalo, L.E. Cross and S.-E. Park,"A Monoclinic Ferroelectric Phase in the $Pb(Zr_{1-x}Ti_x)PbO_3$ Solid Solutions" Appl. Phys. Lett., 74, 2059-2061 (1999)
[20] A. M. Glazer "The Morphotropic Phase Boundary – My Part in Its Downfall" J. Conf. Abs. EMF 2003, Cambridge UK, 8,137 (2003)
[21] W. Wersing "Application of Piezoelectric Materials: an Introductory Review" in Piezoelectric Materials in Devices, N. Setter Ed., page 29(2002)

[22] M. Demartin and D. Damjanovic" Lead-free Piezoelectric Materials" in Piezoelectric Materials in Devices" N. Setter Ed., pag. 389 (2002)
[23] R.C. Turner, P.A. Fuirier, R.E. Newnham and T.R. Shrout "Materials for High Temperature Acoustic and Vibration Sensor" Applied Acoustics, 41, 299-324 (1994)
[24] R.F. Mitchell "Some New Materials for Ultrasonic Transducers" Ultrasonics 112-117 (1968)
[25] R.E. Jacger and L. Egerton "Hot Pressing of Potassium-Sodium Niobates" J. Am. Ceram. Soc., 45 (5) (1962)
[26] G.A. Smolenskii, V.A. Isupov, A.I. Agronovskaya and N.N. Krainik "New Ferroelectrics of complex composition. IV" Sov. Phys. Sol. State, 2 [11] 2651-2654 (1961)
[27] C.F. Buhrer "Some Properties of Bismuth Perovskites" J. Chem. Phys., 36[3]798-803 (1962)
[28] G.O. Jones and P.A. Thomas "The Tetragonal phase of $Na_{0.5}Bi_{0.5}TiO_3$- a New Variant of the Perovskite Structure" Acta Crystallogr. B56, 426-430 (2000)
[29] G.O. Jones and P.A. Thomas "An Investigation of the Crystal Structure and Phase Transitions of $Na_{0.5}Bi_{0.5}TiO_3$" Acta Crystallog. B58, 168-178 (2000)
[30] S-E Park and S.-J.Chung "Ferroic Phase Transitions in $Na_{0.5}Bi_{0.5}TiO_3$ Crystal" J. Am. Ceram. Soc., 79[5] 1290-96 (1996)
[31] I.G. Siny, C.S. Tu, V.H. Schmidt, "Critical Acoustic Behaviour of the Relaxor Ferroelectric Na1/2Bi1/2TiO3 in the Intertransition Region" Phys. Rev. B 51, 5659-5665 (1995)
[32] S.B. Vakrushev, V.A. Isupov, B.E. Kvyatkovsky, N.M. Okuneva, I.P. Pronin, G.A. Smolensky, P.P. Syrnikov " Phase Transitions and Soft modes in Sodium Bismuth Titanate" Ferroelectrics, 63, 153-60 (1985)
[33] I.P. Pronin, P.P. Syrnikov, V.A. Isupov, V.M. Egorov, N.V. Zaitseva "Peculiarities of Phase Transitionsin Sodium-Bismuth Titanate" Ferroelectrics 25, 395-397 (1980)
[34] K. Roleder, I. Franke, A.M. Glazer, P.A. Thomas, S. Miga and J. Suchanicz "The piezoelectric Effect in $Na_{0.5}Bi_{0.5}TiO_3$ Ceramics" J. Phys: Condens. Matter 14, 5399-5406 (2002)
[35] V.A. Isupov, P.L. Strelets, I.A.Serova, N.D. Yatenko and T.M. Shirobokikh "Peculiarities on Ferroelectric Phase Transition in Solid Solutions of the $Na_{0.5}Bi_{0.5}TiO_3 - PbTiO_3$ System" Soviet Physics-solid state , 6[3] 615-619 (1964)
[36] S.B. Vakrushev, B.E. Kvyatovkii, R.S. Malysheva, N.M. Okuneva and P.P. Syrnikov " Investigation of a Broad Phase Transition in $Na_{0.5}Bi_{0.5}TiO_3$ by the Neutron Scattering Method" Sov. Phys. Solid State 27[3] 455-457 (1985)
[37] K. Roleder, J. Suchanicz and A. Kania " Time Dependence of Electric Permittivity in $Na_{0.5}Bi_{0.5}TiO_3$ Single Crystal" Ferroelectrics 89, 1-5 (1989)
[38] J. Suchanicz and W.S. Ptak " On the Phase Transition in $Na_{0.5}Bi_{0.5}TiO_3$" Ferroelectric, 12, 71-78 (1990)
[39] T. Takenaka and H. Nagata "Present Status of Non-lead Piezoelectric Ceramics" Key Eng. Mat., 157-58, 57-64 (1999)
[40] T. Takenaka, A. Hozumi, T. Hata, and K. Sakata "Mechanical Properties of $Na_{0.5}Bi_{0.5}TiO_3$-based Piezoelectric Ceramics" Sil. Ind., 7-8, 136-142 (1993)
[41] T. Takenaka, K. Maruyama and K. Sakata "$Na_{0.5}Bi_{0.5}TiO_3$-$BaTiO_3$ System for Lead-free Piezoelectric Ceramics" Jpn. J. Appl. Phys., 30 [9B] 2236-2239 (1991)

[42] O. Elkechai and J.P. Mercurio "Ferroelectric Ceramics in the $Na_{0.5}Bi_{0.5}TiO_3$ - $K_{0.5}Bi_{0.5}TiO_3$, $Na_{0.5}Bi_{0.5}TiO_3$- $PbTiO_3$ and $K_{0.5}Bi_{0.5}TiO_3$- $PbTiO_3$ systems" Proceeding of the 9th IEEE International Symposium on Applications of Ferroelectric ISAF '94, 253-56 (1994)
[43] A. Herabut and A. Safari "Processing and Electromechanical Properties of $(Na_{0.5}Bi_{0.5})_{(1-1.5x)}La_xTiO_3$ Ceramics" J. Am. Ceram. Soc., 80[11] 2954-58 (1997)
[44] H. Nagata and T. Takenaka "$Na_{0.5}Bi_{0.5}TiO_3$-based Non-lead Piezoelectric Ceramics" J. Kor. Phys. Soc. 32, S1298-300 (1998)
[45] H. Nagata and T. Takenaka "Lead-free Piezoelectric Ceramics of $Na_{0.5}Bi_{0.5}TiO_3$-½(Bi_2O_3.Sc_2O_3) System" Jpn. J. Appl. Phys. 36[9B] 6055-6057 (1997)
[46] T. Takenaka and K. Sakata " New Piezo- and Pyroelectric Sensors Materials of $Na_{0.5}Bi_{0.5}TiO_3$-based Ceramics" Sensors and Materials, 3, 123-131 (1988)
[47] T. Takenaka and K. Sakata "Dielectric, Piezoelectric and Pyroelectric Properties of $Na_{0.5}Bi_{0.5}TiO_3$ – based Ceramics" Ferroelectrics, 95, 153-156 (1989)
[48] N. Ichinose and K. Udagawa "Piezoelectric Properties of $Na_{0.5}Bi_{0.5}TiO_3$ Ceramics" Ferroelectrics, 169, 317-325 (1995)
[49] T. Takenaka "Piezoelectric Properties of Some Lead-free Ferroelectric Ceramics" Ferroelectrics, 389, 87-98 (1999)
[50] T Takenaka, K. Sakata, K. Toda "Piezoelectric Properties of $Na_{0.5}Bi_{0.5}TiO_3$-based Ceramics" Ferroelectrics, 160, 375-380 (1990)
[51] O. Elkechai, M. Manier and J.P. Mercurio "$Na_{0.5}Bi_{0.5}TiO_3$- $Na_{0.5}Bi_{0.5}TiO_3$ (NBT-KBT) System: a Structural and Electrical Study" Phys. Stat. Sol. 157, 499-506 (1996)
[52] T. Wada, K. Toyoike, Y. Imanaka and Y. Matsuo " Dielectric and Piezoelectric Properties of $(A_{0.5}B_{0.5})TiO_3$-$ANbO_3$ (A=Na,K) Systems" Jpn. J. Appl. Phys., 40, 5703-5705 (2001)
[53] X. Wang , H. L.-W. Chan, C.-L. Choy "Piezoelectric and Dielectric Properties of CeO_2-added $(Bi_{1/2}Na_{1/2})_{0.94}Ba_{0.06}TiO_3$ Lead-free Ceramics" Solid State Comm., 125, 395-399 (2003)
[54] B.-J. Chu, D.-R. Chen, G.-R. Li, Q.-R. Yin "Electrical properties of $Na_{1/2}Bi_{1/2}TiO_3$–$BaTiO_3$ ceramics" J. Eur. Ceram. Soc., 22, 2115-2121 (2002)
[55] Y. Wu, H. Zhang, Y. Zhang, J. Ma, D. Xie "Lead-free Piezoelectric Ceramics with Compositions of (0.97-x)$Na_{1/2}Bi_{1/2}TiO_3$-0.03$NaNbO_3$-x$BaTiO_3$" J. Mater. Science, 38, 987-994 (2003)
[56] B. Aurivillius "Mixed Bismuth Oxides with Layer Lattice I.$Ca_2Nb_2O_6$" Arkiv Kemi, 1, 463 (1949)
[57] E.C. Subbarao, "Ferroelectricity in $Bi_4Ti_3O_{12}$ and its Solid Solutions", Phy. Rev., 122[3] 804-807 (1961)
[58] X. Duand, I-W Chen "Ferroelectric Thin Film of Bismuth-containing Layered Perovskites: Part I, $Bi_4Ti_3O_{12}$", J. Am. Ceram. Soc., 81[12] 3253-3259 (1998)
[59] R.L. Withers, J.G. Thompson, and A.D. Rae "The Crystal Chemistry Underlying Ferroelectricity in $Bi_4Ti_3O_{12}$, Bi_3TiNbO_9, and $BiWO_6$" J. Solid State Chem., 94, 404-417 (1991)
[60] J.P. Mercurio and B. Frit "Transitions de Phases dans les solutions solides de type $Bi_{4-x}Pb_xTi_{3-x}M^V_xO_{12}$ (M^V = Nb, Sb)" Sil. Ind. , 9-10, 143-146 (1989)
[61] E.C. Subbarao "Systematics of Bismuth Layer Compounds" Integr. Ferroelectrics, 12, 33-41 (1996)

[62] T. Rentschler "Substitution of Lead into the Bismuth Oxide Layer of the n=2 and n=3 Aurivillius Phases" Mater. Re. Bull., 32[3] 351-69 (1997)
[63] R.E. Newnham, R.W. Wolfe and J.F. Dorrian "Structural Basis of Ferroelectricity in the Bismuth Titanate Family" Mat. Res. Bull., 6, 1029-1039 (1971)
[64] E.C. Subbarao "A Family of Ferroelectric Bismuth Compounds" J. Phys. Chem. Solids, 23. 665-676 (1962)
[65] A. Pignolet "Growth, Structure and Properties of non c-oriented Epitaxial Bismuth-Layered Perovskite Ferroelectric Thin Films on Oxide-Buffered Silicon Substrates" Talk held at Cranfield University 10/05/2001
[66] K. Srinivas, A.R. James "Dielectric Characterisation of Polycrystalline $Sr_2Bi_4Ti_5O_{18}$" J. Appl. Phys., 86[7] 3885-3889 (1999)
[67] I.G. Ismailzade, V.I. Nesterenko, F.A. Mirishili and P.G. Rustanov "X-ray and Electrical Studies of the System $Bi_4Ti_3O_{12}$-$BiFeO_3$" Soviet Physics-Crystallography, 12[3] 400-404 (1967)
[68] J.M. Perez-Mato, P. Blaha, K. Parlinski, K. Schwarz, M. Aroyo, L. Elcoro and Z. Izaola " Competing Instabilities in Ferroelectric Aurivillius Compounds" J. Conf. Abs. EMF 2003, Cambridge UK, 8,259 (2003)
[69] B. Frit and J.P. Mercurio "The Crystal Chemistry and Dielectric Properties of Aurivillius Family of Complex Bismuth Oxides with Perovskite-like Layered Structures" J. All. Comp., 188, 27-35 (1992)
[70] S. Seong, K.-A. Yee and T.A. Albright "Interlayer Communications in Some Two-dimensional Materials" J. Am. Chem. Soc., 115, 1981-1987 (1993)
[71] E.C. Subbarao "Ferroelectricity in $Bi_4Ti_3O_{12}$ and its Solid Solutions" Phys. Rev., 122[3] 804-807 (1961)
[72] R. Maalal, M. Manier & J.P. Mercurio "Dielectric Properties of the Mixed Aurivillius Phase $M^{II}Bi_8Ti_7O_{27}$ (M^{II} = Ca, Sr, Ba and Pb)" J. Europ. Ceram. Soc., 15, 1135-1140 (1995)
[73] T. Kikuchi "Synthesis of a New, Mix-Layered Bismuth Titanate $SrBi_8Ti_7O_{27}$" J. Less-Common Metals, 52, 163-165 (1977)
[74] J. Golapalakrishnan, A. Ramanan, C.N. Rao, D.A. Jefferson and D.J. Smith "A Homologous Series of Recurrent Intergrowth Structures of the Type $Bi_4A_{m+n-2}B_{m+n}O_{3(m+n)+6}$ Formed by Oxides of the Aurivillius Family" J. Solid State Chem., 55, 101-105 (1984)
[75] V.K. Yanovskii, V.I. Voronkova "Structure, Polyphormism and Ferroelectric Properties of Mixed Layered Bismuth-containing Compounds" Inorg. Mat., 22[12], 1777-1781 (1986)
[76] C.N. Rao and J.M. Thomas "Intergrowth Structures: the Chemistry of Solid-solid Interfaces" Acc. Chem. Res., 18, 113-119 (1985)
[77] G.N. Subbanna, T.N. Guru Row and C.N.R. Rao "Structure and Dielectric Properties of Recurrent Intergrowth Structures Formed by the Aurivillius Family of Bismuth Oxides of the Formula $Bi_2A_{n-1}B_nO_{3n+3}$" J. Solid State Chem., 86, 206-211 (1990)
[78] S. Horiuchi, T. Kikuchi and M. Goto " Structure Determination of a Mixed-Layer Bismuth Titanate, $Bi_7Ti_4NbO_{21}$, by Super-High-Resolution Electron Microscopy" Acta Crist., A33, 701-703 (1977)

[79] F. Chu, D. Damjanovic, O. Steiner and N. Setter "Piezoelectricity and Phase Transitions of Mixed-layer Bismuth Titanate Niobate $Bi_7Ti_4NbO_{21}$" J. Am. Ceram. Soc., 78[11] 3142-44 (1995)
[80] P. Boullay and D. Mercurio "Structural Behaviour of the Mixed-Layer Aurivillius Phase $Bi_7Ti_4NbO_{21}$" J. Conf. Abs. EMF 2003 Cambridge UK, 8, 82 (2003)
[81] W.L. Warren, B.A. Tuttle and D. Dimos "Ferroelectric Fatigue in Perovskite Oxides" Appl. Phys. Lett., 67 [10] 1426-28 (1995)
[82] B.H. Park, B.S. Kang, S.D. Bu, T.W. Noh, J.Lee and W. Jo "Lanthanum-substituted Bismuth for Use in Non-volatile Memories" Nature, 401, 682-684 (1999)
[83] T.W. Noh, B.S. Kang, Y.W. So, B.H. Park and S.D. Bu "A New Ferroelectric Material for FRAM Applications: Lanthanum-substitued Bismuth Titanate" J. Korean Phys. Soc. 39, S35-S38 (2001)
[84] W.L. Warren, D. Dimos, B.A. Tuttle, R.D. Nashby and G.E. Pike "Electronic Domain Pinning in $Pb(Zr,Ti)O_3$ Thin Films and its Role in Fatigue" Appl. Phys. Lett. 65[8] 1018-1020 (1994)
[85] E.L. Colla, D.V. Taylor, A.K. Tagantsev and N. Setter "Discrimination Between Bulk and Interface Scemarios fo the Suppression of the Switchable Polarisation (Fatigue) in $Pb(Zr,Ti)O_3$ Thin Films Capacitors with Pt Electrodes" Appl. Phys. Letters, 72 [19] 2478-80 (1998)
[86] Y. Wang, K.H. Wong, C.L. Choy "Fatigue Problems in Ferroelectric Thin Films" Phys. Stat. Sol. (a) 191 [2] 482-488 (2002)
[87] J.F. Scott and M. Dawber "Oxygen-vacancy Ordering as a Fatigue Mechanism in Perovskite Ferroelectrics" Appl. Phys. Lett., 76 [25] 3801-3803 (2000)
[88] Y. Noguchi, M. Miyayama "Large Remanent Polarisation of Vandium-doped $Bi_4Ti_3O_{12}$" Appl. Phys. Lett., 78[13] 1903-1905 (2001)
[89] H. Nagata, N. Chikushi and T. Takenaka " Ferroelectric Properties of Bismuth Layer-structured Compound $Sr_xBi_{4-x}Ti_{3-x}Ta_xO_{12}$ ($0 \leq x \leq 2$)" Jpn. J. Appl. Phys., 38, 5497-5499 (1999)
[90] B.H. Park, S.J. Hyun, S.D. Bu and T. Noh "Differences in Nature of Defects Between $SrBi_2Ta_2O_9$ and $Bi_4Ti_3O_{12}$" Appl. Phys. Lett. 74[13] 1907-1909 (1999)
[91] C. Jovalekic, M. Pavlovic, P. Osmokovic, Lj. Atanasoska " X-ray Photoelectronic Spectroscopy Study of $Bi_4Ti_3O_{12}$ Ferroelectric Ceramics" Appl. Phys. Lett., 72[9] 1052-1053 (1998)
[92] S.-H. Hong, S. Trolier-McKinstry and G.L. Messing "Dielectric and Electromechanical Properties of Textured Niobium-doped Bismuth Titanate Ceramics" J. Am. Ceram. Soc., 83[1] 113-118 (2000)
[93] T. Takenaka, K. Sohji and K. Sakata "Ferroelectric and Dielectric Properties of Press-forged $Bi_4Ti_3O_{12}$ Ceramics" " Proc. Jpn Cong. Mater. Res., 19, 230-33(1976)
[94] H. Nagata, Y. Fujita, H. Enosawa and T. Takenaka "$Bi_4Ti_3O_{12}$-based Lead-free Piezoelectric Ceramics with Grain Orientation" Proceedings of the IEEE Conference on Ferroelectric Materials 2002, 303-306 (2002)
[95] T. Takenaka and K. Sakata "Electrical Properties of Grain Oriented Ferroelectric Ceramics in Some Lanthanum Modified Layer-structure Oxide" Ferroelectrics, 38, 769-772 (1981)
[96] S. Swartz, W.A. Schulze and J.V. Biggers "Fabrication and Electrical Properties of Grain Oriented $Bi_4Ti_3O_{12}$ Ceramics" Ferroelectrics, 38, 765-768 (1981)

[97] J. A. Horn, S.C. Zhang, U. Selvarag, G.L. Messing, S. Troiler-McKinstry and M. Yokoyama "Fabrication of Textured $Bi_4Ti_3O_{12}$ by Template Grain Growth" Proceeding IEEE on Electroceramics 1996, 943-946 (1996)
[98] H. Holmes, R.E. Newnham and L.E. Cross "Grain-oriented ferroelectric Ceramics" Am. Ceram. Soc. Bull., 58[9] 872 (1979)
[99] T. Takeuchi, T. Tani and Y. Sato "Unidirectionally Textured $CaBi_4Ti_4O_{15}$ Ceramics by the Reactive Template Grain Growth with an Extrusion" Jpn. J. Appl. Phys., 39, 5577-5580 (2000)
[100] J. A. Horn, S.C. Zhang, U. Selvaray, G.L. Messing and S. Trolier-McKinstry "Templated Grain Growth of Textured Bismuth Titanate" J. Am. Ceram. Soc., 82[4] 921-926 (1999)
[101] Y. Kan, P. Wang, Y. Li, Y.-B. Cheng, D. Yan "Fabrication of Textured Bismuth Titanate by Template Grain Growth Using Aqueous Tape Casting" J. Europ. Ceram. Soc., 23, 2163-2169 (2003)
[102] L. Nistor, G. Van Tandeloo and S. Amelinckx "The Paraelectric-ferroelectric Phase Transition of $Bi_4Ti_3O_{12}$ Studied by Electron Microscopy" Phase Transitions, 59, 135-153 (1996)
[103] A.D. Rae, J.G. Thompson, R.L Withers and A.C. Willis " Structure Refinement of Commensurately Modulated Bismuth Titanate, $Bi_4Ti_3O_{12}$" Acta Cryst., B46, 474-487 (1990)
[104] H.S. Shulman, M. Testorf, D. Damjanovic, and N. Setter "Microstructure, Electrical Conductivity, and Piezoelectric Properties of Bismuth Titanate" J. Am. Ceram. Soc. ,79 [12] 3124-3128 (1996)
[105] J.F. Dorrian, R.E Newnham, D.K. Smith and M.I. Kay "Crystal Structure of $Bi_4Ti_3O_{12}$" Ferroelectrics, 3, 17-27 (1971)
[106] S.E. Cummings and L.E. Cross "Electrical and Optical Properties of Ferroelectric $Bi_4Ti_3O_{12}$ Single Crystal" J. Appl. Phys., 39[5] 2268-2274 (1968)
[107] K. Singh, D.K. Bopardikar and D.V. Atkare " A Compendium of Tc-Ps and Ps-Dz Data for Displacive ferroelectrics" Ferroelectrics, 82, 55-67 (1998)
[108] S.C Abrahams, S.K. Kurtz, and P.B. Jamieson "Atomic Displacement Relationship to Curie Temperature and Spontaneous Polarisation in Displacive Ferroelectrics" Phys. Rev., 172 [2] 551-553 (1968)
[109] S.S. Lopatin, T.G. Lupeiko, T.L. Vasil'tsova, N.I. Basenko and I.M. Berlizev "Properties of Bismuth Titanate Ceramics modified with Group V and VI Elements" Inorganic Materials, 24, 1328-1331 (1998)
[110] Y. Lu, D.T. Hoelzer, W.A. Schulze, B. Tuttle, B.G. Potter "Grain-oriented Ferroelectric Bismuth Titanate Thin Film Prepared from Acetate Precursors" Mat. Sci. and Eng., B39, 41-47 (1996)
[111] M.Villegas, C. Moure, J.F. Fernandez and P. Duran "Low Temperature Sintering of Submicronic Randomly Oriented $Bi_4Ti_3O_{12}$ Materials" Ceram. Inter.,22, 15-22 (1996)
[112] R.A. Armstrong and R.E. Newnham "Bismuth Titanate Solid Solutions" Mater. Res. Bull., 7, 1025 (1972)
[113] S.H. Hong, S. Troiler-Mckinstry, and G.L. Messing "Dielectric and Electromechanical Properties of Texture Niobium-doped Bismuth Titanate Ceramics" J. Am. Ceram. Soc., 83 [1] 113-118 (2000)

[114] H.S. Shulman, D. Damjanovic, and N.Setter "Niobium doping and Dielectric Anomalies in Bismuth Titanate" J. Am. Ceram. Soc., 83 [1] 528-532 (2000)
[115] S.H. Hong, J.A. Horn, S. Troiler-Mckinstry, and G.L. Messing "Dielectric and Ferroelectric Properties of Ta-doped Bismuth Titanate" J. Mater. Sci. Lett., 19, 1661-1664 (2000)
[116] A. Megriche, L. Lebrun, M. Troccaz "Materials of $Bi_4Ti_3O_{12}$ Type for High Temperature Acoustic Piezo-Sensors" Sensors and Actuators, 78, 88-91 (1999)
[117] M.Villegas, A.C. Caballero, C. Moure, P. Duran, and J.F Fernandez "Low Temperature Sintering and Electrical Properties of Chemically W-doped $Bi_4Ti_3O_{12}$ Ceramics" J. Europ. Ceram. Soc. 19,1183-1186 (1999)
[118] Y. Shimazawa, Y. Kubo, Y. Tauchi, T. Kamiyama, H. Asano, F. Izumi "Structural Distortion and Ferroelectric Properties of $SrBi_2(Ta_{1-x}Nb_x)_2O_9$" Appl. Phys. Lett., 77(17) (2000)
[119] Y. Shimakawa, Y. Kubo, Y. Tauchi, H. Hasano, T. Kamiyama, F. Izumi, Z. Hiroi "Crystal and Electronic Structures of $Bi_{4-x}La_xTi_3O_{12}$ Ferroelectric Materials" Appl. Phys. Lett., 79(17) (2001)
[120] R.W. Wolfe and R.E. Newnham "Rare Earth Bismuth Titanates" J. Electrochem. Sc.: Solid State Science, 116(6) 832-835 (1969)
[121] H.Nagata, N. Chikushi, T. Takenaka "Ferroelectric Properties of Bismuth Layered-Structured Compound $Sr_xBi_{4-x}Ti_{3-x}Ta_xO_{12}$ ($0 \leq x \leq 2$) " Jpn. J. Appl. Phys., 38, 5497-5499 (1999)
[122] B.H Park, B.S. Kang, S.D. Bu, T.W. Noh, J. Lee and W. Jo "Lanthanum-substituted Bismuth Titanate for Use in non-volatile Memories" Nature, 401, 682-685 (1999)
[123] T. Kojima, T. Sakai, T. Watanabe,H. Funakubo, K. Saito, M. Osada "Large Remanet Polarization of $(Bi,Nd)_4Ti_3O_{12}$ Epitaxial Thin Films Grown by Metalorganic Chemical Vapour Deposition" Appl. Phys. Lett., 80 [15] 2746-48 (2002)
[124] A.D. Rae, J.G. Thompson and R.L. Withers, Acta Cristallog. Sect B: Struct. Science, 48, 418 (1992)
[125] J.A. Horn, S.C. Zhang, U. Selvaray, G.L. Messing and S. Trolier-Mckinstry "Template Grain Growth of Textured Bismuth Titanate" J. Am. Ceram Soc., 82 [4] 921-926 (1999)
[126] V.K. Seth, W.A. Schulze "Fabrication and Electrical Properties of Grain-oriented Bismuth Titanate Ceramics" Ceramica, 11/12, 11-15 (1986)
[127] E. C. Subbarao "A Family of Ferroelectric Bismuth Compounds" J. Phys. Chem. Solids, 23. 665-676 (1962)
[128] E.C. Subbarao " Systematics of Bismuth Layer Compounds" Integ. Ferroelectrics, 12, 33-41 (1996)
[129] I.G. Ismailzade "X-Ray Investigation of the Ferroelectric Phase Transition in $Ba_2Bi_4Ti_5O_{18}$ and Phase Transitions in the Compounds $A_{m-n+1}Bi_nB_mO_{3m+3}$ ($A=Ca^{2+}$, Sr^{2+}, Ba^{2+}, Pb^{2+}, Bi^{3+}; B= Nb^{5+}, Ta^{5+}, Ti^{4+})" Soviet Physic-Crystallography, 8, 686-690 (1963)
[130] I.G. Ismailzade, V.I. Nesterenko, F.A. Mirishili and P.G. Rustamov "X-ray and Electrical Studies of the System $Bi_4Ti_3O_{12}$-$BiFeO_3$" Soviet Physics-Crystallography, 12[3], 400-404 (1967)

[131] A.L Micheli, J.V. Mantese and N.W. Schubring "Characteristics of Some (MOD) Thin-Film Layer Type Compounds in The Bismuth Titanate-Lead Titanate System" Integr. Ferroelectrics, vol. 12, 1-9 (1996)
[132] L.V. Korzunova, V.G. Osipyan, L.A. Shebanov and E.Zh. Freidenfel'd "Crystal-chemical Conditions for Formation of New Layered Compounds of Bismuth" Inor. Mater., 20, 12, 2074-2076 (1984)
[133] R. Maalal, M. Manier & J.P.Mercurio "Dielectric Properties of the Mixed Aurivillius Phases $M^{II}Bi_8Ti_7O_{27}$ (M^{II} = Ca, Sr, Ba and Pb)" J. Europ. Ceram. Soc, 15, 1135-1140 (1995)
[134] Miyayama M., Yi I.-S "Electrical Anisotropy in Single Crystals of Bi-layer Structured Ferroelectrics" Ceram. International, 26, 529-533 (2000)
[135] B Aurivillius and P.H. Fang "Ferroelectricity in the compound $Ba_2Bi_4Ti_5O_{18}$" Phys. Rev. 126, 3, 893-896 (1962)
[136] K. Srinivas, A.R. James "Dielectric Characterisation of Polycristalline $Sr_2Bi_4Ti_5O_{18}$" J. Appl. Phys., 86, 7, 3885-3889 (1999)
[137] V.A. Isupov "Curie Temperature of $A_{m-1}Bi_2M_mO_{3m+3}$ Layered Ferroelectrics" Inorg. Mater., 33, 9, 936-940 (1997)
[138] A. Srinivas, S.V. Suryanarayana, G.S. Kumar and M. Mahesh Kumar "Magnetoelectric measurement on $Bi_5FeTi_3O_{15}$ and $Bi_6Fe_2Ti_3O_{18}$" J. Phys.: Condes. Matter, 11, 3335-3340, (1999)
[139] A. Srinivas, M. Mahesh Kumar S.V. Suryanarayana and T. Bhimasankaram "Investigation of dielectric and magnetic nature of $Bi_7Fe_3Ti_3O_{21}$" Mat. Res. Bull., 34, 6, 989-996 (1999)
[140] N.V. Prasad, G. Prasad, S.V. Suryanarayana and G.S. Kumar " Dielectric Measurements on Rare Hearth-substituted $Bi_6Fe_2Ti_3O_{18}$ Ceramic" Phase Trans.,76[6] 575-585 (2003)
[141] S.-L. Ahn, Y. Noguchi, M. Miyayama, T. Kudo "Structural and electrical characterization of $Bi_5Ti_3Fe_{1-x}Mn_xO_{15}$ system" Mat. Res. Bull., 35, 825-834 (2000)
[142] T. Takenaka "Lead free and Low-lead-content Piezoelectric Ceramics for Environment" Proc. Int. Symp. Ceram. Trans., 70, 271-283 (1995)
[143] H.S. Shulman, M. Testorf, D. Damjanovic and N. Setter "Microstructure, Electrical Conductivity and Piezoelectric Properties of Bismuth Titanate" J. Am. Ceram. Soc., 79[12] 3124-3128 (1996)
[144] S.L. Swartz and T.R. Shrout "Fabrication of Perovskite Lead Magnesium Niobate" Mater. Res. Bull., 17 [10] 1245-50 (1982)
[145] Crystallographica 1.0 by Oxford Cryosystem, 2-3, Bleheim Office Park, Lower Road. Long Hanborough, UK
[146] D.A. Fletcher, R.F. McMeeking, and D. Parking "The United Kingdom Chemical Database Service" J. Chem. Inf. Comput. Sci., 36, 746-749 (1996)
[147] W.D. Kingery, H.K. Bowen, D.R. Uhlmann, "Introduction to ceramics" John Wiley & sons Edition ,2nd Edition, 1976
[148] R. M. German, "Powder Metallurgy Science" MPIF Editor, 2nd Edition, 1994
[149] IEEE Standard on Piezoelectricity, American National Standard, 1987
[150] A. Sanson "Sintesi e Caratterizzazione di un Materiale Piezoelettrico Senza Piombo" Tesi per il corso di laurea in Chimica Industriale, Università di Padova, Italy, 2000

[151] A.J. Moulson and J.M. Herbert "Electroceramics: Materials-properties-application" Chapman & Hall, (1997)
[152] F. Jona and G.Shirane "Ferroelectric crystals" Pergamon Press, 1962
[153] IEEE Standard on Piezoelectricity, American National Standard, 1987
[154] C.-H. Lu, C.-H. Wu "Preparation, Sintering and Ferroelectric Properties of Layered-structured Strontium Bismuth Titanium Oxide Ceramics" J. Eur. Ceram. Soc., 22, 704-714 (2002)
[155] H. Yan, C.Li, J. Zhon, W. Zhu, L. He, Y. Song, Y. Yu "Influence of Sintering Temperature on the Properties of High Tc Bismuth Layer Structure Ceramics" Mater. Science and Eng., B88, 62-67 (2002)
[156] A.I. Kingom, J.B. Clark "Sintering of PZT Ceramics: I, Atmosphere Control" J. Am. Ceram. Soc., 66[4] 253-256 (1983)
[157] A.I. Kingom, J.B. Clark "Sintering of PZT Ceramics: II, Effect of PbO Content on Densification Kinetics" J. Am. Ceram. Soc., 66[4] 256-260 (1983)
[158] M. Hammer and M. Hoffman "Sintering Model for Mixed-Oxide-Derived Lead Zirconate Titanate Ceramics" J. Am. Ceram. Soc., 81[12] 3277-84 (1998)
[159] S.G. Brodie, J. Ricoh and C.E. Millar "Hot Isostatic Pressing of Aurivillius Compounds for High-Temperature Device Applications" Electroceramics: Production Properties and Microstructure, Proc. Symp. Leeds, Inst. of Metals, 195-203 (1993)
[160] M.V. Gelfuso, D. Thomazini and J.A. Eiras "Synthesis and Structural, Ferroelectric ad Piezoelectric Properties of $SrBi_4Ti_4O_{15}$ Ceramics" J. Am. Ceram. Soc., 82[9] 2368-72 (1999)
[161] M. Zhao. C. Wang, W. Zhong, J. Wang and H. Chen "Ferroelectric, Piezoelectric and Pyroelectric Properties of $Sr_{1+x}Bi_{4-x}Ti_{4-x}Ta_xO_{15}$ (x = 0-1)" Jpn. J. Appl. Phys., 41, 1455-1458 (2002)
[162] H. Oka, M. Hirose, T. Tsukada, Y. Watanabe and T. Nomura "Thickness-Shear Mode Characteristics of $SrBi_4Ti_4O_{15}$-Based Ceramics" Jpn. J. Appl. Phys., 39[9B] 5613-15 (2000)
[163] E.C Subbarao "Systematics of Bismuth Layer Compounds" Integrated Ferroelectrics, 1233-41(1996)
[164] R.D. Shannon and C.T. Prewitt "Effective Ionic Radii in Oxides and Fluorides" Acta Cryst. B25,925 (1969)
[165] T. Kikuchi "Stability of Layered Bismuth Compounds in Relation to the Structural Mismatch" Mat. Res. Bull., 14, 1561 (1979)
[166] O. Furukawa, Y. Yamashita, M. Harata, T. Takashi and K. Inagaki "Dielectric Properties of Modified Lead Zinc Niobate Ceramics" Jon. J. Appl. Phys., 24, S24-3, 96-99 (1985)
[167] B. Jaffe, W.R. Cook Jr. and H. Jaffe "Piezoelectric ceramics" Academic Press London and New York, 1971
[168] I.G. Ismailzade, V.I. Nesterenko, F.A. Mirishili and P.G. Rustamov "X-ray and electrical studies of the system $Bi_4Ti_3O_{12}$-$BiFeO_3$" Soviet Physics- Crystallography, 12 (3) (1967) 400-404
[169] C. Kittel "On infinitely Adaptive Crystal Structure" Solid State Comm., 25,519-520 (1978)
[170] R.A. Armstrong and R.E. Newnham, "Bismuth Titanate Solid Solutions", Mater. Res. Bull., 7, 1025-1034 (1972)

[171] N. Wakiya, N. Ishizawa, K. Shinozaki and N. Mizutani "Thermal Stability of $Pb(Zn_{1/3}Nb_{1/3})O_3$ (PZN) and Consideration of Stabilization Conditions of Peroskite Type Compounds" Mater. Res. Bull., 30[9] 1121-1131 (1995)
[172] I.M. Reaney, M. Roulin, H.S. Shulman and N. Setter, "In situ Observations of Octahedral Tilt Transitions in Strontium Bismuth Titanate Layered Perovskites", Ferroelectrics, 165, 295-305 (1995)
[173] K.S. Aleksandrov and J. Bartolome', "Octahedral Tilt Phases in Perovskite-like Crystals with Slabs Containing an Even Number of Octahedral Layers", J.Phys.:Cond. Matter, 6, 8219-8235 (1994)
[174] F.K. Lontgering "Topotactical Reactions with Ferrimagnetic Oxides Having Hexagonal Crystal Structures-I" J. Inorg. Nucl. Chem., 66[2] 113-123 (1959)
[175] C.-H. Lu and Y.C. Chen "Sintering and Decomposition of Ferroelectric Layered Perovskites: Strontium Bismuth Tantalate Ceramics" J. Eur. Ceram. Soc., 19, 2909-2915 (1999)
[176]K. Srinivas, A.R. James: "Dielectric Characterisation of Polycristalline $Sr_2Bi_4Ti_5O_{18}$" J. Appl. Phys., 86[7] 3885-3889 (1999).
[177] H.S. Shulman, M. Testorf, D. Damjanovic and N. Setter: J. Am. Ceram. Soc., **79** (1996) No. 12, 3124.
[178] H. Irie, M. Miyayama and T. Kudo: J. Am. Ceram. Soc., "Electrical Properties of a Bismuth Layer-structured $Ba_2Bi_4Ti_5O_{18}$ Single Crystal" 83[11], 2699-2702(2000).
[179] V.K. Seth, W.A. Shultze "Grain Oriented Bismuth Ceramics" La Ceramica 11 (1986)
[180] S. Ehara and alt.: Jpn. J. Appl. Phys. 20 (1981) No. 5, 877
[181] D. Damnjanovic, M. Demartin Maeder, P. Duran Martin, and N. Setter "Maxwell-Wagner Piezoelectric Relaxation in Ferroelectric Heterostructures" J. Appl. Phys., 90[11]5708-5712 (2001)
[182] D. O'Neill, R.M. Bowman, and J.M. Gregg "Dielectric Enhancement and Maxwell-Wagner Effects in Ferroelectric Superlattice Structures" Appl. Phys. Lett., 77[10] 1520-1522 (2000)
[183] A.V. Turik and G.S. Radschenko " Maxwell-Wagner Relaxation in Piezoactive Media" J. Phys. D: Appl. Phys., 35, 1188-1192 (2002)
[184] M. Shen, S. Ge, W. Cao "Dielectric Enhancement and Maxwell-Wagner Effects in Polycrystalline Ferrolectric Multilayered Thin Films" J. Phys. D: Appl. Phys., 34, 2935-2938 (2001)
[185] A. von Hippel " Dieelctrics and Waves" Artech House Ed., (1996)
[186] R. Maalal, M. Manier & J.P.Mercurio "Dielectric Properties of the Mixed Aurivillius Phases $M^{II}Bi_8Ti_7O_{27}$ (M^{II} = Ca, Sr, Ba and Pb)" J. Eur. Ceram. Soc., 15, 1135-1140 (1995)
[187] C. Giacovazzo, H.L. Monaco, D. Viterbo et al "Fundamentals of Crystallography" Oxford Science Publications, 1995
[188] Rentschler T. "Sustitution of Lead into the Bismuth Oxide Layers of the n=2 and n=3 Aurivillius Phases" Mater. Res. Bull., 32, 3, 351-369 (1997)
[189] Suchow L. "Bismuth Magnesium Titanate, an Unusual New Perovskite" J. Inorg. Nucl. Chem., 30, 87-95 (1968)
[190] K. Tajima, H.J. Hwang, M. Sando and K. Niihara "PZT Nanocomposites Reinforced by Small Amount of Oxides" J. Eur. Ceram. Soc., 19, 1179-1182 (1999)

[191] R.L. Withers, J.G. Thompson and A.D.Rae "The Crystal Chemistry Underlying Ferroelectricity in $Bi_4Ti_3O_{12}$, Bi_3TiNbO_9 and Bi_3WO_6" J. Solid State Chem. 94, 404-407 (1991)
[192] C.H. Hervoches and P. Lightfoot "A Variable-Temperature Powder Neutron Diffraction Study of Ferroelectric $Bi_4Ti_3O_{12}$" Chem. Mater., 11, 3359-3364 (1999)
[193] A.D. Rae, J.G. Thompson and R.L. Withers "Structure Refinement of Commensurably Modulated Bismuth Strontium Tantalate, $Bi_2SrTa_2O_9$" Acta Cryst., B48, 418-428 (1992)
[194] L. Nistor, G. Van Tendeloo and S. Amelinckx "The Paraelectric-Ferroelectric Phase Transition of $Bi_4Ti_3O_{12}$ Studied by Electron Microscopy" Phase Transitions, 59, 135-153 (1996)
[195] D. Saha, A. Sen, H.S. Maiti "Low Temperature Liquid-phase sintering of Lead Magnesium Niobate" Ceram. Int., 25, 145-151 (1999)
[196] T.V. Koladiazhnyi, A. Petric, G.P. Johari, A.G. Belous "Effect of Preparation Conditions on Cation Ordering and Dielectric Properties of $Ba(Mg_{1/3}Ta_{2/3})O_3$ Ceramics" J. Europ. Ceram. Soc., 22, 2013-2021 (2002)
[197] C.-L. Huang and C.-L. Pan "Low-Temperature Sintering and Microwave Dielectric Properties of $(1-x)MgTiO_3 - xCaTiO_3$ Ceramics Using Bismuth Addition" Jpn. J. Appl. Phys., 41, 707-711 (2002)
[198] L. Zhou, P.M. Vilarinho and J.L. Baptista " Solubility of Bismuth Oxide in Barium Titanate" J. Am. Ceram. Soc., 82[4] 1064-1066 (1999)
[199] D. Saha, A. Sen. H.S. Maiti "Effect of Humidity on Dielectric Properties of Lead Magnesium Niobate Containing Excess MgO" Mater. Res. Bull., 35, 305-314 (2000)
[200] M. Villegas, A.C. Caballero, C. Moure, P. Duran, J.F. Fernandez "Factors Affecting the Electrical Conductivity of Donor-doped $Bi_4Ti_3O_{12}$ Piezoelectric Ceramics" J. Am. Ceram. Soc., 82, 2411-2414 (1999)
[201] H. Irie, M. Miyayama and T. Kudo "Electrical Properties of a Bismuth Layer-Structured $Ba_2Bi_4Ti_5O_{18}$ Single Crytal" J. Am. Ceram. Soc., 83[11] 2699-704 (2000)
[202] B. Guiffard, L. Lebrun. D. Guyomar, E. Pleska "Dielectric and Piezoelectric Properties of Mf-F Co-doped PBSZT Ceramics" Ann. Chim. Sci. Mat., 2, 113-119 (2001)
[203] R.A. Dorey, S.B. Stringfellow, R.W. Whatmore "Effect of Sintering Aid and Repeated Sol Infiltrations on the Dielectric and Piezoelectric Properties of a PZT Composite Thick Film" J. Eur. Ceram. Soc., 22, 2921-2926 (2002)